Scale up and Development of a Microbial Electrolysis Cell for Domestic Wastewater Treatment and Energy Recovery

EngD

Sarah Elizabeth Cotterill

A thesis submitted to Newcastle University for the degree of Doctor of Engineering in the Faculty of Science, Agriculture and Engineering

Supervisor: Professor Tom Curtis

Co-supervisors: Dr Elizabeth Heidrich and Dr Jan Dolfing

Industrial Supervisor: Chris Jones, R&D Manager, Northumbrian Water Group

School of Civil Engineering and Geosciences

Date of Submission: March 2017

ii

Abstract

Microbial Electrolysis Cells (MECs) have the potential to transform wastewater treatment, but many studies have been carried out at a very small scale with implausible temperatures and synthetic substrates. The value of laboratory-scale controlled experiments is not questioned, but these studies do not inform us of the realities and challenges that occur when operating MEC in the real world at realistic scales.

Addressing this issue led to the installation and operation of a pilot scale MEC which failed within 6 months. It was consequently dissected and analysed, to systematically understand failure, through fault tree analysis (FTA). This process identified areas for further development to move towards a more robust MEC prototype. Meta-analyses and experiments were used to asses some of the challenges still to be overcome, before the commercialisation of MEC is a realistic prospect.

With this knowledge, a re-design led to the successful operation of a second pilot, which moved from the L to the m^3 scale, thanks to a 16-fold increase in electrode surface area (1 m^2 each) and a 5-hour hydraulic retention time (HRT). After nine months, 0.8 L of H_2/d (0.003 L-H_2/L-MEC/d) was produced from primary treated domestic wastewater where the wastewater temperature was as low as 5.3℃. The European Urban Wastewater Treatment Directive consent of 125 mg/L was achieved 55% of the time, with 64% of the chemical oxygen demand (COD) removed. To break-even energetically each module would need to produce 4 L-H_2/day. This is possible, if hydrogen loss through scavenging can be addressed and improvements to the current density can be achieved. Recommendations for both are proposed.

A cost benefit analysis (CBA) and multi criteria assessment (MCA) is used to compare four potential MEC products. The model is based on current and realistic projections of MEC performance, to assess the net present value (NPV) of the technology and the potential savings that could be gained in wastewater treatment.

Acknowledgements

I have been extremely fortunate to forge some long-lasting collaborations during this EngD. Zach Stoll and Pei Xu (at New Mexico State University), hosted me for a month-long collaboration on MEC in 2014. This was at a difficult time in my EngD, after my first pilot had failed. They helped me to explore ideas to understand why failure had occurred. This collaboration continued beyond the visit, as Zach and I planned international webinars and mini-conferences to link to STREAM and ReNUWIt industrial doctoral centres. Additionally, I would like to thank Albert Guisasola and Juan Baeza at Universitat Autónoma de Barcelona, for hosting my visit to their Genocov lab in 2015.

I am grateful to the support provided by Paul Jeffrey, Ewan McAdam and Tania Rice at Cranfield. Being part of the STREAM programme has provided countless opportunities, exciting experiences and life-long friendships. I have been part of an immensely supportive cohort during this doctoral process.

Finally, I would like to thank my family and friends for listening to me moan and doing their utmost to keep me smiling. Most of all, I must thank my mum and dad, who first instilled my thirst for learning. They have been tremendously supportive: providing encouragement, motivation and emotional guidance when it was needed most. I could not have done this without them.

Contents

List of Figures

List of Tables

Chapter 1. Introduction

1.1 Background

Wastewater is defined as "a combination of the liquid or water-carried wastes removed from residences …and commercial and industrial establishments, together with groundwater, surface water and storm water" (Tchobanoglous *et al.,* 2004). Untreated wastewater can lead to the production of malodorous gases, the accumulation of pathogenic microorganisms, and the stimulation of aquatic plant growth (Tchobanoglous *et al.,* 2004). Wastewater treatment is therefore a necessity to protect public health and the environment. Currently, UK sewage companies are legally obliged to treat wastewater to the Urban Wastewater Treatment Directive standards (91/271/EEC).

Conventional wastewater treatment is a series of unit processes to provide different levels of treatment: preliminary, primary, and secondary. Preliminary treatment involves the removal of gross solids, grease and grit to prevent damage to downstream processes (Tchobanoglous *et al.,* 2004). Primary treatment removes settleable solids through sedimentation, and may be enhanced by chemical coagulants. Secondary treatment aims to remove biodegradable organic matter, suspended solids and nutrients, depending on site specific requirements (Tchobanoglous *et al.,* 2004).

Secondary treatment can be classified by the metabolic function of the bacteria (aerobic, anaerobic, anoxic or facultative) or the type of biological process (suspended-growth, attached-growth, combined or lagoon). In the UK, secondary treatment typically involves the activated sludge (AS) process (suspended-growth, aerobic) or trickling filters (TF) (attached-growth, aerobic). AS is widely used, due to the high effluent quality achieved from aerating wastewater. AS involves the suspension and aeration of microorganisms, and the sedimentation and recirculation of solids (Tchobanoglous *et al.,* 2004).

Removal of organic contaminants through aeration is a costly process. It accounts for 50% of the energy use in wastewater treatment, at 0.3 kWh/m^3 (Olsson, 2012; McCarty *et al.,* 2011). Energy is wasted by the process of aeration (which uses 1.08 kJ/L wastewater treated) and the failure to recover the chemical energy (estimated to be 7.6 kJ/L by Heidrich *et al.,* 2011).

Wastewater is increasingly viewed as a resource (McCarty *et al.,* 2011, Verstraete and Vlaeminck, 2011). Changes to conventional practice can reduce energy use in wastewater treatment and increase opportunities to recover energy. A switch to complete anaerobic treatment may provide the best opportunity to achieve this (McCarty *et al.,* 2011). Yet, anaerobic treatment of wastewater has limitations, including its performance at low temperatures and with low strength wastewaters (McCarty *et al.,* 2011). Before the introduction of upflow anaerobic sludge blanket (UASB) reactors in the late 1970s, secondary anaerobic treatment of wastewater was fairly uncommon (Lettinga *et al.,* 1980; Seghezzo *et al.,* 1998).

UASB reactors contain no packing or supporting material. Instead, their design contains an influent distribution system at the base of the reactor and gas-solids separator (GSS) (Tchobanoglous *et al.,* 2004). This allows suspended solids to settle at the top of the reactor and a sludge blanket (with 50-100 g/L solids) to form at the bottom (Lettinga *et al.,* 1984; Tchobanoglous *et al.,* 2004). The process is used to treat a range of wastewaters and can achieve 55-70 % chemical oxygen demand (COD) removal at temperatures between 13-17°C (Seghezzo *et al.,* 1998). Below this temperature range, significant suspended solids accumulation can lead to a reduction in methanogenesis and an overloading of the system (Seghezzo *et al.,* 1998). Wastewater composition, organic loading, pH, temperature and VFA concentration are some of the factors that influence the performance of a UASB (Leitão *et al.,* 2006; Tchobanoglous *et al.,* 2004).

New technologies, such as anaerobic fluidised membrane bioreactors (AFMBRs) or bioelectrochemical systems (BES) also provide an opportunity to reduce energy input and recover chemical energy whilst treating wastewater. AFMBRs combine a membrane system with a suspended particulate, such as granular activated carbon (GAC). As the biofilm grows on the GAC, the system can be effective for low strength wastewaters, previously seen as a barrier to anaerobic treatment (McCarty *et al.,* 2011).

BES, an overarching term for microbial fuel cells (MFCs) and microbial electrolysis cells (MECs), directly convert organic matter into electricity or chemicals. MFCs can produce "combustion-less, pollution-free bioelectricity directly from the organic matter in biomass" (Rittmann, 2008). Developing carbon-neutral alternatives, such as BES, may help to reduce the reliance on fossil fuels, which are predicted to increase in cost and continue to contribute to global warming (Rittman, 2008).

In 2005, it was discovered that hydrogen could be generated from MFCs, by providing additional current (Rozendal *et al.,* 2006; Liu *et al.,* 2005a). This technology, initially called a bioelectrochemically assisted microbial reactor (BEAMR) (Ditzig *et al.,* 2007), became known as microbial electrolysis cell (MEC) by 2008. Hydrogen production in MECs occurs at greater efficiencies than by fermentation, and with less electrical energy input (0.2-0.8 V) than required for traditional water electrolysis (1.8-3.5 V) (Lu and Ren, 2016).

MECs make use of exoelectrogens (electrochemically-active microorganisms) to oxidise organic matter, releasing electrons and protons (Ditzig *et al.,* 2007). These electrons are transferred in a circuit from anode to cathode (Figure 1.1). In wastewater, cations such as sodium (Na^+), potassium (K^+) and calcium (Ca^{2+}) are found at much higher concentrations than protons (H^+ ions). Therefore, although shown in many simplified schematics, cathodic protons are not replenished by protons generated at the anode (Logan *et al.,* 2008). Instead, a pH imbalance occurs across the membrane, creating alkaline conditions at the cathode, and acidic conditions at the anode. Under alkaline conditions, water is reduced to hydrogen and hydroxide at the cathode (Eq. 1.2). This reaction is endothermic and does not occur spontaneously. The electrons supplied by bacteria must be "topped up" from an external source to overcome the thermodynamic barrier (Lu and Ren, 2016).

Cathodic reaction under acidic conditions,	$2H^+ + 2e^- \rightarrow H_2$	(1.1)
Or under alkaline conditions,	$2H_2O + 2e^- \rightarrow H_2 + 2OH^-$	(1.2)
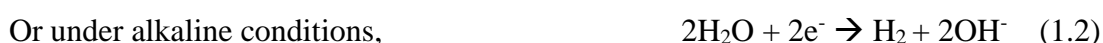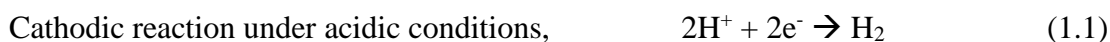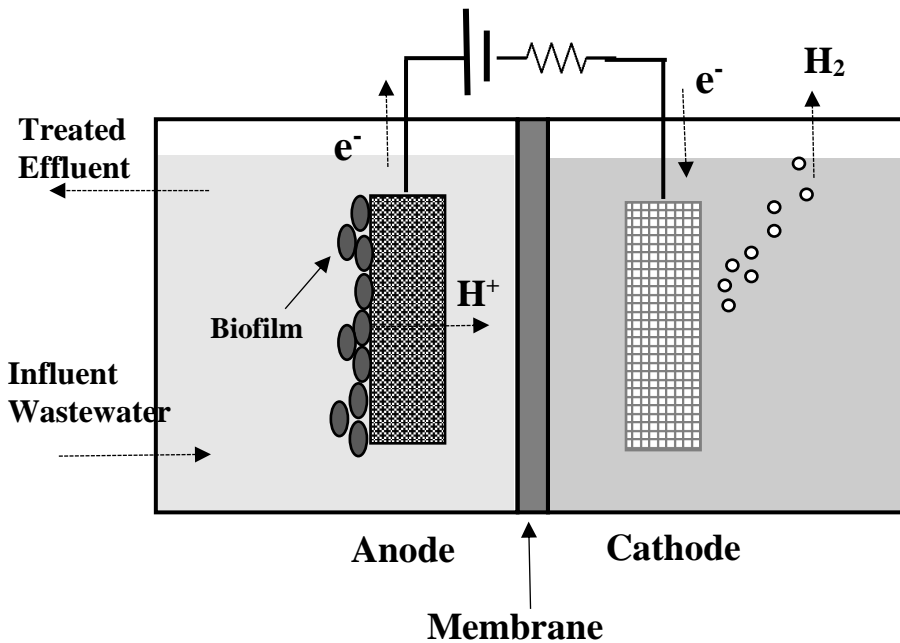
Figure 1.1 Schematic of MECs for hydrogen production. Electrons (e-) travel in a circuit from anode to cathode, supplemented by an external power supply. Ion transport across the membrane causes a pH imbalance. Under alkaline conditions at the cathode, water is reduced to hydrogen (H_2) and hydroxide (OH⁻) at the cathode

The key difference between MECs and MFCs is that both the anode and cathode chamber are anaerobic in the former, but only the anode is anaerobic in the latter. An entirely anaerobic configuration means that MECs can be more easily designed for retrofit, such as submersion in an activated sludge lane (European Commission, 2013). Providing oxygen at the cathode requires aeration of the electrolyte, or an air cathode, but both are undesirable. The aeration of a liquid is expensive and large air cathodes are problematic to engineer. The manufacturing of cathodes more than a few hundred cm^2 is difficult (Logan *et al.,* 2015). Alternatively, diffusion of oxygen into the cathode would require an additional compartment (often not reported in lab scale MFCs) (Yang, Feng and Logan, 2012).

The commercialisation of BES is likely to be facilitated by a modular design (Logan *et al.,* 2015). In this study, and the study that preceded it (Heidrich *et al.,* 2013, 2014), MECs have been designed as a series of cassette-style electrode assemblies, creating a modular design which, in theory, could be installed into existing wastewater tanks (if volumetric loading rates of MEC are similar to conventional processes).

MECs are promoted as a technology with the potential to improve the energy balance of wastewater treatment (Foley *et al.,* 2010; Escapa *et al*., 2016). The last decade has seen a 10%

4

increase in UK water sector energy use (Water UK, 2012) and industrial electricity prices have risen dramatically (78% increase) (DECC, 2016). Providing clean drinking water and treating waste accounts for 3-5% of the energy use of developed countries (EPA, 2016; Curtis, 2010). This has sparked a growing interest in the benefits of reducing energy use and carbon emissions by up to 80% by 2050 (Anglian Water, 2015; Northumbrian Water Ltd, 2009).

1.2 Rhetoric or reality?

The future of BES for low-energy treatment cannot be fairly assessed without testing the technology under realistic conditions. As few as 2 % of BES studies involve reactors larger than 1 litre (Zhang et al., 2013). Only 16 % of MECs evaluated by Escapa *et al.,* 2016 (using real wastes to produce hydrogen gas) involved reactors greater than or equal to 10 litres. There is little evidence of long-term performance of MECs. Most MECs operated more than a year are small, fed synthetic substrates and kept at a constant temperature (Liu *et al.,* 2008; Moon *et al.,* 2006; Zhang *et al.,* 2011 and Zhang *et al.,* 2012a).

The value of small-scale, controlled research is not questioned, but these studies do not inform us about the challenges of operating MEC at realistic scales in the real world. Real world conditions will depend on the site in question and will vary seasonally and diurnally. For example, the average annual US wastewater temperature ranges between 3-27 ℃ (Tchobanoglous *et al.,* 2004). By contrast, most laboratory studies use controlled conditions. Furthermore, there is a lack of consistency in reporting data. Critical variables such as energy efficiency, scale and temperature are often not collected, recorded or reported in publications (Fig. 1.2). Therefore, assessing performance and predicting potential of MEC is difficult.

Many technologies exist that can treat wastewater to a high standard, through the oxidation of dissolved and particulate solids, and the biological removal of nitrogen and phosphorous (Tchobanoglous *et al.,* 2004). There is, therefore, a need for MEC to provide additional benefits to encourage their commercial uptake. The benefit may be as simple as matching the level of treatment provided by conventional technology at a lower energy demand. Without adequate data on energy and treatment efficiency, MEC's prospects in the 'real world' cannot be justly compared or considered.
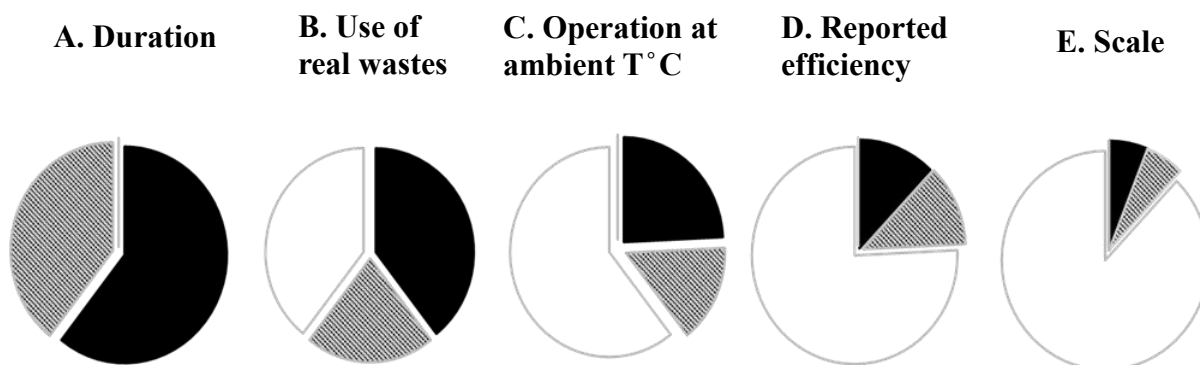
Figure 1.2 Review of 33 papers on MEC performance from 2005-2015 (Appendix A) (Cotterill et al., 2016). Papers were assessed for the following; duration of experiment (A), use of real wastewater (B), operation at 'ambient' temperatures (not fixed or controlled) (C), energy efficiency (D), large scale (E). Only 6% met all five criteria. Studies where the criteria were recorded are shown in solid black, those that did not are shown with black stripes. Studies that failed to meet prior criteria are shown in white.

COD is a core wastewater quality indicator. Effluent discharge in the UK must be below 125 mg/L of COD, per the Urban Wastewater Treatment Directive (91/271/EEC). Removal of COD is often used to reflect wastewater treatment efficiency in BES. When operated with a synthetic substrate, the treatment efficiency of MECs is comparable with conventional technologies [Table 1.1], removing 67 – 98 % of the influent COD (Fig. 1.3). When operated with real wastes, COD removal is far less predictable ranging from 19-100 % (Fig. 1.3) [Appendix A].

Total and electrical energy efficiencies of MECs are also under-reported [Appendix A]. Electrical energy efficiency describes the amount of electrical energy put into the reactor recovered as hydrogen (η_E). Total energy efficiency accounts for the energy recovered as hydrogen, from the electrical input and the energy stored in the wastewater combined (η_{E+S}) [Appendix B]. Worked examples of these calculations are provided in Appendix B. By either measure, MEC fed synthetic substrates tend to be more efficient than those fed real wastewaters (Fig. 1.4). However, total energy efficiency (η_{E+S}) assumes energy is equivalent to COD. This is a simplification: there is currently no empirical formula to calculate the energy content from COD (Heidrich *et al.,* 2011). A more accurate method involves the use of bomb calorimetry to determine the actual energy in the substrate [Appendix C] (Chapter 3).
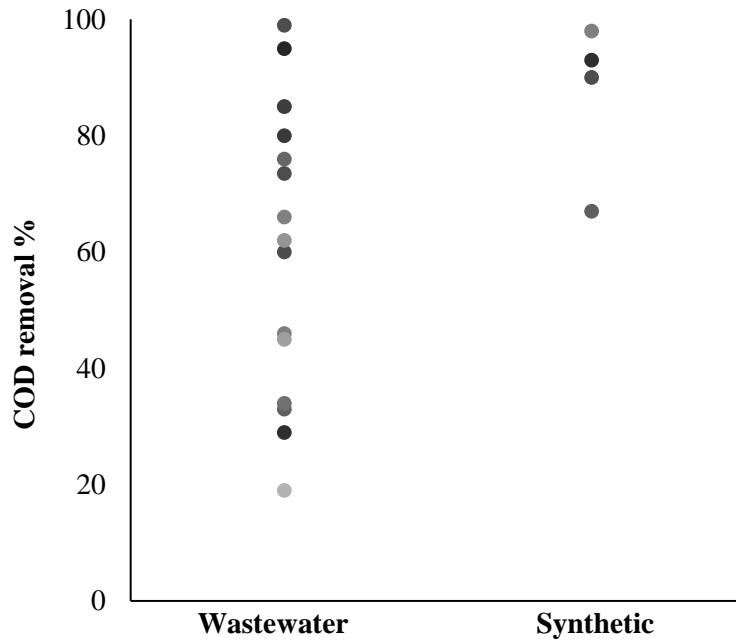
Figure 1.3. Comparison of COD removal in MEC fed real and synthetic wastewaters [Appendix A]. Where a range was reported in the table, the smallest value was taken throughout.
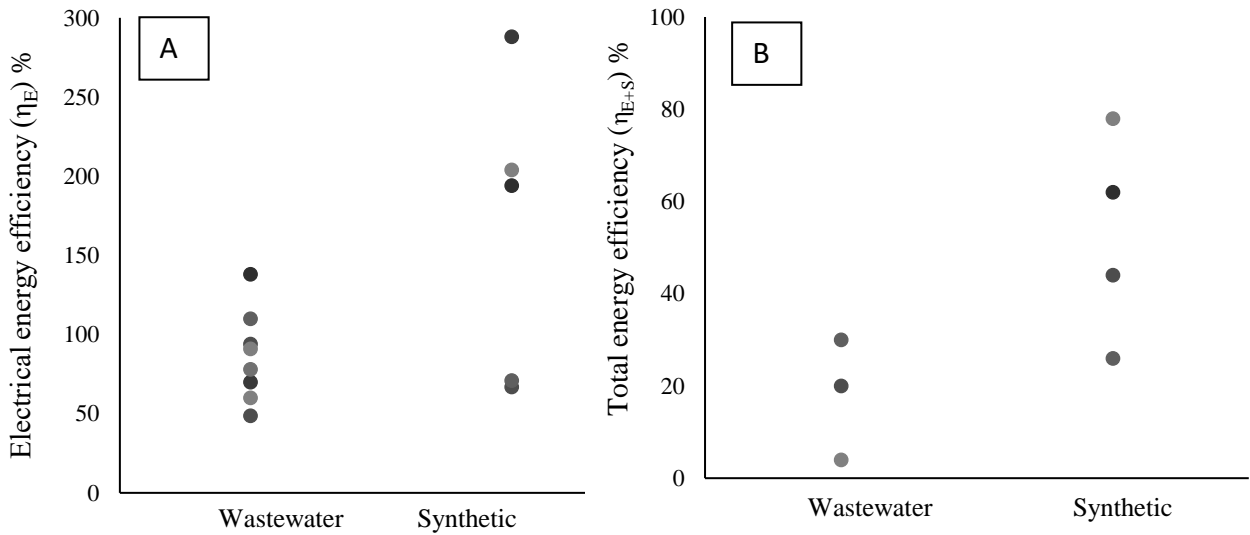
Figure 1.4 A) Electrical energy efficiency (η_E) and B) total energy efficiency (η_{E+S}) of MEC fed real and synthetic wastewaters [Appendix A]. Where a range was reported in the table, the smallest value was taken throughout.

Technology	COD Removal %
AS	<95
MBR	<95
TF	80-90
Reed bed	70
UASB	70

Table 1.1 Comparison of COD removal by secondary wastewater treatment technologies; Activated Sludge (AS), Membrane bioreactor (MBR), Trickling Filter (TF), Reed bed and Upflow Anaerobic Sludge Blanket reactor (UASB) (Tchobanoglous et al., 2004). Some values are temperature sensitive.

The use of real wastewaters, affordable materials and real-world conditions at large scale is riskier than carrying out small, controlled experiments. Pilot studies take longer to set up and usually cost more than laboratory scale studies. Additionally, those operated with real wastewaters exhibit a poorer performance (Fig. 1.3-1.4). Yet the biggest risk is in the likelihood of failure. The importance of failure in technological development is well established (Thomke and Reinertsen, 2012) and cannot be avoided. Evidence of failure in pilot scale research is demonstrated in chapter 2. Fault tree analysis (FTA), a top-down hazard-analysis tool, uses Boolean logic to identify process changes, human error and system component failures. FTA is explored in Chapter 2 to systematically understand the MEC's failure, identifying improvements to move towards a more robust MEC prototype.

1.3 Challenges

MEC commercialisation depends on several challenges being overcome, many related to cost (Chapter 6). MECs are structurally more complicated than a conventional wastewater tank, therefore investment costs are likely to be higher. Challenges relating to materials, electrochemical losses and long term durability may hinder the uptake of MEC, if solutions are not found.

The high cost associated with ion-exchange membranes and platinum catalysts used in laboratory MEC prohibits their use at large scale. The use of stainless steel cathodes has been described as 'promising' (Logan, 2010). Some brush configurations, including stainless steel, are comparable to high performing platinum cathodes, at a fraction of the cost (Logan, 2010). Most studies have moved away from costly Nafion proton exchange membranes (PEM)

(Rozendal *et al.,* 2008). Some have removed the membrane altogether, operating as a membraneless system (Escapa *et al.,* 2015). Creating a physical barrier between the anode and cathode in MECs often results in a higher level of hydrogen purity obtained (Clauwaert and Verstraete, 2008). However, membranes are rarely 100 % selective, leading to some mixing of anolyte and catholyte. The material costs of MEC from this study, and their effect on the capital cost of the technology, are outlined in chapter 6.

In MECs designed to produce hydrogen, loss of product probably presents the greatest problem. Before considering problems associated with hydrogen storage, hydrogen must be produced and captured in sufficient quantities from the MEC. The risk of hydrogen scavenging by H_2-oxidizing and homoacetogenic bacteria is discussed in chapter 3. Furthermore, the bottlenecks to scale-up are also assessed in chapter 3, to determine whether they relate to the engineering of the system or the biology underpinning it.

The design life of a water or sewerage asset is often more than 25 years (Institution of Civil Engineers 2010; Drainage Services Department 2013). The predicted lifespan of MEC electrodes and membranes is 5 years (Rozendal *et al.,* 2008a). The most realistic pilot study prior to this research (Heidrich *et al*., 2013, 2014), was 0.1 m^3 and in operation for just 1 year. A scale and timeframe too small and too short a duration to test industrial feasibility. Therefore, larger scale, long term studies of BES are required.

1.4 Beyond Hydrogen

Hydrogen as a product is more valuable than the production of methane from other anaerobic technologies, or electricity from MFCs (Foley *et al*., 2010). Yet, the ability to reduce protons (and potentially carbon dioxide) at the cathode, provides opportunities to generate products with more value, and a direct end-use in the water industry.

When the electrodes in MECs are separated by a membrane, a pH gradient is formed creating alkaline conditions at the cathode. These conditions can be exploited to produce caustic soda (NaOH) or hydrogen peroxide (H_2O_2): products with values an order of magnitude higher than electricity produced from MFCs (Rabaey *et al.,* 2010; Logan and Rabaey, 2012).

Microbial electrosynthesis (MES) is the catalysis of biofuels and biochemicals from reduced carbon dioxide in a BES (Sharma *et al.,* 2014). This process provides the combined benefit of

using waste carbon to generate sustainable chemicals such as acetate, methanol, and 1,3-propandiol (Sharma *et al.,* 2014; Gildemyn *et al.,* 2015).

Exploiting these options may help to create opportunities to recover value at small treatment plants where, at present, generating hydrogen or methane would not be economic. High value products could be allowed to accumulate, perhaps over months at small or remote treatment plants, and then harvested periodically.

In chapter 6, some of the potential products from MECs are explored through cost-benefit analysis (CBA), and their environmental and economic impact on the UK water industry is evaluated. Sensitivity analysis is carried out on: i) material costs of the MEC ii) market value of the products and iii) MEC performance. The CBA feeds into a multi criteria analysis (MCA) tool to propose site-specific solutions for value recovery from MECs.

1.5 Towards a usable technology

Deploying working MECs will not be simple. As noted above, wastewater treatment plants have extremely long design lives (Institution of Civil Engineers 2010; Drainage Services Department 2013). Therefore, the most financially efficient approach might be to replace traditional assets when they reach the end of their design lives.

Alternatively, the technology may be deployed as a package plant, functioning as a pre-treatment for the existing infrastructure. In chapter 3, consideration is given as to where best to install MECs in the treatment chain, based on wastewater constituents and desired outcomes of the technology. The commercial prospects of MECs are discussed in chapter 6, with an evaluation of net present value (NPV) under differing scenarios.

In the concluding chapter (7), the steps necessary to move towards a usable technology are explored, including opportunities for future research. An assessment of technology readiness level (TRL) is made, and the outlook for further scale-up on reactor configuration is discussed.

1.6 Aims and objectives

1.6.1 Aims

The STREAM Industrial Doctoral Centre stipulates that 75 % of a researcher's time is spent within their sponsoring organisation. This affects the direction of the project and opportunities

for practical delivery, such as the installation of pilot trials on wastewater treatment plants. This industrially-funded project sought to develop the prototype designed by Heidrich *et al.,* (2013, 2014), which demonstrated that MECs can work with real wastewaters at realistic temperatures. The aims of this research were to achieve a larger scale, improved performance and greater understanding of the technology. To achieve this, four objectives and nine research questions were established.

1.6.2 Objectives

Objective 1:

Develop a series of pilot scale MECs to trial on a domestic wastewater treatment plant

Research and development processes often require an element of trial and error, through problem-solving practices such as computer simulations, laboratory experiments and pilot scale prototypes (Pisano, 1996). 'Learning-by-doing' is a term used to describe this process in manufacturing (Arrow,1962; Von Hippel and Tyre 1995). Heidrich's 'proof of concept' (Heidrich *et al.,* 2013, 2014) provided a benchmark for MEC design. The first objective involved 'learning-by-doing': building a pilot scale prototype to understand factors underlying performance.

Research questions:

1a. What influences or inhibits the performance of MECs? **(Chapter 2)**

1b. How robust are MECs? How will MECs respond to scaling, fouling, temperature fluctuations and a variable influent load? **(Chapter 2)**

1c. Does scale affect the performance of MECs? **(Chapter 4)**

Objective 2:

Assess the impact of external variables on the performance of the technology

Trialling a technology in the real world (i.e. on a wastewater treatment plant) limits the ability to control environmental variables: organic load, rate of flow, and wastewater composition are likely to fluctuate. Understanding how these factors influence the performance of the technology formed the second objective.

Pilot scale MECs were trialled at two different stages in the treatment process: primary, after screening and grit removal **(Chapter 2)**; and secondary, after primary settlement **(Chapter 4).** Upstream processes, in the treatment works (e.g. chemical dosing), the sewer network and the

catchment (e.g. source of the wastewater: domestic, agricultural, industrial), could influence wastewater composition and consequently, the performance of the MECs **(Chapter 3).**

This gave rise to the following research questions:

2a. What is the goal of MECs: low-energy treatment or energy-recovery? **(Chapter 3)**

2b. Is the technology widely applicable? **(Chapter 3)**

Objective 3: Characterise the anodic microbiological community in a pilot scale MEC

Bioelectrochemical systems are driven by microbial processes. Therefore, an understanding of community ecology and assembly may help to explain MEC performance. Identifying where community variation occurs, through 16S DNA sequencing, may support observations between community, function and performance.

Research questions:

3a. Does 16S DNA community influence MEC performance? **(Chapter 5)**

3b. Does the assembly and structure of the biofilm affect performance? **(Chapter 5)**

Objective 4: Identify how to recover the most value from the technology

The sponsoring organisation's interest was to decide if the technology is viable, practically and economically. Identifying economic and environmental value may help to offset investment costs. A cost-benefit and sensitivity analysis, consider the net present value (NPV) of MEC. A multi criteria analysis tool is used to support decisions on product and value recovery.

Research Questions:

4a. How and where can value be recovered in MECs? **(Chapter 6)**

4b. Are MECs economically viable? **(Chapter 6)**

Chapter 2. An examination of failure in a pilot scale microbial electrolysis cell

2.1 Introduction

An Environment Agency report on "transforming wastewater treatment to reduce carbon emissions" discussed redeveloping existing processes and switching to anaerobic technologies (EA, 2009). It suggested research was necessary "to understand how a significant process change will affect existing systems" (EA, 2009). Additionally, it stressed the importance of considering "the applicability across many works" (EA, 2009). This thinking helped to shape the objectives. The primary objective was to build and operate a pilot-scale MEC reactor. Heidrich's 'proof of concept' (Heidrich *et al,* 2013) was used as a benchmark for the design. The configuration was replicated, but with increased opportunities for monitoring. It was hoped this would provide a better understanding of the factors underpinning performance.

The MEC design was slightly modified. The number of modules was increased from six (in Heidrich *et al.,* 2013) to ten, creating a larger electrode surface area relative to the tank volume, which remained consistent. It was hoped a trend may be observed between the number of modules and the COD removed. This trend could, in theory, be used to rationally design future MECs for improved COD removal.

Fishburn sewage treatment works (STW) in County Durham was selected for this study. It was chosen due to its small population equivalent (with low and variable flows), lack of trade-waste, ease of access to power supply, and amount of space available to construct a pilot plant. It provided a stark contrast to the site chosen by Heidrich, which treated "an average of 246,500 m^3 of domestic wastewater" daily (Heidrich *et al.,* 2013). Fishburn STW, serves a small village of 2,500 people and is directly next to a farm. The wastewater was expected to be domestic and agricultural.

2.2. Methods

2.2.1 MEC design

Heidrich's 'proof of concept' for scaling up MECs for wastewater treatment highlighted design issues, relating to the engineering and hydrodynamics, which were potentially inhibiting performance (Heidrich *et al.,* 2013). Modifications were made with the aim of improving treatment capacity, energy recovery and opportunities for monitoring.

The result was a 135 L PVC tank (dimensions 1.36m x 0.26m x 0.38m) containing ten separate MEC modules that functioned individually. The modules were submerged in wastewater and placed on alternate sides of the reactor. They were secured in PVC tracks to provide structural stability, enable removal for maintenance, or in the case of failure. Sampling ports were located on the side of the tank between each MEC module (Fig. 2.3) to allow for collection of anolyte at set intervals through the tank.

An applied voltage of 1.0 V was supplied to the ten modules via two multichannel variable DC power supplies (PSM 2/2A, Caltek Instruments, Hong Kong) during start-up, which was increased to 1.2 V after 30 days of operation. Cell voltage was measured across a 0.1 Ω fixed resistor (Farnell, UK) using a 4-differential input (ADC-20) and an 8-differential input (ADC-24) data logger (Pico Technology, UK).

Each module was constructed from 10 mm PVC sheet with a volume of 2.6 L. The modules included two carbon felt anodes (Olmec Advanced materials ltd, UK), one on each side of the module. The total anode surface area to liquid volume ratio was 12 m^2/m^3. The carbon felt was sandwiched between two sheets of stainless steel mesh. These sheets were secured with bolts to act as a current collector.

The cathode was housed in a sealed chamber between the two anodes. The cathode was composed of 20 grams of stainless steel wool (Merlin Ltd, UK), pressed under a 500-tonne weight. This reduced the cathode thickness, which enabled a smaller electrode spacing, and a thinner module design. The electrodes were separated by a low cost microporous battery separator of ultra-high molecular weight polyethylene (UHMWPE) called Rhinohide (Entek Ltd, UK). Cathodic gas was captured into ten Tedlar™ 1L gas bags (Sigma Aldrich, UK), connected to each module using 3 mm ID Tygon F-4040 tubing (VWR International, UK).

Phosphate-buffered saline (PBS) solution is frequently used at concentrations of 50 mM to control pH in the cathode chamber (Kyazze *et al.,* 2010 and Qu *et al.,* 2012). A buffered catholyte, theoretically, prevents overpotential increases of -59 mV per pH unit (Zhuang *et al.,* 2010). However, phosphate-based salts are unsuitable, economically and environmentally, for use in large-scale wastewater treatment (Pant *et al.,* 2011). The catholyte was changed from pH 7 PBS (Heidrich *et al.,* 2013) to 0.1M NaCl. The increased conductivity of the latter should give rise to a higher rate of hydrogen production (Nam and Logan, 2012).

Additionally, NaCl is a more affordable chemical than PBS and provides less challenges for removal, if it leaches into the anodic wastewater.

2.2.2 Operating Conditions

Three Watson Marlow 520s peristaltic pumps were used to circulate raw domestic wastewater from the head of the works through the pilot system (Watson Marlow, UK). After problems with clogging, a pilot scale clarifier was installed prior to the MEC. Wastewater was fed from the clarifier at 75 mL/min. This resulted in a hydraulic retention time (HRT) of 1 day in the MEC. Wastewater left the MEC under gravity. It was then pumped from the storage tank into the STW and returned to the existing process chain (Fig. 2.1).
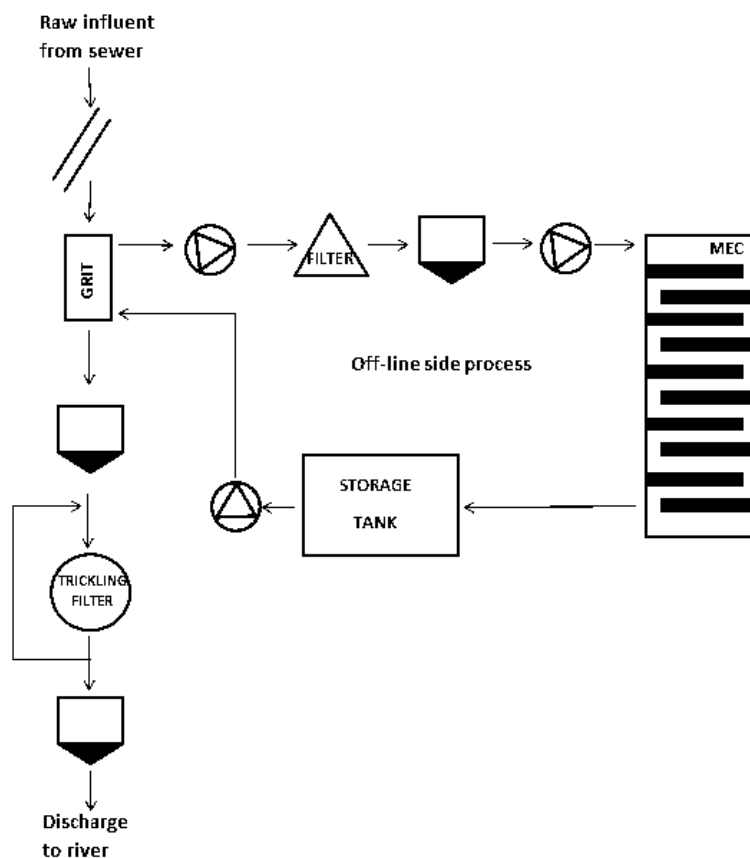
Figure 2.1 Schematic of Fishburn STW with pilot MEC side stream process. The vertical process (right hand side) shows the regular treatment line; screens, grit removal, primary settlement, trickling filters, final settlement and discharge to the river. The side process loop shows the experimental set-up; pyramid filter, primary settlement, microbial electrolysis cell, and effluent storage tank.

The aperture of a course screen in preliminary treatment is usually between 6 and 150 mm (Tchobanoglous *et al.,* 2004). At Fishburn, the coarse screen had 24 mm apertures. This is sufficient to remove bulky items that may block pipes, cause damage to fixtures, or wrap

around monitoring equipment. The pilot MEC had 12 mm diameter tubing. As such, there was a risk of clogging from items passing through the site's course screen. Therefore, a pyramid filter (Fig. 2.2) was installed in the open channel. The filter was designed with the help of Ray Armstrong at Northumbrian Water Ltd. The design was modified from baskets used to trap bulky solids on combined sewer overflows (CSOs). The stainless steel mesh was punctuated with 6 mm apertures and bolted to the channel.

Figure 2.2 Photograph of stainless steel pyramid filter installed in the open channel at Fishburn STW. The filter, which had 6 mm apertures, was designed to prevent clogging in the pilot scale MEC.

2.2.3 Installation of electrical connections and monitoring equipment

Wires from MEC modules were hardwired into a weatherproof box, connecting the anode and cathode to the power supply and data logging equipment. Data loggers were used to continuously record the current produced by each module. Each box was labelled with the module, data logger and channels the wires corresponded to (Fig. 2.3). Wires and electrical equipment (peristaltic pumps, variable DC power supplies and data logging equipment) were earthed. All external cables running from the building to the pilot installation had mechanical and environmental protection (armoured cable or PVC coated steel conduit). Power supplies and data logging equipment were stored in IP65 rated weatherproof boxes. The number indicates the level of ingress protection (IP) the box provides against solid particles (first digit, rated from 0 to 6) and liquid particles (second digit, rated from 0-8) (IEC/EN 60529).

Figure 2.3. Photograph of MEC wiring and IP65 rated weatherproof boxes at Fishburn. Boxes were labelled with the corresponding module, data logger and channel for ease of identification. Liquid sampling ports can be seen protruding the tank (green and blue taps).

2.2.4 Analytical Methods

Chemical and microbiological data were collected throughout operation. A 50 mL sample was taken from each sampling port. This sample was used for analysis of total (tCOD) and soluble chemical oxygen demand (sCOD). The samples were measured using colorimetric COD test kits (25-1500 mg COD/L, Merck & Co. Inc., USA) on a Spectroquant Pharo 300 in line with manufacturer's instructions (Merck & Co. Inc., USA).

Hydrogen gas measurements were initially taken on site with a Hy-Alerta hydrogen probe. This showed >85 % hydrogen purity. After this, gas bags were periodically taken for analysis on a GC-TCD using argon as a carrier gas (Thermo Scientific, USA). A five-point calibration was carried out prior to each set of samples with a 99.999 % hydrogen standard (Calgaz, USA).

Conductivity, pH, temperature and dissolved oxygen (DO) spot samples were taken twice weekly. These samples were analysed using a Hach HQ40D multi portable meter with a PHC10105 pH gel probe, LDO10105 DO probe and CDC40105 conductivity probe (Hach Lange, UK). Continuous temperature readings were taken with a K-type thermocouple (RS Components, UK) connected to an EL041 thermocouple converter and an EL005 data logger (Pico Technology, UK). Values were recorded onto a computer every 30 minutes. Cell voltage was measured every 30 minutes across a fixed resistor.

Calculations were carried out to determine the efficiency of the reactor [Appendix B]. Cathodic coulombic efficiency (CCE) [Appendix B, Eq. 12-14] is calculated as the amount of hydrogen gas captured relative to the theoretical value derived from the current, noted as (N_{CE}). The latter is calculated as the sum of the current, multiplied by the time interval, divided by two times Faraday's constant. This value should not exceed 100%. The applied voltage supplied sets the upper limit of electrical efficiency. The theoretical maximum energy efficiency (based on Gibbs free energy or heat of combustion) decreases with increasing applied voltage, such that the maximum recovery would be 246 % at of 0.5 V, or 154 % at 0.8 V (Logan *et al.,* 2008) [Appendix B, Eq. 4-8]. However, as the energy is generated as hydrogen, it would need to be converted in to electricity to supply power. The typical efficiency for conversion of hydrogen in a PEM fuel cell is 50-60 % (DOE, 2017).

In December 2014, 160 days into operation, the MEC was disassembled. Samples of the anolyte were taken from each sampling port; gas bags were removed and catholyte was removed from modules with a syringe. Liquid samples were frozen for later analysis. Fouling on the membrane was analysed by inductively coupled plasma mass spectrometry (ICP), x-ray diffraction (XRD) and scanning electron microscopy (SEM). Solid was scraped from the membrane using a laboratory spatula. This created a powdered solid which was stored in a glass vial for XRD analysis. Partial digests of 0.2 g of the white powdered solid (found on the membranes) was dissolved in nitric acid and filtered through a 0.45-micron filter for ICP analysis.

All statistical tests were carried out using IBM SPSS statistics 23 (IBM Corp. NY, USA)

2.2.5 Molecular and microbiological methods

A small core boring device (Sigma Aldrich, UK) was used to take a 9.5 mm diameter sample from the top corner of each anode. This method was chosen, because the biofilm appeared to grow around individual carbon fibres, rather than as a flat layer (Section 5.3.3). Once bored, the sample was placed immediately into sterile filtered PBS and ethanol and frozen on site. Samples were taken from each module at five time periods during start-up, operation and failure. Samples were taken from similar locations to enable a direct comparison.

DNA extraction of the anode samples was carried out using BIO 101 FastDNA Spin Kit for soil (MP Biomedical, USA) per manufacturer's instructions. The bored sample was added to a lysing matrix tube and the weight of each sample was recorded. Each tube contained 0.205 g ± 0.117 g of anode. The manufacturer's instructions were followed for cell lysis, DNA

isolation and purification. Then, the sample was eluted into 50 μl of DES (DNase/Pyrogen-Free Water) prior to amplification using polymerase chain reaction (PCR).

Bacterial and archaeal 16S DNA genes were amplified by PCR using a PCR Hot Master Mix (5 Prime, Germany). The samples were labelled with a Golay barcode, a 515F forward oligonucleotide primer (Thermohybaid, Germany), and an 806 reverse primer. Following amplification, all PCR products were checked for size on a 2.5 % w/v agarose gel. Clean- up of the PCR products followed, using MinElute 96 UF Purification kit (Qiagen). After this, each PCR amplicon was quantified using Invitrogen Quant-IT dsDNA Assay Kit (Invitrogen), which uses Picogreen as the fluorescent nucleic acid stain. Once the amplicon had been quantified, it's possible to calculate the volume of each sample required to produce an equimolar bulked sample pool. The pooled sample was then cleaned using the AMPureXP protocol, and an agarose gel was run to ensure any existing primer-dimer was removed. The pooled sample library was then sent to the University of Liverpool on dry ice, where paired-end sequencing (2 x 250bp) was run on the Illumina MiSeq platform. The resulting FASTQ files were run through Newcastle University's School of Civil Engineering and Geoscience's bioinformatics pipeline to generate QIIME outputs.

A phylogenetic tree was built using defaults (Price *et al.,* 2010). A 'core diversity' QIIME script was run, which included OTU picking and chimera detection. This script served to establish the number of taxa detected, and the differences between samples. Taxonomy was assigned using RDP (Wang *et al.,* 2007) and Greengenes 13_8 (McDonald *et al.,* 2012, Werner *et al.,* 2012). The mean abundance of known exoelectrogens (e.g. *Shewanella, Geobacter* etc.) was compared between various sample groupings. These groupings included separating the samples by i) time of sample taken, ii) location in the tank and iii) performance of module the sample was taken from.

2.2.6 Fault tree analysis

Pilot scale research often fails to perform at levels observed in a laboratory (Fig.1.3-1.4). Fault tree analysis is a top-down hazard-analysis tool to identify process changes, human error and system component failures. It is used in this chapter to understand why modules may have failed. It is hoped FTA can be used to identify improvements to move towards a more robust MEC prototype.

The concept of fault tree analysis (FTA) was first conceived in 1961 by Watson of Bell Telephone Laboratories. Two years later, it was recognised as a 'significant safety tool' by Haasl of Boeing. By 1965 there was worldwide interest (Ericson, 1999). FTA is predominantly used in safety and reliability engineering to understand how systems fail and how to reduce risk.

Biological systems, however, do not always behave in the expected manner and therefore the application of FTA is rare (Hayes, 2002). Despite this, the use of FTA was chosen to increase understanding of the individual components of MECs, enabling a complex system to be deconstructed. However, if the complex system is not fully understood, solutions proposed from the FTA may be sub-optimal, and the FTA may require recalibration and amendments later. One of the major benefits of undertaking FTA, is its ability to substantiate understanding and identify areas of knowledge uncertainty: a welcome side effect in research.

After a process has been described in detail, FTA can be conducted to assess the root cause(s) of failure in a process. It is a top-down hazard-analysis tool, in which all possible scenarios that lead to top events are considered. It is a graphical model (Table 2.1) - arranged with branches - using Boolean logic (OR and AND functions) to identify all combinations of events that may have caused the specified failure. External events, such as floods or earthquakes, may influence the likelihood of failure, but are usually excluded.
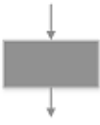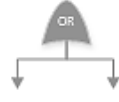
Symbol	Meaning	Description
	TOP EVENT	The primary event of interest i.e. the failure
	INTERMEDIATE EVENT	Caused by events described below
	UNDEVELOPED EVENT	Not developed further because information beyond this point is not useful or relevant to the fault tree or because data are unavailable
	TRANSFER GATE	Transfer to another branch of the fault tree
	BASIC INITIATING EVENT	Does not need to be developed further
	OR GATE	Logic gate where output occurs if any of the input occurs
	AND GATE	Logic gate where output occurs only if all of the inputs occur

Table 2.1. Description of the symbols used in the fault trees illustrated in this chapter.

2.3 Operational Results

2.3.1 Wastewater treatment

COD removal, representing wastewater treatment was poor. Prior to decommissioning in December 2014, tCOD removal by the MEC process was 34.3 %. This was marginally lower than sCOD removal, at 43.6 %. COD removal did not appreciably decrease over time: the operational average tCOD removal was 31.9 % (Fig. 2.5).

A Pearson's correlation was run to determine the relationship between anode surface area and tCOD removal. There was a strong, positive correlation between the surface area and the amount of COD removed (Fig. 2.4), which was statistically significant (r^2=0.816, n=10, p=0.000). To achieve an effluent COD <125 mg/L (assuming a linear relationship), 22 modules would be required, increasing total surface area from 1.2 m^2 to 2.6 m^2. In a 135L tank, this would provide a surface area to volume ratio of 20 m^2/m^3. It is not known whether the relationship will continue to be linear as COD concentration decreases further.
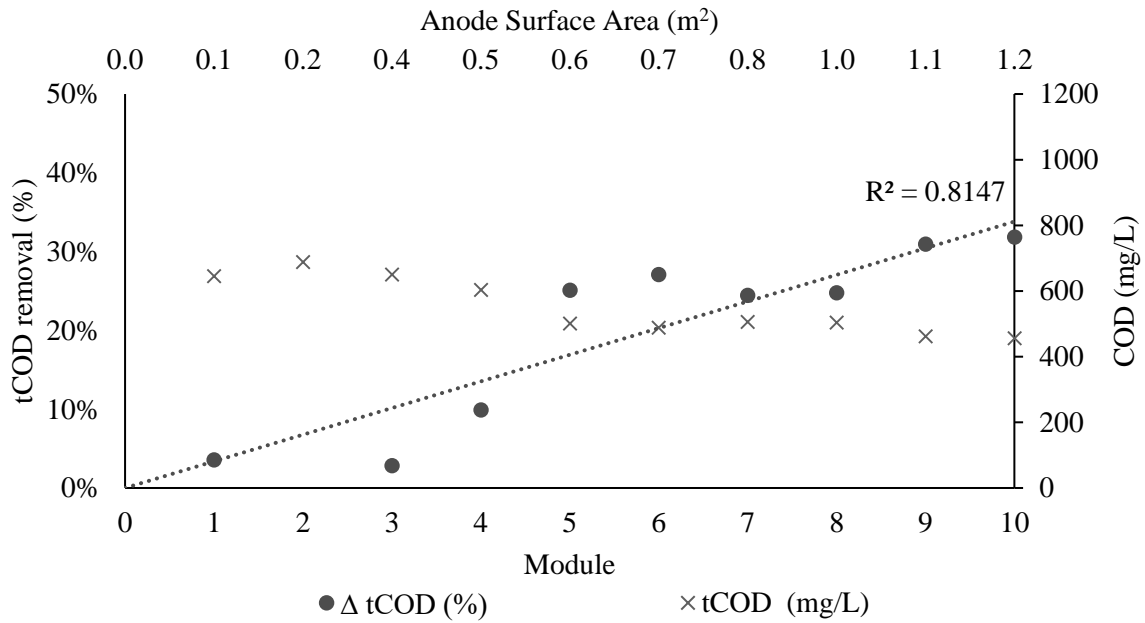
Figure 2.4. Mean cumulative tCOD removal relative to the anode surface area of the modules in pilot 1. Each black dot represents the mean tCOD removal of each module. Grey crosses represent the average COD concentration. Measurements were taken between each of the ten modules during 6 months of operation.

COD removal fluctuated tremendously, due to a variable influent and a long HRT. Influent COD varied daily during operation (Fig. 2.5), in line with data collected by Northumbrian Water at Fishburn STW between 2008 and 2013. Northumbrian Water reported a mean influent of 670 mg/L ranging between 170 -1500 mg/L, during this 5-year period. The variability of the influent (and lack of composite sampling) occasionally resulted in an increase in COD through the MEC and negative removal. There was no correlation with the percentage of tCOD removal over time, implying this did not improve (or become worse) during MEC operation. The volumetric loading rate was 0.21 kgCOD/m^3/day. This is at the lower end of the range for activated sludge (AS), 0.2-2 kgCOD/m^3/day (Grady *et al.,* 1999). This implies that MEC could, in theory, have a similar footprint to AS, supporting a future retrofit application.
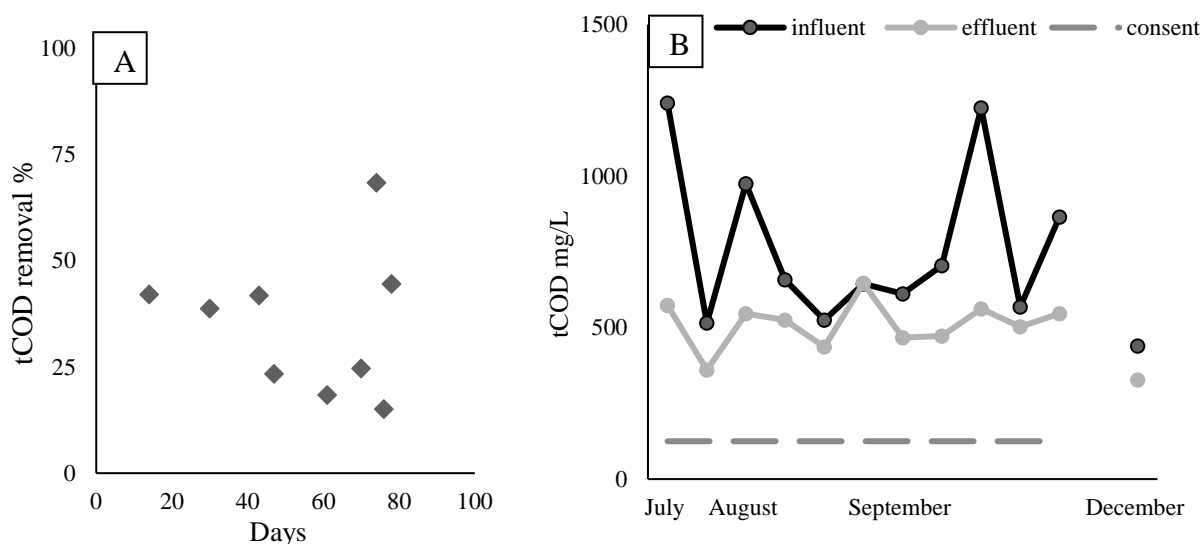
Figure 2.5. Effluent tCOD concentration and tCOD removal in Fishburn MEC. A) Mean percentage tCOD removal between July and October. B) Influent (solid black) and effluent (solid grey) concentration. MEC effluent did not meet EU consent of 125 mg/L (dashed grey).

Similarly, volatile fatty acid (VFA) concentration varied considerably. During start-up, acetic acid varied between 50-400 mg/L; a value consistent with the influent COD concentration (500-700 mg/L). When two modules failed (modules 1 and 3), VFA concentration was considerably higher (acetic 1400-2100 mg/L; isobutyric 200-600 mg/L and propionic 200-500 mg/L) than the influent COD (600-1000 mg/L). Acetic acid was, on average, 2.2 times larger than tCOD.

	Fluoride (mg/L)	Chloride (mg/L)	Bromide (mg/L)	Nitrite (mg/L)	Nitrate (mg/L)	Phosphate (mg/L)	Sulphate (mg/L)
August (Working)	4.8 ± 0.7	76 ± 3	0.2 ± 0.2	9.8 ± 6.5	0.01 ± 0.03	23.7 ± 1.4	92 ± 22
September (Failure)	3.8 ± 0.4	73 ± 5	0.04 ± 0.05	0.56 ± 0.54	0.4 ± 0.1	20.8 ± 1.5	72 ± 13

Table 2.2 Average anions concentration in August (gas production) and September (when several modules failed). All anions are measured as milligrams per litre (mg/L).

Concentrations of fluoride, chloride, bromide and phosphate were not significantly different between the gas production phase and failure (Table 2.2). However, a paired t-test showed significantly more sulphate in the MEC's wastewater during the gas production phase (92 mg/L ± 22) than at the point of failure (72 mg/L ± 13) (n = 20, p= 0.04). Furthermore, there was significantly more nitrite (9.8 mg/L ± 6.5) in August, than September (0.56 mg/L ± 0.54)

(p=0.001). Nitrate concentration was significantly higher in September (0.4 mg/L $\pm$ 0.14) than August (0.01 mg/L $\pm$ 0.03) (p = 0.000). On average, there was 22 mg/L sulphate removed per day, using 14.4 mg/L of COD. Based on an average COD removal of 210 mg/L/d, sulphate removal accounted for 7% of the total COD removal.

2.3.2 Hydrogen production

The MEC began to produce hydrogen gas after 44 days. Gas was first observed in module 6, followed by modules 1, 2, and 8 a few days later (Table 2.3). Hy-Alerta probe measurements were supported by analysis on GC –TCD. Gas purity showed an increasing trend during the first 14 days of gas production. Gas purity stabilised at 98.4% $\pm$ 2.5% for the remaining gas-producing phase of operation.

Module	Started after (days)	$N^{o.}$ of days of gas production
1	47	24
2	47	10
3	51	20
4	n/a	0
5	n/a	0
6	44	115
7	n/a	0
8	47	7
9	n/a	0
10	48	110

Table 2.3. Time taken to start-up, and the number of days of gas production, in the six modules that produced hydrogen gas.

Gas production was promising initially. Between day 44 and day 69, the MEC produced more than 28 L of hydrogen gas; equivalent to more than a litre a day. The initial volumetric rate (0.005 L-H_2/L/d) was higher than that of Heidrich's 'proof of concept' (<0.001 L-H_2/L/d, Heidrich *et al*., 2013, 2014) in days 0 to 5 (Fig. 2.6). Moreover, the rate of hydrogen production increased more rapidly over 20 days (Fig. 2.6). By day 25, the volumetric rate was 0.016 L-H_2/L/d, double that of the previous MEC (0.008 L-H_2/L/d, Heidrich *et al.,* 2013, 2014).
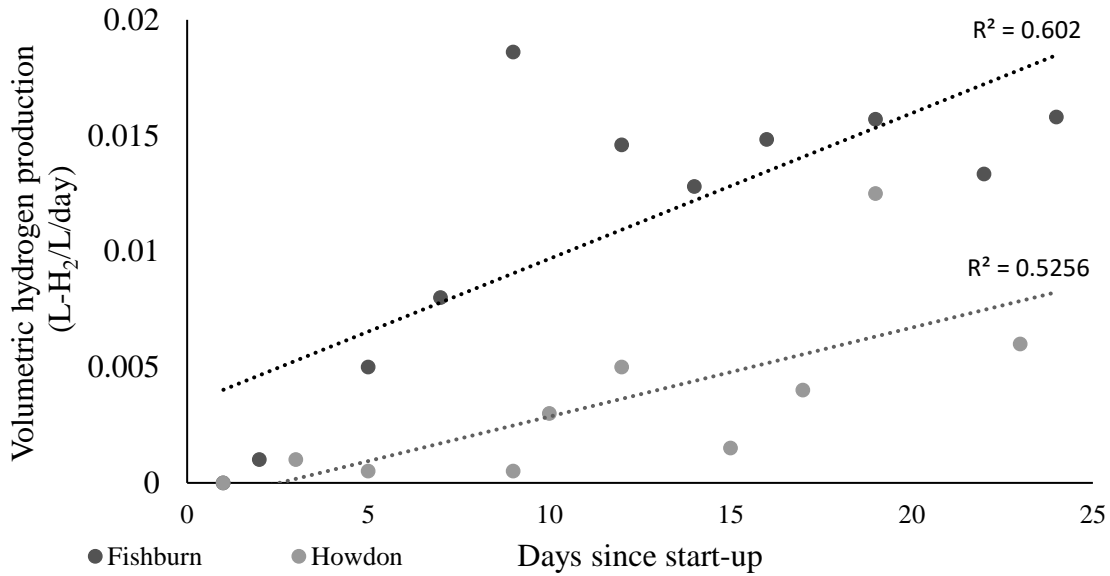
Figure 2.6. Volumetric hydrogen production (L-H₂/L/d) in the first 25 days after start-up in the Howdon (Heidrich et al., 2013; 2014) (grey line) and Fishburn pilot MECs (black line).

However, this did not continue. Some modules failed within a week, others within a month. Some modules never produced hydrogen gas. By day 72, (28 days after gas was first observed) there were only two modules still producing hydrogen (Fig. 2.7). These two modules produced gas until the end of operation.
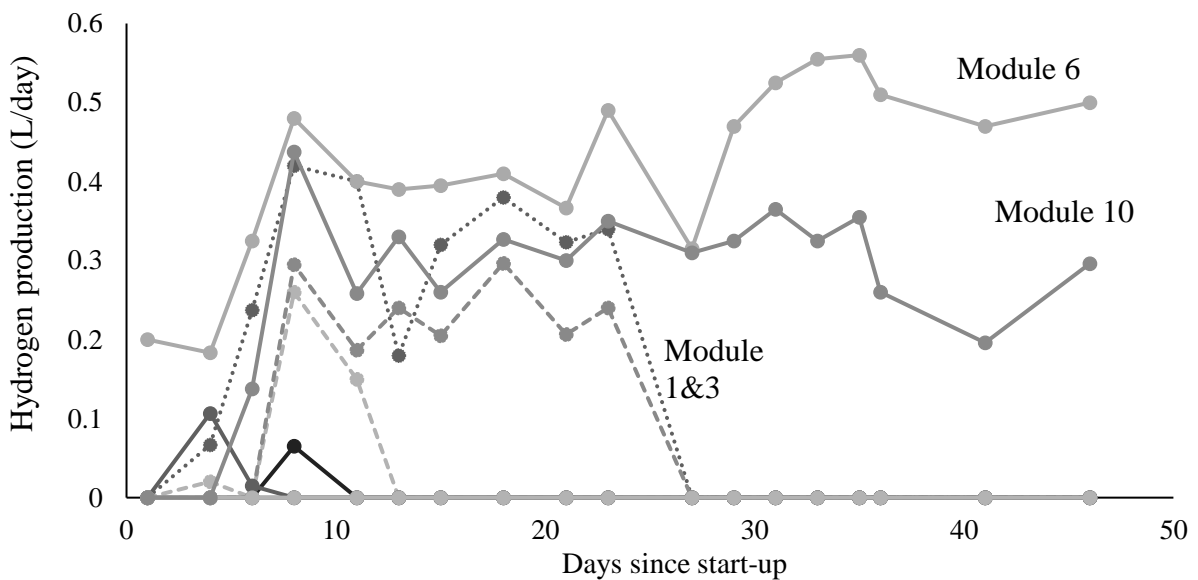
Figure 2.7. Litres of hydrogen gas produced per module per day (during day 45-95). This represents a period of operation (50 days) in which a steady-state voltage was achieved, directly following the start-up period.

2.3.3 Cathodic coulombic efficiency

Cathodic coulombic efficiency (CCE) was determined for the working cells (i.e. those that produced hydrogen during operation) (Table 2.4). This was to assess how much of the current

generated was being recovered as hydrogen. A low percentage indicates hydrogen loss. High values may, at times, be indicative of hydrogen cycling across the membrane (Call *et al.,* 2009).

CCE is expressed as a percentage and should not exceed 100 % (Appendix B). A Pearson's correlation was run to determine the relationship between CCE and number of days of hydrogen gas production across all ten modules. There was a positive correlation between CCE and number of days of hydrogen gas production, which was statistically significant ($r^2 = 0.484$, n = 10, p = 0.025).

Module	N^o. of days of H$_2$ production	Cathodic Coulombic Efficiency (CCE) / %
1	27	76
2	11	42
3	23	77
4	0	n/a
5	0	n/a
6	115	93
7	0	n/a
8	7	68
9	0	n/a
10	110	74

Table 2.4. Cathodic coulombic efficiencies (CCE) and number of days of hydrogen production for each of the 10 modules. CCE was calculated from the average current and gas produced.

2.4 Results from decommissioning the reactors

2.4.1 Molecular data: 16S DNA sequencing

Module 6 had the largest hydrogen gas output (0.6 L/d) and CCE (93 %). At day 42, two days before gas production, the relative abundance of taxonomic groupings in module 6 was not significantly different to the other modules (p>0.05), except module 9 (p = 0.04) (Fig 2.8).
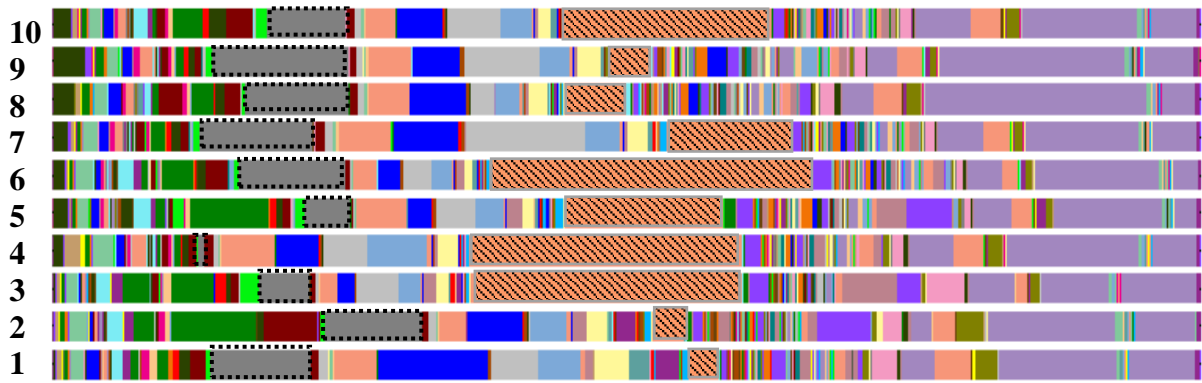
Figure 2.8 Bar chart taxa summary after 42 days of operation. This shows the composition of genera across the 10 modules (listed 1-10) two days before the onset of gas production. Each coloured bar represents a different genus. Two of the most notable genera present were Geobacter (grey bar with black dotted outline, ~7% of the anode) and Hydrogenophaga (pink bar with diagonal black stripes, ~13% of the anode).

At day 51, module 6 had produced hydrogen gas continuously for 7 days. Additionally, modules 1, 2, 3 and 10 were all producing gas. However, the remaining half (modules 4, 5, 7, 8 & 9) were not. There were no significant differences in the MEC anode communities (p>0.05) (Fig. 2.9). The result was the same at day 79, despite the cessation of gas production in modules 1, 2 and 3.
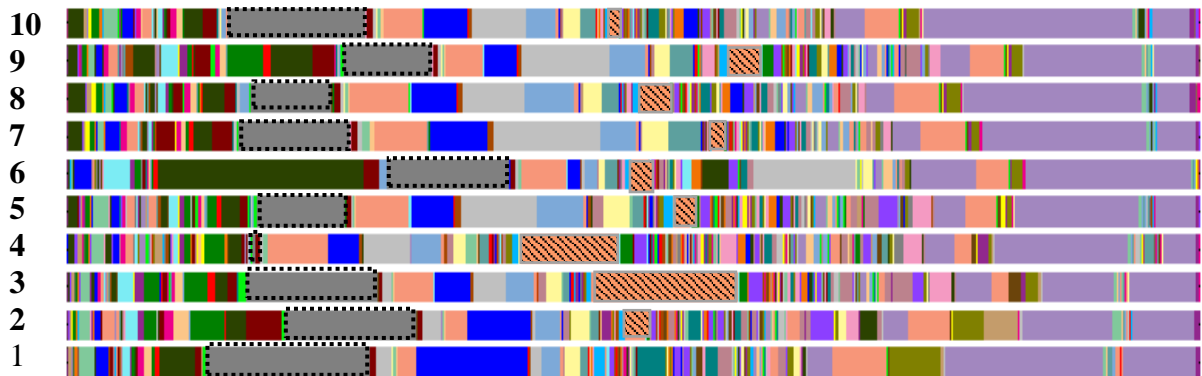
Figure 2.9 Bar chart taxa summary after 51 days of operation. This shows the composition of genera across the 10 modules (listed 1-10) during gas production. Geobacter is present (grey bar with black dotted outline, ~9.5% of the anode) but the relative abundance of Hydrogenophaga has decreased considerably (pink bar with black diagonal stripes, ~3% of the anode). There are no significant differences in any of the 10 anode communities.

By day 160, when the MEC was decommissioned, almost half of the modules were significantly different to module 6; including 5 (p=0.04), 8 (p= 0.02) and 9 (p= 0.01) which had all failed, as well as module 10 (p=0.02) which was still producing hydrogen gas (Fig. 2.10)

Gas producing modules, 6 and 10, showed a significant change between start-up and stable operation, but no change once they had started to produce gas. Modules 5, 8 and 9 showed considerable variation throughout operation with significant changes at every sampling point. Modules 5 and 9 failed to produce any hydrogen gas throughout operation, whereas module 8 produced hydrogen gas in very small quantities (<0.05 L/d) for less than a week.
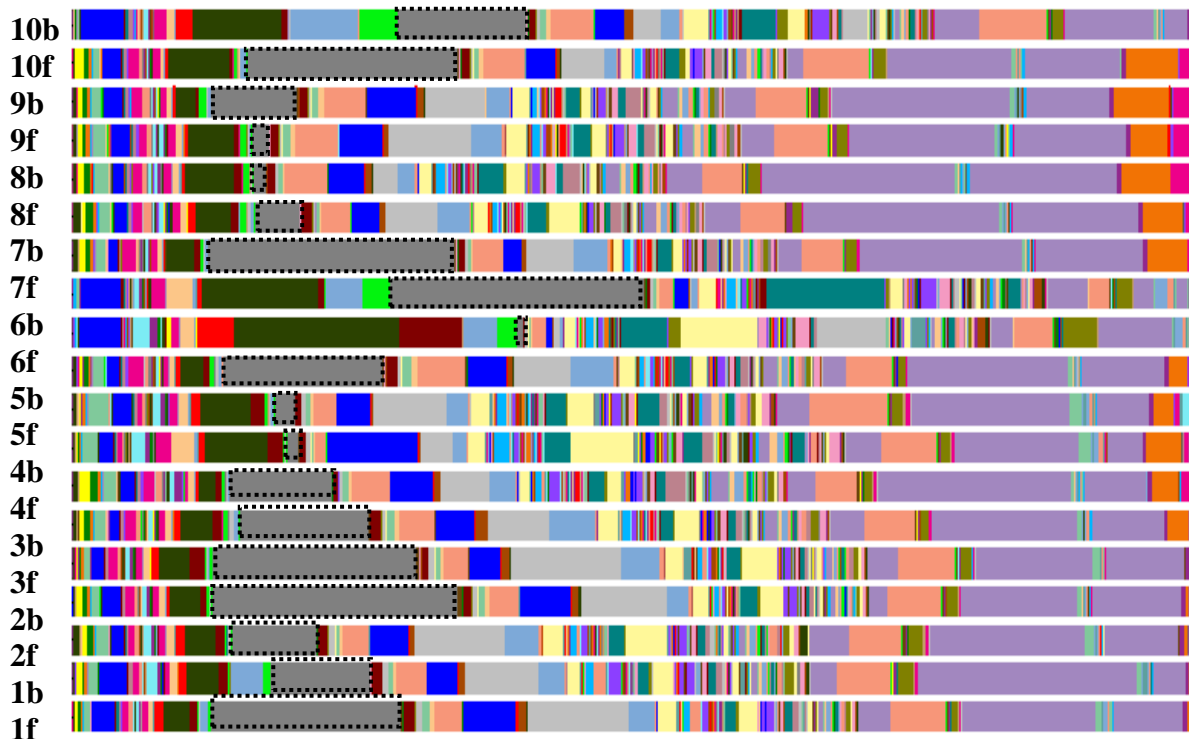
Figure 2.10 Bar chart taxa summary at day 160. This shows the composition of genera across the 10 modules in the MEC after decommissioning. Two samples were taken per module (listed 'b' for the back of the module and 'f' for the front). Module 6, the highest performing module, is significantly different to half of all the modules at day 160, including module 5 (p=0.04), module 8 (p=0.02), module 9 (p=0.01) and module 10 (p=0.02). Geobacter is still present (grey bar with black dotted outline) but Hydrogenophaga is no longer visible.

Modules 1, 2, 3 and 7 all show significant changes at a single time point in the sampling series, although that time point is not the same for each module. Module 1 showed a significant change between day 79 and day 160 (p=0.01), whereas module 2 displayed a shift earlier, with a significant change between day 51 and day 79 (p=0.02). This does not align with time of module failure.

Further microbial (Scanning Electron Microscopy imaging, SYBR gold staining) and molecular analysis (16S sequencing) was undertaken. It is discussed in Chapter 5.

2.4.2 Structural integrity and fouling

The membranes were all intact when the MEC was decommissioned. A fine coating of solids was present on the surface of each of the membranes. After the membranes were left to dry,

variation was observed in their condition (Fig. 2.11). Some had a visible coating of a rust-like deposit, others had a white powdered precipitate coating the surface. ICP analysis revealed the main cations in the powder were calcium and magnesium (Table 2.5).

The amount of white precipitate varied between modules, with noticeably more on those that performed better. In a Tukey's multiple comparison test, there was a statistically significant difference (p=0.000) between the amount of white precipitate on the two modules that continued to produce gas until the end of operation (coverage = 75 % ± 21) and the amount present on the modules that had failed (coverage = 2.5 % ± 3.2). There was no significant difference between the extent of fouling on the front-facing and the rear-facing membranes for the white powder (p=0.994) or the rust-like deposit (p= 0.998).

	Ca mg/L	Mg mg/L	Na mg/L	K mg/L	Fe mg/L	Mn mg/L	Al mg/L	Zn mg/L	Pb mg/L	Cu mg/L	Ni mg/L
Cathode sample	7870	677	49	68	7.5	3.3	3.4	0.4	0.6	0.1	3.8
Anode sample	426	3055	34	30	7.3	4.9	1.2	0.1	0.1	1.2	1.2

Table 2.5 Results from inductively coupled plasma mass spectrometry (ICP) analysis. The concentration, in milligrams per litre (mg/L), of each cation in the 0.2g partial digests of white powdered precipitate from the UHMWPE membrane from module 6 is reported.

The powders scraped from the membranes varied in their colour, texture and grain size. The sample from the inside of the cathode chamber from module 6, was paler in colour and finer in texture (Fig. 2.12a). The sample from the outside (Fig 2.12b), which was in contact with the wastewater, was darker in colour and coarser in grain.

XRD analysis confirmed ICP results. The predominant XRD peaks were for calcium and magnesium carbonates. Both samples from module 6 showed peaks for calcite, magnesian calcite and monohydrocalcite. However, the outer sample (anode-side) also showed peaks for brucite (magnesium hydroxide). Samples taken from the rust-coloured powder observed on the membranes of module 2 and 3 (Fig. 2.12c and 2.12d), showed peaks for elemental sulphur and gypsum. Scanning electron microscopy (SEM) was used to visualise the membranes at microscopic level (Fig. 2.13 and 2.14).
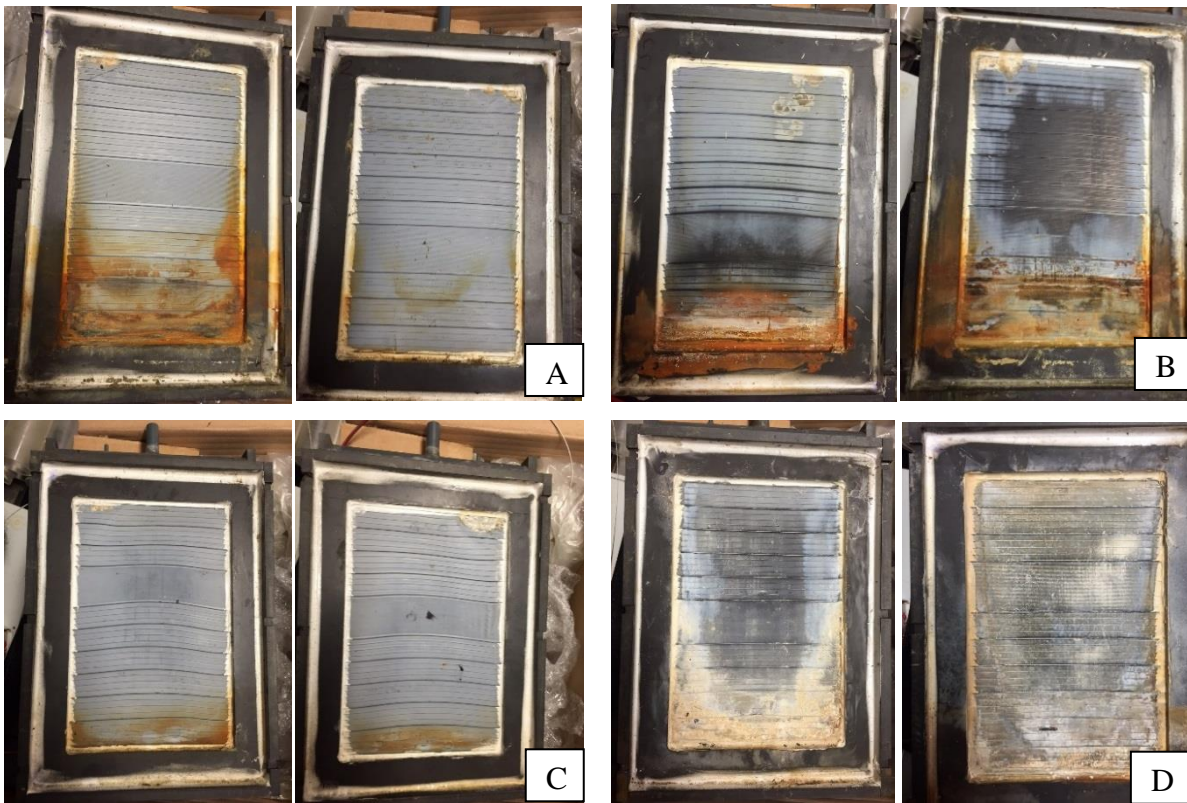
Figure 2.11 Photographs showing fouling of the membranes: module 2 front and back (A); module 3 front and back (B); module 5 front and back (C) and module 6 front and back (D).
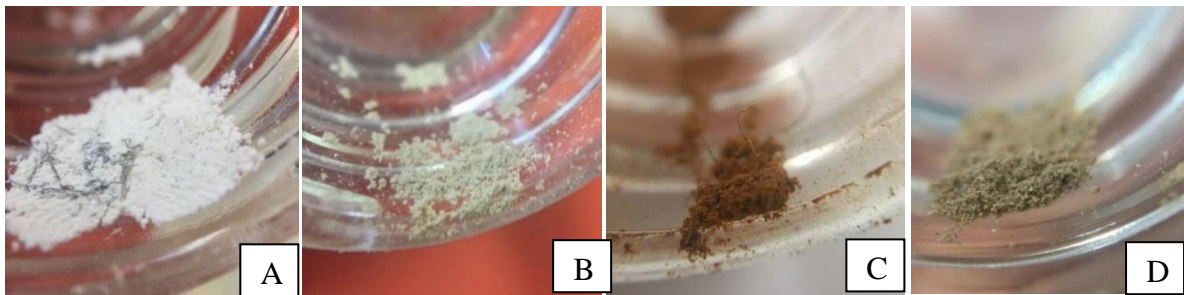
Figure 2.12. Photographs of the powdered samples sent for XRD analysis. Samples A and B were taken from the cathode-side (A) and anode-side (B) of module 6's membrane, and visualised with a 10x macro lens. Sample C was taken from the membrane of module 2 and D from the membrane of module 3. Both C and D were visualised with a 15 x macro lens.
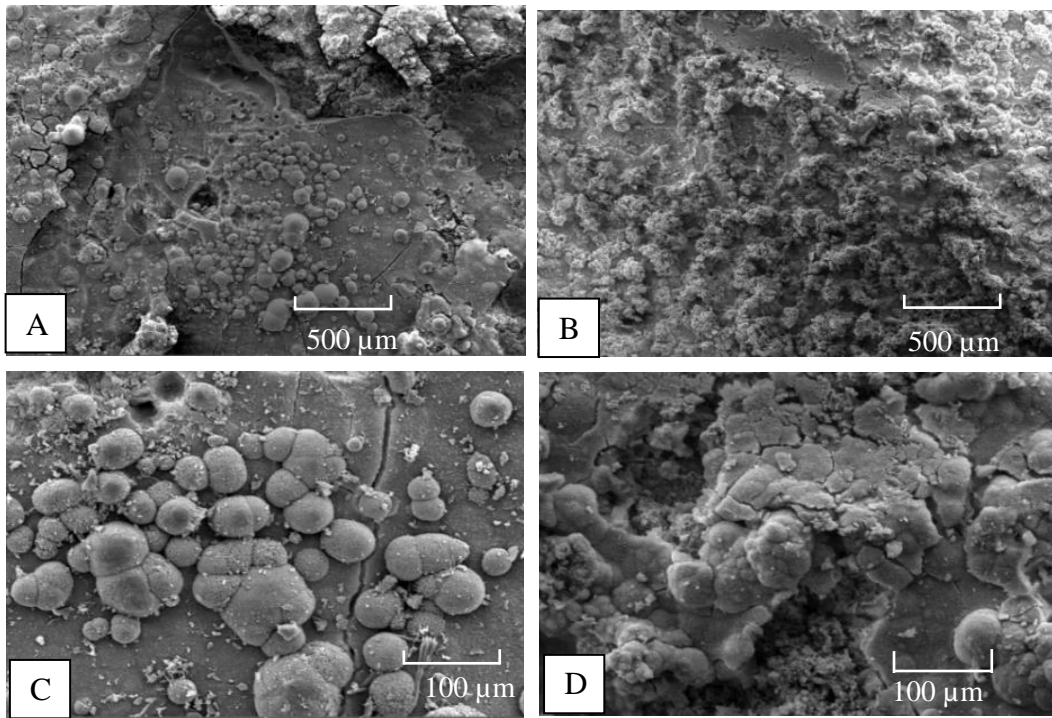
Figure 2.13 Scanning electron micrographs of scaling on (A) front and (B) back of module 6's membrane at 100 x magnification, and (C) front and (D) back at 500 x magnification.
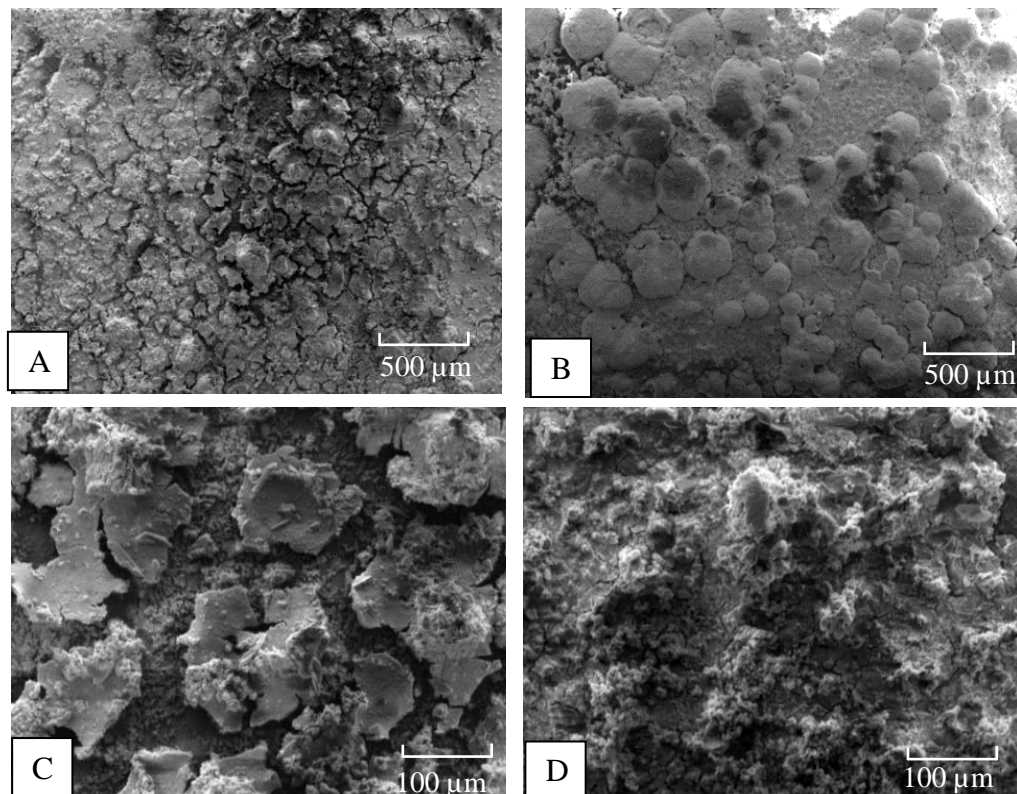
Figure 2.14 Scanning electron micrographs of scaling on (A) module 2's membrane and (B) module 3's membrane at 100 x magnification, and (C) module 2's membrane and (D) module 3's membrane at 500 x magnification.

2.4.3 Anodic resistance

The integrity of each of the modules' electrical connection was highly variable when the MEC was decommissioned. This was evident in both electrodes, but particularly on the cathode side. Module 5 had a very loose connection, and was assumed to be an incomplete circuit. The anodic resistance from module 5 was difficult to record (Table 2.6). Module 5's values are recorded as an asterisk (Table 2.6), because a stable value could not be achieved for either anode. The readings fluctuated between 0 and 5 Ω in the front-facing anode, and 4 and 10.8 Ω in the rear-facing anode.

Anode	1	2	3	4	5	6	7	8	9	10
Front-facing	3.3	25.3	26.4	25.0	*	2.6	1.7	2.8	15.8	1.2
Rear-facing	2.4	2.4	22.1	22.2	*	<DL	1.8	2.8	18.9	<DL

Table 2.6 Anodic resistance, measured in ohms (Ω), of the front-facing and rear-facing anodes of each module. Values for module 5 are left blank due to fluctuation. Two anodes recorded a value below the detection limit (DL) of the multimeter.

The back-facing anode of the highest performing modules (6 and 10) both recorded a resistance below the detection limit of the instrument (<0.5 Ω). The multimeter is operational between 0 and 50°C, however it is accurate to 0.1Ω when operated at 23°C $\pm$ 5 and <75 % relative humidity. When the measurements were taken, it was 6°C and the relative humidity around the multimeter's probe would have exceeded 75%. A one-way ANOVA showed there was no significant difference in the resistance of the front-facing ($F_{(2,9)} = 0.905$, p= 0.453) or rear-facing anodes ($F_{(2,9)} = 1.414$, p= 0.314) between the failed modules (4,7 and 9), the deteriorated modules (1,2,3 and 8) and the gas producing modules (6 and 10) (Table 2.6).

2.4.4 Chemical results

At decommissioning, anolyte pH and conductivity were consistent throughout the MEC (pH 7.82 ±0.2, conductivity 1.053 ± 0.015 mS/cm). This was comparable with the pH and conductivity when gas production was first observed (pH 7.34 ± 0.35, conductivity 1.002 ±0.006 ms/cm). However, pH varied considerably throughout the 6 months' operation. After 72 days there was a sharp shift in pH at the front of the tank (Fig. 2.15). For more than 60 days, the pH gradient was almost 2 pH units (front pH 5.4 ± 0.5, back pH 7.18 ± 0.15).
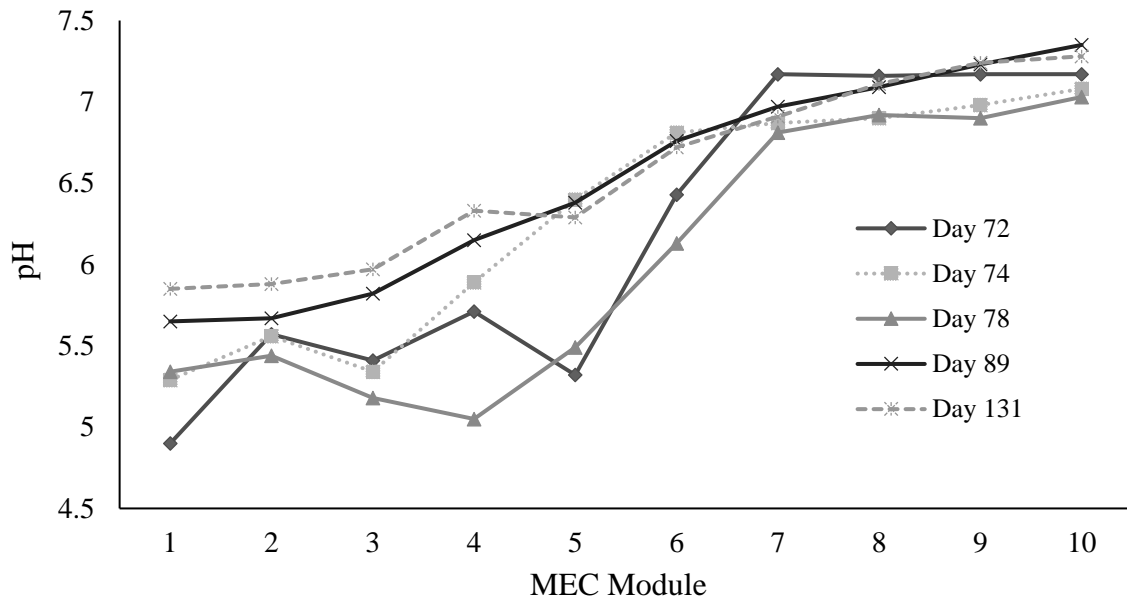
Figure 2.15. Changes to the measured pH in the MEC reactor over a 2-month period (September-October) during the gas-producing phase of operation.

Catholyte conductivity and pH at decommissioning reflected module performance. The pH of the catholyte in module 6 and 10 was very alkaline (12.5 and 11.3 respectively). The failed modules' catholyte pH was markedly lower, on average 9.1 ± 0.5. The conductivity of the working modules' catholyte (3.2 mS/cm ± 0.1) was almost 3 times that of the failed modules (1.1 mS/cm ± 0.2).

2.5 Fault Tree Analysis

Six of the ten MEC modules produced hydrogen gas, but four of those ceased to work before the end of operation. To deduce the root cause(s) of failure in these modules, FTA was applied. It is thought that there were at least two modes of failure. Modules 4, 5, 7 & 9 failed to start-up, never producing current or gas. Modules 1, 2, 3 & 8 produced current and gas for a period of 7 to 27 days before deteriorating to the point of failure.

2.5.1 Failure to start up

Despite being subject mostly to the same conditions (as the modules were hydraulically connected, COD was not the same for each module, but power supplied, type of wastewater, temperature, DO *etc.* were the same), four of the ten modules did not achieve stable current. The three following fault trees (Fig. 2.16 - 2.18) cover scenarios that may have led to complete failure at the outset. These include: all modules failing to start up (2.5.1a), which was not observed in this study; and some modules failing to start up (2.5.1b), which was observed.

Discounting repeated events, there are 13 basic events that may have resulted in instant module failure.

2.5.1a All modules fail to start-up

This fault tree, which is split into two parts due to size, was developed to understand why all modules may fail to start-up. Part 1 (Fig. 2.16) considers the build of the MEC modules, including the reactor architecture and the electrical connections within the circuit. The latter, includes loose wires resulting in an incomplete circuit, as well as significant corrosion of electrical connections. Both means prevent the external supply of power reaching the electrodes. If the electrons produced by the bacteria (as well as those supplied externally) are not transferred to the circuit, current will not be recorded by the data loggers.

Modules are presumed to have 'failed' at start-up, if they are unable to generate current or hydrogen gas. The design of the reactor architecture - including the electrode materials, their configuration within the module, and the solution within which they are placed – will have a direct impact on the modules' resistivity and ability to generate current and hydrogen. Each of the reactor architecture factors could be prohibitive individually or in combination.

Part 2 (Fig. 2.17) describes how the MEC' biofilm may have led to outright failure in all modules. There are four basic events which may have prevented current generation and hydrogen production. These include absence of exoelectrogenic bacteria in the inoculum; competition with methanogens and anaerobic heterotrophs; and inability to adhere to the anode material.
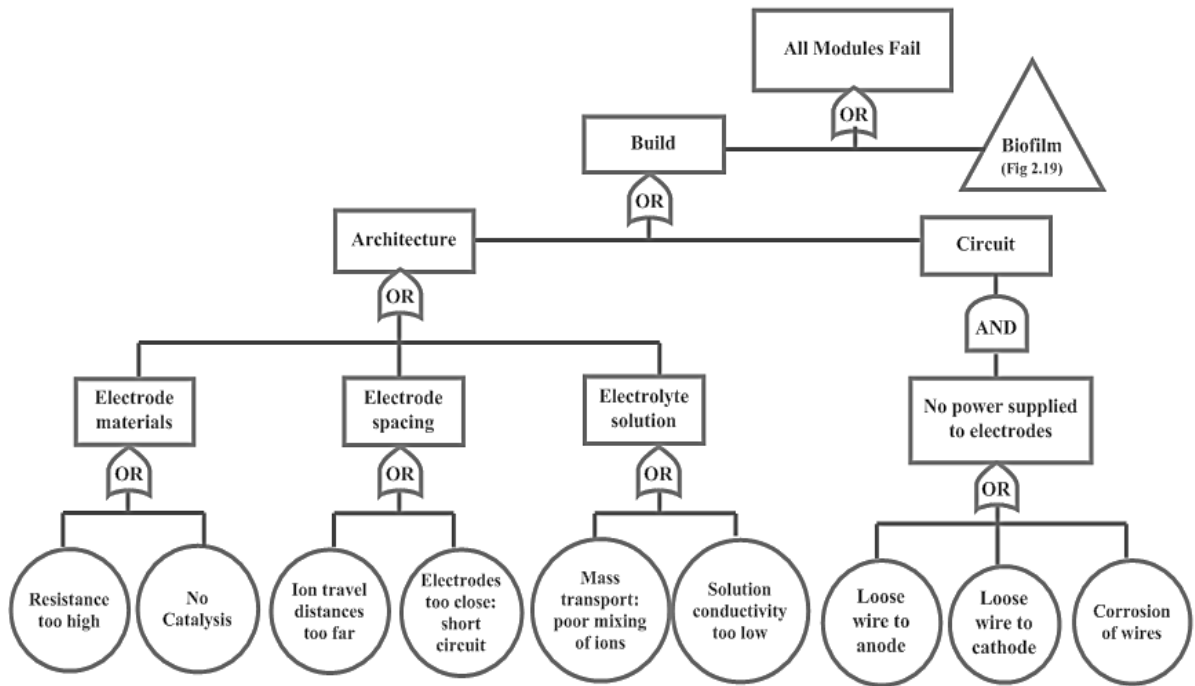
Figure 2.16. Part 1 of the fault tree developed to understand why all modules may fail to start-up. This fault tree examines 9 basic events stemming from faults and inadequacies in the reactor build, including configuration and electrical connections.
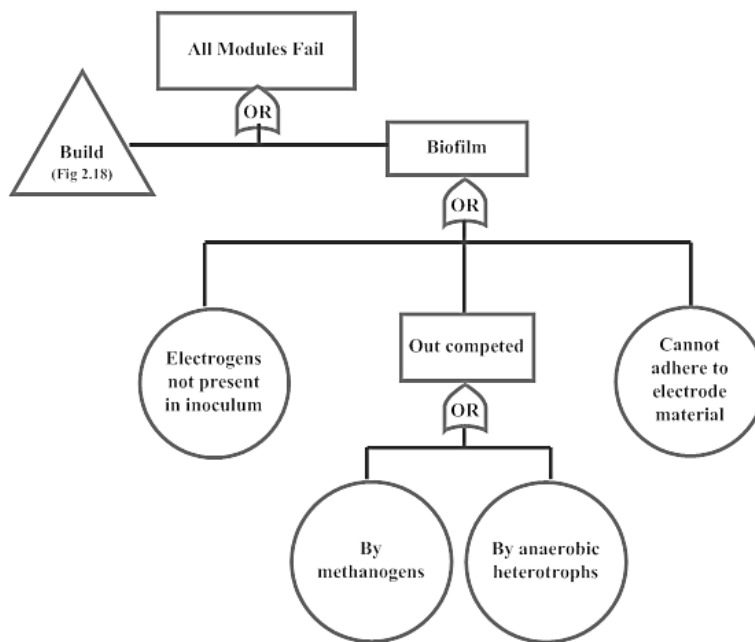
Figure 2.17. Part 2 of the fault tree developed to understand why all modules may fail to start-up. If the biofilm does not contain exoelectrogens, it will not be able to transfer electrons to the circuit and generate current. This fault tree considers four basic events which may lead to an absence of exoelectrogens in the MEC anode.

2.5.1.b some modules fail to start-up

This fault tree describes why some (not all) modules may fail to start-up, while other modules achieve stable current and gas generation (Fig 2.18). There are three basic events and one

undeveloped event. The undeveloped event relates to inconsistencies in the MEC build. This corresponds with the faults outlined in Fig. 2.16, provided the faults only apply to individual modules (not all). It is unlikely that electrode materials and spacing would have contributed to the failure of some, but not all, of the MEC modules. It is more likely, that inconsistencies in the build relate to the integrity of the electrical connections.

The three basic events in this fault tree all relate to the wastewater characteristics. The presence of a toxic compound is likely to have a greater impact on the first module in the tank, than the last. If the toxic compound caused bacterial cell death, it may cause failure in the first module, with no detrimental effect on later modules. Localised pH changes could affect the exoelectrogens' metabolism. A pH change below 5.5 above 9 would lead to a cessation of the exoelectrogens' metabolism (Kim and Lee, 2010; Nevin *et al.,* 2005). Increasing scale, increases the likelihood of variation in the modules' wastewater environment. If influent COD is low, there may be insufficient organic material available for the biofilm of latter modules, after COD has been removed earlier in the tank.
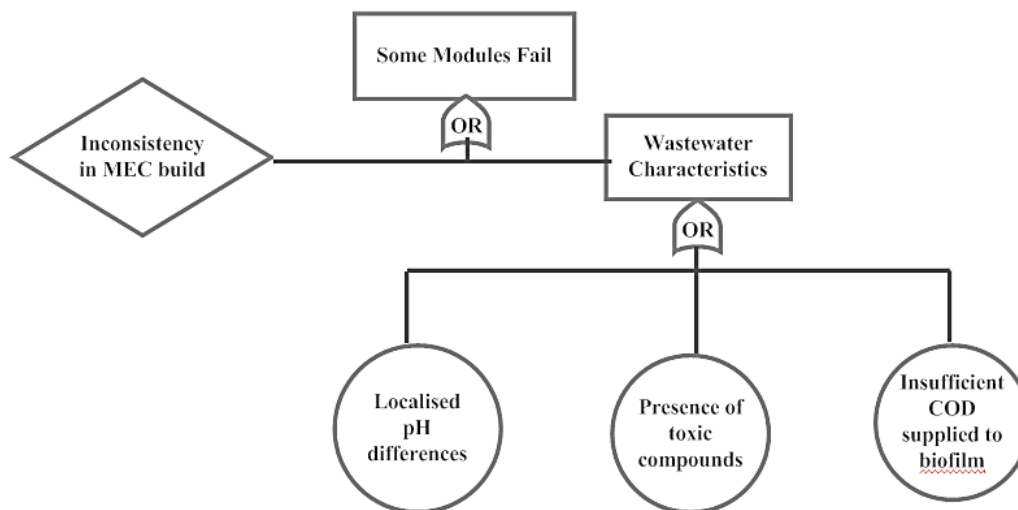
Figure 2.18 Fault tree developed to understand why some modules may fail to start up, whilst other modules achieve stable current and gas generation. This fault tree considers inconsistencies in the modules' themselves, and in their environments. There are three basic events and one undeveloped event.

2.5.2. Module deterioration

Six modules produced hydrogen gas during operation. However, four of these six had stopped producing gas long before the end of operation. The two following fault trees (Fig. 2.19-2.20) cover scenarios that may have led to deterioration of modules, resulting in failure. This is considered from the perspective of two or more modules failing simultaneously (2.5.2a) and an

individual module failing independently (2.5.2b). Discounting repeated events, there are 15 basic events (and one undeveloped event) which may have resulted in failure.

2.5.2.a Simultaneous deterioration

This fault tree (Fig. 2.19) was developed to understand why two or more modules may fail simultaneously, after previously producing current and/or hydrogen gas. This fault tree focuses on changes to the surrounding environment of each of the modules, which may lead to deterioration. It considers changes large enough to encompass several modules, which would lead to deterioration of one or more modules simultaneously.

This includes a change in the supply of substrate, such as significant variation in pH or COD concentration, or complete cessation of supply (in the event of a pump failure or blockage). Additionally, the impact of widespread fouling is considered. This would include clogging from fats, oils and greases, or the accumulation of biofilm shedding (during seasonal temperature change). These factors could affect the flow of waste through the tank and therefore, the supply of substrate to certain modules. Additionally, they could foul the module architecture itself, increasing electrode spacing, or creating an impermeable barrier preventing the transfer of ions.

Furthermore, failure could arise in simultaneous modules due to a fault in an individual power supply, however this was deemed to be an external event and was not included in the fault tree.
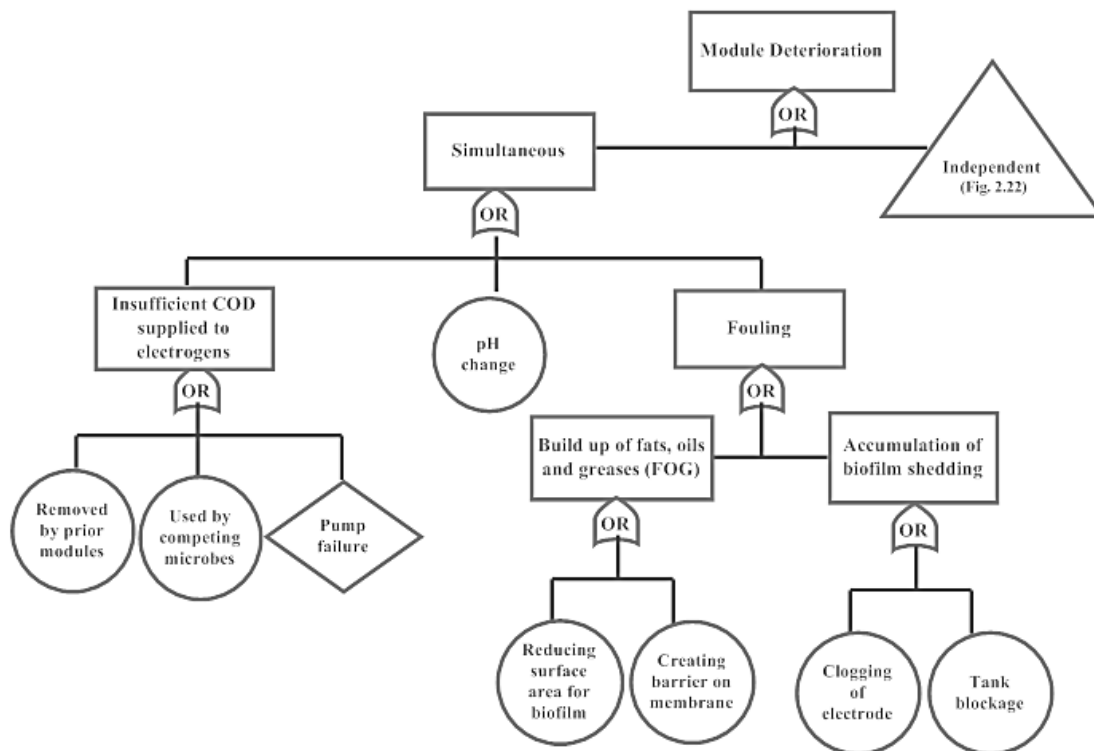
Figure 2.19 Fault tree developed to understand why two or more modules may deteriorate to the point of failure. There are six basic and one undeveloped event described in this fault tree.

2.5.2b Independent deterioration

This fault tree was developed to understand why a single module may fail independently, having previously produced current and/or hydrogen gas (Fig. 2.20). This tree considers the deterioration of electrical connections, fouling of the membrane and deterioration of the membrane's seal. Additionally, it considers fouling of the cathode's catalytic sites and the risk of hydrogen scavenging. Furthermore, failure could occur independently due to human error or sabotage (not depicted in fault trees).
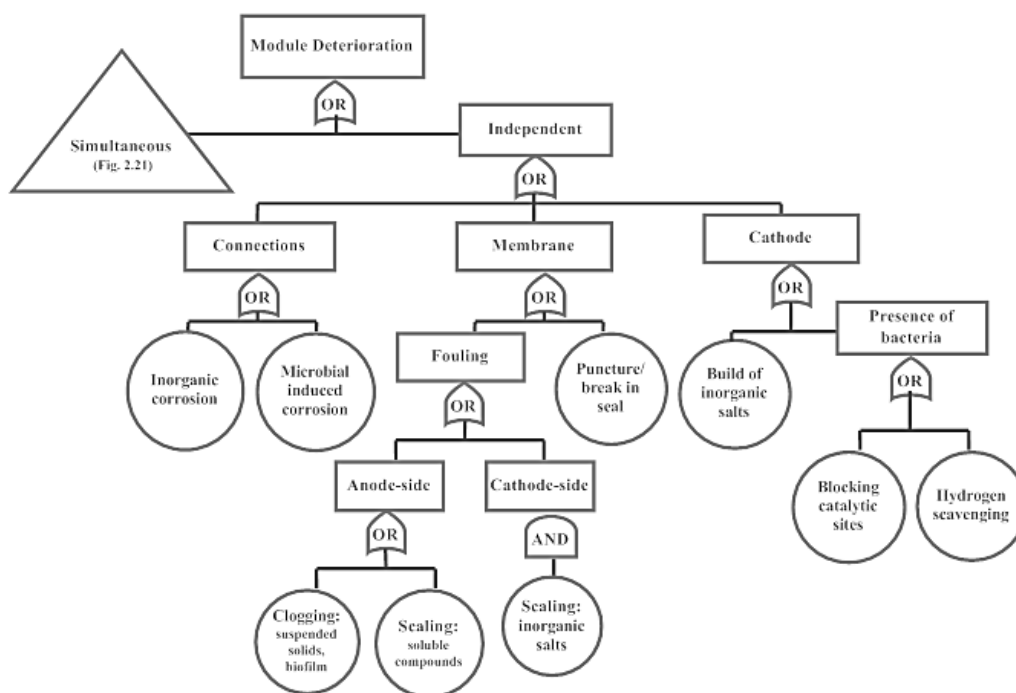
Figure 2.20 Fault tree developed to understand why an individual module may deteriorate to the point of failure. This tree considers 9 basic events.

2.6 Discussion

This study confirms work carried out by Heidrich *et al.,* (2013; 2014) showing that MEC can produce almost pure (98 % ± 3) hydrogen gas from raw domestic wastewater at ambient temperatures (average 16.3˚C). The technology can work on small isolated sites, providing opportunities for energy recovery on sites with low and variable flows, as well as larger sites, where energy recovery is common.

The MEC did not achieve effluent consent (<125 mg/L) during operation. However, tCOD removal (32 %), sCOD removal (44 %) and organic loading rate (0.21 kgCOD/m^3/day) were comparable with the previous pilot (34 % tCOD removal; OLR 0.14 kgCOD/m^3/day). For a viable technology, COD removal would need to be improved and achieved consistently. If a linear relationship between anodic surface area and COD removal is assumed, 22 modules (each with two 0.06 m^2 anodes) would be required to achieve a COD <125 mg/L in this study. This is equivalent to a surface area to volume ratio of 20 m^2/m^3.

Poor mixing within the MEC led to accumulation of fats and solids and the front of the tank which ultimately, resulted in fermentation. This was noticed when acetic acid in the MEC was 2.2 times larger than the influent tCOD, after 72 days of operation, and a pH of 4.9 was

recorded. An increase in VFA concentration, from fermentation, may have resulted in a drop in pH and the cessation of exoelectrogen activity.

Known genera of exoelectrogens, such as *Geobacter* and *Shewanella*, grow between pH 6 and 8 (Kim and Lee, 2010; Wang *et al.,* 2010; Sun *et al.,* 2014) with optimum growth in a slightly narrower range (pH 6.7-7.3). Wang *et al.,* showed that even a very slight drop in pH, below 6, had a considerable effect on the microbial anode potential (raising it above -250mV) and consequently on the rate of hydrogen produced (Wang *et al.,* 2010). A more significant drop in pH (below pH 4) was shown to cause irreversible damage to the anodic biofilm, with no indication of recovery after return to neutral conditions. Similarly, Kim and Lee (2010) found no growth of *G. sulfurreducens* below pH 5.5, a result comparable with Nevin *et al.,* (2005) who reported two species of *Geobacter* which could not be grown at pH 5. However, when the pH was increased, even after a sustained period at pH 12, the biofilm could recover and produce current on return to neutral conditions (Wang *et al.,* 2010).

Analysis of module 1, 2 and 3 - all of which failed at the same time as the observed shift in wastewater pH - showed no significant difference in the relative abundance of *Geobacter,* whilst functioning at day 51 (0.13 % ± 0.02) and immediately after failure at day 79 (0.17 % ± 0.07), t (4) = -0.885 p=0.426). However, the analysis carried out (16S DNA sequencing) does not indicate whether the *Geobacter* present is alive or dead. Therefore, it is unlikely that a change in relative abundance would be observed by this method. Furthermore, *Geobacter* is used as an example, but does not represent all known (and unknown) exoelectrogens' response to the pH shift. For this reason, variation in the entire anodic community, rather than exoelectrogenic bacteria alone, was used to assess potential root causes of failure.

Controlling and maintaining a near neutral pH is one of the factors paramount to successful operation. Consideration will be given to the following modifications:

- Recirculation: preventing accumulation and settlement of VFA, solids and fats which may lead to fermentation. Recirculation should also support mixing and mass transfer.
- Reducing the amount of settleable and non-biodegradable solids which may not be used by the electrogenic biofilm. This suggests testing the technology as a secondary process.
- A shorter retention time and higher flow rate may improve mixing. This may prevent mass transfer limitations, increasing the organic load reaching the electrogenic bacteria.
- Specific pH control: chemical dosing or buffering to maintain pH within a narrow range.

Whilst it is likely that the shift in anodic pH played a role in failure, the statistical analysis of the modules' microbiological communities showed no significant difference between high performing and failed modules during start-up. It is unlikely therefore, that there is a biological basis for the modules' failure at the outset: eliminating many branches of the FTA.

The role played by elemental sulphur and gypsum, observed by XRD and SEM imaging, in the modules that deteriorated, remains to be investigated. It is widely accepted that formation of a scale on the surface of a membrane is likely to decrease its performance and life span (Shih *et al.,* 2005; Al-Amoudi and Lovitt, 2007). Sulphate-reducing bacteria (SRB) found in the anodic biofilms, are likely to convert the influent sulphate into hydrogen sulphide under anaerobic conditions in the MEC (Parker, 1945; Rauch and Kleidorfer, 2014). Spontaneous electrochemical oxidation of aqueous sulphide has been demonstrated at neutral pH, leading to a build-up of elemental sulphur ($H_2S/HS^- \rightarrow S(s) + 2e^- + 2H^+/ H^+$) (Dutta *et al.,* 2008).

Deposition of elemental sulphur in an electrochemical reactor, has been shown to increase ohmic resistance 10-fold, in as little as 60 days, decreasing the reactor's performance (Dutta *et al.,* 2008). It is unclear whether this mechanism is electrochemical (Dutta *et al.,* 2008) or microbiological (Rabaey *et al.,* 2006). Rabaey *et al.,* (2006) did not determine the long-term impact of sulphur precipitation on the process of electron transfer. This precipitation may form a barrier, reducing electrochemical performance (Dutta *et al*., 2008).

It can be assumed that the sulphur deposition in this study contributed negatively to MEC performance, possibly resulting in module failure. However, the extent of fouling observed at decommissioning may not fairly reflect the amount that was present at the point of failure. The oxidation of sulphur requires potentials higher than -0.274 V, but higher potentials result in greater oxidation (Rabaey *et al.,* 2006). Immediately following module failure, the applied voltage of failed modules was increased from 1.2 V, to 1.4 V then 1.6 V, to determine whether gas production had stopped due to an increase in module overpotential.

It is unclear whether the sulphur and gypsum fouling, which was proportionally greatest on modules which deteriorated, was the cause, or a consequence, of failure. Based on this, it would not be fair to make predictions of a threshold level of sulphur precipitation beyond which becomes prohibitive to MEC performance. However, it may suggest that factors such as influent sulphate concentration - arising from the catchment and the sewer feed to the site - may be more influential in determining site suitability than flow or population equivalent.

The applied voltage supplied, at 1.2 V, was too high for the MEC to be a net-energy producer (Logan *et al.,* 2008). The theoretical maximum energy efficiency at 1.2 V is 103 % [Appendix B, Eq. 4-8]. As the limit of energy recovery is set by the applied potential, future trials should be operated at a lower applied voltage. To support a lower applied voltage, improvements should be made to decrease the modules' internal resistance.

Analysis at decommissioning suggests several modules failed, whether outright or during operation, due to poor electrical connections. Variation in anodic resistance was observed. Whilst not statistically significant, the modules which continued to function over 6 months recorded lower anodic resistance than those which had failed. Moreover, the cathode could be improved in the next pilot by:

- Providing a firm connection that will not deteriorate, short circuit or break
- Combining a strong connective material (for transporting current) with a material of high surface area required for the catalytic reactions at the cathode
- Maximising surface area and minimising chamber volume (i.e. electrode spacing)
- Optimising the catholyte – taking account of cost, chemical composition and impact on electrochemical losses in the MEC.

The greatest improvement still to be made relates to the stability of the technology. Despite periods of success, including high yields of hydrogen per module and comparable COD removal, the MEC failed to show robustness or stability. Robustness can be defined as the ability to "reach steady state performance under certain environmental and operational conditions" (Leitão *et al.,* 2006). Only 60% of the modules achieved this. Stability is defined by the variability of the effluent, or by the capacity to cope with more severe fluctuations in conditions (Leitão *et al.,* 2006). The MEC failed to achieve stability by either definition.

The aims of the study were met, albeit indirectly. It was hoped that repeating a pilot scale study of comparable scale to Heidrich *et al.,* (2013) would increase opportunities for monitoring. Data from operation of the MEC brought little further understanding. However, the dissection arising from decommissioning provided information on how and why MEC may fail. Future development of the FTA, to include probabilities, would help to determine the likelihood, as well as the mode, of failure. The fault tree could also be used for gap analysis, to identify where to focus future research effort to support the design of a more robust technology.

Chapter 3. Bottlenecks and Challenges to the Scale up of Microbial Electrolysis Cells

Several challenges must be overcome, before the commercialisation of MECs can be considered a realistic proposition. MECs are intrinsically complicated. Making better MECs requires an understanding of a wide field of subjects including: materials science, electrochemistry and microbiology. Technological challenges such as material choice, electrochemical losses and hydrogen gas capture are well documented (Logan and Regan, 2006; Hamelers *et al.,* 2010; Zhang and Angelidaki, 2014; Escapa *et al.,* 2015). Yet there are still several practical challenges to be addressed when moving from bench to pilot scale.

In this chapter, meta-analyses and experiments are collated to assess some of the challenges to the scale up of MEC, including; the effect of temperature; where best to place the technology in the treatment chain; how resistances in wires will dictate the power supplied; and whether hydrogen scavenging bacteria affect the hydrogen yield.

3.1. Electrical Resistivity

MEC technology needs an input of electrical energy to drive the transfer of electrons in a circuit. The materials chosen must provide a low electrical resistivity. Resistivity is described as an "electrical property of a material due to which, it impedes or resists the flow of electricity" (Rajput, 2004). The most conductive material may not always be the best choice. There may be a trade-off between the most suitable electrical conductor; the cost of the material; and its suitability to the application.

There are numerous reasons for resistivity in MECs. Individual electrochemical losses can occur due to electrode kinetics, ohmic resistances or limited mass transport (Hamelers *et al.,* 2010). When the electron transfer step (or a process linked to this) is slow, losses can occur at the anode or cathode. Ohmic resistances are caused by opposition to the flow of ions and electrons through a bioelectrochemical system (Rozendal *et al.,* 2008). This may be resistance of the flow of ions in the electrolyte, or by the resistance of the flow of ions in an electrode and its associated wiring; the latter of which, is likely to become more problematic with scale up (Rozendal *et al.,* 2008; Hamelers *et al.,* 2010).

When MECs is scaled up, so too is the peripheral equipment. Where crocodile clips and short wires can suffice in a laboratory, more robust connections are necessary for a pilot. This is

particularly true for one installed *in situ* on a treatment works, where exposure to changes in temperature and moisture is more likely than in a laboratory.

With larger MEC and storage tanks, the wires need to stretch further to the power packs and monitoring equipment. This increases the distances that the ions must travel, thereby increasing electrical resistivity. Resistance in a wire is calculated as: $R = \rho L/A$, where R is resistance, ρ is the wire's resistivity, L is length and A is cross-sectional area. Therefore, increasing the length will directly increase the resistance.

Materials used in scaled up MEC are primarily chosen for their low cost and compatibility with an electrochemically active biofilm (Rozendal *et al.,* 2008a). The resistivity of a material is influenced by the temperature at which the measurement is carried out, the purity of the metal and the mechanical processes subject to the material (Rajput, 2004). The values detailed below, for common materials used in MEC systems, are indicative of the resistivity of each at 20°C assuming no impurities or deterioration (Table 1). Their market value is listed alongside, highlighting the magnitude of the trade-off between cost and conductivity.

Material	Resistivity ρ (10^{-8} Ω m)	Market value (USD/kg)	Max current density* ($\mu A/cm^{-2}$)	Biofilm thickness** (μm)
Gold	2.3	8,723[a]	1200	127
Nickel	7.1	7[b]	380	77
Platinum	10.5	6754[a]	-	-
Titanium	39	12.5[b]	-	-
Stainless Steel	71	0.9[b]	700	-
Graphite Felt	<3000[c]	63[c]	1000	117

*Table 3.1. Resistivity coefficients and market value of MEC electrode materials (Baudler et al., 2015). All market values were obtained on 03 October 2016. Sources: A, Bloomberg (2016), B, Metal Miner (2016), and C, SGL (2016) SIGRACELL battery felt (used in Chapter 4). *Current densities obtained with acetate at 35 ̊C (Baudler et al., 2015) ** corresponding biofilms measured using CLSM (Baudler et al., 2015)*

If the wire's characteristics remain unchanged with scale up, resistance will increase proportionally with scale (Table 3.2). Scale up for retrofit into an activated sludge lane, may lead to wire lengths of up to 10m. This would increase the measured resistance of titanium wire used in the laboratory by 200-fold. Therefore, the thickness of wire must be increased, or

its length must be reduced. The latter could be achieved by increasing the number of power supplies, which would carry an additional cost. This has implications for MEC module design; particularly, whether the module size will be limited by resistance.

Scale	Material	R (Ω)	ρ(Ω)	L (cm)	A (cm^2)
Lab	Titanium	0.2	0.0004	5	0.01
Pilot	Stainless steel	3.5	0.0007	50	0.01
Commercial	Stainless steel	70	0.0007	1000	0.01

Table 3.2. Hypothetical resistance of MEC wires at three different scales. The calculation assumes the cross-sectional area of the wire (A) remains constant.

The ability to support an electrogenic biofilm may have implications on the conductivity of the electrode material. Baudler *et al.,* (2015) showed a correlation between biofilm thickness and current density in tests on gold, nickel and graphite (Table 3.1). This result supports studies which have shown current density is proportional to biofilm thickness (Ishii *et al.,* 2008; He *et al*., 2011). Despite the high electrical resistivity of graphite felt (Table 3.1), it may provide one of the best options for achieving a high current density with an affordable material. The maximum current density achieved by Baudler *et al.,* (2015) with a graphite electrode was 83% of that achieved with a gold electrode, despite a market value less than 1% of gold's. Furthermore, He *et al.,* (2011) implied a fibrous electrode material, such as graphite felt, can support a thick and continuous biofilm necessary to achieve high current densities. Biofilm thickness and distribution across the electrode is discussed in Chapter 5.

3.2 Wastewater composition and energy content

3.2.1. Total COD vs. calorific energy

Chemical oxygen demand (COD) is often used as a proxy for wastewater 'strength'. Whilst the test provides a relatively simple indication of the number of organic compounds present, there is no empirical formula to calculate the energy content from the amount of COD (Heidrich *et al.,* 2011). Bomb calorimetry has been used to measure the energy content of solid waste (Rodriguez-Anon *et al.,* 1998), wastewater sludges (Zanoni and Mueller 1982; Vesilind and Ramsey 1996) and domestic wastewater (Shizas and Bagley, 2004; Heidrich *et al.,* 2011). Shizas and Bagley (2004) suggest that the high VS:TS ratio in the primary sludge sample indicates much of the energy in wastewater is locked into the settleable volatile solids.

Many volatiles are driven off in the drying process which, at 103°C, is above the boiling point of ethanol (78.4°C) and formic acid (101°C) (Heidrich *et al.,* 2011).

Heidrich proposed a freeze-drying method, yielding values 20 % higher than Shizas and Bagley (2004). Higher recovery of COD was observed during freeze-drying (74-82 %) than oven drying (51-56 %) (Heidrich *et al.,* 2011). This improved method suggests domestic wastewater contains 7.6 kJ/L ± 0.9, and mixed (domestic and industrial) wastewater contains 17 kJ/L ± 3 (Heidrich *et al.,* 2011).

An adapted version of this method (Appendix C) was used to calculate the energy content in the influent and effluent of the large MEC from pilot 2 (Chapter 4) (Table 3.3). The sample was dried in a Rocket Synergy evaporator, which makes use of low temperature steam to dry the sample under a vacuum (Genevac Ltd, UK). After drying, the samples were analysed on an adiabatic bomb calorimeter. This measures the heat of combustion, calculating the temperature rise (in ℃) and the calorific value of the sample (kJ/g). This was used to calculate the calorific value of the wastewater (kJ/L) and the energy per gram of COD (kJ/g-COD) (Table 3.3).

	Calorific Value (kJ/g – dry solid)	Calorific Value (kJ/L- wastewater)	Calorific Value (kJ/g-COD)
Settled Wastewater (MEC influent)	4.0 ± 1.1	1.8 ± 0.7	7.5 ± 1.2
MEC effluent	2.5 ± 0.4	0.9 ± 0.1	6.4 ± 0.6
MEC sludge	13 ± 5	15 ± 7	18 ± 7

Table 3.3 Calorific values of the MEC influent, effluent and sludge in pilot 2. Values were determined via Rocket evaporation of the liquid wastewater sample and bomb calorimetry of the dry solid.

The energy content of the settled wastewater (1.8 kJ/L ± 0.7) was considerably lower than values obtained for raw wastewater (7.6 kJ/L ± 0.9, Heidrich *et al.,* 2011). This is consistent with the findings of Shizas and Bagley (2004), who reported that 66 % of the energy in the wastewater is found the in the primary sludge following the primary settlement process.

3.2.2. Low-energy treatment vs. energy production

The values determined by Heidrich *et al.,* (2011) suggest that placing the technology at the head of the works, where the COD is highest, provides the best opportunity for recovering energy. This will, to some extent, depend on the chain of processes present and the extent of sludge return. The potential benefits of high COD, for current generation, must be set against the likely reduction of effluent quality. MEC operated on primary wastewater require a longer residence time for a poorer effluent quality (Zhang *et al.,* 2015). Therefore, operating MECs on primary wastewater is likely to require downstream processing before discharge to the environment.

The relationship between organic loading rate (OLR) and hydrogen production and current generation has been shown to fit a Monod-type trend (Escapa *et al.,* 2012), with hydrogen evolution occurring only at OLRs greater than 448 mgCOD per litre of anode per day. Increasing the OLR beyond 2000 mgCOD/L_a/day had negligible effect on current and hydrogen production, suggesting a maximum value or saturation at this point (Escapa *et al.,* 2012). This would suggest that unless the HRT is particularly low, installing MECs later in the treatment process, where COD is likely to be lower, is unlikely to generate current and/or yield hydrogen.

Despite this, there may be benefits to foregoing some of the energy content, to position the technology after primary settlement. Zhang *et al.,* (2015) compared substrate removal rates in MFCs fed acetate, filtered domestic wastewater and raw domestic wastewater. The wastewater was filtered to remove the particulate matter, making the substrate more physically comparable with dissolved acetate and preventing production of additional soluble substrate from the particulate COD (Zhang *et al.,* 2015). The removal rates of both acetate and filtered domestic wastewater fit a first order reaction, calculated as $\ln(COD_0/COD_t) = -kt$ (Zhang *et al.,* 2015). However, the rate constant in wastewater-fed reactors was double that of the acetate-fed reactors. This equated to COD removals of 76 % (to 51 mg/L) in filtered wastewater-fed MFCs and 78 % (to 58 mg/L) in acetate-fed MFCs over a period of 8 hours, comfortably meeting effluent standards (Zhang *et al.,* 2015).

However, when the wastewater was not filtered, the COD removal process was more complex and did not fit a first order reaction. Instead, there were two stages. During the first 4 hours, there was high current production and a rate constant 15 % higher than observed in filtered wastewater-fed MFCs. There was marked decline in COD removal and current production in

the second stage. As the rate constant was 3.5 times slower than the first stage, COD removal to 72 mg/L took a further 20 hours. The MFCs failed to generate current after 4 hours, when the tCOD dropped below 200 mg/L (a similar value to that of the filtered WW). Therefore, raw wastewater-fed MFCs required a longer residence time (24 hours) to achieve an effluent COD which was 25-40 % higher (72 mg/L) than MFCs fed a substrate with reduced particulate matter (Zhang *et al.,* 2015).

3.2.3. Sludge

Placing the MEC before primary settlement may reduce the volume and/or quality of sludge recovered from the clarifiers. Shizas and Bagley (2004) suggested primary sludge contains the largest fraction of energy in the wastewater treatment process. If the amount of sludge sent to the digesters from primary settlement is reduced, it is likely that the amount of energy recovered from the treatment process would also be reduced. It is unlikely that the MEC would produce sludge in sufficient quality (i.e. energy content) and quantity (i.e. volume) to match that of conventional primary clarification.

The MEC sludge from this study (Chapter 4) contained 13 kJ/g of dry solid. This value is lower than the energy content of primary sludge, shown to contain 15.0 – 15.9 kJ/g of dry solid (Shizas and Bagley, 2004; Zanoni and Mueller 1982). The MEC sludge is more comparable with the sludge from a secondary biological process (such as a trickling filter or activated sludge) which contains 12.4 - 13.5 kJ/g of dry solid, or the sludge that results from anaerobic digestion, which contains 11.4 - 12.7 kJ/g of dry solid (Shizas and Bagley, 2004; Zanoni and Mueller 1982). This supports placement of the MEC after primary settlement, to allow for energy recovery from separate processes. This would reduce the likelihood of making the existing sludge digestion process redundant, through the reduction of high energy-content primary sludge.

3.2.4. COD fractionation

COD concentration is usually about twice the concentration of BOD_5. McCarty reported that over a third (36 %) of COD in domestic wastewater is refractory (McCarty *et al.,* 2011). Refractory COD includes detergents and pesticides which can be chemically oxidised, but are not readily biodegradable.

If the MEC is fed raw wastewater, it may be possible to biodegrade up to 64 % of the COD (both the suspended and dissolved fractions). If it is placed after primary, in theory, this value

will be reduced, leaving only 30-40 % of the original COD accessible to the exoelectrogens. In a typical domestic wastewater treatment plant, where raw influent COD is between 400-600 mg/L, this would imply that only 120- 240 mg/L COD would be bioaccessible to a secondary MEC process. This concentration (120-240 mgCOD/L) is unlikely to generate current (Zhang *et al.,* 2015).
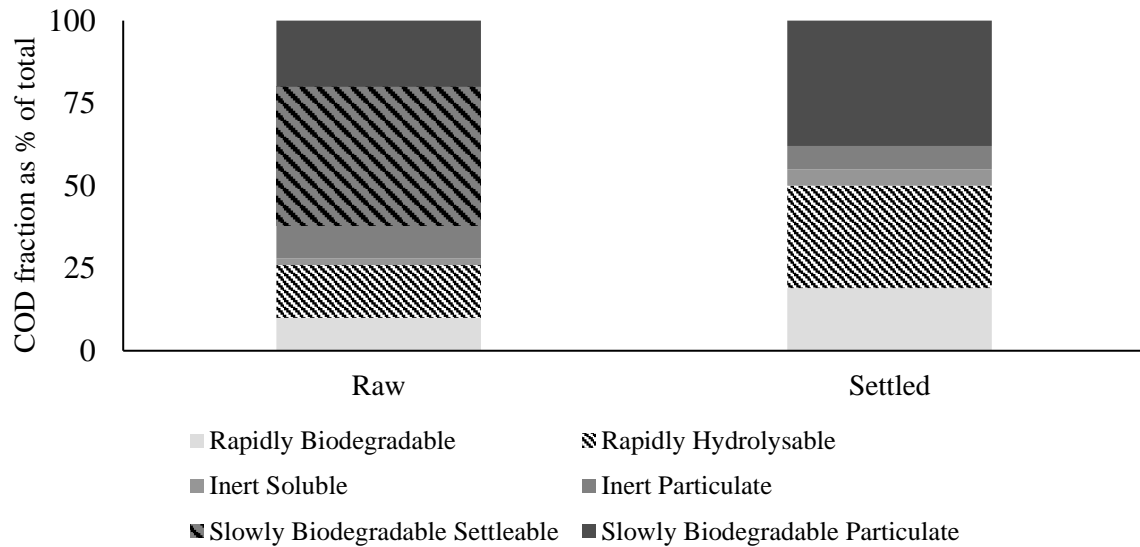
Figure 3.1. Fractions of chemical oxygen demand (COD) as a percentage of the total COD in raw and settled wastewater. Adapted from Table 1 in Orhon et al., (2002).

Orhon *et al.,* (2002) found that the proportion of rapidly biodegradable and hydrolysable fractions of COD (relative to total COD) are twice as high in settled wastewater compared to raw. For example, with an influent tCOD of 425 mg/L, the primary settlement process may remove 175-180 mg/L (40 % of the tCOD) through the removal of slowly biodegradable settleable COD, but almost all 110 mg/L of rapidly biodegradable and hydrolysable fractions will remain in the settled wastewater (Fig. 3.1). Therefore, the composition of COD present in the settled wastewater, if delivered at a sufficient OLR (> 450 mg/L/d; Escapa *et al.,* 2012) should, theoretically, be more favourable for a biological process than the COD present in the raw wastewater.

The ratio of BOD/COD in the raw and settled wastewater was examined at the three sites that had housed pilot MEC; Howdon (Heidrich *et al.,* 2013, 2014); Fishburn (Pilot 1, Chapter 2) and Chester le Street (Pilot 2, Chapter 4), as a simplified means of determining the bioavailability of the organic material present (Table 3.4).

BOD/COD %	Howdon	Fishburn	Chester Le Street
Raw	43 ± 6	39 ± 8	46 ± 7
Settled	46 ± 6	44 ± 2	43 ± 4

Table 3.4 Ratio of BOD/COD in raw and settled wastewater on three sites which have housed pilot MEC: Howdon, Fishburn and Chester le Street STW.

There was no significant difference in the ratio of BOD/COD across treatment process between the three sites ($F_{(2, 68)} = 1.64$, p=0.202). However, when the treatment stages were considered individually, there was a significant difference ($F_{(5, 68)} = 2.489$, p = 0.04) between the raw wastewater at Fishburn and Chester le Street. Raw influent at Fishburn had significantly less (39 % ± 8) BOD relative to COD than raw influent at Chester le Street (46 % ± 7) (p= 0.039) (Table 3.4).

3.2.5. Fats, Oils and Grease (FOG)

Fats, oils and greases (FOG) often form a large part of the wastewater fraction. It is estimated that 31- 45 % of the COD in municipal wastewater can be attributed to lipids, but these values may vary seasonally (Heukelekian and Balmat 1959; and Raunkjaer *et al.,* 1994). Despite this, the interaction of FOG and treatment process is poorly understood (Chipasa and Mędrzycka, 2008). This can be particularly challenging, when it comes to resolving issues such as sludge floatation and the promotion of filamentous microorganisms (Chipasa and Medrzycka 2008). It was thought that FOG reduced the performance of the MEC in pilot 1 (Chapter 2), causing what appeared to be clogging, from sludge floatation between MEC modules (Fig. 3.2)
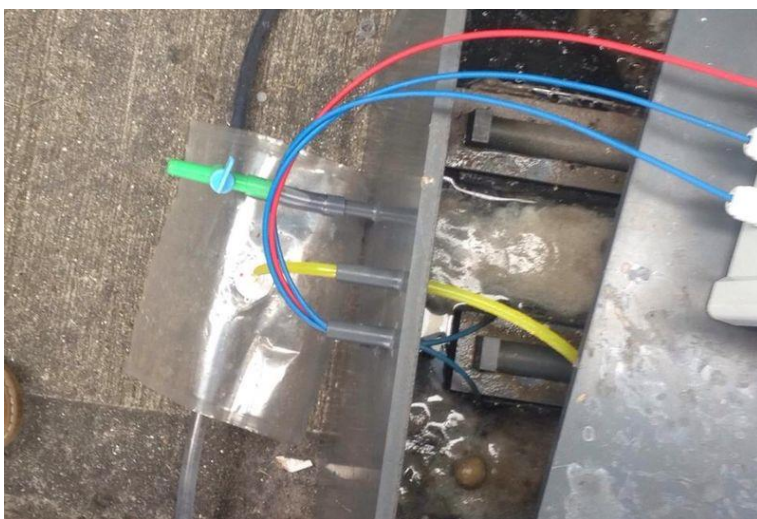
Figure 3.2. Photograph of solids accumulation on the surface of the wastewater between modules 1 and 3 in pilot1.

A short study was conducted to determine the amount of FOG in the wastewater, to compare the three sites that had housed pilot scale MEC (Table 3.5). Evidence of a FOG issue had not been recorded in Heidrich's pilot at Howdon (Heidrich *et al.,* 2013, 2014).

FOG/COD %	Howdon	Fishburn	Chester le Street
Raw	9 ± 4	7 ± 2	10 ± 4
Settled	7 ± 3	10 ± 9	11 ± 6

Table 3.5 Ratio of fats, oils and greases (FOG) concentration (in mg/L) relative to COD (mg/L) at three sites which have housed pilot MEC: Howdon, Fishburn and Chester le Street.

There was no significant difference in FOG as a percentage of COD between raw and settled for any site ($F_{(5, 68)}$ = 1.296, p = 0.277) (Table 3.5). A Tukey's post hoc test showed no significant difference between sites or stage of treatment (p>0.05). When samples were grouped by site alone, there was no significant difference ($F_{(2, 68)}$ = 1.961, p = 0.149) between Howdon and Fishburn (p=0.834) or Howdon and Chester le Street (p= 0.136). Additionally, there was no significant difference between Fishburn and Chester le Street (p= 0.386).

The median FOG concentration in the wastewater at each of the sites (Howdon 16 mg/L, Fishburn 27 mg/L and Chester le Street 19 mg/L) (Fig. 3.3) was lower than expected values (50-150 mg/L, Tchobanoglous *et al.,* 2004). Based on the measured FOG concentration, it is unlikely that insoluble FOG salts were contributing detrimentally to MEC performance.
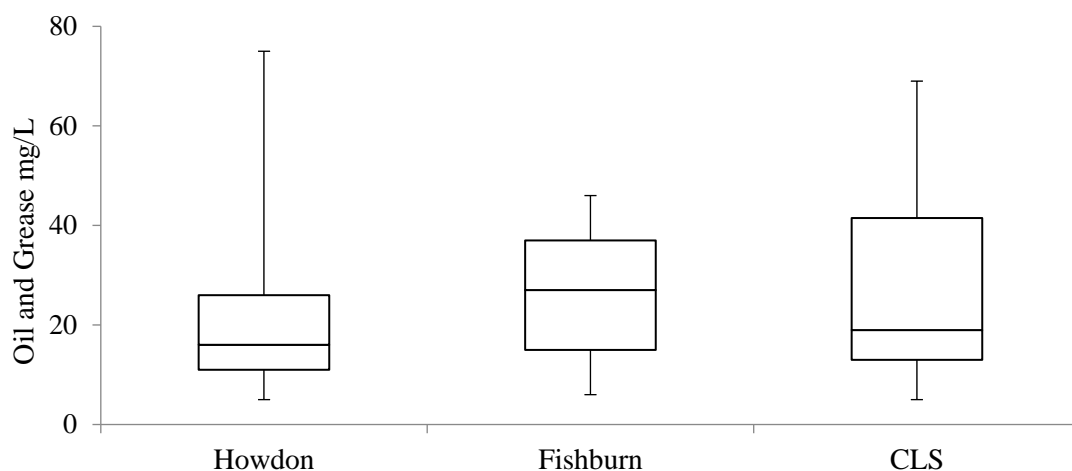
Figure 3.3. Concentration of Oil and Greases (mg/L) in the wastewater at three sites which have housed pilot MEC: Howdon, Fishburn and Chester le Street.

Furthermore, analysis of the fat composition of a scraping taken from the header tank, assumed to be FOG, contained negligible oil and grease (<1 %). Clogging on the surface of the wastewater between MEC modules was observed in both pilot 1 and 2 (Chapter 2 & 4). At the

time of sampling in January 2016, there did not appear to be an issue with FOG clogging at Chester le Street, as observed at Fishburn (in July/August 2014) (Fig. 3.2). Later in operation, an accumulation of solids on the surface of the wastewater in the MEC coincided with a period of biofilm shedding in the trickling filters on the main site (March to July 2016).

Biofilm shedding, or sloughing, occurs largely due to the activity of insect larvae (Tchobanoglous *et al.,* 2004). These larvae dislodge thick biofilms which have accumulated over winter, as temperatures rise during spring (Tchobanoglous *et al.,* 2004). This process, which affects the COD and suspended solids measured in the effluent, was observed in the MEC. When sloughing ceased in the trickling filters, so too did the volume of solids accumulation in the MEC. Given that MEC have a fixed biofilm, it is highly likely this would be subject to a period of shedding with seasonal environmental changes, most notably temperature.

3.2.6. Chemical dosing
The electrochemically active bacteria present in the MEC biofilm contribute to the system via extracellular electron transfer (EET). This process can be direct or indirect. In direct EET, direct contact is necessary between the bacteria and the electrode to transfer electrons from the inside of the cell to the circuit (Rozendal *et al.,* 2008). In indirect EET, the electrons are transferred to the electrode via redox cycling of electron shuttling compounds. These compounds are either produced by the bacteria themselves or naturally occurring in the wastewater (Rozendal *et al.,* 2008).

Samples were taken prior to, within and post-MEC in the large MEC from pilot 2 (Chapter 4). These samples were used to analyse the relative concentration of iron species (Fe^{2+} and Fe^{3+}) (Table 3.6). Quantification of reduced iron (Fe^{2+}) and total iron was performed using the 1,10-phenanthroline method (Appendix E). The aim was to determine whether *Geobacter*, which was assumed to be present in the anodic community, was donating electrons to Fe^{3+} present in the wastewater, rather than to the graphite electrode. This would interrupt the redox cycling necessary for indirect EET, and lower current production. Fe^{3+} was expected to be present in the wastewater due to chemical dosing prior to the MEC.

In natural environments, iron oxides, which are usually in crystalline form in soils and sediments (Weber *et al.,* 2006a; Weber *et al.,* 2006b), can be reduced by mixed cultures containing *Geobacter* and *Shewanella* species. The family Geobacteraceae are one of the most

studied and most abundant contributors to the process of dissimilatory Fe (III) reduction and oxidation of organic matter (Caccavo *et al.,* 1994; Weber *et al.,* 2006a; Weber *et al.,* 2006b).

It was initially thought that this attribute required the formation of extracellular appendages such as pili or flagella, to directly attach to the surface of the iron oxide. It has since been reported that the function of the pili is to act as an electrical connection, rather than as an anchoring mechanism (Weber *et al.,* 2006a). This enables cells to release electrons extracellularly, to Fe^{3+} or electron acceptors such as the anode in a bioelectrochemical system. Therefore, if *Geobacter* was present in the anodic community, it is possible that electrons may have been donated to Fe^{3+} in the wastewater, rather than to the graphite electrode, lowering current production and the efficiency of the MEC.

	Sample condition	Fe (II) mg/L	Fe(tot) mg/L
MEC influent	Unfiltered	0.40	5.02
	1.2μm filtered	0.13	2.82
	0.2 μm filtered	0.06	0.31
MEC tank	Unfiltered	1.26	16.3
	1.2μm filtered	0.15	0.56
	0.2 μm filtered	0.05	0.44
MEC effluent	Unfiltered	0.47	3.74
	1.2μm filtered	0.15	0.71
	0.2 μm filtered	0.06	0.52

Table 3.6 Iron speciation prior to, within and post-MEC after ferric sulphate dosing in the raw wastewater. Each sample was analysed in duplicate under triplicate conditions: unfiltered, and with a coarse (1.2μm) and fine (0.2μm) filter.

The amount of unfiltered Fe^{2+} showed a three-fold increase from the settled domestic wastewater influent (taken from the site) to the tank, where the exoelectrogenic biofilm was present. This observation is perhaps misleading, as the amount of Fe^{2+} relative to the total Fe in the wastewater remained consistent between influent (Fe^{2+} = 8% of total Fe) and MEC tank (Fe^{2+} = 7.7% of total Fe). The fact that Fe^{2+} concentration remained consistent implies that both

Fe^{2+} and Fe^{3+} increased within the MEC reactor. An accumulation of both Fe species in the liquid phase in the tank may occur because of electron cycling between the two (i.e. dissimilatory Fe^{3+} reduction and Fe^{2+} oxidation coupled with reduction of NO_3^- to NH_4^+), or as an artefact of the variable ferric dosing rate and 5-hour retention time. The former would have a direct impact on current production, reducing the number of electrons reaching the MEC electrode. The latter would have no consequence on current production.

It is possible, but unlikely that the removal of nitrate (from 1.1 mg/L to 0.6 mg/L) can be attributed to the oxidation of Fe^{2+} (which is coupled with reduction of NO_3^- to NH_4^+). It is unlikely because the amount of ammonium decreases in the MEC (18 mg/L to 13 mg/L) (Table 3.7). Whilst redox cycling is possible, it is unlikely (given the values recorded in Table 3.6-3.7) to be having a significant detrimental effect on current production.

	Ammonium (NH_4^+ mg/L)	Nitrate ($mgNO_3^-$/L)	Nitrite ($mgNO_2^-$/L)
MEC influent (1°settled wastewater)	18 ± 6	1.1 ± 1.1	0.4 ± 3.5
MEC effluent (after 2°anaerobic treatment)	13 ± 5	0.6 ± 1.1	0.4 ± 1.1

Table 3.7 Average wastewater characteristics, including ammonium, nitrate and nitrite, (all recorded in mg/L) of the influent and effluent wastewater from pilot 2.

Raw wastewater with a chemical oxygen demand (COD) in the range of 250-430 mg/L typically contains between 12 and 25 mg/L of ammonium, and 0 mg/L of nitrate and nitrite (Tchobanoglous *et al.,* 2004; Henze and Comeau, 2008). The values observed in the second MEC pilot (Chapter 4) (Table 3.7) indicate that there has been some, but not complete, nitrification and therefore, whilst the nitrate concentration is low (and shows evidence of removal within the MEC) this is not a consequence of good denitrification, but rather a lack of full nitrification of the waste.

3.3 Temperature

A drop in performance, in terms of power density, is associated with a drop in temperature. This occurs in systems that are acetate-fed (Liu *et al.*, 2005b; Patil *et al.,* 2010; Behera *et al.,* 2011; Cheng *et al.*, 2011; Lu *et al.*, 2012; Li *et al.*, 2013; Wei *et al.,* 2013; Gonzalez de

Campo *et al.,* 2013; Zhang *et al.*, 2014) and those using more complex wastes (Ahn and Logan, 2010; Larroso-Guerrero *et al.,* 2010). Linear relationships between temperature and performance were reported by Cheng *et al.* (2011) and Lu *et al.* (2012) showing that as temperature drops, so does power output (Fig. 3.4). This drop was reported as 33 mW/°C (Cheng *et al.,* 2011) but varies between 5-60 mW/°C across studies (Fig 3.4).
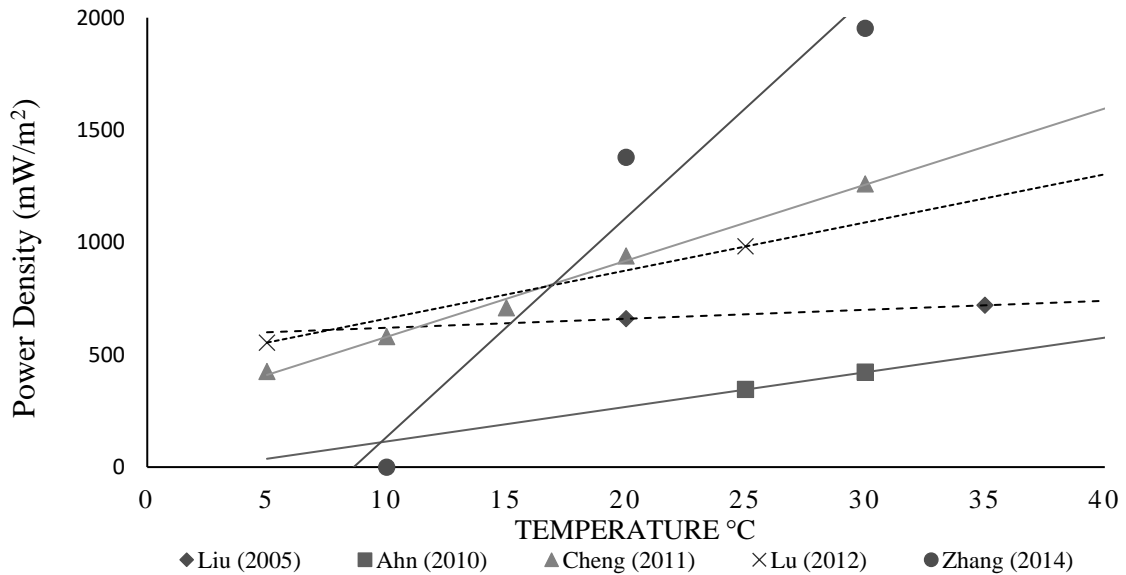
Figure 3.4. Relationship between power density (mW/m^2) and temperature (°C) between 5 and 35°C. As temperature decreases so does power density; shown to drop 5 - 60 mW/°C.

MEC could be applied over a wide range of temperatures but it is unlikely, in a real-world application, that a constant fixed temperature will be maintained. The MECs in this study were operated in the north east of England. The Met Office historic climate data suggests a yearly maximum average temperature of 13.1°C and a yearly minimum average temperature of 5.6 °C, taken from an average of monthly data across five years (2010-2014 inclusively, Table 3.8).

	Summer		Winter	
	Max °C	Min °C	Max °C	Min °C
Durham	19.5	9	8.8	2.2

Table 3.8. Maximum and minimum average temperatures for summer and winter in Durham, UK. Taken as an average of Met Office Historic Climate Data from 2010 -2015.

Zhang *et al.,* (2014) studied the effect of a fluctuating temperature, mirroring diurnal temperature fluctuations that may occur in a warm temperate climate. A warm temperate climate includes: those with dry summers (classified as Cs), usually known as a 'Mediterranean' climate, including the countries bordering the Mediterranean Sea, south-western Australia, California, and south-western South Africa; and more humid temperate

climates (classified as Cf), such as the east coast of the USA and Japan and much of Europe (Kottek *et al.,* 2006).

Zhang *et al.*'s observed that fluctuating the temperature of MFCs diurnally generated a higher power density than MFCs operated at a fixed temperature (Zhang *et al.,* 2014). This observation was most notable for the MFC operated at 6 °C; when operated at a fixed temperature, the MFC had no power output; when the temperature was fluctuating between 6 and 18 °C, the power density at 6 °C was 759 mW/m^2. The increase in power density achieved through diurnal fluctuation was not limited to the lower end of the temperature range (Fig. 3.5). The power density achieved at 30 °C in the MFC fluctuating between 18 and 30 °C was 11 % higher than the value obtained when it was operated constantly at 30°C.
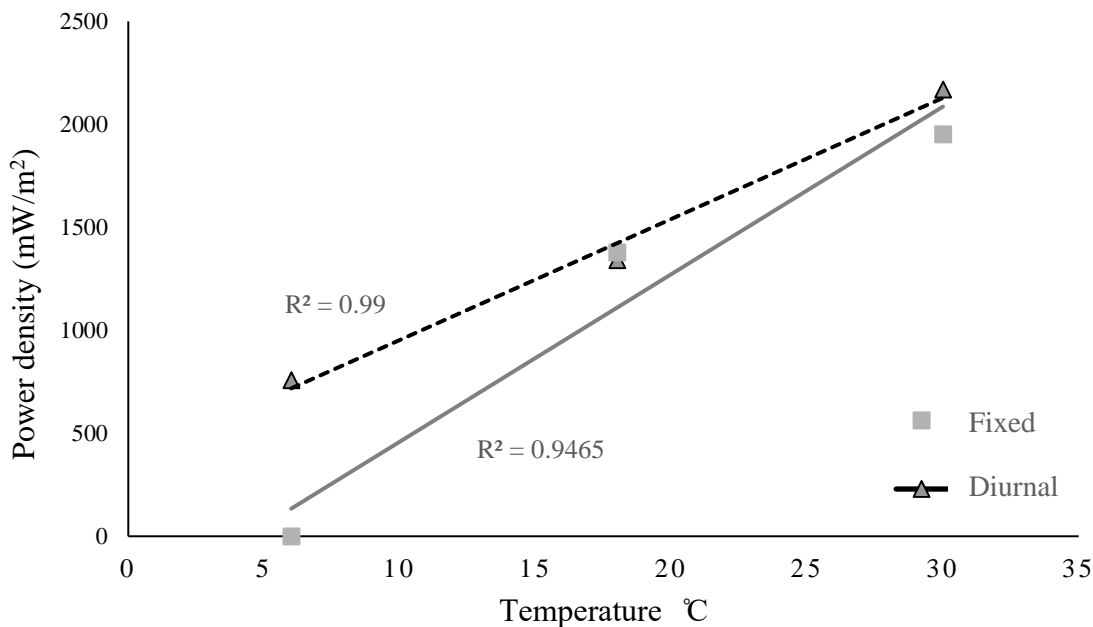
Figure 3.5. Effect of diurnal temperature fluctuation (°C) on power density (mW/m^2). This shows the results of three reactors operated at a fixed temperature of 6, 18 and 30°C (grey), and two reactors where the temperature fluctuated between 6/18°C and 18/30°C (black).

Assuming the temperature in Durham is as described in Table 3.6, the temperature drop from summer to winter would be expected to lower the power density by 300 mW/m^2 to 500 mW/m^2, based on the assumptions of 33 mW/°C (Cheng *et al.,* 2011) and 58 mW/°C respectively (Zhang *et al.,* 2014). By contrast, Heidrich *et al.,* (2014) did not report a significant correlation between temperature and performance (Fig. 3.6). When energy recovery is plotted against temperature (Fig. 3.6), they follow a similar trajectory, suggesting that performance drops during the winter and peaks in the summer, but this result was not significant (Pearson's correlation, 0.306, *p* = 0.009) (Heidrich *et al.,* 2014).
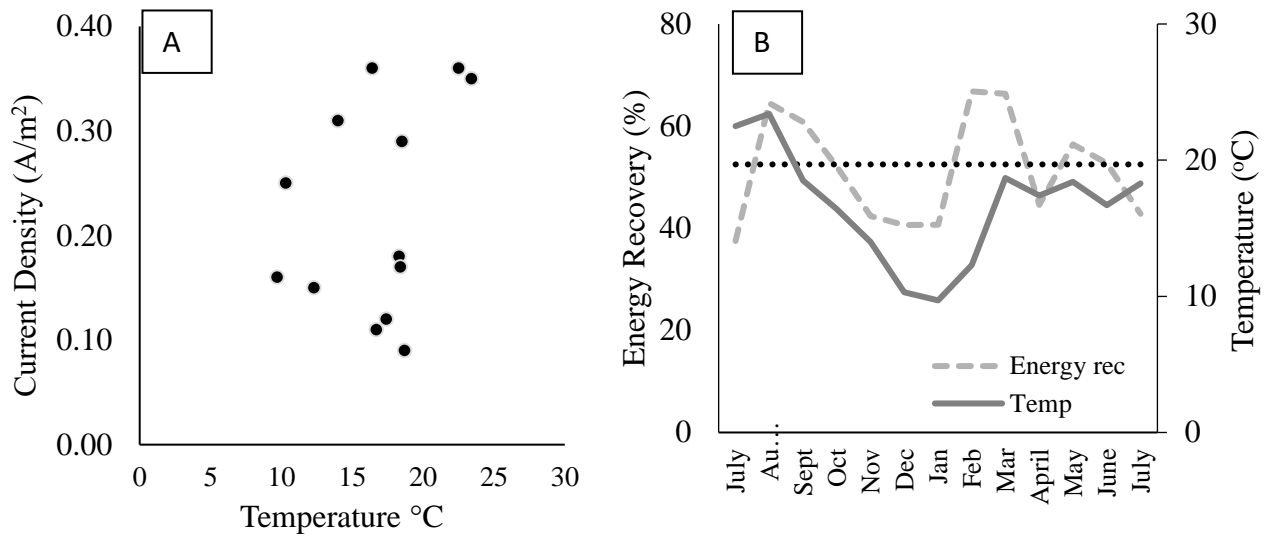
Figure 3.6. Effect of temperature on MEC performance in a pilot scale MEC (Heidrich et al., 2014). A) effect of temperature on current density, B) relationship between energy recovery (solid line) and temperature (dashed line) over a 12-month period.

	Energy Recovery (%)	Deviation from Mean (%)
August	64.5	12
September	60.8	8.3
October	52.1	-0.4
November	42.4	-10.1
December	40.6	-11.9
January	40.7	-11.8
February	66.8	14.3
March	66.3	13.8
April	44.6	-7.9
May	56.4	3.9
June	52.7	0.2
July	42.8	-9.7

Table 3.9 Average monthly energy recovery of a pilot scale MEC (Heidrich et al., 2014). Average energy recovery was 53%. Deviations from the mean show gains and losses.

The energy recovery in Heidrich's reactor across 12 months (Aug-July) averaged 53 % (Table 3.9) (Heidrich *et al.,* 2014). The average deviation from the mean during summer months (May-October) was +2.38 %, in comparison to -2.27 % for winter (Nov-April). This suggests gains in the summer offset the losses in the winter. This raises questions over whether the

microbes that acclimate during start up can work year-round, or if their optimal performance is seasonal.

Michie *et al.,* (2011) investigated whether temperature during the start-up period influenced the performance of BES during operation. To cover a temperate range, they acclimated reactors at 10, 20 and 35 ℃, which each showed a varied response to changing temperature. The reactor acclimated at 20 ℃ could adapt to the range of operational temperatures, achieving optimal steady-state voltage in each condition. However, the 35 ℃ acclimated reactor showed a rapid drop in voltage output with decreasing operational temperature. The 10℃ acclimated reactor, whilst able to cope with increases to 20 ℃, was negatively affected by a temperature increase to 35 ℃ (Michie *et al.,* 2011). This implies, that for countries with seasonal temperature changes, the time of year in which the reactor is started up will influence how well it can maintain performance throughout the year. For cold temperate climates, starting up between spring and autumn may provide the best conditions for developing a biofilm that is robust to the temperatures it is likely to endure.

Temperature at start up is also likely to affect the length of time it takes the biofilm to develop. Reactors acclimated at 35 ℃ may take as little as 20 % of the time to reach optimal steady-state voltage as rectors started up at 10 ℃ (Michie *et al.,* 2011). Furthermore, Cheng *et al.,* (2011) noted that reactors acclimated at temperatures below 10 ℃ failed to start-up altogether. However, those acclimated at >15 ℃ could maintain performance when temperature dropped below 10 ℃ after optimal steady-state voltage had been achieved (Cheng *et al.,* 2011). This supports the previous suggestion that spring-autumn start-up times may be optimal for MEC robustness in the UK, allowing for colonisation of the anode at milder temperatures with adaptation to colder periods during winter.

3.4 Sulphate

Sulphate-reducing bacteria (SRB) are anaerobic prokaryotes, found in a variety of natural environments ranging from soils and sediments to the guts of animals. They primarily use sulphate or sulphur as terminal electron acceptors, but some strains can use other molecules such as nitrate (Cordas *et al.,* 2008). Furthermore, the versatility of their metabolism, which is well documented (Hansen, 1994; Fauque and Ollivier, 2004), demonstrates that they can make use of a variety of carbon sources and respiratory substrates providing the capacity to rapidly adapt to fluctuations in their environment (Carepo *et al.,* 2002).

A versatile metabolism is a useful trait to have in a wastewater biofilm, where fluctuation in carbon source and availability of electron acceptors and donors is likely. Hydrogen also plays an important and diverse role in the metabolism of SRB species: it can be used (to support redox reactions in sulphate respiration) or produced (in the absence of sulphate) (Carepo *et al.*, 2002).

SRB genera *Desulfobacter*, *Desulfobulbus*, *Desulfobacterium* and *Desulfovibrio* were found in the biofilms of Heidrich *et al.*,'s MEC (2013, 2014) and the first pilot MEC from this study (Chapter 2) (with 3.6 %, 3.8 %, 3 % and 1.2 % of the anode comprised of each of the aforementioned genera respectively). These SRB may influence MEC performance, by contributing to current generation and/or using the hydrogen produced (Carepo *et al.*, 2002; Ishii *et al.*, 2014). The relative abundance of bacteria present in the anodic communities of both MEC from this study are discussed in Chapter 5.

SRB are commonly found in sewer systems, where anaerobic conditions facilitate the reduction of sulphate to hydrogen sulphide, causing significant corrosion of concrete assets when the sulphide is exposed to air and oxidised to sulphuric acid (Parker, 1945; Rauch and Kleidorfer, 2014). Utilities have focused on removing sulphide thus far, in the prevention of deterioration of pipe networks and assets, seeing the presence of sulphates in wastewater and sewers as unavoidable (Pikaar *et al.*, 2014).

Sulphates arrive in wastewater from a variety of sources, but most commonly from the inorganic coagulants used in treatment processes, including aluminium sulphate used to remove solids during flocculation in potable water treatment (Pikaar *et al.*, 2014) and ferric sulphate used to aid phosphorous removal in the treatment of wastewater. The nature of the sewer itself - whether a gravity fed combined sewer, or a pressurised rising main - will also affect the likelihood of the conversion of sulphate to sulphide and subsequently to sulphuric acid. Septicity is more widely documented downstream of rising mains (Alibahi *et al.*, 1994), but can also occur in gravity fed sewers if the self-cleaning velocity is not maintained.
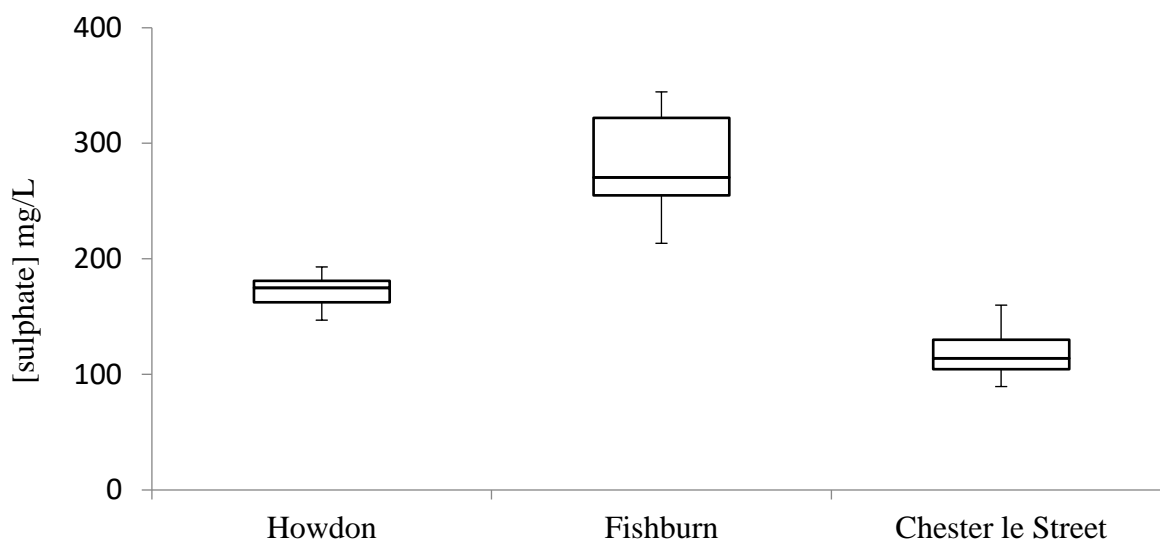
Figure 3.7 Comparison of sulphate concentration (mg/L) in the raw wastewater at three pilot sites: Howdon, Fishburn and Chester le Street.

A one-way ANOVA showed a statistically significant difference between measured sulphate concentration in the raw wastewater at the three STW's that housed MEC pilot plants ($F_{(2,45)}$ = 157.642, p = 0.000). A Tukey's post hoc test revealed that the amount of the sulphate in the wastewater was statistically significantly higher at Fishburn (284 mg/L ± 41) than Howdon (170 mg/L ± 14, p =0.000) and Chester le Street (118 mg/L ± 18, p=0.000) (Fig. 3.7). Chester le Street is the only site of the three with a phosphate consent, and consequently the only site to dose ferric sulphate. Despite this, the wastewater at Fishburn STW contained significantly more sulphate (than Chester le Street or Howdon) and therefore, it was likely that there was another factor influencing the amount of sulphates present in the wastewater. This could be an artefact of the sulphate concentration in the potable water, as each of the sites are associated with different water treatment works.

All three sites were located in the north east of England; the former (Heidrich *et al.,* 2013, 2014) in Tyne and Wear and the latter two (Chapter 2 and 4) in County Durham. However, the site that had significantly more sulphate present in the wastewater was located in the heart of Durham's collieries. Sulphate is often associated with abandoned mines: a typical characteristic of the ground and surface waters from mines is a high concentration of sulphate. This occurs as a consequence of the oxidative dissolution of pyrite (FeS_2) which becomes exposed, and thus oxidised, during mining (Edwards *et al.,* 1999). The disulphide (S_2^{2-}) then dissolves in water before it is oxidised further to sulphate (SO_4^-). The sulphate concentration recorded in these sewage treatment works may be elevated from pervasive sulphur

compounds in the environment. This concentration may be elevated by ingress to the wastewater network through surface water, drainage or infiltration.

Fishburn colliery operated for over 60 years before it closed in 1973 (Durham County Record Office, 2016) and the location of the sewage treatment works is within the boundaries of the colliery (Fig. 3.8a). Comparatively, Chester le Street STW is further away from its nearest colliery (approx 2km as the crow flies away from Pelton Fell Colliery) (Fig. 3.8b). The pervasive nature of mine water pollution, which can persist for centuries, makes it plausible that the elevated sulphate observed in the wastewater network could be related to the proximity of the abandoned coal mine.
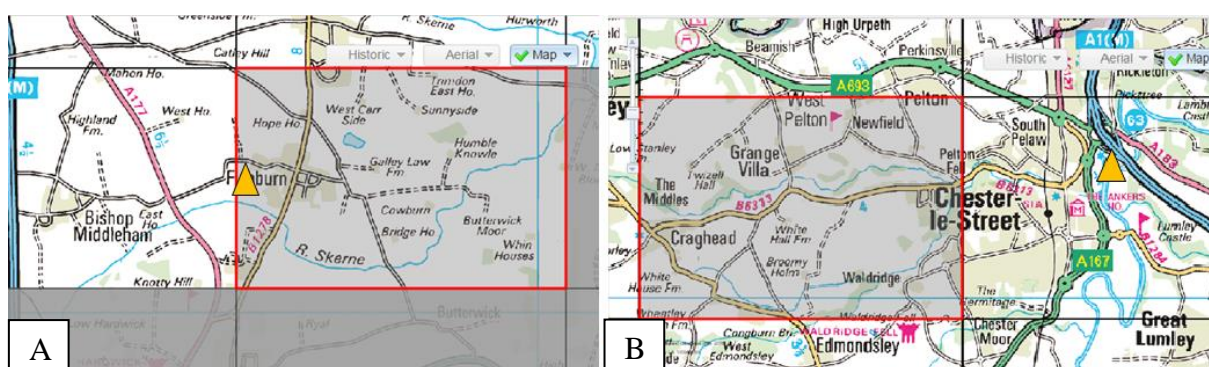
Figure 3.8. Location of pilot sites (yellow triangle) relative to their nearest collieries (solid red line) (which are now closed). A) Fishburn STW relative to Fishburn Colliery. B) Chester le Street STW relative to Pelton Fell.

It is likely to be a combination of factors, rather than one direct cause, influencing the influent sulphate concentration. As sulphate concentration is not routinely measured by Northumbrian Water, the cause of elevated influent sulphate concentration in this study cannot be defined.

3.5 Hydrogen-scavenging

The cathode of MECs, arranged in the configuration outlined in Chapter 2, should theoretically be abiotic. However, when operated for long periods with high hydrogen retention times (to readily capture hydrogen from the system), proliferation of H_2-consuming microorganisms may occur. These microorganisms, such as homoacetogenic bacteria (which are strictly anaerobic), would undermine the performance of the MEC through the conversion of hydrogen to acetate (Ruiz *et al.,* 2013). The activity of homoacetogenic bacteria in the cathode may lead to the formation of a H_2-acetate loop: increasing the energy requirement of the MEC and lowering the yield of hydrogen recovered from the system (Lee *et al.,* 2009; Parameswaran *et al.,* 2009; Ruiz *et al.,* 2013; Rago *et al.,* 2015). Furthermore, if hydrogen

leaks into the anode chamber, the growth of H_2-oxidizing anode-respiring bacteria (ARB) would be encouraged, further decreasing hydrogen yield and performance.

Creating a physical barrier between the anode and cathode has obvious benefits; a larger yield and higher purity of hydrogen can be achieved with a membrane, which would limit the opportunity for scavenging to occur. However, even when a barrier is used, if the pore size is large enough to permit bacteria through (like the separator used in this research), then they likely to be found in the cathode.

Six cathode samples were taken for 16S DNA sequencing. The environment in the cathode was cold (8.1℃ ± 0.6), salty (0.1M NaCl), alkaline (pH = 11 ± 2) and nutrient-poor relative to the anode (cathodic COD 15-20% of anodic COD at ~50 mg/L). This environment would not be expected to support as many microorganisms as the anode compartment, which had a less alkaline pH (8.06 ± 0.23) and more abundant supply of organic material (COD = 342 mg/L ± 200). Analysis of the samples sent for 16S DNA sequencing showed that fewer taxa of microorganisms were found in the cathode (545 taxa, Simpson's index = 0.945) than the anode (887 taxa, Simpson's index = 0.964) (Fig. 3.9).
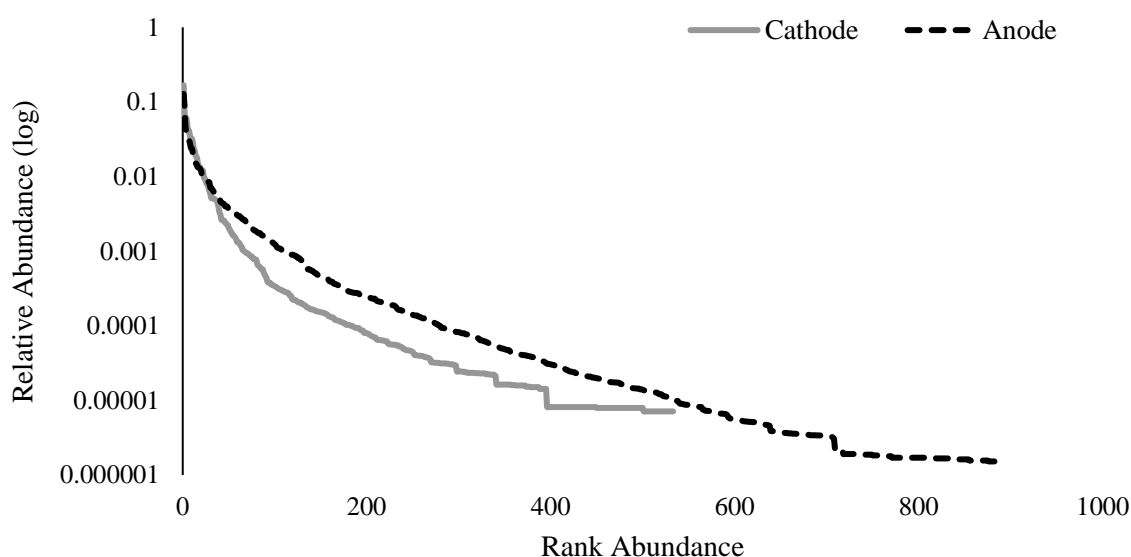
Figure 3.9 Rank abundance curve for anodic and cathodic communities from pilot 2. Log relative abundance of anode (dashed black line) and cathode (solid grey line) samples taken from the Medium MEC in this study (Chapter 4).
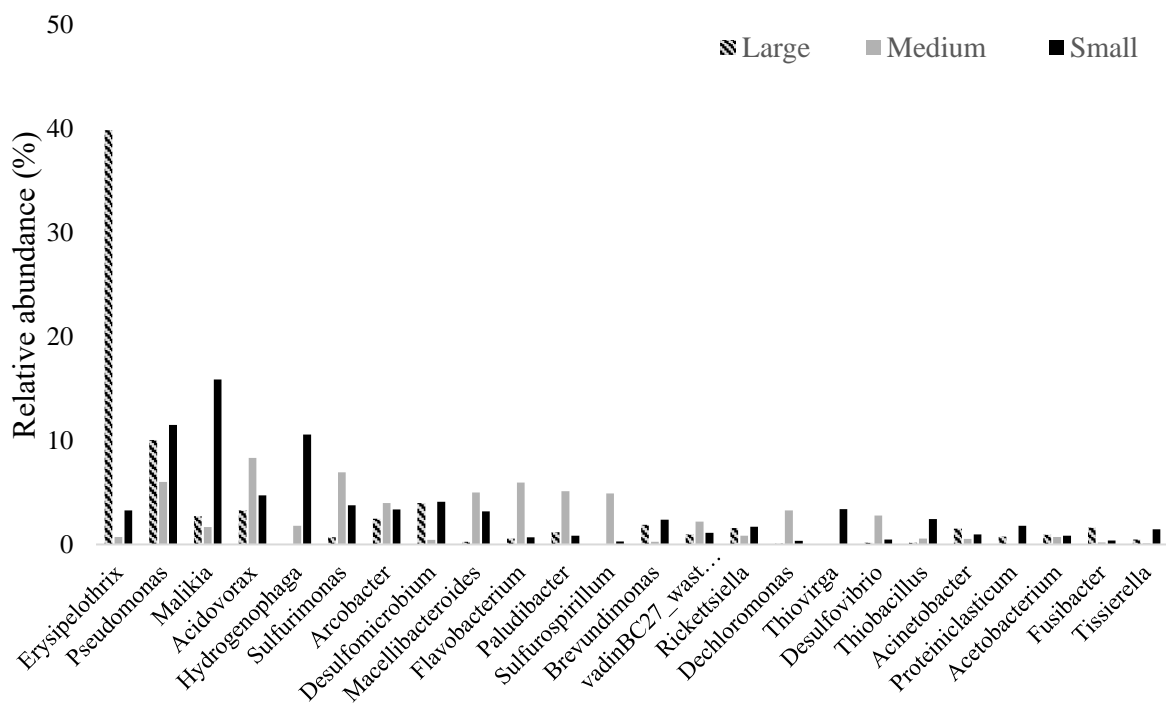
Figure 3.10 Most abundant genera in the MEC cathodic communities in pilot 2 (Chapter 4). Hydrogen-scavenging bacteria including Acetobacterium, a homoacetogenic genus which converts hydrogen into acetic acid; Sulfurimonas, a genus of bacteria which uses hydrogen as an electron donor; and Hydrogenophaga, a facultative hydrogen autotroph, are present.

The most prevalent genera were considered for each of the cathode samples (Fig. 3.10). The relative abundance of each genus varied between the three samples, however these genera constitute 73 % ± 9 of each catholyte community. The microorganisms capable of oxidising hydrogen in anaerobic respiration are usually acetogens, methanogens and SRB. All cathode samples analysed via 16S DNA sequencing included several genera of sulphate- and sulphur-reducing deltaproteobacteria, totaling 5% of each sampled community (Fig. 3.10). These included *Desulfomicrobium* and *Desulfovibrio*, genera which are unable to oxidise acetate and use hydrogen as an electron donor for anaerobic respiration; and *Sulfurospirillum,* a dissimilative sulphur reducer which uses hydrogen to reduce elemental sulphur (Madigan *et al.,* 2012).

Similarly, an acetogen, *Acetobacterium, was* observed in all three samples (Fig 3.10). *Acetobacterium* is an obligate anaerobe usually found in sewage and sediment. A homoacetogen, *Acetobacterium,* would use available hydrogen, produced in the cathode, to generate acetic acid. Besides the acetogens and SRB, there are many other organisms which use hydrogen as a sole electron donor. These are grouped as the chemolithotrophic hydrogen-oxidising bacteria (Madigan *et al.,* 2012). In the three cathode samples, hydrogen-oxidisers

such as *Acidovorax, Hydrogenophaga* and pseudomonads such as *Pseudomonas* and *Brevundimonas* were found (Fig. 3.10). Pseudomonads are usually obligate respiratory bacteria; however, many can grow in anoxic conditions using nitrate or fumarate as an electron acceptor (Madigan *et al.,* 2012). Other bacteria of note included anaerobic haloterant genera such as *Fusibacter and Macellibacteroides:* fermentative bacteria able to grow in up to 2-3% NaCl w/v. Both genera produce volatile fatty acids as products of glucose fermentation (Ravot *et al.,* 1999; Jabari *et al.,* 2012)

It was of interest to determine whether hydrogen loss was possible by the scavenging bacteria listed above. The ten genera described above accounted for 25-46 % of the sampled cathode communities. It is likely that hydrogen loss (to acetogenic bacteria) was common across all modules, even though the yield of hydrogen obtained from each module varied considerably.

The concentration of VFAs in the cathodes of MECs where hydrogen scavenging bacteria were found (Large MEC = 16 mg/L ± 2, Medium MEC =27 mg/L ± 6 and small MEC = 20 mg/L ± 6) was similar or slightly higher than the concentration of VFAs in the anode (Large MEC = 18 mg/L ± 1, Medium MEC = 16.95 mg/L ± 0.05 and 14.4 mg/L ± 0.2). Furthermore, the VFA concentration accounted for 42 % ± 11 of the cathodic tCOD compared with 6.6 % ± 0.8 of the anodic tCOD. The cathodic VFA concentration, combined with the community composition observed, may be indicative of hydrogen loss to acetogenic processes in the cathode. The cathodic VFA concentration is equivalent to the production of 110-140 mg of acetate (2 mmol), which would account for the consumption of approximately 8 mmol of H_2 (i.e. 200 mL). This may be a conservative estimate of hydrogen loss, as the mixed consortia in the cathode suggests that hydrogen may be scavenged by more than one pathway.

The presence of hydrogen-scavenging bacteria in the cathode chamber is problematic for the efficiency of MECs system producing hydrogen. A low cathodic coulombic efficiency suggests that the current generated at the anode is not being converted into measurable hydrogen gas. If the hydrogen scavenging bacteria proliferate, then their consumption of hydrogen could approach or equal the production. As such, yield would continue to decrease until complete cessation of gas capture. This problem could be solved by: eliminating the bacteria from the cathode, or removing the hydrogen from the system before it can be scavenged. The former could be achieved by modifying the pH or sterilizing the catholyte solution periodically, inhibiting the anaerobic acetogenic bacteria. Recovering hydrogen more efficiently from the system, may be more achievable than creating and maintaining a sterile

environment in the cathode whilst submerged in wastewater. Recirculating the catholyte would decrease the retention time of the hydrogen in the cathode, limiting the potential for the hydrogen to be scavenged (Baeza *et al.,* 2017). Another possibility would be to design the MEC architecture to decrease the distance for the H_2 to travel from the site of production to capture (i.e. wide, shallow cassettes).

An alternative option may be to harvest acetate, with hydrogen as the secondary product (Gildemyn *et al.,* 2015, Patil *et al.,* 2015). The value of acetate is reported to be 0.5 €/kg (Andersen *et al.,* 2014). However, there is a large potential to exploit this. Acetate is the precursor to a variety of chemical products and 10 million tons of acetate/year are produced petrochemically (Schiel-Bengelsdorf and Dürre, 2012). Acetogenic bacteria, such as *Acetobacterium* and *Clostridium*, make use of the Wood–Ljungdahl pathway (Schiel-Bengelsdorf and Dürre, 2012). Production of acetate through the Wood-Ljungdahl pathway would provide environmental benefits through the conversion of greenhouse gases to industrial products (Schiel-Bengelsdorf and Dürre, 2012 and Spirito *et al.,* 2014).

Chapter 4. Domestic wastewater treatment in a 200L MEC

Parts of this chapter are submitted for publication as Cotterill, S.E., Dolfing, J., Jones, C., Curtis, T.P and Heidrich, E.S. Upscaling MEC Technology - Domestic Wastewater Treatment in a 200 L Microbial Electrolysis Cell.

4.1. Introduction

The results in this chapter arise from the second pilot study in this thesis and the third pilot from a collaboration between Newcastle University and their industrial partner, Northumbrian Water Ltd. The first pilot (Heidrich *et al.,* 2013, 2014) functioned as a 'proof of concept'; the second failed within 6 months, providing opportunities for learning (Chapter 2).

In this study, three MECs of increasing scale were designed, built and operated for 9 months, from October 2015 until May 2016. Two of the MECs were operational at the time of writing, but the results from June until December 2016 are not included. The smallest of the three, containing eight modules with anodes measuring 0.06 m^2, was comparable in electrode size and surface area to the previous two pilots (Chapter 2 and Heidrich *et al.,* 2013, 2014), however the volume of the tank was much smaller at 30 L, giving a surface area to volume ratio of 32 m^2/m^3. The medium sized MEC was scaled up by a factor of 4. The 45 L tank contained three modules, each with anodes measuring 0.24 m^2, giving a surface area to volume ratio of 32 m^2/m^3. Finally, the largest MEC, which was 16 times bigger than the original, contained three modules with anodes measuring 1 m^2 in a tank with an empty bed volume of 175 L and a surface area to volume ratio of 34 m^2/m^3. The three MECs were installed on a domestic sewage treatment works (STW) in the north east of England, with the aim of operating for a period over 12 months.

The pilot plant was fed settled domestic wastewater (average influent COD of 340 mg/L) which had been dosed with ferric sulphate and sodium hydroxide to meet the STW's ammonia (<10 mg/L) and phosphorous (<2 mg/L) consents. The reactor was not supplemented with acetate, and buffers were not used to control pH. There was no temperature control on the reactor; it was housed in a modified shipping container (Fig. 4.1) and operated during winter and spring at ambient temperatures (wastewater 5.3-16.6℃).

The largest MEC in this study achieved: effective wastewater treatment to the European Urban Wastewater Treatment Directive (UWWTD) consent for chemical oxygen demand

(COD); recovery of energy from wastewater; and a robust ability to produce hydrogen and remove COD at low temperatures, with low strength wastewater.

Figure 4.1 Photographs of the modified shipping container at Chester le Street STW. Modifications were made to the outside (A-B) and inside (C) of the container for it to house three MEC pilots of increasing scale (D).

4.2 Methods

4.2.1 MEC design

Each of the three scales of MEC reactor were based on a cassette-style design previously described by Heidrich *et al.,* (2013, 2014) for a reactor with a volume of 100 L. The three MECs were scaled up in terms of electrode surface area, by a factor of 1, 4 and 16 for the small, medium and large trials in this study, respectively (Table 4.1). The small MEC housed eight modules, to enable comparison with the prior studies which had six (Heidrich *et al.,* 2013, 2014) and ten modules (Chapter 2) respectively. The medium and large MECs, however, only contained three modules, because of the need to provide replicability and the limitations of space in the pilot plant.

Each cassette-style module contained two anodes, thus in the large MEC there was a total anodic surface area of 6 m^2, an effective anodic volume of 175 L and a surface area-to-volume ratio of 34 m^2/m^3 (Table 4.1). Each module had a cathode, measuring 0.8 m^2 in the large MEC, which was contained within a chamber that was filled with 0.1M NaCl, with a total volume of 7.2 L (Table 4.1).

Scale	Anode (m^2)	Cathode (m^2)	Anodic tank volume (L)	Cathodic volume (L)	Anodic surface area to volume ratio (m^2/m^3)
Small	0.06	0.05	30	0.5	32
Medium	0.24	0.20	45	1.8	32
Large	1.00	0.80	175	7.2	34

Table 4.1 Dimensions of the three MEC in pilot 2, including anode, cathode and tank sizes.

Samples of graphite felt were assessed for resistivity prior to the purchasing of materials for the pilot plant. Samples were obtained from two suppliers, (Olmec, UK and SGL, Germany) and assessed for different material thicknesses (Table 4.2). A handheld voltmeter was used to measure the resistance in two dimensions. The first measurement was across the plane of the surface, where an average was taken of the two diagonal measurements: top left to bottom right and top right to bottom left. The second measurement was through the thickness of the material, where an average was taken of three spot measurements between the front and back surfaces (Table 4.2). Following this comparison, 4.6 mm felt from SGL was selected.

The structure of each module was based on a 9 mm thick PVC frame, measuring 1.2 m x 0.8 m (large), 0.8 m x 0.6 m (medium) and 0.3 m x 0.2 m (small). This frame housed the stainless steel cathode and the 0.1M NaCl catholyte. The cathode was comprised of a flat sheet of 316 stainless steel mesh (Patterson Ryan Wireworkers Ltd., UK) with stainless steel wire wool (Merlin, UK) woven throughout (Fig. 4.2a). The cathode chamber was sealed on both sides by a non-selective battery separator (Entek, UK) (Fig. 4.2b) and sandwiched by a graphite felt anode (SGL, Germany) and stainless steel current collector (Patterson Ryan Wireworkers Ltd. UK) (Fig. 4.2c). Low cost materials were used throughout: the largest reactor cost £1,308 of which the cathode and membrane represented only 9% of the total outlay.

The modules were spaced 10mm apart, on alternate sides of the MEC to create a serpentine flow path through the tank (Fig 4.3a). Wastewater was delivered to the MEC through an inlet (positioned in the top left hand corner of the tank), flowed past the surface of each module,

and then exited via an outlet (in the bottom right hand corner of the tank). Recirculation pipework was built in, midway between these two points (vertically) to increase mixing to prevent mass transfer limitations (Fig 4.3b)
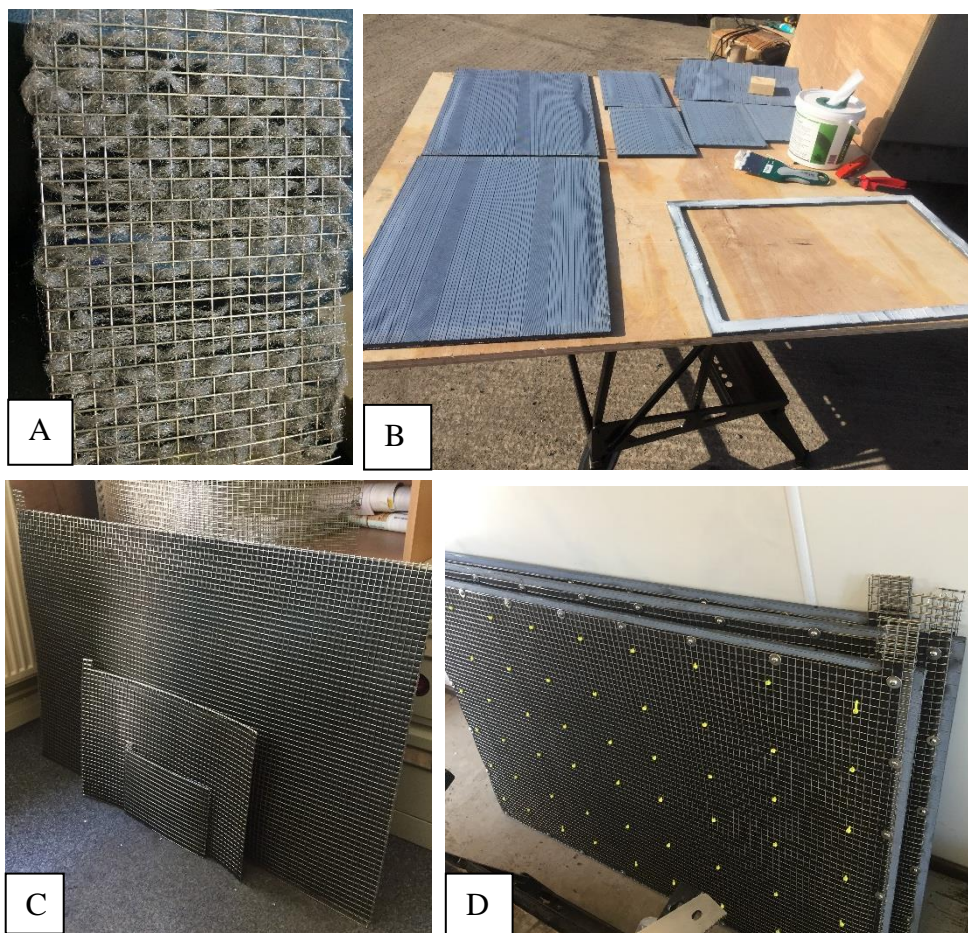
Figure 4.2 Structural components of each MEC module: A) a stainless steel wire wool and mesh cathode from the small MEC, B) the PVC frame and membrane for the medium and small MECs, C) three graphite felt anodes, one from each scale and D) the three assembled modules for the large MEC.
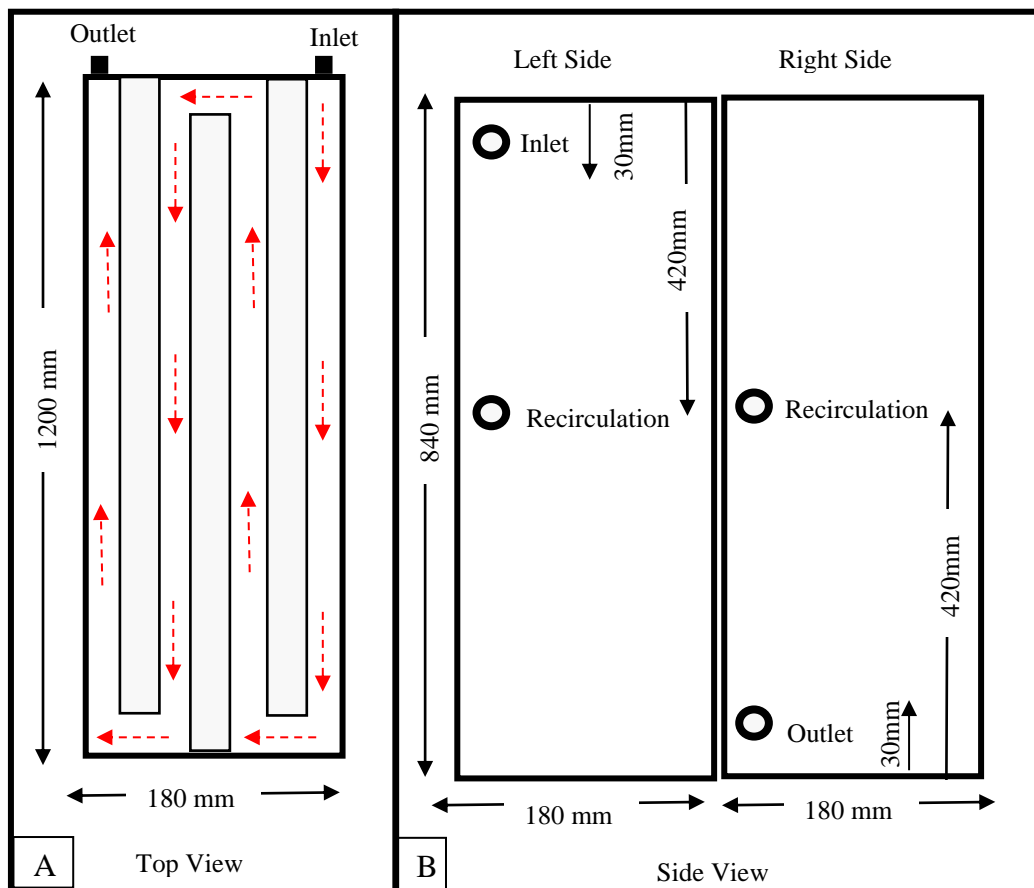
Figure 4.3. A) Top view schematic of the large MEC showing the positioning of the three modules. The dashed red arrows highlight the flow of the influent through the reactor. B) Side view schematic showing the location of the inlet, outlet and recirculation pipework.

4.2.2 Operating conditions

The MEC was installed in an unheated shipping container on a domestic sewage treatment works (STW) in the north east of England. The site has a population equivalent of 24,581, a dry weather flow of 8356 m³/day (97 L/s) and a full flow to treatment consent of 194 L/s. A small submersible pump drew settled wastewater into a header tank from a distribution chamber used to distribute wastewater to the trickling filters following primary settlement and dosing of sodium hydroxide. A peristaltic pump (Watson Marlow 520S, UK) was used to pump the wastewater into each of the MEC at a hydraulic retention time (HRT) of 5 hours. In the large MEC this was a pumping rate of 575 mL/min resulting (HRT = 304 minutes), the medium was 147 mL/min and the small was 98 mL/min. The wastewater left the MEC via gravity. The reactor was operated in continuous flow mode and a voltage of 0.9 V was applied from a PSM 2/2A variable DC power supply (Caltek Industrial Ltd., Hong Kong). No acetate or synthetic substrates were used to supplement the wastewater, which was low strength due to primary sedimentation upstream. The three reactors were operated for 217 days from October 2015 until May 2016. After this, the medium-sized MEC was decommissioned for

dissection and comparison with the previous pilot (Chapter 2). The small and large-sized MEC were gifted to a colleague beginning his EngD to continue operation beyond 12 months.

4.2.3. Sample collection and analysis

Each of the three MECs had the same process of sample collection and analysis during operation. The voltage from each module was recorded every 15 minutes across a 1 Ω resistor (RS Components, UK) using 4-differential input (ADC-20) and 8-differential input (ADC-24) data loggers (Pico Technology, UK). This was used calculate the current produced by each module. Conductivity, pH, and temperature measurements were taken from the front and back of the reactor twice weekly using a Hach HQ40D Multi portable meter with a PHC10105 pH gel probe and CDC40105 conductivity probe (Hach Lange, UK).

Gas was captured from the cathode into Tygon F-4040 tubing (VWR, UK) and a Tedlar gas bag (Sigma Aldrich, UK). The gas volume was measured using a 100 mL borosilicate glass syringe (SGE Analytical, Australia) twice weekly (or more regularly where it permitted). Gas composition was analysed on a GC-TCD using argon as a carrier gas (Thermo Scientific, USA). A five-point calibration was carried out prior to the analysis, with a 99.999% hydrogen standard (Calgaz, USA). Later, these measurements were duplicated using a HPR40 Membrane Inlet Mass Spectrometer (Hiden Analytical Ltd, UK), confirming the results from the GC-TCD.

Liquid samples of influent and effluent were taken three times per week. Total chemical oxygen demand (tCOD) was measured in duplicate using Hach LCK314 (range 40-150 mg/L) and LCK 514 (range 100-2000 mg/L) COD cuvette test kits with a LT200 laboratory analysis dry thermostat and a DR3900 spectrophotometer (Hach Lange, UK). Volatile fatty acids were measured twice weekly on site using LCK365 kits, and confirmed in the laboratory using a Dionex Ion chromatograph (IC). Sulphate (LCK153), sulphide (LCK653), nitrite (LCK341), nitrate (LCK339) and ammonium (LCK305) were measured weekly on site using Hach cuvette kits. These results were supported by anions analysis using a Dionex IC.

Samples were also sent to Northumbrian Water's United Kingdom Accreditation Service (UKAS) accredited laboratories. Two 1 litre samples were taken once a week from the large MEC for the following analyses: total suspended solids (TSS), ammonium, nitrate, nitrite, biological oxygen demand (BOD_5), chemical oxygen demand (COD), soluble BOD, soluble COD and alkalinity. These results are reported separately (Table 4.3).

A prototype was assembled using the new materials in the new configuration (Fig. 4.2). The cell ohmic resistance of two cassette-style modules, one from pilot 1 (Chapter 2) and one of comparable size from pilot 2, were compared using electrical impedance spectroscopy (EIS). Both prototypes were analysed after 24 hours of submersion in a sterile solution of phosphate buffer (PBS). The conductivity of the PBS matched that of domestic wastewater (0.1 mS/cm). The cathode chamber had been filled with 0.1M NaCl, to mirror the catholyte used in the experiments.

EIS was carried out with an Autolab N series potentionstat/galvanostat (Metrohm Autolab) and Nova 1.11 software. Results were obtained using a standard programmable procedure (FRA impedance potentiostatic) with a potential of 0 and a frequency range of 0.1-100,000 Hz for 50 frequencies. Measured impedance can be plotted as a complex plane (Fig. 4.4) or a bode plot (Manohor *et al.,* 2010). In a complex plane plot, the x-axis is denoted as the 'real impedance', labelled Z' (Ω), and the y-axis is the 'imaginary impedance' and labelled -Z" (Ω). When a small amplitude AC voltage is imposed on an electrode or a BES circuit, the response can be measured using a small excitation signal of around 10mV (Manohar et al., 2010; Scott, 2016). When the real impedance is plotted against the imaginary impedance, each point on the plot represents the impedance at one frequency (Scott, 2016). The right-hand side of the plot represents the low frequency impedance, and the left-hand side represents the high frequency impedance (Scott, 2016).
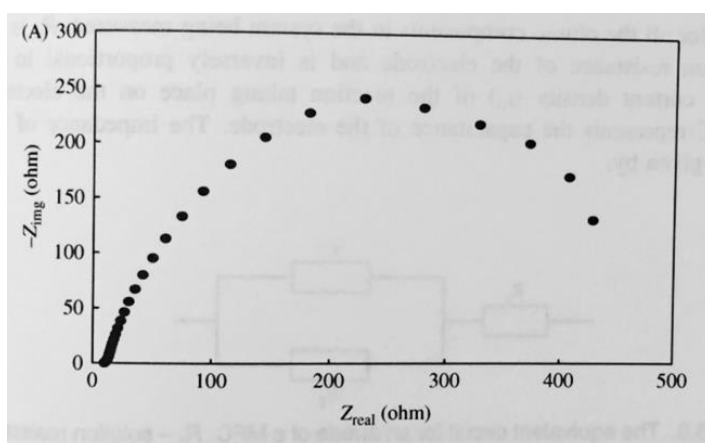
Figure 4.4 Example of a complex plane (Nyquist) plot showing the impedance of an MFC anode in an acetate solution (taken from Manohar et al., 2010).

Calculations were carried out to determine the efficiency of the reactor based on the electrical and substrate energy supplied [Appendix B]. These included: coulombic efficiency [CE]

which is the ratio of coulombs recovered as current, divided by the coulombs available in the substrate (i.e. in COD removed); cathodic efficiency [CCE] calculated as the amount of hydrogen gas captured relative to the theoretical value derived from the current; electrical energy recovery (η_E) calculated as energy out versus electrical energy in; substrate efficiency (η_S), calculated as the amount of hydrogen produced relative to the theoretical amount possible from the COD removed; and total energy efficiency (η_{E+S}) which is the energy recovered from the combination of input energies (electrical and substrate). The equations used have been described previously (Heidrich *et al.,* 2013; Logan, 2008). Further calculations were carried out to determine the amount of hydrogen gas needed to cover the energetic cost of the power supply. All statistical tests were carried out using IBM SPSS statistics 23 (IBM Corp. NY, USA)

A tracer study, carried out by an MSc student (Ben Birkhead), was used to assess the MEC hydrodynamics and residence time. Rhodamine stock dye solution was prepared to give a final concentration of 1 mg/L (Birkhead, 2016). Effluent from the MEC outlet was used to calibrate the fluorescent probe and Turner databank. Two ten-point calibration curves were prepared; 0 to 1 μg/L and 1 to 10 μg/L (Birkhead, 2016). After calibration, 17.5 mL of rhodamine solution was injected at the inlet. The concentration of dye was recorded at the outlet over time.

The tracer study was supported by a multi-phase transient computational fluid dynamics (CFD) model (Birkhead, 2016). The model represented a suspended solids concentration of 160 mg/L, assuming a relative solids density of 1.2, a maximum particle size of 67 μm, and a Stokes number of 3.22×10^{-8} (Birkhead, 2016). The 'mixture model' was selected in Fluent to allow for two phases: water-liquid phase and suspended solids phase (Birkhead, 2016). Mass flow rate was determined for each phase for the inlet and recirculation flows. Recirculation ratio was varied across a range (1 to 3.5) to assess the impact on mixing and flow velocity in the MEC (Birkhead, 2016).

4.3 Results

4.3.1. MEC module resistivity and electrical impedance spectroscopy (EIS)

The MEC was re-designed (Fig. 4.2) to decrease electrode spacing and increase the quality of the connections to the power supply. It was hoped this would reduce internal resistance,

minimising the voltage necessary to generate hydrogen. In the previous pilot (Chapter 2), 10 mm felt (Olmec) was used. A comparison of material resistivity was made (Table 4.2).

Supplier	Material Thickness (mm)	Left-Right Diagonal Plane (Ω)	Front-Back Thickness (Ω)
Olmec	3	3.2	0.90
	5	2.9	1.30
	10	2.5	1.40
SGL	4.6	1.8	0.75
	6	2.7	1.20

Table 4.2 Electrical resistivity of five samples of graphite felt of varying thickness, ranging from 3mm to 10mm, from two suppliers, Olmec, UK and SGL, Germany.

EIS was used to assess the individual electrochemical losses that contribute to a module's overpotential such as ohmic resistance, charge transfer resistance and capacitance (Lisdat and Schäfer, 2008). The module from pilot 2 had a lower ohmic resistance (1.369 Ω at $\gamma = 0.1$ mS/cm) than the ohmic resistance of the module from pilot 1 (Chapter 2) (3.903 Ω at $\gamma = 0.1$ mS/cm) (Fig. 4.5). This is likely due to reduced electrode spacing in the module re-design. The archetypal semi-circle usually observed after plotting EIS data was not present for either module (Fig 4.5). Only a part of the semi-circle is visible in the plot. Solution resistance can be calculated from the high frequency intercept of the real axis (Manohar *et al.,* 2010). However, charge transfer resistance cannot be calculated from this plot. This may suggest that the frequencies selected were not low enough to determine the complete semi-circle.
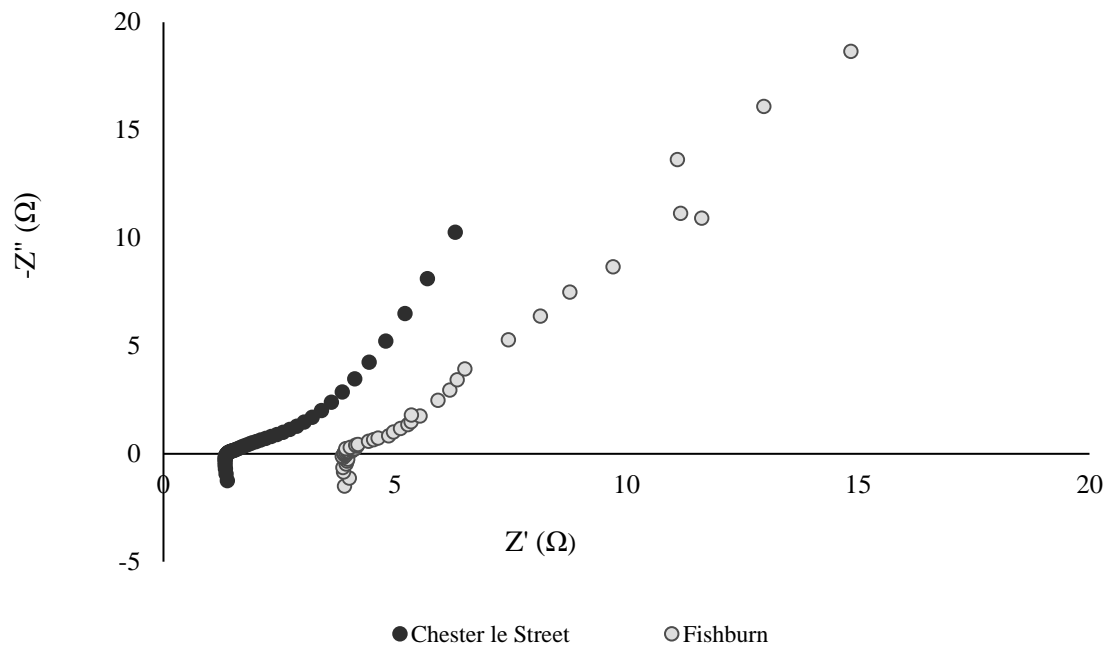
Figure 4.5 Nyquist plot showing the ohmic resistance in prototypes from the Fishburn and Chester le Street MECs. The cell ohmic resistance of each module is shown by the x-intercept.

4.3.2. Start up

The MECs began to produce gas after 90 days. This was a longer start up period than in the previous two trials (44 days, Chapter 2 and 64 days, Heidrich *et al.,* 2013). This is likely due to lower temperatures and the use of lower strength wastewater. This trial started-up in autumn-winter, with wastewater temperatures averaging $10\,°C \pm 2$. In comparison, the previous two trials were started up in spring-summer with wastewater temperatures averaging $17\,°C \pm 1$. A switch to primary treated wastewater led to an average COD of 340 mg/L $\pm$ 200 with a conductivity of 0.8 mS/cm $\pm$ 0.1. These values are slightly lower than the raw wastewater (average COD 450 mg/L, ranging from 147-1976 mg/L, and conductivity =1.8 mS/cm $\pm$ 0.4) used by Heidrich *et al.,* 2013 and considerably lower than the raw wastewater in pilot 1 (average COD 670 mg/L $\pm$ 370 and conductivity = 1.05 mS/cm $\pm$ 0.02). During start-up, current production in the large MEC increased from 0.18A (0.03 A/m^2) at day 10 to 0.45A (0.075 A/m^2) at day 70. There was some COD removal (average 54 % $\pm$ 22 removed), but the average effluent did not reach the European consent of <125 mg/L of COD.

4.3.3 Wastewater Treatment

After gas production began (in January, air temp <0 °C), treatment efficiency and current production (Fig. 4.6) improved. During 127 days of gas production (Jan-May), average effluent COD from the large MEC was 120 mg/L $\pm$ 42, achieving the European consent of <125 mg/L in 56% of the measurements (Fig. 4.6). An independent-samples t-test, run to compare average COD removal during start-up and stable operation, showed no significant

difference [t (107) =0.87, p=0.386] between average COD removal before and after the onset of gas production (Fig. 4.7)
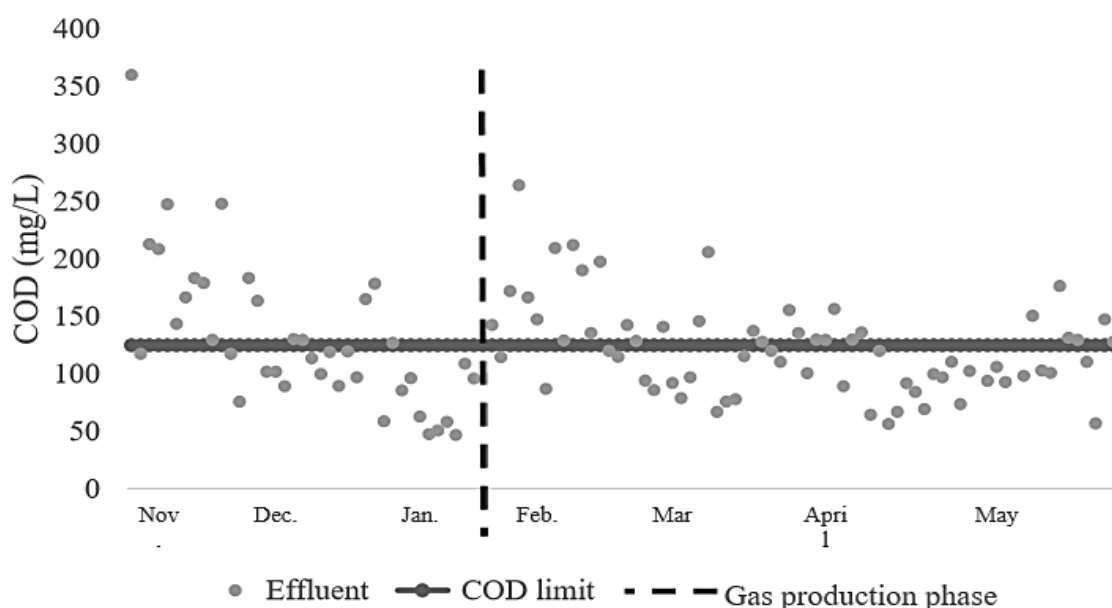
Figure 4.6 Effluent COD concentration (in milligrams per litre) from the large MEC throughout the 217 days of operation. The UWWTD consent (horizontal grey line) is shown. The end of the start-up and beginning of gas production is shown (vertical dashed black line).

Over 217 days, the average measured COD of the effluent from the large MEC (120 mg/L ± 50) was statistically significantly lower [t (434) =15.496, p = 0.000] than the MEC influent (340 mg/L ± 200), equating to a removal efficiency of 64 % (Table 4.3). A Spearman's rank-order correlation was run to determine the relationship between the strength of the influent COD and the percentage of COD removed. There was a strong, positive correlation between the two variables, which was statistically significant (r_s (109) = 0.693, p = 0.000). Therefore, COD removal was larger, when the strength of the influent COD coming in to the reactor was higher.

Gil-Carrera *et al.,* (2013b) found that COD removal improved with increasing OLR. They suggest that exoelectrogenic activity is limited at low COD concentrations, reducing COD removal and hydrogen production (Gil-Carrera *et al.,* 2013b). Furthermore, a Pearson's correlation of data presented by Escapa *et al.,* (2012), shows a significant positive relationship (r (6) = 0.917, p = 0.010) between influent COD and percentage of COD removed, provided a voltage is applied (i.e. excluding V_{app} =0).

Scale	Average Effluent COD (mg/L)	Percentage COD removal (%)
Small	120 ± 60	63
Medium	140 ± 60	36
Large	120 ± 50	64

Table 4.3 Average effluent COD (in milligrams per litre) and percentage COD removal of the three MECs during operation between October 2015 and May 2016: the medium MEC did not achieve the European consent of <125 mg/L for COD.

Removal of Biological Oxygen Demand (BOD) and Total Suspended Solids (TSS) occurred at 66 % and 74 % respectively; yet, with average effluent concentrations of 35 mgBOD/L ± 15 and 42 mgTSS/L ± 12, neither test achieved the UWWTD consent through this process alone (Table 4.4). The effluent VFA concentration, of which acetic acid comprised on average 20 %, was 43 mg/L ± 18. This was 46 % lower than in the influent (80 mg/L ± 43). This result was statistically significant (t (64) = 4.32, p =0.0000).

There was an average of 7.8 g/day of sulphate removed from the reactor. An independent samples t-test showed that the amount of sulphate in the effluent (105 mg/L + 16) was significantly (t (40) = 3.722, P = 0.001) lower than in the influent (141 mg/L ± 41). This value fluctuated considerably, but the sulphate was never completely depleted. Removing 1 mol of sulphate (98 g) requires 64 grams of COD. Therefore, 23 mg/L of COD would have been used to remove 36 mg/L of sulphate. This accounts for 11% of the COD removal in the MEC. Nitrite and nitrate were both present in the effluent, on average 0.87 mg/L and 1.1 mg/L, respectively.

The soluble COD (45 mg/L ± 22) and soluble BOD (15 mg/L ± 10) in the effluent were very low (Table 4.4), suggesting that availability of organic material for the electrochemically-active bacteria could be limiting current and gas production. This has been observed in laboratory BES: when total influent COD drops below 200 mg/L (or sCOD below 100 mg/L) current production declines drastically (Zhang *et al.,* 2015).

Analysis	Influent (mg/L)	Effluent (mg/L)	Percentage removal (%)	UWWTD Consent (mg/L)	Minimum % removal
TSS	161 ±50	42 ±12	75	35 Or 60 for <10,000 PE	90 Or 70 for <10,000 PE
BOD$_5$	101 ± 33	35 ± 16	66	25	70 – 90 Or 40 for <10,000 PE
COD	261 ±85	103 ± 40	61	125	75
sBOD	18 ± 10	15 ±11	19	-	-
sCOD	57 ±24	45± 23	21	-	-
Alkalinity	183 ±39	143 ±24	22	-	-
Ammonia	15 ±4	13 ± 2	19	Total N 15 (10,000-100,000 PE) 10 (100,000 + PE)	Total N 70- 80
Nitrate	1.3 ±0.9	1.1 ±0.9	15		
Nitrite	1.8 ±2.3	0.87 ±0.79	51		

Table 4.4 Analysis of total suspended solids (TSS), biological oxygen demand (BOD$_5$), chemical oxygen demand (COD), soluble BOD, soluble COD, alkalinity, ammonia, nitrate, and nitrite in the influent and effluent of the large MEC, carried out in parallel by Northumbrian Water's UKAS accredited Scientific Services. The consent for discharge of wastewater to the environment, as depicted in the urban wastewater treatment directive (UWWTD, 1991) is listed alongside, including variations for population equivalent (PE) i.e. the pollution load produced during 24 hours by one person.

Current production fluctuated significantly during storm conditions, when influent COD was affected by increased surface water runoff. In December and January, prior to the beginning of the gas production phase, there were periods of sustained heavy rainfall in the north of England. This was evident on site, when the MCERTS flow meters' alarms were triggered by a flow more than Chester Le Street STW's consent (194 L/s). This tripped the site into 'storm protection mode' where the flow is diverted to the storm tanks. A Spearman's rho analysis shows a weak negative correlation which was statistically significant, between the onset of 'storm protection mode' and the current produced by module 1 (r_s (62) = -0.267, p = 0.036) and module 2 (Rs (62) = -0.277, p = 0.029) in the large MEC (Fig 4.5). There was no significant correlation between the onset of 'storm protection mode' and the current produced by module 3 (p= 0.078).

An independent-samples t-test was run to deduce whether there was a significant difference in current production before and after the onset of gas production. This was analysed over the two-month period (from 02/12/15 – 01/02/16) that led up to and followed stable gas production (which began on 21/1/16) (Fig 4.5). All modules in the large MEC showed a statistically significant difference in current produced before (1= 149 mA ± 32, 2= 139 mA ± 25 and 3=146 mA ± 27) and after (1= 161.4 mA ± 0.05, 2= 151.1 mA ± 0.02, 3= 161.2 mA ±0.04) the onset of gas production (Fig. 4.7). The measured current after the onset of gas production was higher and less variable than during the start-up period.
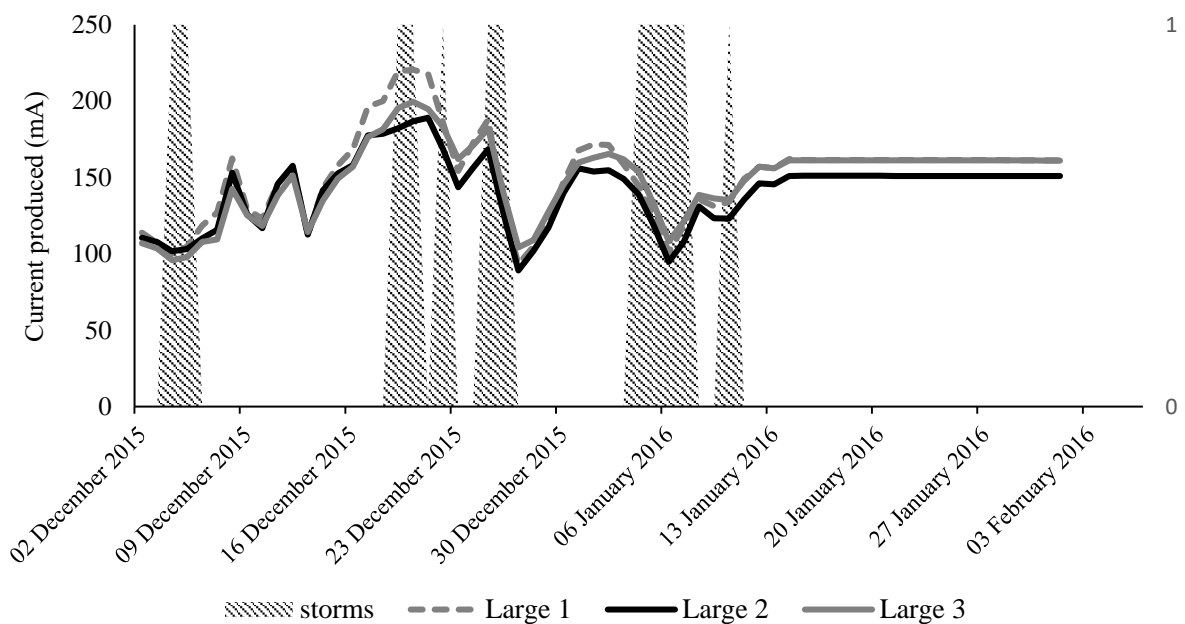
Figure 4.7 Current production (recorded as milliamps) in the large MEC at Chester le Street STW during December 2014 and January 2015.This reflects a two-month period during which there were periods of heavy rainfall. Striped shaded blocks indicate when the sites' MCERTS storm alarm was triggered.

4.3.4 Hydrogen Gas Production

The first gas measurements recorded a hydrogen purity of 60 % ± 19. Composition of the remaining 40% was not determined quantitatively, but qualitative analysis showed carbon dioxide, oxygen, and water vapour. In the following two weeks, hydrogen purity increased to 78 % ± 18 and then stabilised at 93 % ± 7 for 4 months. It is possible that the gases diluting the purity of the early measurements, may have been trapped in the process of assembling the modules. The cathode chamber was not sparged with nitrogen at the start of the experiment.

	January (mL/d)	February (mL/d)	March (mL/d)	April (mL/d)	May (mL/d)
Small	20	127	212	111	152
Medium	0	0	35	28	27
Large	183	237	622	857	705
Combined	203	464	869	996	884
Average temperature (ºC)	8.6 ± 0.5	10 ± 1	11 ± 1	13 ± 1	16 ± 1
Average influent COD (mg/L)	330 ± 200	410 ± 160	270 ± 150	350 ± 150	270 ± 120

Table 4.5 Average yield (in millilitres) of hydrogen gas per MEC per day during the gas production phase at Chester le Street STW. Variation in temperature and influent COD per month is shown.

The total volume of hydrogen produced increased each month, from 0.203 L/d in January to 0.996 L/d in April. This value dropped to 0.884 L/d in May (Table 4.5). The maximum gas yield obtained, 0.857 L/d in the large MEC in April, is equivalent to 0.005 L-H_2/per L of anode volume/day. This is considerably lower than typical values obtained in laboratory studies with acetate (0.12 m^3 H_2/m^3/day, Jia *et al.,* 2012) or real wastes (0.061 m^3 H_2/m^3/day, Jia *et al.,* 2010). However, whilst the applied voltage in the laboratory example (at 1V) is comparable with this study, the influent COD was much higher, at 1298 mg/L (Jia *et al.,* 2010). Adjusting for variation in influent COD, the values achieved in laboratory MEC are three times larger than the yield obtained in this study. Furthermore, the yield achieved in pilot 1 (before failure), was 0.016 L-H/per L_a/day. Adjusting for influent COD (670 mg/L), the yield obtained in pilot 1 is half the value obtained by Jia *et al.,* (2010). The low hydrogen yield obtained in both pilot MEC could be a result of an under loaded system or hydrogen scavenging.

A Spearman's rho was used to determine the relationship between the volume of hydrogen gas produced and the temperature of the wastewater. There was a positive correlation which was statistically significant (r (24) = 0.567, p = 0.004), suggesting that more hydrogen gas is produced when the temperature of the wastewater is higher, as observed in April and May. (Fig. 4.8). Gas analysis (volume and composition) was completed indoors at room temperature, and therefore the relationship observed is not a result of the ideal gas law (which states that volume must increase with temperature if other factors remain constant). However,

a partial correlation was run to control for the month in which the sample was taken. The partial correlation was not significant, when controlling for month (r (21) = -0.226, p=0.300). Therefore, the increase in hydrogen obtained at warmer wastewater temperatures may be an artefact of a winter start-up, as the MEC reached maturity during the spring when temperatures happen to increase.
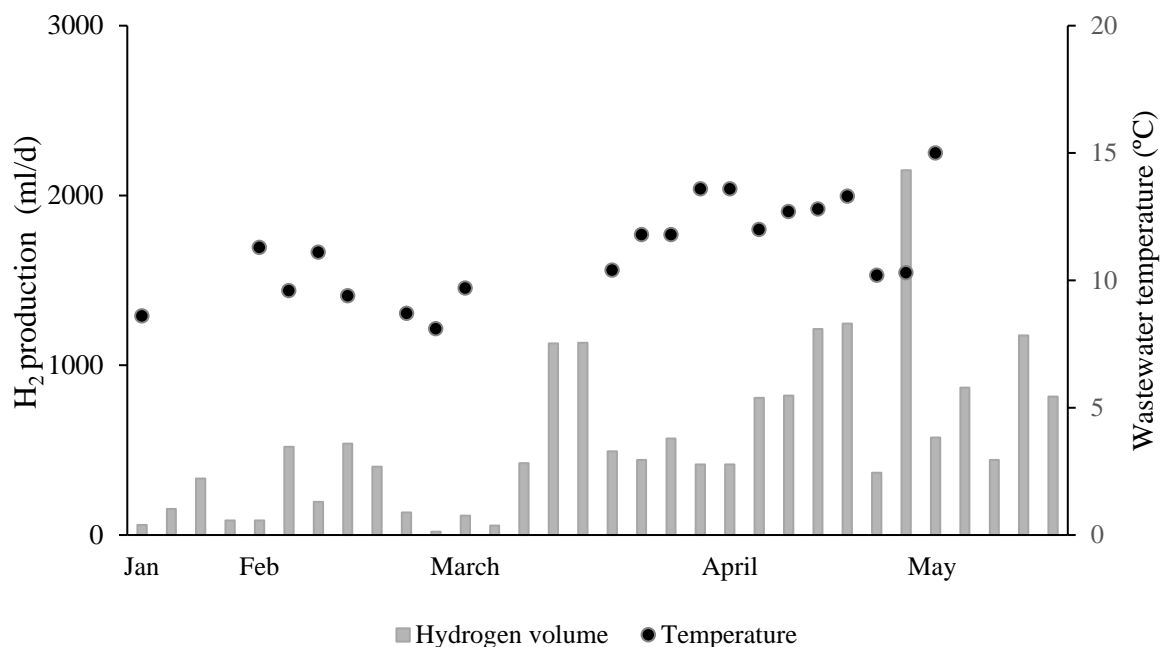
Figure 4.8 Volume of hydrogen gas produced by the MEC, in millilitres per day, relative to the temperature of the wastewater at the time of the gas measurement, in degrees Celsius.

.

4.3.5 Energy Efficiency

Current production was highly variable throughout operation. The mean current produced in the gas production phase was 300 mA ± 180. A Pearson's correlation showed there was not a significant relationship between the current produced and the amount of hydrogen gas obtained r (15) = -0.079 p = 0.780). In the large MEC, module 1 produced more gas (475 mL/day ± 300) than module 2 (22 mL/day ± 9) or 3 (24 mL/day ± 17). However, module 2 produced more current (330 mA ± 220) than module 1 (200 mA ± 40) or 3 (190 mA ± 30) (Fig. 4.9).
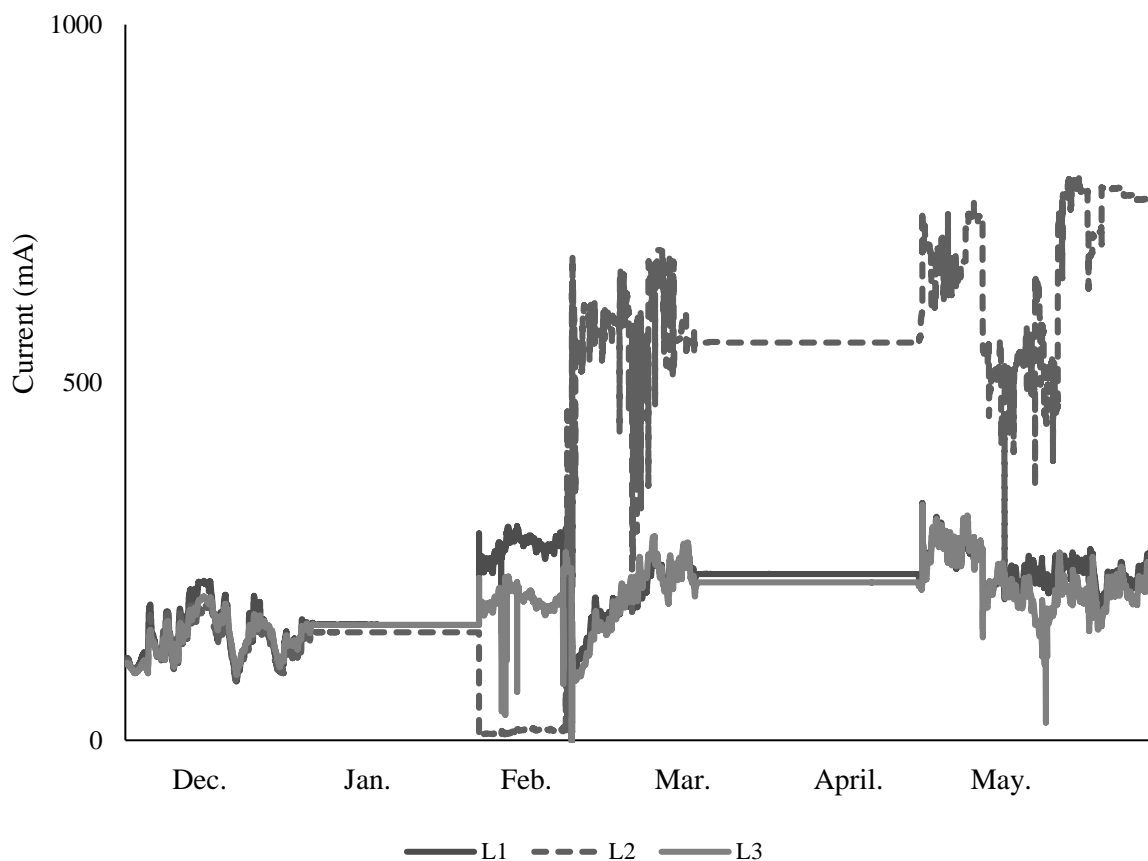
Figure 4.9 Current production (in milliamps) in the three large MEC modules throughout the start-up and gas-production phases of operation.

The MECs' efficiencies were particularly low during the start-up phase (October 2015 to January 2016), but showed an increase throughout operation (Figure 4.9). A maximum coulombic efficiency (CE) of 28 % was achieved, 6 months into the period of operation. Cathodic coulombic efficiency (CCE) peaked at 20 % in April, but was below 10 % for the remaining period of operation, implying significant hydrogen losses. Electrical energy recovery (η_E) was very poor, below 3.5% throughout operation (Figure 4.10).
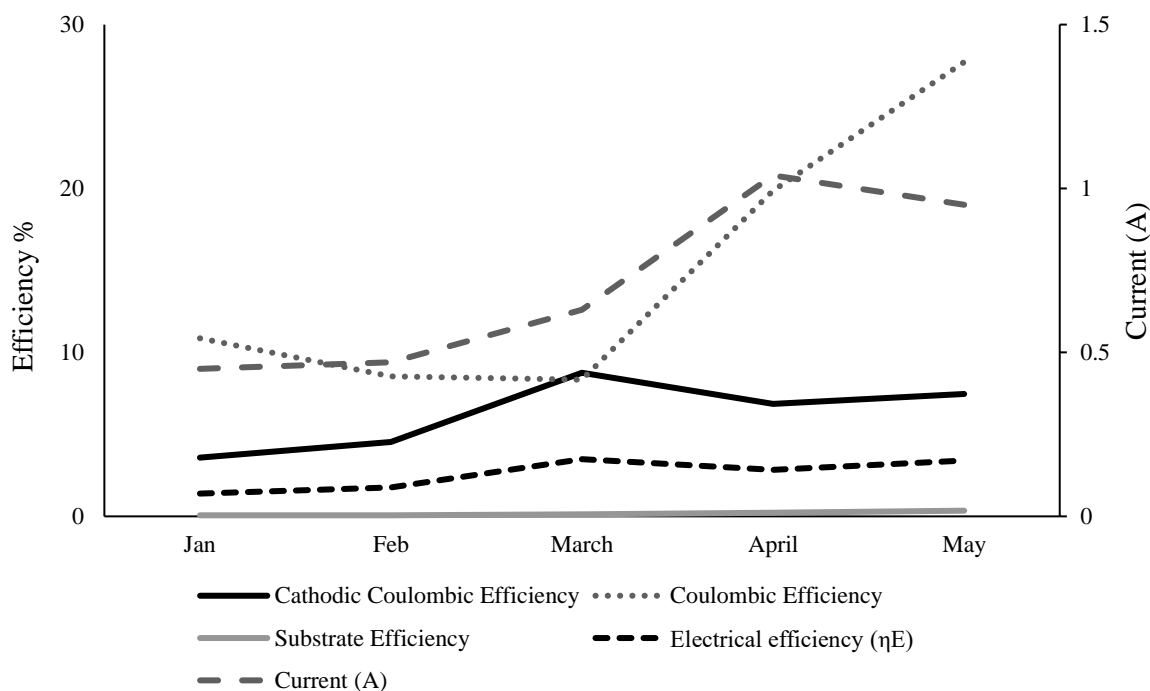
Figure 4.10 Average MEC reactor efficiencies per month during the period of stable gas production (day 90-200). Most of the efficiencies (coulombic efficiency [CE], cathodic efficiency [CCE], and electrical energy recovery [ηE]) show an increasing trend during this time. Substrate efficiency [ηs], remains very low throughout.

4.3.6 Energy required to 'break even'

The operation of the large MEC in this study occurred at an energetic cost (from the power supplies) of 0.1 kWh/kg-COD, or 1 kWh/kg-COD if pumping requirements are accounted for. The applied voltage used in this trial (0.9 V), would permit a theoretical maximum energy recovery of 137 % (Appendix B, Eq. 4-8). However, to recover the energy generated, the hydrogen gas would need to be converted to electricity using a PEM fuel cell, with a typical efficiency of 50-60% (DOE, 2017).

During March and May, the MEC produced on average 0.73 L of hydrogen gas per day. To meet the energy requirements of the power supply, the MEC would need to produce on average 12 L/d: 16 times more than the average achieved in this pilot trial. If the yield obtained from modules 2 and 3 had matched module 1, then total yield would be 2.45 L/d: a volume 4.9 times lower than required to meet the energy requirements of the power supply.

The low reactor efficiencies are, in this instance, paradoxically promising. The low cathodic efficiency, which was predominantly below 10 %, implies sufficient current was generated at the anode to break-even energetically. Unfortunately, the low efficiency implies that gas is

83

simply not being captured. This is most likely due to hydrogen-scavenging bacteria, which were found to be present in the catholyte of all three MEC reactors in this trial (Fig. 3.11). It was previously estimated, based on cathodic VFA concentration in January, that a maximum of 110-140 mg of acetate was produced in cathode, accounting for the consumption of 200 mL of H_2 per day. If acetogenic bacteria account for the loss of 200mL of H_2 per day, the yield captured in January (183 mL) was only 48% of the total yield. In April, when gas yield was highest, a percentage loss of 52 % to acetogenic conversion, would equate to a loss of 936 mL of H_2 per day.

4.3.7 Effect of Scale

The effect of scale, on the performance of the three MEC reactors, was considered (Table 4.6). There was negligible difference in the volumetric gas production (0.003 to 0.004 L-H_2/L-MEC/d) and level of COD removal (63-64 %) of the small and large MECs (Table 4.6). However, the average hydrogen production, relative to the anode surface area, was four times larger in the small MEC (2 L/m^2 of anode) than the large MEC (0.5 L/m^2 of anode) (Table 4.5).

The current density was an order of magnitude larger in the biggest MEC (Table 4.6). This may have been a true effect of scale; however, it is more likely the effect was masked by a high margin of error on the samples from the small and medium MEC. The standard deviation on the current observed in the small MEC was 2.08 times the value recorded (Table 4.5). Pico ADC 20/24 data loggers are operational between 0 and 45 °C, but accuracy can only be guaranteed between 20 and 30 °C. Air temperature was below this for most of the operational period reported (Fig. 4.8).

The medium MEC performed poorly in comparison, with limited gas production and COD removal, and hence was selected for decommissioning early. The most limiting factor in scale-up was the structural stability of the module. The medium and large modules both showed signs of bowing: a spacer would be recommended for future trials of comparable scale and configuration.

	Small	Medium	Large
Size of electrode (m^2)	0.06	0.24	1.0
Current (mA)	2.2 ± 4.7	17 ± 25	294 ± 185
Current density (A/m^2)	0.04	0.07	0.29
COD removal (%)	63	36	64
Daily ΔCOD (kg-COD/day)	0.03	0.02	0.18
Average H_2 production (mL/d)	124	18	521
Average H_2 production relative to scale (L/d/size of electrode)	2.07	0.08	0.52
Volumetric H_2 yield (L-H_2/L-MEC/day)	0.004	0.0004	0.003

Table 4.6 Effect of scale on MEC performance. Data are reported both as raw values (current, COD removal and H_2 production) and subsequently adjusted relative to scale (current density, daily removal of COD and volumetric yield of hydrogen).

4.3.8. Tracer Study and CFD model

Tracer studies can identify dead zones, short-circuiting and channelling (de Nardi *et al.,* 1999). Non-ideal flow can be caused by: density currents due to temperature differences; inadequate mixing; poor design; and axial dispersion (Tchobanoglous *et al.,* 2004). Concentration plotted over time was typical of a plug-flow reactor with recirculation (Birkhead, 2016) (Fig. 4.11).

Tracer study hydraulic retention time (HRT) was measured as 273 minutes (Birkhead, 2016). This value is 31 minutes less than the calculated HRT from the flow supplied by calibrated pumps. The reduced HRT could indicate short-circuiting and stagnant zones (de Nardi *et al.,* 1999). Alternatively, the lower HRT could be a consequence of a reduced anodic volume due to sludge accumulation or blockages. The long tail observed in the plot (Fig. 4.8) is expected with the use of a fluorescent tracer in a reactor with a biofilm.

Typically short-circuiting is indicated by a HRT which is 30-80% of the theoretical HRT (Stairs, 1993). This study's tracer HRT was 90% of the calculated HRT. The area under the curve represents the rhodamine recovered (130 µg of the 175µg applied) (Birkhead, 2016). The loss of rhodamine is likely caused by sorption to attached biomass or solids in the tank (Giraldi *et al.,* 2009). Ideally, 90% should be recovered. (Tchobanoglous *et al*., 2004; Teefy & Singer, 1990): 74 % of rhodamine was recovered in this study (Birkhead, 2016).
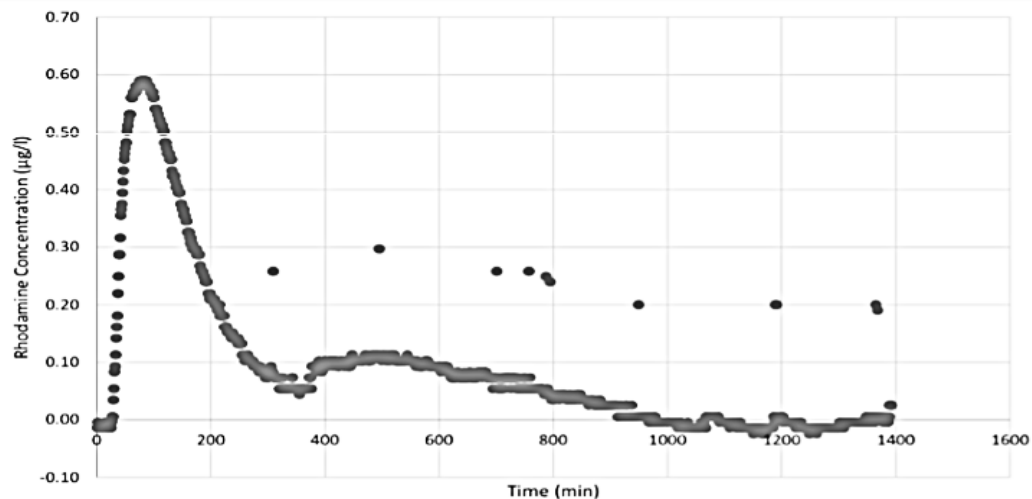
Figure 4.11 Tracer study plot showing rhodamine concentration in MEC outlet over time. Figure taken from Birkhead, 2016 p.52.

The multiphase transient CFD model shows flow pattern is largely dictated by the position of the inlet and outlet (Birkhead, 2016). Dead space accounts for 15-20% of the velocity contour without recirculation (Fig. 4.12). It is most noticeable in the corners opposing the direction of flow (i.e. bottom left below inlet, and top left above outlet) (Fig. 4.12). Recirculation improves velocity considerably. Without recirculation, the predominant velocity in the contour is 0.6×10^{-3} m/s (Fig 4.12). Velocity is markedly higher with recirculation at 1.5×10^{-3} m/s (Fig 4.13). However, recirculation does not eliminate dead space (Fig 4.13). There is considerable room to improve mixing in the tank, thereby reducing mass transfer limitations. This may be achieved through the installation of multiple inlets, creating a more distributed flow. Alternatively, the effect of flow direction, e.g. making use of a gravity feed, could be explored.
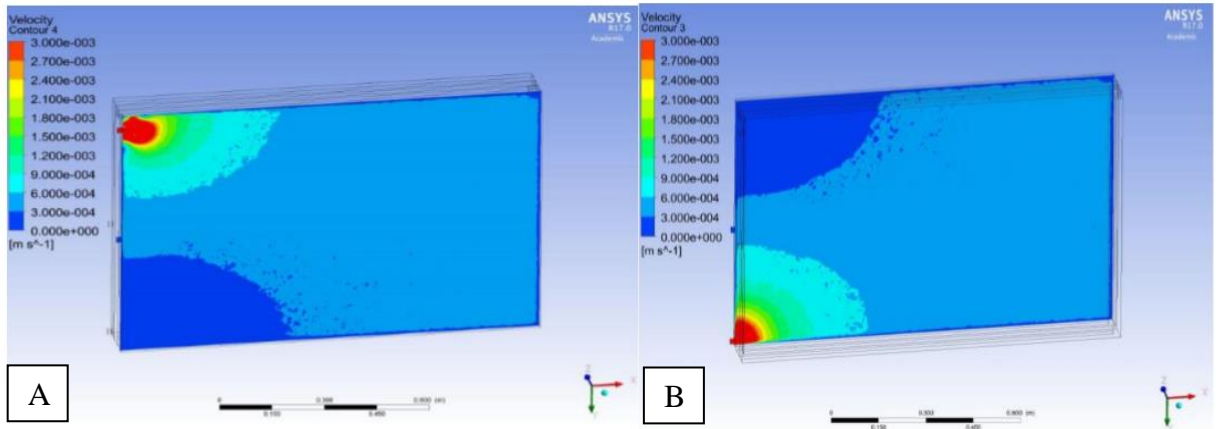
Figure 4.12 Velocity contour from multiphase transient CFD, without recirculation, modelled in Fluent. A) Front plane of MEC (including inlet). B) Rear plane of MEC (including outlet). Dead space is shown (dark blue) in opposite corners to direction of flow. Figure adapted from Birkhead 2016 pp. 82-83.
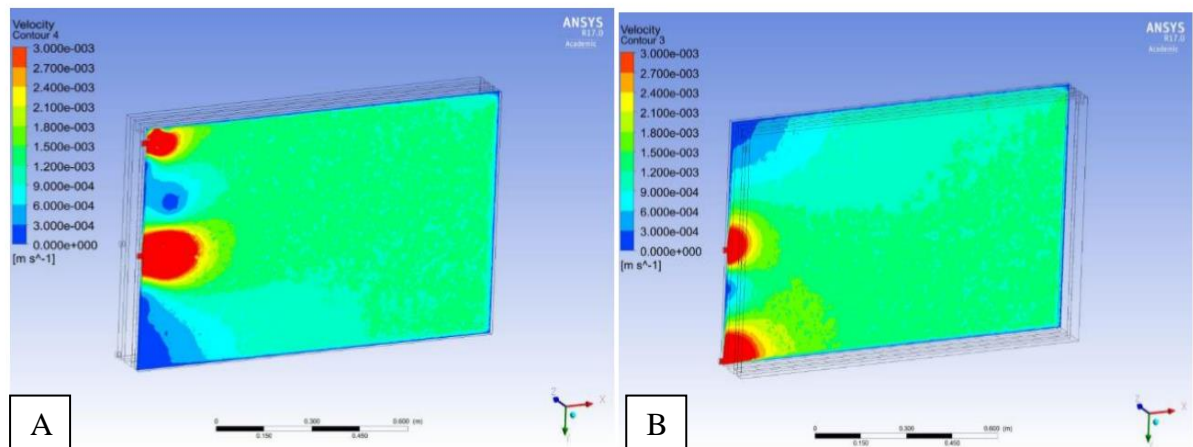
Figure 4.13 Velocity contour from multiphase transient CFD, with recirculation equal to 2 x flow, modelled in Fluent. A) Front plane of MEC (including inlet). B) Rear plane of MEC (including outlet). Dead space is shown (dark blue) in opposite corners to direction of flow. Figure adapted from Birkhead 2016 pp. 101-102.

4.4 Discussion

Pilot scale MECs of increasing size, made from low cost-materials, produced high-purity hydrogen gas from low-strength domestic wastewater at ambient temperatures. The most important result was the technology's capability of treating wastewater to an industrially viable level: meeting the European UWWTD standard for COD removal (<125 mg/L) at 120 mg/L $\pm$ 42. TSS removal in the MEC did not meet the UWWTD standard (< 35 mg/L), with an effluent concentration of 42 mg/L $\pm$ 12. However, the regulations for TSS are usually relaxed on smaller sites (<10,000 PE), requiring an effluent of <60 mg/L.

There was a relationship between the amount of COD removed and the strength of the influent COD. The effect of influent COD and OLR has previously been explored by Gil Carrera *et al.,* (2013b) and Escapa *et al.*, (2012), who showed COD removal is proportional to OLR. Furthermore, current production has been shown to be limited at low COD concentrations (Zhang *et al.,* 2015). Therefore, it is likely that exoelectrogenic activity is reduced when COD is low, affecting COD removal as well as current and hydrogen production (Gil-Carrera *et al.,* 2013b). The relationship observed between strength of COD and COD removal may be indicative of an underloaded system.

Effluent COD concentration was improved on previous trials (Chapter 2; Heidrich *et al.,* 2013, 2014), but removal was still inconsistent across the operational period. Consistency in COD removal is required before the technology could be reliably tested inline. The MECs showed poor nutrient removal, with limited nitrification and denitrification, as would be expected with an anaerobic technology. The lack of nutrient removal remains a challenge for the uptake of MECs in domestic wastewater treatment: MECs may require a chemical or biological downstream process to remove nitrogen and phosphorous. The combined cost of these technologies will determine the likelihood of utilities' investment in MECs.

Hydrogen was produced for 127 consecutive days, showing the technology is capable of long term gas production. The total volume of hydrogen produced increased each month, but the yield was relatively low compared with values obtained in laboratory studies with real wastes (Jia *et al.,* 2010). Adjusting for variation in influent COD, the values achieved in laboratory MEC are three times larger than the yield obtained in this study. The low volumetric yield achieved may be indicative of underloading, as COD falls below the threshold required to generate current and hydrogen; or it may be a result of hydrogen losses and scavenging.

Hydrogen yield decreased towards the end of the trial. Cathodic efficiency was consistently poor (below 10 %), implying the system is limited by hydrogen losses. Hydrogen scavenging bacteria were found in all cathode samples. If hydrogen scavenging bacteria proliferate, hydrogen gas yield will decline, as was observed between April and May 2016. Reducing hydrogen loss is a priority for improving the efficiency of the technology. The applied voltage supplied to the MEC (0.9 V) would permit a maximum energy recovery of 137%, suggesting that addressing hydrogen losses is a critical factor in attaining energy-neutrality. Reducing losses could be achieved by capturing the hydrogen more efficiently; through recirculation of

catholyte, modifying reactor architecture, or by maintaining a sterile environment: the last of which, is likely to be problematic in a wastewater application.

When the effect of scale was assessed, the volumetric gas production (L-H_2/L-MEC/d) and COD removal were comparable in the small and large MECs. Yet when performance was evaluated relative to the size of the anode, rather than the volume, there was a factor of four difference in the average hydrogen production. The small MEC produced between 0.3 and 3.5 L of H_2/m^2_{anode}/d, compared with 0.2-0.9 L of H_2/m^2_{anode}/d in the large MEC. This may be due to a combination of factors. It could be due to increased hydrogen losses in the large MEC. These losses may be more likely in the large MEC due to the risk of gas permeation through a larger surface area of materials. Alternatively, it could be due to more rapid capture of hydrogen in the small MEC, due to a decreased distance between the cathode and the gas bag. This would make losses to scavenging bacteria less likely. There is a possibility that the observation indicates a higher conversion efficiency in the small MEC, suggesting performance decreases with increasing scale, although this is unlikely with the current densities recorded. It is unusual that the hydrogen yield is greater, per unit of electrode area, in the small MEC than the large MEC, despite the former generating less current. The current density reported may be artificially low in the small MEC due to error caused by operating the logging equipment outside of operational tolerance levels.

The tracer study and CFD model identified some areas with limited mixing in the MEC, with dead space accounting for 15-20 % of the total area. The actual hydraulic retention time calculated from the tracer was 10 % less than expected, based on calibrated pump flows. The pattern of flow is largely dictated by the position of the inlet and outlet. Consequently, dead space is most apparent in the corners opposing the direction of flow. Recirculation was shown to improve mixing within the tank, increasing the average velocity by 2.5 times. However, recirculation does not eliminate dead space entirely. Although short-circuiting and dead space can be identified using a tracer study and CFD, these results may not translate well with scale. Distribution of flow is likely to vary moving from bench-top to pilot scale, and further still to full scale (Zheng *et al.,* 2012).

Improving mixing in the tank may provide a means to reduce mass transfer limitations and improve MEC performance. The distribution of the flow could be improved, through the installation of multiple inlets; or the direction of flow could be changed, to make use of a gravity feed. Optimising distribution of organic load across the anode surface is likely to

reduce variation in the chemical and biological environment of the biofilm (Mason and Stuckey, 2016), which should have positive effects on MEC performance. Increasing the accessibility of COD to the biofilm may increase COD removal and current generation. Although subject to considerable error, the large MECs' current density (Table 4.6) was an order of magnitude greater than the small and medium MECs'. Improving further on this seems possible, as current density showed an increasing trend through operation. A maximum current density of 0.79 A/m^2 was achieved in April: three times larger than the average value recorded in this study.

Resistance, expected to increase with scale, was expected to negatively affect the current density of larger MEC modules. However, there may have been benefits of scale-up which negated the impact of increased resistivity. Flow through the tank would be expected to improve with scale-up; a reduction in the likelihood of blockages, caused by sludge accumulation, would be expected at scale. Improved flow in the MEC would affect the reactors' hydrodynamics, the treatment efficiency and the biomass activity (Zheng *et al.,* 2012). Positive and negative effects on reactor hydrodynamics and biogas production have been shown with scale up of anaerobic fluidised bed reactors (Buffière *et al.,* 1998). This could be further examined in BES.

Chapter 5. Microbiology

5.1 Introduction

The enrichment of bacteria on an electrode to form an electrochemically active biofilm is critical to the underlying process of an MEC (Ringelberg *et al.,* 2011). Many prokaryotes have the potential to generate electricity, but few will be able to form an electrochemically active biofilm, where electrons are transferred to a terminal electron acceptor (Chabert *et al.,* 2015). Studies of the biofilm in BES report a predominance of known exoelectrogenic genera, such as *Geobacter* and *Shewanella* (Kiely *et al.,* 2011; Cusick *et al.,* 2010, Holmes *et al.,* 2004 and Logan *et al.,* 2005). In mixed consortia, such as domestic wastewater, exoelectrogenic genera are often found in combination with Bacteriodetes and Proteobacteria (Chabert *et al.,* 2015).

Understanding how the biofilm assembles, and where fluctuations in the community occur, may help to explain how the microbial community affects function and performance. Community assembly is an emerging topic in BES research (Zhou *et al.,* 2012; Croese *et al.,* 2013; Ishii *et al.,* 2014; Ruiz *et al.,* 2014 and Jiang *et al.,* 2016). However, our understanding of how that community evolves with scale and time is still limited.

The objectives of the work described in this chapter were to:
- Identify the bacterial communities in a pilot MEC, fed real wastewater for >6 months
- Compare the spatial and temporal variation in the community within individual anodes, across anodes within the same reactor, and across different reactors
- Assess the distribution of biofilm across the anode surface using imaging techniques

The overarching aim of this work was to determine whether differences in biological community influence MEC performance. It is hypothesised that biofilm distribution is uneven. Localised patches of thicker biofilm may occur because of the distribution of current to the electrode, and the availability of substrate from the bulk wastewater flow to the bacteria. This chapters explores variation in biofilm distribution and microbial community composition across two pilot scale MEC.

5.1.1 Biofilms

A biofilm is an 'assemblage of bacterial cells attached to a surface and enclosed in an adhesive matrix' (Madigan *et al.,* 2012). This matrix usually consists of a mixture of

polysaccharides, protein and nucleic acids, all of which are secreted by the cells within the biofilm (Madigan *et al.,* 2012).

Biofilms are the default growth mechanism, formed by 99 % of bacteria in nature (Garrett *et al.,* 2008). Planktonic growth is usually only seen in natural environments with a low nutrient concentration (Madigan *et al.,* 2012). Forming a biofilm is usually advantageous to the individual bacteria, as the surface (to which the biofilm is attached) generally provides greater access to nutrients. This enables more extensive growth than would be possible as planktonic individuals. As more bacteria adhere, the attachment to the surface becomes stronger and cells are less likely to wash off. In addition, the biofilm provides protection (sheltering other bacterial cells) from phagocytosis or penetration of toxic compounds (Madigan *et al.,* 2012).

5.1.2 Biodiversity

Microorganisms are the most diverse and abundant life form on earth. Estimates of bacterial diversity suggest between 10^6 and 10^9 different species, and 10^{30} individuals globally (Curtis *et al.,* 2002; Schloss and Handlesman, 2004; and Prosser *et al.,* 2007). Bacteria have been isolated from extreme environments ranging from near boiling hot springs, to the Antarctic. However, they are particularly diverse in soils and sediments where they can account for up to half of the total biomass (Kennedy, 1999). There can be up to 10^{10} bacterial cells per gram of soil, forming a highly diverse community. This is often due to the variety of energy and carbon sources present in the soil (Kennedy, 1999).

Nutrient and resource heterogeneity are common in wastewater treatment plants. Thus, like soils and sediments, wastewater contains a metabolically diverse mix of bacteria, archaea and viruses (Zhang *et al.,* 2012b). Activated sludge plants contain in the region of 700 genera, with thousands of operational taxonomic units (OTUs) (Zhang *et al.,* 2012b).

Biodiversity can be assessed once microorganisms are identified and quantified. Culture-based (enrichment, isolation) and culture-independent (staining, fluorescent *in situ* hybridisation, PCR and denaturing gradient gel electrophoresis) methods can be used to analyse a microbial community (Madigan, *et al.,* 2012). A limitation of culture-based techniques is that most microorganisms have never been grown in laboratory cultures.

Culture-independent methods (used in this study) identify cells or genes within a microbial habitat. Fluorescent stains, such as DAPI or SYBR Gold, bind to nucleic acids and function as a nonspecific means to identify all cells, dead and living (Madigan *et al.,* 2012). Attaching a

probe to the fluorescent stain, as in fluorescent in situ hybridisation (FISH), can allow direct targeting of a single species or a group of related species (Madigan *et al.,* 2012). The FISH probe binds to the cells' ribosomal RNA; therefore, the cells must be alive when fixed prior to staining. Some diversity studies forego isolation and staining entirely, in favour of gene identification. PCR, DGGE and 16S DNA sequencing can be used to determine a microbial community.

5.2 Methods

5.2.1. Inoculation

Both pilot studies (Chapter 2 and 4) were inoculated with domestic wastewater in the anode compartment. A solution of 0.1M NaCl was used in the cathode chamber. This had been autoclaved before use. The inoculation of both pilot MECs began when the pumps were turned on. However, there were differences in the temperature, treatment stage and dosed chemicals in the wastewater between the two pilots (Table 5.1). Additionally, the surface area to be colonised by biofilm was considerably larger in pilot 2 (Table 5.1).

Start-up conditions	Pilot 1	Pilot 2
Wastewater type	Raw domestic	Primary treated domestic, dosed with ferric sulphate and sodium hydroxide
Wastewater temperature (˚C)	Day 1 = 15.8 At onset of H_2 = 17.4	Day 1 = 11.4 At onset of H_2 = 8.6
Flow	75 mL/min	575 mL/min
Anode surface area	0.06 m^2	1 m^2
Time taken until H_2	44 days	90 days

Table 5.1. Description of the start-up conditions of pilot 1 (chapter 2) and pilot 2 (chapter 4). Both were inoculated with wastewater pumped directly from the sewage treatment works.

5.2.2. DNA extraction of catholyte

Liquid samples of the catholyte were taken from each of the cathode chambers from the small, medium and large MECs during operation (Chapter 4). The samples were stored in PBS and ethanol prior to analysis. For each discrete sample, 4 mL of catholyte was spun

down in a centrifuge to obtain a pellet. The supernatant was discarded and the pellet was re-suspended to create a measured volume of 250 µL. Each 250 µL sample was added to a lysing matrix tube from a BIO 101 FastDNA Spin Kit for soil (MP Biomedical, USA). The manufacturer's instructions were followed for DNA extraction. PCR amplification took place using a PCR Hot Master Mix, Golay barcode, 515F forward oligonucleotide primer and 806 reverse primer. PCR products were checked for size on a 2.5 % w/v agarose gel. There were no visible bands present. This implied that either no DNA was present, or inhibition had occurred in the extraction process.

Samples were analysed via Qubit and Nanodrop. The results showed DNA yields which should have been sufficient for PCR (7.8 ng/µL ± 0.8). As such, the problem was likely to be related to inhibition, caused by a large salt concentration. The ratio of absorbance at 260 and 280nm was 1.99, which falls in between the range of 1.8-2.0 for high purity of DNA and RNA. This implies negligible contamination at 280 nm, by proteins or phenols. The ratio of absorbance for 260 nm and 230 nm, was considerably lower than the expected value of 2.0-2.2, at 0.016. This suggests significant contamination at 230 nm. This contamination may have been by EDTA, carbohydrates or the chemicals used in the DNA extraction process. It was thought that NaCl (catholyte) had interacted with ethanol in the MPBIO kit during the extraction phase and precipitated out with the pellet.

Additional samples were taken, as outlined above, for a second extraction. To minimise disruption to the catholyte, whilst obtaining enough sample for analysis, the samples from each cathode chamber were pooled, to create one sample for each of the MECs (large, medium and small). For each sample, 16 mL of catholyte was centrifuged down into 500 µL. A series of freeze-thaw processes were applied to the samples. The samples were stored in a -80℃ freezer for three minutes, adjusted to room temperature, and incubated in a 95℃ heated block for two minutes. This procedure was repeated five times, manually fracturing the cells to provide access to the DNA. Samples were analysed via Qubit to assess the quantity of DNA prior to PCR. A low yield (2.5 ng/µl), was achieved, but there was no inhibition and the sample was visualised under UV on a 2.5% w/v agarose gel. DNA extracts were pooled with extracts taken from anode samples (5.2.3) and sent for PCR and Illumina MiSEQ 16S DNA sequencing (5.2.4) at LGC Genomics (Berlin, Germany).

5.2.3 DNA extraction of anode samples

A total of 72 samples were taken from the anodes of working MEC electrodes using a core boring device (2.2.5). Samples were taken from module 1 from the medium sized MEC in pilot 2 (24 in total: 12 from front, 12 from back). Samples were taken from module 10 from pilot 1 (48 in total: 24 from front, 24 from back). Samples were taken evenly across the top, middle and bottom of each anode (Appendix D1), to assess the heterogeneity of the community.

BIO 101 FastDNA Spin Kit for soil (MP Biomedical, USA) was used for the DNA extraction of anode samples. The bored sample was added to a lysing matrix tube and the weight of each sample was recorded. Each tube contained $0.14 \text{ g} \pm 0.05$ of anode from pilot 2 (Chapter 4), and $0.26 \text{ g} \pm 0.11$ of anode from pilot 1 (Chapter 2). The average weight was larger in the samples from pilot 1, due to a thicker graphite felt anode in the first trial (10 mm) compared to the second (4.5 mm). The manufacturer's instructions were followed for cell lysis, DNA isolation and purification. Samples were eluted into 50 µL of DES (DNase/Pyrogen-Free Water) prior to PCR.

5.2.4 PCR, amplicon pooling and Illumina MiSeq 16S sequencing

Samples were shipped as DNA extracts in safe-lock Eppendorf tubes to LGC Genomics for further processing. 16S DNA genes were amplified by PCR with a 341F forward primer and 785R reverse primer pair. This was recommended based on Klindworth *et al.,* (2012) who compared the coverage of phylum spectrum of 175 primers and 512 primer pairs. Samples were checked for size, after which a clean-up of the PCR products followed. Each PCR amplicon was quantified to calculate and create an equimolar pool. Quality control of the library preparation took place using an Agilent 2100 Bioanalyzer. The pooled sample library underwent paired-end sequencing (2 x 300bp) on the Illumina MiSeq platform (V3 subunit) to produce up to 5 million paired-end reads. The FASTQ files were submitted to LGC Genomics' bioinformatics service for analysis of the bacterial and archaeal community diversity.

5.2.5 Bioinformatics

The following analysis was carried out by LGC Genomics' bioinformatics service using the FASTQ files of sequenced paired-end reads from the Illumina MiSeq V3 subunit:

- Inline barcode demultiplexing
- Clipping of sequencing adapters from 3' ends of reads

- Amplicon pre-processing with Mothur 1.35.1 including:

    a. removal of sequences with ambiguous bases,
    b. alignment against the 16S Mothur-Silva SEED r119reference alignment,
    c. filtering of short alignments,
    d. subsampling to 5 000-25 000 reads per sample,
    e. 'denoising' to remove sequencing error,
    f. removal of chimera using the uchime algorithm,
    g. taxonomic classification with Silva,
    h. OTU picking by clustering at the 97 % identity level (using the cluster. split method),
    i. *de novo* phylogenetic tree generation using the FastTree method
    j. Creation of OTU tables in the BIOM format

- Species level annotation of OTUs with NCBI BLAST + 2.2.29
- OTU diversity analyses with QIIME 1.9.0 including:

    a. OTU relative abundance heatmaps
    b. Within-sample diversity analyses i.e. taxonomic composition and rarefaction plots
    c. Between-sample diversity analyses with sample distance calculations (UniFrac) and principal coordinate analysis (PCoA).

5.2.6 SYBR gold staining and UV visualisation

Electrode biomass distribution was visualised in a method adopted from section 3.7.4 "Imaging biomass distribution on electrodes" (Popescu, 2016). Sections of anode, measuring 2 cm^2, were cut with a sterile scalpel. Samples were taken from pilot 1 (module 10) and pilot 2 (medium module 1), in line with DNA extraction (5.2.2) and scanning electron microscopy imaging (5.2.6). The surface most exposed to the wastewater was cut from the anode, to create a sample for analysis which was <1 mm thin.

Each sample was placed into a petri-dish and submerged with a nucleic acid stain, SYBR Gold (S11494, Life Technologies). The staining solution had been prepared by adding 5 μL of 10000 x SYBR Gold stock solution to 50 mL PBS (50 mM) (Popescu, 2016). Several batches of this stain were prepared to submerge the anode entirely. The anode was incubated for 30 minutes in the SYBR Gold solution in a Petri dish. The Petri dish was covered in tinfoil to prevent bleaching of the stain. The sample was rinsed in fresh 50 mM PBS buffer, transferred

to a clean Petri dish, and stored in tinfoil to prevent bleaching from ambient light. Each petridish was visualised inside a gel documentation system, as described by Popescu (iBOXR, UVP). UV light (at 340 nm) was applied in epi-illumination mode and emission was imaged using a band-pass filter (485-655 nm) (Popescu, 2016).

The images were converted to 8-bit greyscale files. Using ImageJ software, the 8-bit files were converted to binary images, by adjusting the threshold of the image. This collapsed the 256 levels of pixel intensity to just 2 levels: black (0) and white (255). Parts of the biofilm that picked up the stain were visualised as white, and parts which had not were visualised as black. The number of white pixels relative to black pixels was analysed, giving an indication of the percentage of the biofilm which had been stained. This is not an exact measurement of biofilm coverage (as shown in SEM imaging, 5.4.5), but a proxy for determining variation in biofilm distribution within an anode. Measurements are solely used to compare samples subject to the same preparation and visualisation at the same time.

5.2.7. Fluorescent staining and microscopy

Samples of catholyte were taken (5.2.1) from each of the three MEC reactors (Chapter 4). An aliquot of each sample was pipetted into a 2 mL tube and spun down in centrifuge (at 14,000 rpm) to obtain a pellet. The supernatant was discarded, and the mixture was not re-suspended. The 2mL tube was refilled with a second aliquot of sample and the process was repeated until 20 mL of each catholyte had been spun down. This process produced 3 x 2mL tube of concentrated sample, one for each reactor.

The sample was thoroughly mixed, before transferring a 100 μL aliquot of the sample to a new tube. A diluted fluorescent stain (SYBR Gold, 5.2.5) was added to each of the tubes. The tubes were covered in tinfoil and left to incubate for 30 minutes in the dark. Microscope slides were prepared by adding 1 drop of sample to the centre of the slide. Slides were dried in an incubator before applying a cover slip for visualisation on a Nikon Eclipse Ci fluorescence microscope with COOL LED PE300 laser system (465-495 nm excitation, DC505, emission 525-555 nm).

Images were processed using imageJ (5.2.5). The area of the field of view (125, 640 μm^2) was calculated from the diameter obtained with a 100x objective lens. The area of a known bacteria, *E. coli*, was calculated from assumed dimensions (0.5 μm x 2 μm). These values were used to determine the number of bacterial cells that could theoretically fit into the field of view. Percentage coverage was determined via imageJ (5.2.5). That percentage was applied

to the theoretical number of bacterial cells that could be visualised, to calculate an estimate of the number observed.

5.2.8 Scanning electron microscopy

Samples were taken using the core boring method (2.2.5). Each sample was fixed in 2 % glutaraldehyde in Sorenson's phosphate buffer and refrigerated overnight. Samples were rinsed with phosphate buffer for two 15 minute periods before a series of dehydrations in sequential ethanol concentrations. Samples were dehydrated in 25 %, 50 % and 75 % ethanol for 30 minutes each, before two one hour long dehydrations in 100 % ethanol.

The drying process was completed in Newcastle University's Medical School using a Baltec Critical Point Dryer. Samples were mounted on to an aluminium stub with Achesons Silver ElectroDag, before coating with 15nm of gold using a Polaron SEM Coating Unit.

Each sample was visualised as an overview (approx. 40 x magnification), prior to 500 x and 2000 x magnifications. This level enabled the operator to focus on the biofilm covering an individual graphite felt fibre. This process was carried out for a control sample (i.e. anode with no biofilm), a sample acclimated in wastewater for 21 days, and for 16 samples taken from the highest performing module from pilot 1 (Chapter 2) after 6 months.

5.3 Results

5.3.1   16S DNA sequencing

This section reports on the results from the second batch of 16S Illumina sequencing carried out by LGC genomics in Berlin. Some comparisons may be drawn with a previous batch of 16S Illumina sequencing carried out by University of Liverpool (pilot 1, Chapter 2).

Rarefaction depth

The 78 samples sent to LGC Genomics (Berlin, Germany) were run on an Illumina MiSeq v3 subunit with a maximum of five million sequences per run. This equates to a maximum rarefaction depth of 64,000 sequences per sample. The actual rarefaction depth across all 78 samples was 8,209 sequences per sample, however half of the samples analysed (39 samples) had 32,417 sequences per sample. The samples with a rarefaction depth of 32,417 were used to compare the biofilm within and between anodes. The rarefaction depth was smaller than the first lIlumina run (pilot 1), which had 70,521 sequences per sample.

Evenness

A total of 1247 different genera were identified using a 341F forward primer and 785R reverse primer pair on a v3 Illumina MiSeq run. A rank abundance plot (Fig. 5.1) shows a similarity in the log relative abundance of taxa in pilot 1 and 2. There were 979 taxa identified to genus level in the anodes of pilot 1 and 887 taxa identified in anodes of pilot 2 (Fig. 5.1). In comparison, there were 545 taxa identified in the cathode (Fig 3.10).

Simpson's diversity (D) accounts for abundance and richness, determining the proportion of individuals that each species contributes to the total sample (Table 5.2). It is determined by summing the relative abundance of each species. A sample with low richness but high evenness may have a higher Simpson's diversity value than a sample which is species-rich with poor equitability (Begon *et al.,* 1990). Evenness (E) is calculated by expressing index (D) as a proportion of the maximum possible value. This value lies between 0 and 1. Shannon's index (H) is another measure of determining diversity (Table 5.1). It is calculated by summing the multiple of relative abundance and the natural logarithm of the relative abundance for each species. Evenness (J) is determined by dividing the value for Shannon's index by the natural log of the maximum possible value.
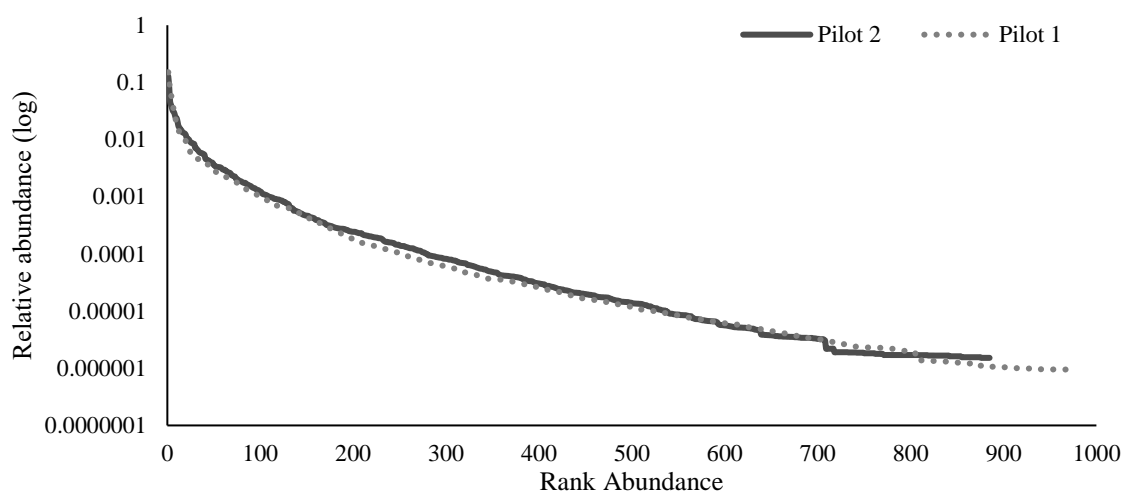
Figure 5.1. Rank abundance curve for anodic communities from pilot 1 and 2. Log relative abundance of pilot 1 (dotted line) and pilot 2 (solid line). There were 979 taxa identified in pilot 1 and 887 taxa identified in pilot 2.

	Number of taxa identified	Simpson's diversity index (D)	Simpson's evenness (E)	Shannon's diversity index (H)	Shannon's equitability (J)
Pilot 1 Anode	979	18.7	0.19	3.91	0.85
Pilot 2 Anode	887	27.7	0.28	4.24	0.92
Pilot 2 Cathode	545	18.4	0.18	3.64	0.79

Table 5.2. Diversity and evenness indices of the three sample groups: pilot 1's anode, pilot 2's anode and pilot 2's cathode.

Using both indices, pilot 2's anodes were more diverse (D = 27.7, H = 4.24) than the cathode samples from the same study (D= 18.4, H= 3.64) and the anodes from the previous pilot (D= 18.7, H= 3.91) (Table 5.2). Pilot 2 had fewer taxa than pilot 1, but greater values for evenness (H) resulting in a higher diversity value.

Community assembly

The relationship between the inoculum and the MEC biofilm was explored using both Illumina sequencing runs (Fig. 5.2-5.4). Individual taxa are plotted, showing their observed frequency in the MEC community and their relative abundance in the source community (Pi). A neutral community model (NCM) provides an alternative to niche-based theory, assuming dispersal-based assembly (Hubbell, 2001; Bell, 2001). Applying NCM to this study would predict an equal opportunity for bacteria in the sewage treatment works to disperse from the source community, and subsequently grow and/or and be lost or removed from the MEC (Venkataraman *et al.,* 2015). This model assumes stochastic processes, such as birth, death and immigration, often referred to as 'ecological drift', are responsible for community assembly. In an NCM, taxa of high relative abundance in the source community should be found at high frequency in the target communities (i.e. the MEC anodes).

Dashed black lines represent the 95 % confidence limits around this NCM assembly prediction (Fig. 5.2). Taxa that have a high frequency in the MEC, but a low abundance in the source community (shown by green dots) are enriched by the MEC environment. Conversely, taxa with a lower frequency in the MEC than would be expected (red dots), based on the taxa's abundance in the source community, are under-represented in the MEC (Fig. 5.2).
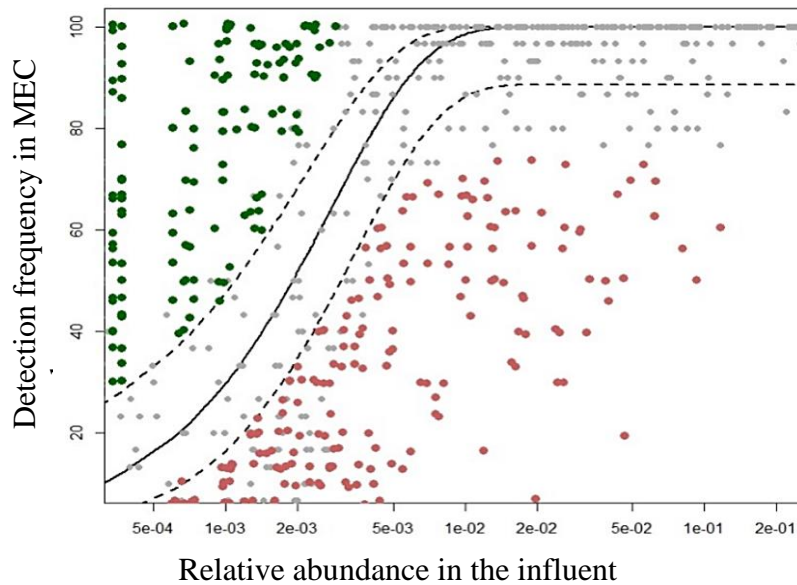
Figure 5.2. Frequency-abundance plot from anodes in pilot 1, showing enriched and under-represented taxa. The detection frequency of each taxon in the MEC community is plotted against its relative abundance in the influent. 95% confidence limits (dashed black line) on the neutral model (solid black line) show the boundaries for the predicted frequency of taxa based on its relative abundance in the influent. Deviation from the model indicates taxa which are enriched (green dots) or under-represented (red dots) in the MEC environment.

There were 1596 taxa identified to species level in the first Illumina run (University of Liverpool). There were 1227 common taxa between samples and used in the NCM model. 845 of these taxa (69 %) were plotted within the 95 % confidence limits of the NCM (Fig 5.2). Of these common taxa, 167 taxa were enriched (14 %), including species of *Geobacter*, *Clostridium*, *Desulfobulbus*, *Desulfomicrobium and Desulfovibrio*, and 215 taxa (18 %) were less frequent in the MEC than the model would predict. The less frequent taxa included one species of *Shewanella*.

Frequency-abundance graphs were plotted from the second Illumina sequencing run (LGC Genomics) to assess their fit to the NCM model (Fig. 5.3-5.4). In all three groups, there was a statistically significant correlation between frequency of detection in the MEC and relative abundance in the influent community (p=0.000). Spearman's rho showed a very strong positive correlation for both anodic communities: pilot 1 (r_s (438) = 0.983, p =0.000) and pilot 2 (r_s (405) = 0.971, p = 0.000) (Fig 5.4). Similarly, despite a smaller sample size, the cathodic community was also aligned with the NCM (r_s (279) = 0.920, p = 0.000). This demonstrates an excellent fit to the model. Deviation from the model shows that the least abundant taxa are slightly more frequent, and the most abundant taxa slightly less frequent than predicted (Fig

5.3). This may be a true observation, or could be a consequence of preferential amplification in the PCR process (Reysenbach *et al.,* 1992).
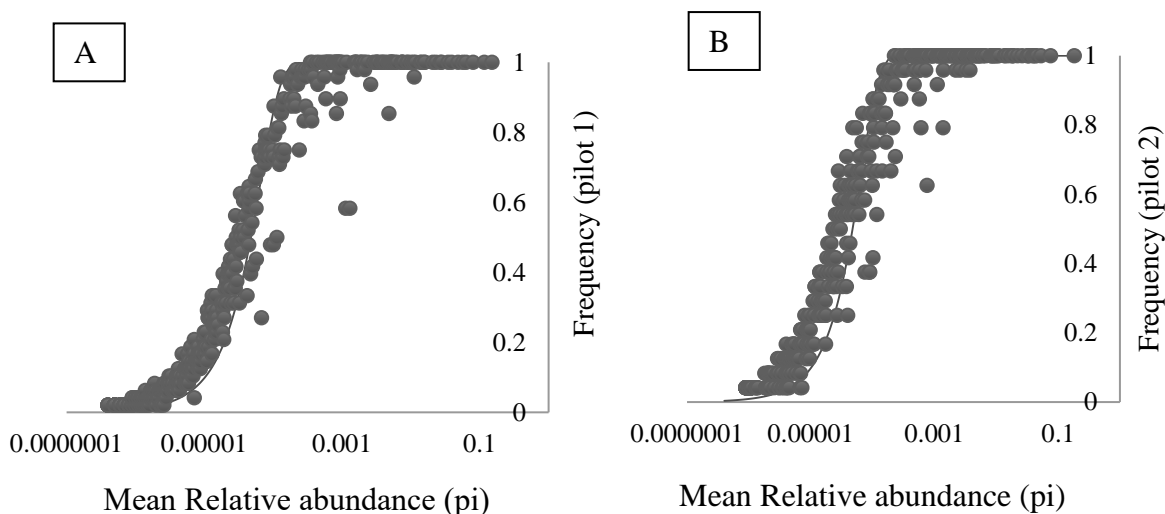
Figure 5.3 Frequency-abundance plots. A) Log relative abundance of taxa in the anodes of pilot 1 against frequency of detection in the sample (grey circles). B) Log relative abundance of taxa in pilot 2 against frequency of detection in the sample (grey circles). Their fit to the neutral community model (NCM) (grey solid line) is shown.

The strong correlation with the NCM model suggests that the MEC community was assembled randomly because of stochastic processes (birth, death, immigration and colonisation).
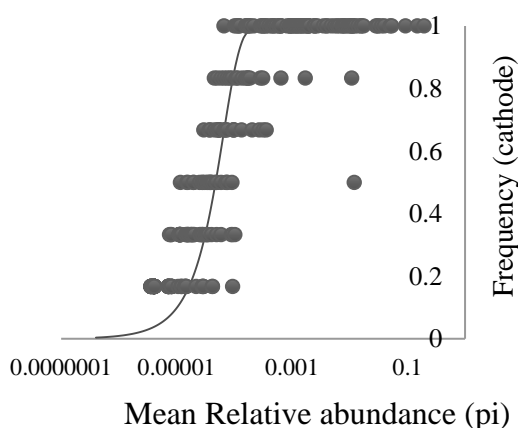
Figure 5.4 Frequency abundancy plot of taxa found in the cathode of pilot 2. Log relative abundance of individual taxa is plotted against frequency of detection in the samples (grey circles). The samples' fit to the neutral community model (NCM) (grey line) is shown.

Rate of immigration

Rate of immigration (m) indicates the likelihood of population of a local community by individuals from the source community, rather than by births within the local community (Ofiteru *et al.,* 2010). N_Tm, calculated in the NCM, describes how the distribution of taxa in a local community deviates from the source community (Ofiteru *et al.,* 2010). N_Tm is the product of immigration probability (m) and the number of individual bacteria (N_T).

The best N_Tm reported by the NCM in Fig. 5.3 was 12501. This was based on the first Illumina sequencing run (carried out by University of Liverpool), resulting in 70,521 reads. A Spearman's Rho showed a strong, positive correlation of the experimental data from the MEC with the theoretical NCM. This correlation was statistically significant (r_s (843) = 0.652, p = 0.2 x 10^{-15}). The immigration probability (m) could not be calculated, as the number of individuals (N_T) had not been previously determined by qPCR. The second sequencing run, carried out by LGC genomics, had a sequencing depth of 32, 417. The N_Tm values reported by the NCM were 18091 (pilot 1's anodes), 18607 (pilot 2's anodes) and 15735 (pilot 2's cathodes).

Principal coordinate analysis (PCoA)

A principal coordinate analysis (PCoA), otherwise known as metric multidimensional scaling, aims to 'calculate a distance matrix and produce a graphical configuration in a two or three-dimensional Euclidean space' (Zuur *et al,* 2007). The distances between the points reflects the samples' dissimilarity.

Samples with a rarefaction depth of 32,417 are shown in three colours on the PCoA plot (Fig. 5.5). Three samples (brown dots) represent the planktonic bacteria from the cathode electrolyte, 14 samples (blue dots) represent the anodic biofilm from the medium MEC in pilot 2 (Chapter 4) and 22 samples (purple dots) represent the anodic biofilm from pilot 1 (Chapter 2).

Distinct groupings can be seen based on colour, and therefore location of sample. The two anodic biofilms (shown in blue and purple) are at opposite ends of the PC1 axis which represents 21.4% of the variation. The biofilm formed under different environmental conditions: the inoculum came from geographically distinct sites (20 miles apart); and start-up took place during different seasons (summer for purple samples, winter for blue samples).

The brown dots, representing the planktonic cathodic bacteria, are at the opposite end of the PC2 axis, which represents 6.31% of the variation, to both (blue and purple) anodic samples, but the same end of the PC1 axis (which represents 21.4% of the variation) as the blue dots (Fig 5.5). The blue and brown dots represent samples which were taken from alternate sides of a membrane in the same reactor, which may suggest why there is some variance across the distinct chambers of the reactor (6.31%), but less than in samples which were taken from a different reactor entirely (21.4%).
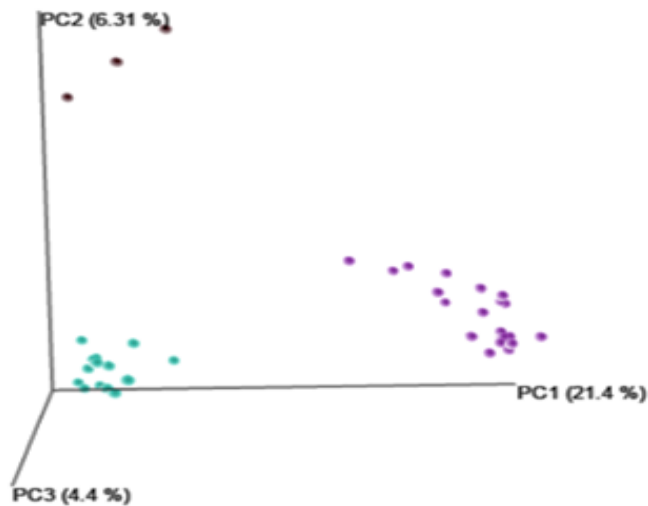
Figure 5.5. Principle co-ordinate analysis (PCoA) plot at rarefaction depth of 32,417. Brown dots (top left) represent the planktonic cathodic bacteria, blue dots (bottom left) represent the anodic biofilm from the medium MEC in pilot 2 (chapter 4) and purple dots (bottom right) represent the anodic biofilm from pilot 1 (chapter 2).

The unweighted UniFrac distance matrices were analysed to determine if there was a statistically significant difference in the distances between groups. A one-way ANOVA, based on distance matrix values, showed distances between groups were larger than variation seen within groups. Therefore, the anodes from the second pilot trial (blue dots) were significantly further away from the anodes from the first pilot trial (purple dots) than could be accounted for by variation within a group (F (2, 65) = 659.872, p = 0.000) (Fig. 5.5).

There was a significant difference between the top, middle and bottom of the anode from the samples from the first pilot trial (F (5,43) = 42.402, p = 0.000). Distances between sample groups (i.e. top vs middle) were significantly larger than within sample groups (i.e. top vs top). There was no significant difference in the variation within groups (i.e. top vs top). Variation within samples at the top of the anode (0.46 ±0.021) was not significantly different

to variation within samples in the middle of the anode (0.49 ±0.016) (p=0.155). Similarly,

variation within samples at the bottom of the anode (0.45 ± 0.023) was not significantly
different to variation at the top (p=0.775) (Table 5.3).

However, there was a significant difference between groups. Matrix distances were
significantly larger between groups (0.55± 0.017, 0.56 ± 0.023, and 0.54 ± 0.021) than
within groups (0.46 ± 0.021, 0.45 ± 0.016, and 0.49 ± 0.023) (p= 0.000) (Table 5.3).

Location of paired samples	Mean unweighted UniFrac matrix distance
Top vs Top	0.46 ± 0.02
Top vs Middle	0.55 ± 0.02
Top vs Bottom	0.56 ± 0.02
Middle vs Middle	0.49 ± 0.02
Middle vs Bottom	0.54 ± 0.02
Bottom vs Bottom	0.45 ± 0.02

*Table 5.3. Mean unweighted UniFrac matrix distances across locations in MEC anode from
pilot 1 (Chapter 2). Paired samples were compared within and between groups to assess
sample dissimilarity.*

Whole anode transects

Samples taken from a high performing module (from pilot 1) were used to assess
homogeneity of the microbial community. This was to determine whether monthly spot
samples, taken during operation (chapter 2), reflected the community fairly. The relative
abundance of key families, such as Geobacteraceae, Desulfobulbaceae and Comamonadaceae,
were compared across 22 sample locations (with a rarefaction depth of 32,714).

Sample locations were grouped as top, middle and bottom. The depth of the anode was 30 cm.
Each group reflects the average microbial community across 10 cm. Analysis of the top 50
families (by proportional abundance) showed 88% were common across the whole anode (Fig
5.6). Only 6 % of families were found solely in the top or the bottom of the anode. Fewer
families (2 %) were found solely in the middle of the anode (Fig. 5.6).
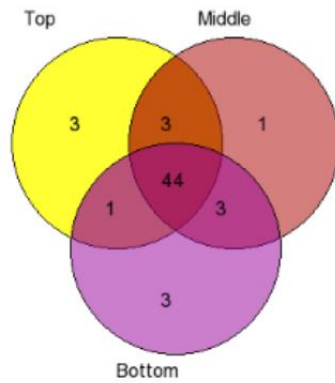
Figure 5.6. Distribution of top 50 families by relative abundance in the top, middle and bottom third of anode transect from pilot 1.

A one-way ANOVA ($F_{(2,22)} = 0.661$, $p = 0.528$) showed no significant difference in relative abundance of Geobacteraceae in the top ($0.011\% \pm 0.009$), middle ($0.4\% \pm 0.9$) or bottom ($0.7\% \pm 1.7$) third of the anode. Similarly, there was no significant difference in the relative abundance of Comamonadaceae ($F_{(2, 22)} = 2.502$, $p = 0.108$), which include hydrogen-oxidisers *Hydrogenophaga* and *Acidovorax*, or the sulphate-reducing Desulfobulbaceae ($F_{(2,22)} = 0.475$, $p = 0.629$) across locations. There was, however, a significant difference in the relative abundance of another family of sulphate reducers, Desulfovibrionaceae ($F_{(2,22)} = 13.462$, $p = 0.000$). The top of the anode ($1.3\% \pm 0.4$) had significantly more Desulfovibrionaceae than the middle ($0.9\% \pm 0.2$) ($p = 0.016$). The middle of the anode had significantly more Desulfovibrionaceae than the bottom ($0.5\% \pm 0.1$) ($p = 0.035$) (Fig. 5.7).
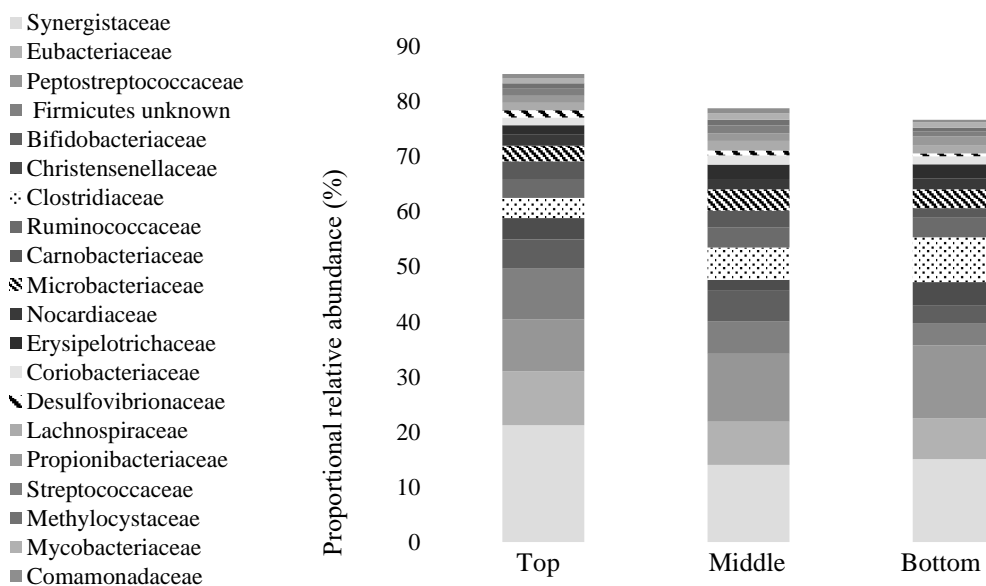
Figure 5.7. Relative abundance of the top 20 families including Comamonadaceae, Synergistaceae and Clostridiaceae. Comparisons are made between the community in the top, middle and bottom of an anode from pilot 1.

106

The process was repeated when the medium MEC from pilot 2 was decommissioned. Transects from pilot 2 showed that 88 % of the top 50 families (by proportional abundance) were common across the whole anode (Fig. 5.8). Despite a four-fold increase in surface area, the depth of the anode was only 10 cm larger as the module was positioned landscape, rather than portrait, in the MEC tank. Each group reflects the average microbial community across a depth of 13.3 cm. Only 4% of families were found solely in the top or middle, whereas 6 % of families were found solely in bottom third of the anode (Fig. 5.8). However, in the second pilot trial, one-way ANOVA ($F_{(2, 22)}$ = 8.410, p =0.006) showed a significant difference in the amount of Geobacteraceae between the bottom (1.8 % $\pm$ 0.75) and both the top (0.6 % $\pm$ 0.2) (p =0.016) and the middle (0.6 % $\pm$ 0.4) (p=0.01) (Fig 5.9).
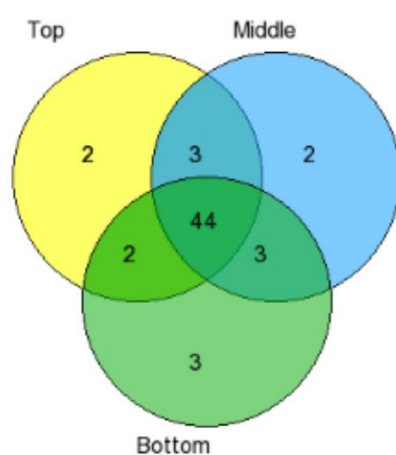
Figure 5.8. Distribution of top 50 families by relative abundance in the top, middle and bottom third of medium MEC pilot 2.
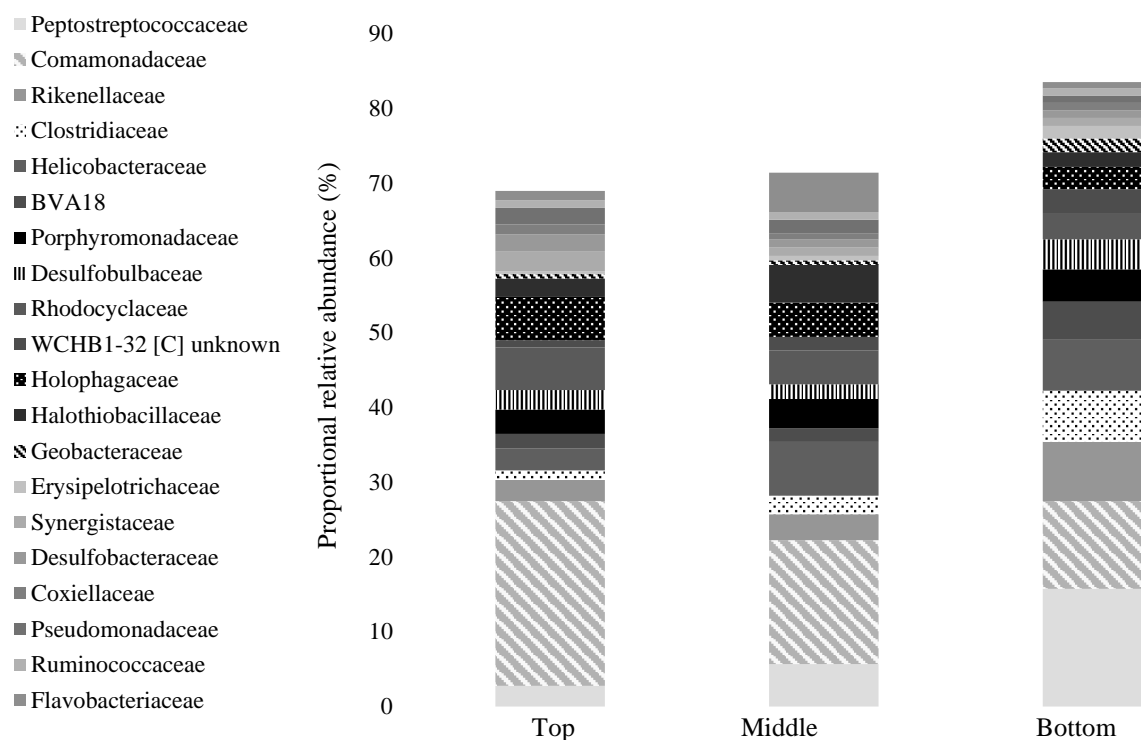
Figure 5.9 Relative abundance of the top 20 families including Comamonadaceae, Desulfobacteraceae and Geobacteraceae. Comparisons are made between the communities in the top, middle and bottom of the medium MEC anode (pilot 2).

5.3.2 SYBR gold staining

A. Anode 10 MEC pilot 1

Distribution of pixels, observed in imageJ after UV visualisation of the first pilot's anodes, showed heterogeneity of SYBR gold staining (Fig. 5.10). The SYBR gold nucleic acid stain was heavily picked up in small localised patches. The majority appeared not to have picked up the stain. This observation was confirmed by calculating the percentage of white to black pixels in the binary image. In the front-facing anode (i.e. facing the flow of wastewater) (Fig. 5.10a) 5% of the sample picked up the SYBR gold stain. Samples taken from the rear-facing anode (Fig. 5.10b) had marginally lower coverage, at 4.3%.

Coverage ranged from 2.4 to 6.9% in the front anode, and 1.9% to 9.5% in the rear anode (Table 5.4). The widest range was recorded in samples located directly next to each other. This corresponded to two taken from the middle vertical plane on the front anode, and two taken from the bottom vertical plane on the rear anode (Table 5.4). In both cases, these two samples were spaced 8 cm apart horizontally.
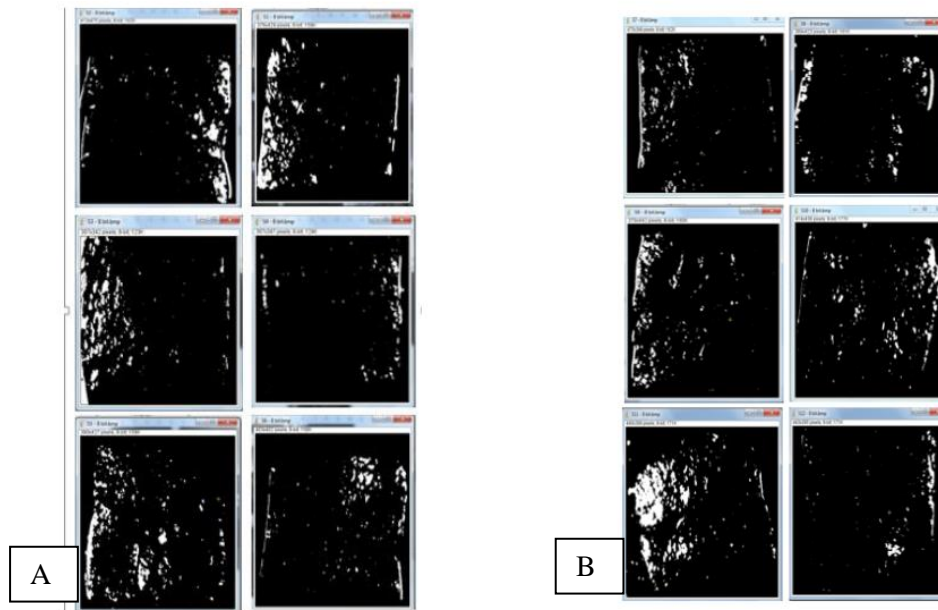
Figure 5.10. A) ImageJ images from the front anode of module 10 from pilot 1. B) ImageJ images from the rear anode of module 10 from pilot 1. Images were created after UV visualisation of SYBR gold staining. The stained biofilm is depicted as white on a black background. Each sample measured 3cm x 3cm.

	Pilot 1 MEC Front Anode		Pilot 1 MEC Rear Anode	
Top	6.5%	5.0%	3.1%	3.4%
Middle	6.9%	2.4%	4.0%	3.8%
Bottom	5.9%	3.1%	9.5%	1.9%

Table 5.4. Percentage of stained biofilm in the samples obtained from the front and rear anodes from module 10 in the MEC from Pilot 1. The percentages were calculated based on the ratio of white to black pixels from the binary images created in ImageJ. Percentages are laid out in the table in accordance with their positioning in Fig 5.11.

B. Anode 1 Medium MEC Pilot 2

Distribution of the white pixels in imageJ appeared, qualitatively, to be more even in Fig. 5.11 than Fig. 5.10. Yet, there was no difference in the average percentage calculated: 5% of each biofilm picked up the SYBR gold stain. Coverage varied from 1% in the bottom right, to 16.6% in the sample immediately left of this sample. These samples were spaced 12 cm apart horizontally and were on the same vertical plane.
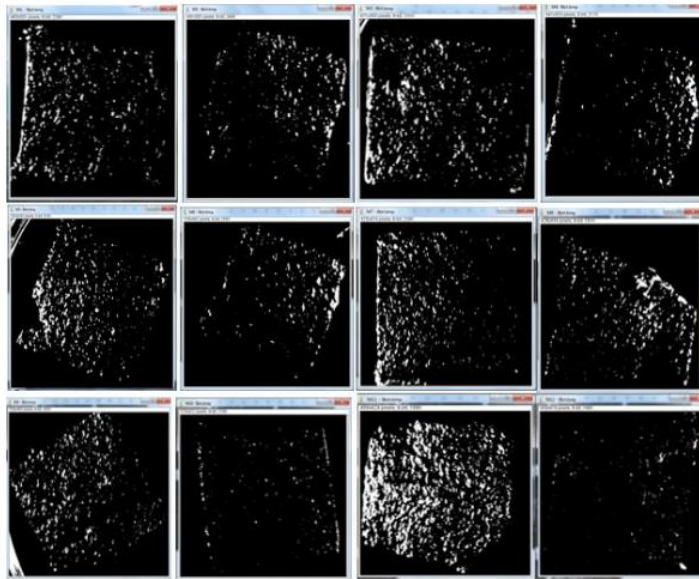
Figure 5.11. ImageJ binary images from the anode of the first module from the medium MEC in pilot 2 (Chapter 4). The binary images were created following UV visualisation after a SYBR gold nucleic acid stain had been applied. The stained biofilm is depicted as white on a black background. Each sample measured 3cm x 3cm.

	Medium MEC Pilot 2			
Top	5.0%	3.4%	6.5%	3.6%
Middle	5.2%	2.6%	5.2%	4.2%
Bottom	5.2%	1.8%	16.6%	1.0%

Table 5.5. Percentage of stained biofilm in the samples obtained from the Medium MEC from Pilot 2. Percentages were calculated based on the ratio of white to black pixels from binary images in ImageJ. Percentages in the table reflect their positioning in Fig 5.12.

5.3.3 Fluorescent staining

SYBR gold staining showed bacterial cells were present in the catholyte. The cathode, which in theory is abiotic, is separated from the anodic biofilm and wastewater by a microporous battery separator. Microscopy showed variation in the heterogeneity of bacterial cell concentration. The cathodic liquid had been concentrated 10-fold prior to visualisation. Estimates suggest there were an average of 3053, 7634 and 6382 cells visualised in the cathodes of the large, medium and small MEC (Chapter 4) respectively. This suggests there were between 7,000 and 15,000 cells per mL in the cathode, based on the visualisation of one drop (50 µL) of 10x concentrated sample.

5.3.4. Scanning Electron Microscopy (SEM) imaging

A. Control

A sample of graphite felt was visualised under the scanning electron microscope to see the surface to which the biofilm would adhere. It was used as a baseline control for comparison with the MEC samples. The graphite fibres can be seen clearly to form a network of interlaced surfaces (Fig. 5.12). These surfaces connect periodically, but gaps between fibres are particularly evident at 500 x (Fig. 5.12b) and 2000 x magnification (Fig. 5.12c).
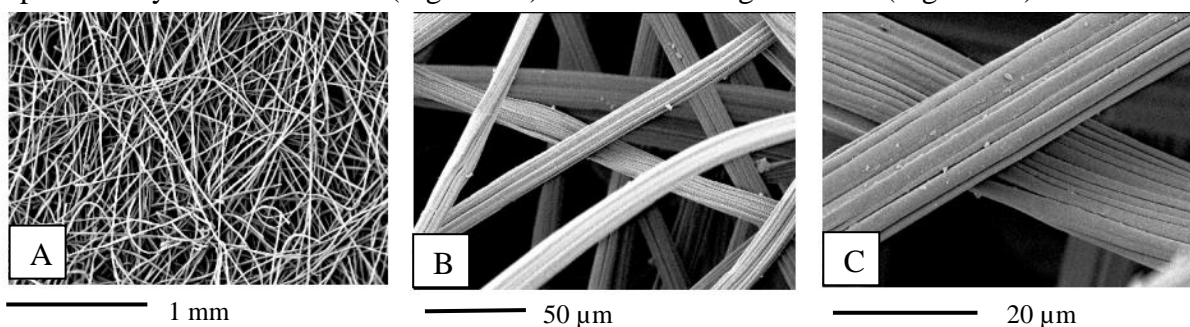
Figure 5.12. Scanning electron micrographs of graphite felt anode with no biofilm enrichment, for use as a control at A) 40 x, B) 500 x and C) 2000 x magnification

B. Batch inoculation (21 days)

A prototype module was placed in a bucket of domestic sewage, in which the substrate was replaced once a week. A sample was taken after three weeks. This would be used for comparison with samples taken from MEC anodes operated for six months. After three weeks' inoculation in domestic sewage, the biofilm distribution is heterogeneous. There are localised clusters of biofilm (evident at 500 x magnification) (Fig. 5.13b). However, the biofilm does not form a complete layer across fibres.
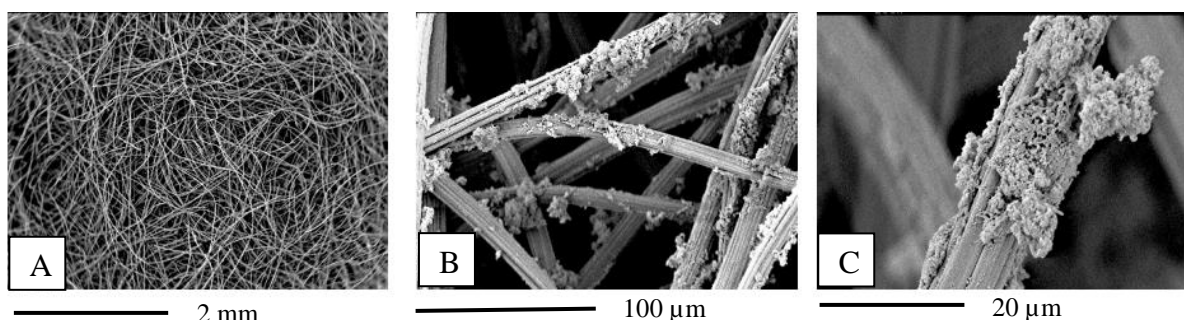
Figure 5.13. Scanning electron micrographs of an anode after inoculation in batch-fed domestic wastewater for 21 days at A) 20 x B) 500 x and C) 2000 x magnification.

C. Six months in continuous flow MEC

After pilot 1 was decommissioned (Chapter 2), 16 samples were taken throughout the highest performing modules. The location of these samples matches the location of the samples taken for 16S DNA sequencing (5.3.1). After six months, the distribution appears uneven and localised at an overview level of magnification (Fig. 5.14). At 2000 x magnification, each fibre is shown to be fully coated in biofilm (Fig. 5.15). Clusters are apparent in the overview (Fig. 5.14). It is unknown whether this cluster is biofilm, or an accumulation of solid or fat from the wastewater that has become clogged in the anode.
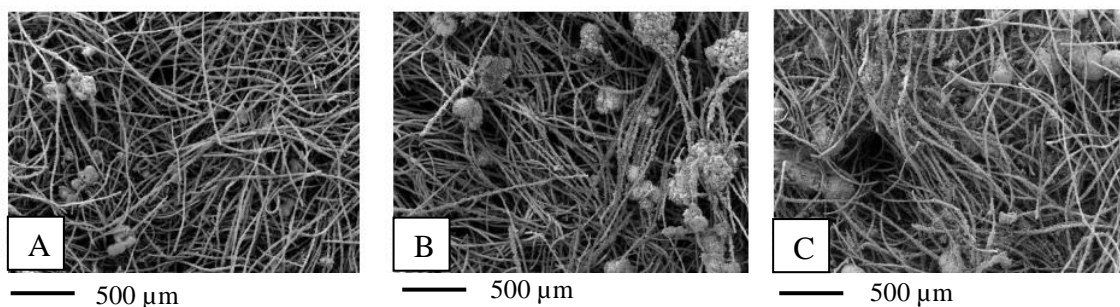
Figure 5.14 Scanning electron micrographs of anodes after six months' inoculation in wastewater in a continuous flow MEC, A-C at 100 x magnification.
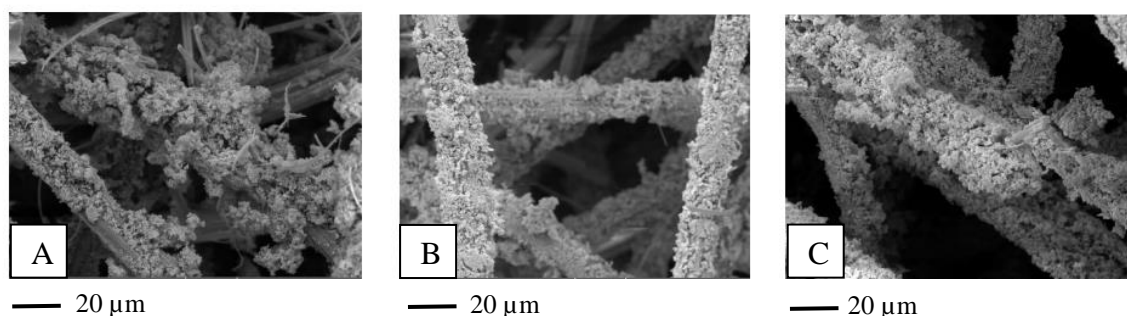
Figure 5.15 Scanning electron micrographs of the biofilm growing around several individual fibres in the graphite felt anode, after six months' inoculation in wastewater after operation in a continuous flow MEC, A-C at 2000 x magnification.

After six months, the biofilm is denser and less heterogeneous than the biofilm observed after 21 days (Fig. 5.13). However, it is still not a solid layer. Therefore, description as a network of individual biofilms is more representative. It is not known how this will influence cell-to-cell communication between separate fibres, and therefore whether this affects current generated by the anode in its entirety.

5.4 Discussion

There was a significant difference in the communities from the first and second pilot MEC (5.3.1). Despite similar inoculation with domestic wastewater, principle co-ordinate analysis showed significant distances between the samples from the two pilots, with statistically distinct communities. Further analysis revealed only half of the order level taxonomic groups were shared. Jiang *et al.,* (2016) found that 45 % of the OTUs (601 in total) were shared between the three anodic biofilm samples, arguing that this suggested a continuous core community. However, one of the samples had a high proportion of unique OTUs (20 %), which they suggest implies a significantly different community.

Studies have shown that substrate and electrode potential can affect exoelectrogenic community composition (Torres *et al.,* 2009; Kiely *et al.,* 2011; Ishii *et al.,* 2014). The bacterial community in this study is likely to be shaped by a combination of the bioelectrochemical process and the influent wastewater community. The MEC community is entirely dependent on the bacteria present in the substrate, but may be influenced by certain environmental conditions (such as applied potential) during start-up.

Zhou *et al.,* (2013) investigated stochastic and deterministic colonisation of microbial communities in controlled laboratory BES (Zhou *et al.,* 2013), finding little overlap in communities between reactors subject to identical environmental conditions. Zhou *et al.,* (2013) suggest that 'ecological drift' may be crucial in shaping these communities, creating considerable site-to-site variation. Ecological drift, which includes the processes of birth, death, colonisation and extinction, leads to a community assembly owing to dispersal rather than adaptation (Hubbell, 2001; Bell, 2001).

Zhou *et al.,* (2013) found that one group of MECs produced 76 times more hydrogen than another group of MECs with a statistically different microbial community. They suggest this difference in performance was likely caused by stochastic variation in community assembly. Variation partitioning analysis showed that gas yields (as an indicator of deterministic processes) accounted for 30 % of the variation in the microbial communities of their replicate MECs (Zhou *et al.,* 2013). This finding supports their implication that deterministic processes, such as species interactions, selection and priority effects, may intensify variation caused by stochastic processes, which they suggest accounts for over half (57 %) of the total community variation (Zhou *et al.,* 2013).

The community in the first pilot trial, analysed in the first Illumina sequencing run, showed a significant, positive correlation with a neutral community model (NCM). This analysis showed 69 % of taxa were located within the 95% confidence limit of the model. Several species of *Geobacter* and SRB were found at greater frequencies within the MEC than would be expected based on their relative abundance in the influent wastewater. These species are likely to be enriched by the environment within the MEC. Moreover, the anodic and cathodic communities from the second pilot, analysed in the second Illumina sequencing run, also showed a very strong correlation with the NCM. This suggest the MEC community is very likely to be randomly assembled by stochastic, rather than deterministic, processes. Immigration probability could not be calculated in this study, as the number of individual bacteria had not been quantified. Future analysis of anodic biofilms in MEC should aim to determine the number of individuals by quantitative PCR (qPCR). This will allow the probability of anode colonisation by the source community to be assessed. This information will provide additional information about the diversity of taxa in the local community and the method of assembly.

Geobacter was shown to comprise 7-10% of the anodic community in the spot sampling during operation of the first pilot (2.4.1). This result may have been affected by the proximity of the sampling location to the point of electrical connection, although this was not specifically tested. The spot samples from pilot 1, which were taken once per month from the top of each anode, accounted for less than 2% of the anode's total surface area. In a second study, transects were taken across an entire anode (5.3.1), showing community heterogeneity. Across 22 samples, reflecting 18% of the anode's surface area, *Geobacter* was shown to comprise <1% of the total community. In the second study, there was several points of electrical connection, compared to the single point of connection in the first study. It is, therefore, unlikely that the variation in *Geobacter* is associated with increased ohmic resistance with increased distance from the point of electrical connection. Furthermore, findings from the transects implied that proportional abundance of *Geobacter* increased with increasing anode depth. There was no significant difference in the variation in community between samples in the same location. Therefore, as temporal sampling (2.4.1) took place within the top section of each anode (to minimise disruption during operation) the reflections made in Chapter 2 are not affected by the heterogeneity presented now.

Proportions of *Geobacter* were low in the anode transects (<1% of relative abundance). Therefore, performance may have been limited by the low relative abundance of *Geobacter*. Ishii *et al.,* (2014) showed that microbial communities with high per-biomass electrogenic activity tend to contain a high relative abundance of known exoelectrogens, such as *Geobacter* and *Desulfuromonas.* It is likely that unreported exoelectrogenic bacteria are contributing to current generation. Sulphate-reducing bacteria can generate electricity from the oxidation of organic material. It is not known whether the relationship between *Geobacter* and SRB is competitive or syntrophic (Ishii *et al.,* 2014). Fermentative bacteria, such as *Clostridium*, have also been linked with electrogenic activity (Ishii *et al.,* 2014).

The anodic biofilms analysed in this chapter are dominated by the Firmicutes, Proteobacteria and Bacteriodetes, as reported in previous studies of BES anodic biofilms (Ishii *et al.,* 2014; Chae *et al.,* 2009; and Holmes *et al.,* 2004). Bacteria may be contributing to the removal of COD, without contributing to the electrochemical process. This could be detrimental for two reasons: COD removal may be carried out by competing methanogenic bacteria (which may increase GHG emissions from the anode); and competitive COD removal reduces the amount of energy that can be recovered bioelectrochemically. Methanogenic bacteria were not detected in the anode from pilot 2. Three orders containing methanogenic bacteria were found in the anodes from the first pilot: Methanobacteriales (<0.1% abundance), Methanosarcinales (<0.1% abundance) and Methanomicrobiales (<0.2% abundance). Six methanogenic species were found to be enriched in the NCM, indicating these species were detected more frequently in the MEC than their relative abundance in the raw wastewater would predict.

Even in a perfectly mixed reactor, transport of nutrients to the biofilm will be heterogeneous (Mason and Stuckey, 2016, Stewart 2003). Diffusion into the biofilm will be limited by the particle boundary layer, and transport within the biofilm will depend on the recycling of nutrients and metabolic products (Mason and Stuckey, 2016). This gives rise to differences in the chemical and biological environment across the biofilm. Such differences could lead to pH gradients, inhibition of metabolic processes or restriction of flow (Mason and Stuckey, 2016), creating an environment in which parts of the biofilm are limited. Gases, such as carbon dioxide or methane released by anodic bacteria, could become trapped in the biofilm creating localised chemical changes which inhibit performance.

It is not yet known whether the heterogeneity observed in biofilm distribution (5.3.2 and 5.3.4) is correlated with performance. SYBR gold staining and UV visualisation (5.3.2)

suggests only 5% of the anode surface area is dominated by biofilm. Current density has been shown to be proportional to biofilm thickness (Ishii *et al.,* 2008 and He *et al.,* 2011). It is unlikely that 5% is the maximum achievable coverage, since 16% coverage was observed in one portion of the anode (5.3.2). Therefore, it is recommended that distribution and biofilm coverage is assessed in high performing reactors to determine if this is a way to improve current density.

Chapter 6. Cost benefit and sensitivity analysis

6.1 Introduction

Life cycle analysis of BES suggests that MFCs may not provide enough direct environmental benefits to justify the replacement of 'conventional' anaerobic treatment (Foley *et al.,* 2010). MECs, however, provide additional benefits through sustainable chemical production, which may surpass the benefits of conventional processes, such as anaerobic digestion (Foley *et al.,* 2010). The pilot MEC from chapter 4 is hypothetically scaled-up in this chapter, to enable economic comparison with an existing wastewater treatment technology. MEC can produce a wide range of chemicals and bioenergy. Cost benefit and multi criteria analysis are used to determine which product provides the most sustainable option for the technology.

6.1.1. What is a cost benefit analysis?

Cost benefit analysis (CBA) is a tool used to support rational decision making, by systematically cataloguing the benefits (advantages) against the costs (disadvantages) (Boardman *et al.,* 2014). It is an economic assessment tool. Benefits and costs are assigned monetary value. The net benefit is a calculation of benefits minus costs. Some variables in the analysis will have direct monetary costs which can be referenced, other variables may have a theoretical value assigned. A theoretical value is assigned if the value is likely to change with time, or because it does not have a direct monetary value. These factors provide cause for disagreement over the suitability of CBA as a decision-making tool by some economists, politicians and philosophers (Boardman *et al.,* 2014).

6.2 Methods

6.2.1. Stages of a cost benefit analysis
Stage 1: Define the project and the alternatives

The primary step defines the boundaries of the analysis, and the variables that will be considered. The greater the number of variables, the greater number of options for each variable in the CBA. Many analysts aim to keep the number of alternatives below six (Boardman *et al.,* 2014). The project definition should consider who the CBA affects, and the scenario in which the resources available will be reallocated (Hanley and Spash, 1993). The latter is often more straightforward to define. Deciding which benefits and costs should be included, is often contentious (Boardman *et al.,* 2014).

Stage 2: Identify the impacts

Stage two involves identifying the impacts arising from the project's implementation. Impact relates to both inputs (i.e. the resources required to complete the project) and outputs (i.e. the economic and/or societal impact) (Hanley and Spash, 1993; Boardman *et al.,* 2014). This stage raises questions of what to count and how to count them. Impacts should only be considered if they have 'standing'; meaning they have a measurable benefit or cost to the population (Boardman *et al.,* 2014). Where there is a risk of uncertainty, assigning probabilities can help to determine quantitative measurements (Hanley and Spash, 1993).

Stage 3: Monetize the impacts

Impacts must be valued in common units: money is the most convenient for comparison (Hanley and Spash, 1993). Some impacts are easier to monetize. Traded goods have a direct market value: the cost of labour can be determined from hourly wages. Other impacts, including those relating to the environment, can be difficult to assign monetary value to (Boardman *et al.,* 2014). An impact may have a monetary value of zero, if no one is willing to pay to prevent or create that impact (Boardman *et al.,* 2014). An impact's value changes in line with global markets. Market value could increase or decrease because of competition. Additionally, a policy change or government intervention could also influence a market change.

Stage 4: Discount benefits and costs to obtain present values (PV)

For projects spanning several years, benefits and costs must be assigned to a specific year. A fixed monetary value is not worth the same from year to year. To account for the effect of time, a discount rate is applied. A discount rate is used to reflect the changing value of money with time, or as a reflection of risk. Present value (PV) is calculated as, PV $(X_t) = X_t [(1+i)^{-t}$, where i = rate of interest and t = time.

Stage 5: Compute net present value of project

The net present value (NPV) of a project asks whether the sum of discounted benefits exceeds the sum of discounted costs, i.e. NPV = PV (benefits) – PV (costs). If NPV > 0, it represents an efficient shift in resource allocation and indicates an improvement in social welfare (Hanley and Spash, 1993). If there are a number of alternatives that all achieve NPV > 0, then the option with the largest NPV would be deemed the most efficient allocation of resources considered and likely to provide the most benefits to those with standing. This provides the

best NPV out of those considered in the CBA. There may be better options in existence that were not considered.

Stage 6: Perform sensitivity analysis

Sensitivity analysis can be used to account for uncertainty of variables. In theory, every variable could be subject to some uncertainty and could undergo sensitivity analysis. However, this would be time consuming and may confuse how best to judge the results from the model. Instead, variables subject to the most uncertainty should be identified for sensitivity analysis in the project definition stage.

6.2.2. Definition of the MEC CBA project

Boundary of analysis

A boundary must be drawn to determine which benefits and costs are to be considered in the CBA. The primary comparison will be between the chemical outputs from the MEC (Fig 6.1). Therefore, it is assumed that pre-treatment and post-treatment are consistent in all scenarios. Pre- and post-treatment are outside of the boundary of analysis. The MEC is assumed to be a secondary biological process, with screening, grit removal and primary sedimentation upstream. Phosphorous and nitrogen are not removed in the MEC. Therefore, all scenarios assume chemical precipitation of phosphorous during primary clarification. The physical or chemical removal of nitrogen is slightly more problematic. The existing options, including air stripping, chemical oxidation and ion exchange are likely to negate the economic and environmental benefits of using an anaerobic process, such as MEC. However, as these options fall outside of the boundary of analysis they are not considered in this CBA.

The CBA does not account for the sale of products externally and their transport commercially (Fig. 6.1). Instead, the outputs' value is calculated from the financial saving gained from not purchasing externally, and the environmental saving from sustainable production of chemicals.
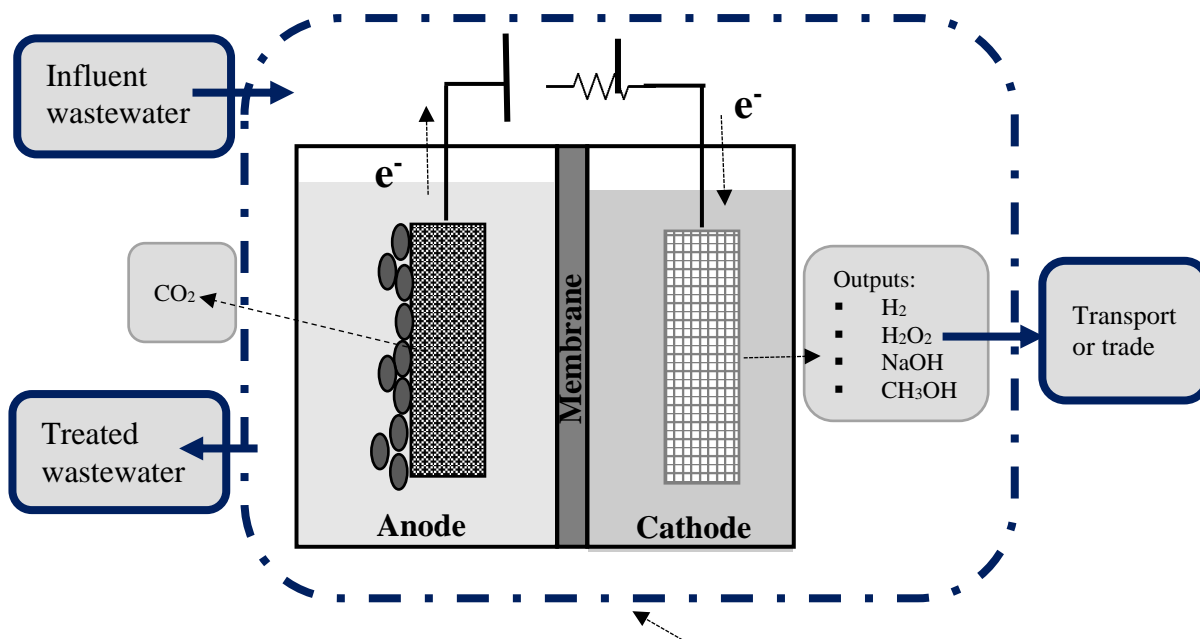
Figure 6.1. Schematic showing boundary of MEC system with chemical production for cost benefit analysis. Product options include hydrogen (H_2), hydrogen peroxide (H_2O_2), sodium hydroxide (NaOH) and methanol (CH_3OH).

Process description and performance

The model MEC is based on a prototype trialled in this study (Chapter 4) in terms of configuration, materials and performance. The model MEC has been hypothetically scaled-up to enable full scale treatment at a medium sized sewage treatment works (STW). This has been scaled up to treat the BOD from a population of 25,000. The pilot MEC (chapter 4) which contained 3 modules, treated a population equivalent of 6. It is assumed that each module is scaled up by a factor of 20: resulting in 625 modules. This is in line with dimensions of an activated sludge lane on a small to medium works.

The level of COD removal is comparable with pilot 2, assuming 65% removal after secondary clarification, achieving the UWWTD consent of <125 mg/L. Maximum current production achieved in pilot 2 was 788 mA/m$^{2.}$ However, this was not consistently achieved in one, let alone all three, of the modules. It is anticipated that current production can be improved significantly. However, a conservative, but realistic, estimate of 1000 mA/m^2 of anode (Aiken, personal communication) is assumed to be the average current output in the model MEC: significantly lower than in previous studies (Foley *et al.,* 2010; Pant *et al.,* 2011). Product yields are calculated based on the current production.

The model system is compared to an aerated system generated using Northumbrian Water's iMOD software. It is assumed that the aerated system is a carbonaceous activate sludge system, with fine bubble diffuser air (FBDA) compressors, submerged aeration pipework and control panel. The model assumes a standard oxygen transfer rate of 200 kg-O_2/hr and a compressor rating of 51.9 kW.

Material Costs

Prices provided for each MEC component are those obtained during fabrication of pilot 2 (Chapter 4). The material and unit size of each component are described along with cost (Table 6.1). These values were used to estimate the cost of a full scale MEC (Table 6.2). The cost of the concrete infrastructure required for the MEC is not included, as this would also be required for the convention technology. Similarly, the cost of replacement parts and maintenance is not considered, as this too would be required for the conventional technology.

MEC component	Material	Cost (£)	Unit size	# of units	Total cost (£)
Anode	4.6mm graphite felt	90	m^2	6	540.00
Current Collector	316 stainless steel mesh	30	m^2	12	360.00
Membrane	Rhinohide UHMWPE	1	m^2	6	6.00
Cathode	stainless steel wire wool	40	per kg (19m)	1	40.00
	316 stainless steel mesh	30	m^2	2.4	72.00
Catholyte	0.1M NaCl	159	25 kg	0.0048	0.76
Structural support	PVC	48.47	Each	3	145.41
Wires	0.2mm wire	11.39	100 m	0.1	1.14
Resistors	0.1Ω resistor	0.84	pack of 5	0.6	0.50
Power supply	Caltek PSM 2/2A	142.4	Each	1	142.40
	Total cost of pilot MEC				**1308.22**

Table 6.1 Actual costs of MEC components in pilot 2 (chapter 4). Total cost of 3 module MEC capable of treating a population equivalent of 6 is £1308.

The full-scale model MEC assumes 625 modules, each with an anode surface area of 20m^2 and a cathode surface area of 16 m^2 (Table 6.2). Length of wire (from power supply to module) is kept to a minimum to limit the effect on electrical resistivity. However, this means that the number of power supplies required is quite large, at 80 units. This increases cost more than increased wire length would, but enables the assumptions of electrochemical performance to be consistent with that of pilot 2.

MEC component	Material	Cost (£)	Unit size	# of units	Total cost (£)
Anode	4.6mm graphite felt	67.5	m^2	25000	1687500.00
Current Collector	316 stainless steel mesh	22.5	m^2	50000	1125000.00
Membrane	Rhinohide UHMWPE	0.8	m^2	25000	20000.00
Cathode	stainless steel wire wool	30	per kg	3600	108000.00
	316 stainless steel mesh	22.5	m^2	10000	225000.00
Catholyte	0.1M NaCl	120	25 kg	60	7200.00
Structural support	PVC	600	Each	625	375000.00
Wires	0.2mm wire	8.5	100 m	33.75	286.88
Resistors	0.1Ω resistor	0.65	pack of 5	125	81.25
Power supply	Caltek PSM 2/2A	107	Each	80	8560.00
Total cost of full scale MEC					3556628.13

Table 6.2 Predicted costs of full scale MEC, assuming 25% discount on unit cost due to economy of scale. Total cost of a 675 module MEC (excluding civil works) capable of a population equivalent of 25,000 is £3.56 million.

The cost of the aerated system was calculated using iMOD for three population equivalents: 10,000, 25,000 and 32,000 (Table 6.3). This estimate did not include the cost of installed pumps for WAS/RAS recycle, estimated to cost £1,500- 5,000 / m^3 of wastewater treated (i.e. £10,000-40,000 for 25,000 PE) (Sedlak, 1991). This value is added on to the total cost, to take the capital cost up to £0.35 million. The cost of mixers is not included, as anoxic/anaerobic zones were not part of the assumption.

PE	Control Panel	FBDA Air Compressor	Submerged Aeration Pipework	Total
	5 starters	2 duty, 1 standby		
33,000	67,981.34	157,621.78	143,178.00	368,781.12
25,000	67,981.34	155,996.68	104,945.42	328,923.44
10,000	67,981.34	151,571.14	44,768.65	264,321.13

Table 6.3 Predicted capital cost of activated sludge system for 10,000, 25,000 and 32,000 PE using Northumbrian Water's iMOD model.

Cost of treatment

Assuming an industrial electricity price of 11.5 p/kWh (based on iMOD model), a standard oxygen transfer rate of consumption 200 kg-O_2/hr, and a compressor rating of 51.9 kW each (one FBDA Air for the contact zone and aeration lane) the cost of treatment is £104,548 per year, or £287 per day. Electricity prices have risen by at least 3-4% per year over the past

decade (DECC, 2016). Therefore, after the first year, the cost of electricity is assumed to be: $[104548 \times 1.03]^{\text{years}}$

Treating the waste via MEC would use approximately 0.04 kWh per m^3 of wastewater. For 8,000 m^3 wastewater (25,000 PE), this equates to £13,140 per year, or £36 per day. Improving the efficiency of the MEC, and reducing the energy input, would reduce this value further.

Products
The four products considered for CBA are: hydrogen, sodium hydroxide, hydrogen peroxide and methanol. The cathodic reactions for their generation in MECs are:

1. Hydrogen: 1 mole of hydrogen requires 2 electrons $\quad\quad 2H^+ + 2e^- \rightarrow H_2$

2. Hydroxide: 1 mole of hydroxide requires 1 electron $\quad\quad 2H_2O + 2e^- \rightarrow H_2 + 2OH^-$

3. Peroxide: 1 mole of peroxide requires 2 electrons $\quad\quad 8H^+ + 4O_2 + 8e^- \rightarrow 4H_2O_2$

4. Methanol: 1 mole of methanol requires 6 electrons $\quad\quad CO_2 + 6H^+ + 6e^- \rightarrow CH_3OH + H_2O$

Thus, reaction two is the most efficient conversion of current into product.

Most of the products listed have a direct-end use in a water or wastewater application. Sodium hydroxide has a relatively high cost, but is one of the most widely used chemicals for pH adjustment on small wastewater treatment plants. Lime is a cheaper alternative, but less convenient due to a slower rate of reaction, a limited range of application and challenges posed by the disposal of the sludge formed (Tchobanoglous *et al.,* 2004). Northumbrian Water Ltd typically pay £170- £220 /m^3 for a 28 % solution of sodium hydroxide (including transportation). Methanol is commonly used as an external carbon source for post-anoxic denitrification, although this is not common practice in the UK (Tchobanoglous *et al*., 2004).

Hydrogen peroxide is used in potable water applications, in advanced oxidation processes (AOP) as an alternative to chlorine (Tchobanoglous *et al.,* 2004). It can be used in combination with ozone or UV. However, Northumbrian Water primarily use sodium hypochlorite at a cost of £154-234 /m^3 for a 14 % solution. This value is used in the sensitivity analysis, as it is deemed to reflect what the utility would pay. The actual cost of laboratory grade sodium hydroxide solution is approximately 5 times higher than sodium hypochlorite (Sigma Aldrich, 2017). Hydrogen does not have a direct end-use in wastewater treatment. It is assumed it would either be blended with the biogas to generate energy, or transferred to a fuel cell to generate electricity. Both options are limited: neither enables the full recovery of hydrogen's value. However, these options prevent the need for additional infrastructure to compress and store hydrogen gas.

6.2.3. Environmental assumptions

The environmental costs and benefits are not monetized in the cost benefit analysis. The negative impacts associated with the MEC are primarily concerned with electricity consumption. The power supplies require approximately 0.04 kWh/m^3 of wastewater. However, this is ~85% less than the electricity required for aeration in activated sludge (McCarty *et al.,* 2011). This is equivalent to a greenhouse gas emissions saving of 0.15 kg-CO$_2$-e/m^3 of wastewater treated (Foley *et al.,* 2010), or 1,200 kg-CO$_2$-e/day in this model.

Positive environmental impacts arise from the displacement of chemical production through traditional processes. MEC could, in theory, replace: steam reforming or traditional water electrolysis (hydrogen); electrolysis of brine in the Castner-Kellener process (sodium hydroxide); the Riedl-Pfleiderer AO or anthraquinone process (hydrogen peroxide); and methanol production from syngas. The benefits obtained from displacing traditional chemical production can be significant, particularly in relation to: carcinogens, global warming and non-renewable energy (Foley *et al.,* 2010). For example, life cycle carbon emissions from MEC-generated H$_2$O$_2$ are approximately 60 % lower than the emissions released from H$_2$O$_2$ generated by the Riedl-Pfleiderer AO process (Foley *et al.,* 2010).

Factors involved with storing and processing the products are not captured in the CBA. It is impractical to store hydrogen gas at ambient temperature and pressure; therefore, the product would require additional energy and infrastructure for compression (Pant *et al.,* 2011). This is not accounted for in the model. However, benefits gained from using the products directly on site (reducing transportation costs) are also not included in the model.

Finally, the impact of a reduced volume of sludge produced from secondary treatment is not considered economically. Primary sludge, which accounts for two-thirds of sludge to digestion is not influenced by the MEC process. An activated sludge plant for a population equivalent of 25,000 should produce 80-140 m^3 sludge per day (von Sperling and Gonçalves, 2007). The pilot MEC (Chapter 4) produced very little sludge (<1 L/d). Scaled-up to the flow of the model, this equates to ~5 m^3/d: substantially lower than a trickling filter (>35 m^3/d for 25,000 PE) or comparable to an Upflow Anaerobic Sludge Blanket (UASB) reactor (5-15 m^3/d for 25,000 PE) (von Sperling and Gonçalves, 2007). Energy recovered from secondary sludge may, therefore, be reduced by 92 % (trickling filter) to 96 % (activated sludge). An evaluation of how this affects the anaerobic digestion of sludge, and the net-energy balance of the entire treatment process, has not yet been made. The reduced sludge volume may have a

positive effect on operational costs, due to a decrease in frequency of sludge collection and processing from small to medium sites, which do not have on site digestion.

6.2.4. Multi criteria assessment tool

Multi criteria assessment (MCA) is used to analyse problems which may have conflicting objectives or a high degree of uncertainty (Wang *et al.,* 2009). A single criterion approach is often used to determine the most cost effective solution. However, MCA are increasingly used to include environmental impact (Wang *et al.,* 2009). The decision-making process is often described as a matrix: plotting a given number of considered options against a given number of criteria (with respective weightings) (Wang *et al.,* 2009).

'Economic value' considers: the operational and maintenance costs required to produce each product, the net present value of the technology (NPV) and the potential savings from producing the products in-house (Table 6.4). The 'environmental aspects' consider the greenhouse gas emissions avoided (by sustainable product production and reduction of transportation) and the electricity saved through a lack of aeration.

'Market need' is assessed on whether the product has a direct end use, and if the quality achieved can meet the market need. 'Technology status' considers the maturity of MEC in producing each product: from conceptual to commercial in line with technology readiness levels (TRL). 'General risk' includes social acceptability and likelihood of operational risk i.e. health and safety, loss of product, failure to comply with wastewater treatment consent *etc*.

Criteria	1	2	3	4	5
Economic Value	High cost Low value No profit NPV less than conventional process	High cost Medium value No profit NPV exceeds conventional in <30 years	Medium cost Medium value No profit NPV exceeds convention in <15 years	Low cost Medium value Profit in 50 years Positive NPV	Low cost High value Profit in <25 years Positive NPV
Environmental Aspects	High carbon emissions High energy consumed Pollution Reliance on fossil fuels	Some carbon emissions High energy consumption Reliance on fossil fuels	Reduced emissions Less energy consumed Predominant use of fossil fuels	Reduced emissions/ energy use Renewable energy/ chemicals Net-energy neutral	Low emissions Significant renewable generation Net-energy positive
Market Need: End Use	No market need. Product not used in water industry.	Product used occasionally in water industry, but not in short supply	Product used regularly in water industry	Product used regularly in water industry and costly to obtain	Product essential to industry and cannot obtain elsewhere
Market Need: Quality	Poor quality, could not be used for market need	Low quality, would require significant processing	Acceptable quality, but does not outperform existing market	Good quality, meets current market level	Exceptional quality, outperforms current market
Technology Status	Conceptual	Research	Lab scale	Pilot Scale	Commercial
General risk	High risk of loss of product AND high risk of danger	High risk of loss of product OR high risk of danger	Medium risk of loss of product OR risk of danger	Low risk of loss of product OR risk of danger	No risk of loss of product OR risk of danger

Table 6.4 Scoring categories for each criterion in the MCA. Each product is considered with respect to these six categories and is allocated a score accordingly. Scores of one and two are deemed unfavourable, scores of five are highly suitable.

6.3 Results

6.3.1 Sensitivity Analysis

Seven scenarios were considered for sensitivity analysis (Table 6.5). The first scenario (A) considers the baseline performance, assuming 1 A/m^2 current generation, a module size of 20 m^2 and capital cost (CAPEX) of £3.56 million. Scenario B considered a 25% increase in current production, from 1 A/m^2 to 1.25 A/m^2. Scenario C considered a 25% decrease in CAPEX, such that each module cost £4,271 instead of £5,695. The latter three scenarios assumed a 25% increase in throughput: therefore, each module was treating a larger volume

of wastewater per day. Scenario G is the 'best case' scenario, with an increase in throughput and current production, combined with a decrease in CAPEX (Table 6.5).

Scenario	Description	25 % ↑ current	25% ↓ CAPEX	25% ↑ throughput
A	Baseline performance of MEC model			
B	Baseline performance with 25% increase in current produced	X		
C	Baseline performance with 25% decrease in CAPEX		X	
D	Baseline performance with 25% increase in current produced and 25% decrease in CAPEX	X	X	
E	Baseline performance with 25% increase in throughput			X
F	Baseline performance with 25% increase in throughput and 25% decrease in CAPEX		X	X
G	Baseline with 25% increase in throughput and current, and 25% decrease in Capex	X	X	X

Table 6.5 Description of the seven scenarios for sensitivity analysis in the cost benefit analysis on the model MEC and its products.

The sensitivity analysis suggests sodium hydroxide (NaOH) is the best product to produce for financial revenue. The value generated per day from sodium hydroxide was 30 % more than hydrogen, twice as much as hydrogen peroxide and almost three times that of methanol (Table 6.6). Despite the higher market value of methanol, sodium hydroxide is more efficient in its conversion of current to product: one electron produces one mole of NaOH, compared to six electrons required for one mole of CH_3OH.

	A	B	C	D	E	F	G
Size of module (m²)	20	20	20	20	20	20	20
PE of module	40	40	40	40	50	50	50
Cost/ module (£)	5695	5695	4271	4271	5695	4271	4271
# modules for full flow	625	625	625	625	500	500	500
Current/module (A)	20	25	20	25	20	20	25
Total current for full flow (A)	12500	15625	12500	15625	10000	10000	12500
CAPEX (millions £'s)	3.559	3.559	2.669	2.669	2.847	2.135	2.135
m³H₂/day/ module	0.2	0.25	0.2	0.25	0.2	0.2	0.25
m³H₂/day @full flow	125	156.25	125	156.25	100	100	125
L-NaOH/day/module	0.717	0.896	0.717	0.896	0.717	0.717	0.896
L-NaOH/day @full flow	447.88	559.85	447.88	559.85	358.30	358.30	447.88
L-H₂O₂/ day/module	0.3047	0.3809	0.3047	0.3809	0.3047	0.3047	0.3809
L-H₂O₂/ day @full flow	190.45	238.06	190.45	238.06	152.36	152.36	190.45
L-CH₃OH/ day/module	0.0957	0.1196	0.0957	0.1196	0.0957	0.0957	0.1196
L-CH₃OH day @full flow	59.79	74.74	59.79	74.74	47.83	47.83	59.79
Market value £/kg-H₂	5	5	5	5	5	5	5
Market value £/kg-NaOH	0.15	0.15	0.15	0.15	0.15	0.15	0.15
Market value £/kg-H₂O₂	0.17	0.17	0.17	0.17	0.17	0.17	0.17
Market value £/kg-CH₃OH	0.4	0.4	0.4	0.4	0.4	0.4	0.4
Value per day (£) H₂	£52.08	£65.10	£52.08	£65.10	£41.67	£41.67	£52.08
Value per day (£) NaOH	£67.18	£83.98	£67.18	£83.98	£53.75	£53.75	£67.18
Value per day (£) H₂O₂	£32.38	£40.47	£32.38	£40.47	£25.90	£25.90	£32.38
Value per day (£) CH₃OH	£23.92	£29.90	£23.92	£29.90	£19.14	£19.14	£23.92

Table 6.6 Sensitivity analysis on predictive inputs and outputs of the CBA model. Seven scenarios are considered for sensitivity analysis (A-G) (Table 6.5).

6.3.2. Net Present Value

Sensitivity analysis provided four estimated capital costs for MEC, ranging from £2.14 million to £3.56 million. The capital cost of the conventional process is £0.33 million. The operational expenditure is not calculated in full: power requirements are accounted for; maintenance, replacements, disposal, transport and labour are not accounted for. The reason for this is due to the uncertainty of the maintenance and replacement requirements of the model MEC system, as it has not yet been tested for a long enough period to provide adequate data. Disposal costs and transport costs are likely to be greater in the conventional system

than in the MEC, due to reduced sludge production and the generation of products for direct use on site in the latter. Labour costs are likely to be comparable between the two processes.

To determine NPV, costs (the electricity cost of the power supplies and the process of aeration) are deducted from benefits (calculated solely from the value generated by the products): NPV = value of products – (capital cost + electricity cost). The value of the products is subject to inflation. This value should increase year on year. Inflation is currently at 1% in the UK. This was used to calculate the NPV of the outputs from the system. The inputs (capital cost and electricity) are also subject to change with time. The asset value will depreciate. Depreciation was fixed at 6% (Comisari *et al.,* 2012), which was consistent with Northumbrian Water's assumptions. A conservative estimate of a 3% increase in electricity cost was assumed per year (DECC, 2016). Therefore, after the first year, NPV was calculated as: (products' value x 1.01) ^{years} - [(capex x 0.94) ^{years} + (electricity x 1.03) ^{years}]
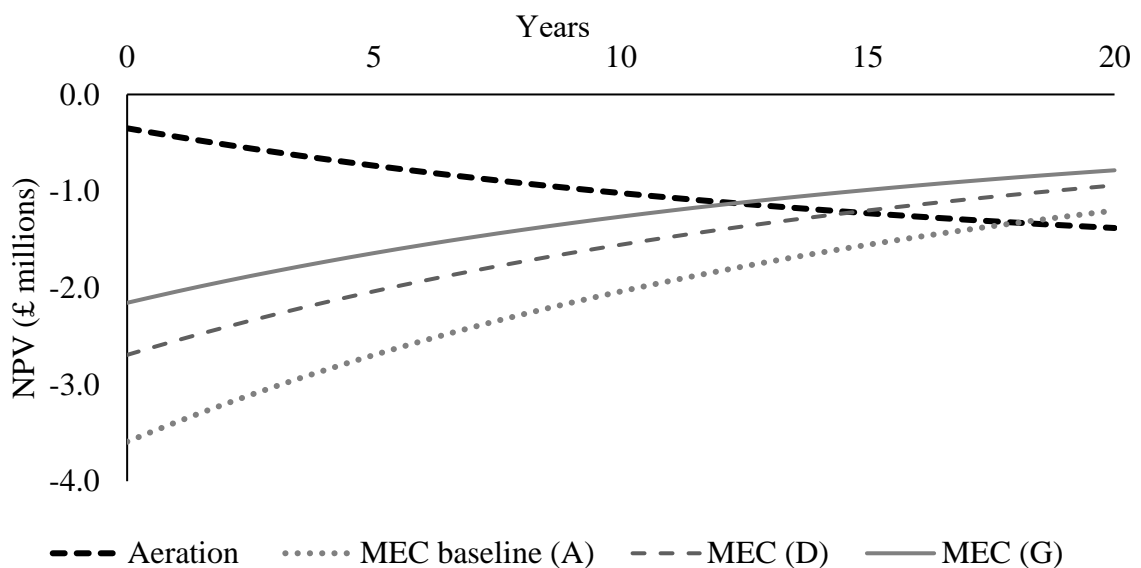
Figure 6.2 Net present value (in millions of pounds) of a conventional aerated process (black dotted line), and three MEC scenarios A, D & G (grey solid and dashed lines) over 20 years.

NPV was calculated for MECs producing caustic, as this was deemed to be the most financially viable option (Table 6.6). Despite a much larger capital cost than a conventional aerated process, the MEC has the potential to dramatically reduce operational costs, thereby producing more net benefits. After 18 years, the baseline MEC model has a better NPV than the conventional aerated process. Under scenarios D and G, this time is reduced to 15 and 13 years, respectively (Fig. 6.2). Therefore, MEC producing caustic would be a more financially attractive option than conventional aeration within three AMP cycles (Fig. 6.2). The most

influential factor (for NPV) is the capital cost of the MEC; particularly the anode and current collector components, which, combined, account for 70% of the total outlay.

Looking further ahead, MEC may have the potential to produce a net-profit, although this was not achieved in the scenarios tested (Fig. 6.3). However, this calculation is subject to a large amount of uncertainty, due to factors omitted from the calculation (maintenance, replacements, labour *etc.*), and the length of time involved: during which market value and inflation are likely to change.
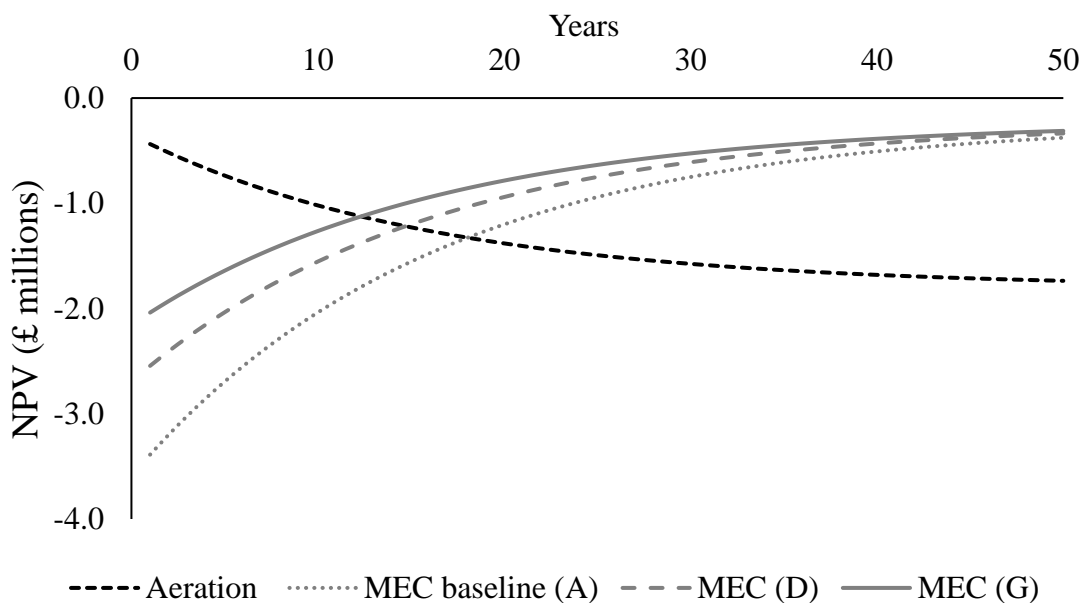
Figure 6.3 Net present value (in millions of pounds) of a conventional aerated process, and three MEC scenarios (A, D and G) over 50 years.

6.3.3. Multi criteria assessment (MCA) tool

In the baseline scenario MEC all four products scored poorly for economic value. None of the four managed to achieve a profit within 50 years, assuming the current market value. To achieve a net-profit within 50 years (under the scenarios tested), the value gained from caustic production needed to be several orders of magnitude higher (i.e. £20,000 per day, rather than £100). To achieve this increase in value, a dramatic increase in market value, and / or an increase in volume produced would be required. It is more likely, that if a profitable scenario occurs, it will be due to a combination of increased value (e.g. an increase in output at double the market value) and lower capital investment costs.

Sodium hydroxide achieved the highest net score of 3.1. Hydrogen peroxide is the second highest weighted score at 3.0. Hydrogen and methanol scored 2.85. In 'market need', hydrogen scored a low value for end use, but scored highly for quality. Conversely, caustic scored a high value for end use and a low value for quality. There was little difference in the economic value, of the products, at the current scale of production. The variation in their economic value would be magnified if larger volumes of product could be achieved.

Criteria	Weight (%)	H_2		NaOH		H_2O_2		CH_3OH	
Economic Value	25	3	**0.75**	3	**0.75**	3	**0.75**	3	**0.75**
Environmental Aspects	25	4	**1**	3	**0.75**	3	**0.75**	3	**0.75**
Market Need: End Use	20	1	**0.2**	4	**0.8**	3	**0.6**	2	**0.6**
Market Need: Quality	20	3	**0.6**	2	**0.4**	3	**0.6**	3	**0.6**
Technology Status	5	4	**0.2**	4	**0.2**	3	**0.15**	3	**0.15**
General risk	5	2	**0.1**	4	**0.2**	3	**0.15**	4	**0.2**
Combined score		**2.85**		**3.1**		**3.0**		**2.85**	

Table.6.7 Multi-criteria analysis tool to assess the best option for product recovery from the MEC considering economic, environmental and risk factors. The value in bold is the score multiplied by the weighting. The highest combined score is the most favourable option.

6.4 Discussion

A cost benefit analysis (CBA), with sensitivity analysis and multi criteria assessment (MCA) suggested caustic soda (sodium hydroxide) production in an MEC is the most economically desirable product for use in a water industry application. The model, which was based on a hypothetical scaled-up version of the pilot trial from chapter 4, supported the production of caustic soda over hydrogen, methanol or hydrogen peroxide in MECs, partly due to a viable end use: caustic soda is regularly used for pH adjustment in wastewater treatment. Caustic is a significant cost to the water industry, thereby making the market need greater. In addition, of the four products considered, caustic provided the most efficient conversion of electrons to product, ensuring the current produced was realised as economic value. Therefore, in all scenarios, it generated the largest value per day in pounds (£).

The production of sodium hydroxide in BES with NaCl catholyte may be used to support chemical nutrient removal. Martin *et al.,* (2009) demonstrated 80 % phosphorous removal

from final effluent in a one-step process using a solution of 4 % NaOH ad 2 % NaCl. This was carried out using an ion exchange media with high selectivity for phosphate (Martin et al., 2009). This would further support the use of MEC in domestic wastewater treatment, as the MEC's product could be used to counter the MECs weakness i.e. its lack of nutrient removal.

The 'technology status' of MEC-caustic production is similar to hydrogen production. A large scale (1 m^3) pilot MEC, operated on wastewater to produce sodium hydroxide, was trialled by the University of Queensland, leading to a start-up: Bilexys (UniQuest, 2012). The potential concerns for MEC-caustic production were the quality of the product produced. Caustic's current end use in the water industry is at a markedly higher concentration (28 %) than has been demonstrated in trials. Unless this can be improved, the product would need to be used in larger quantities to meet the market need. Furthermore, the production of caustic would require a more robust membrane than is currently being used. Build-up of product within the cathode chamber could lead to piercing of the UHMWE membrane. Therefore, a ceramic membrane would be necessary to permit regular rinsing and prevent damage. This will alter the upfront cost of MECs: ceramic membranes currently cost 10-100 times more than the separator used in this study. However, it will reduce the long-term cost, by reducing the frequency of replacement and maintenance.

Using MECs for caustic production as the baseline, scenarios were considered to determine the net present value (NPV) over 20 and 50 years: values, which are likely to be subject to a large amount of uncertainty. This uncertainty is partly caused by the limitations of the model, whereby the cost of maintenance and replacement of parts is not considered. However, uncertainty is magnified by the unknown lifespan of the technology and its component parts: there have been too few large scale, long term experiments testing the durability of MEC. Furthermore, the timespan considered (up to 50 years) is longer than we are reliably able to predict. Change to a variety of factors, such as wastewater regulation, cost of materials, or scientific knowledge (all of which underpin the assumptions in the model), are possible within this timeframe. Any of these changes could alter or falsify the prediction made in the 50-year model.

The NPV of MECs producing caustic exceeded the NPV of a conventional aerated process within 13-18 years, depending on which MEC scenario was used. Therefore, the benefits of MEC-caustic production could, in theory, outweigh the benefits of conventional wastewater

treatment within a few AMP cycles. Decreasing the capital cost of MEC further provides the best opportunity to improve this further. This prediction is subject to uncertainty, but the amount of deviation from the model's assumptions is likely to be considerably less in a decade, than observed in almost half a century.

There were a few factors excluded from the boundary of analysis due to limitations in the data available. A more detailed life cycle assessment of the technology is recommended after further trials at pilot scale. This presents the best opportunity to reduce the likelihood of uncertainty in the model and create the most realistic predictions of NPV for MEC.

Chapter 7. Conclusions and recommendations

The overall aim of this research was to scale-up MECs for domestic wastewater treatment and energy recovery. This research involved the design, building and testing of four successively larger MECs, in two pilot trials. The result was an increased anode surface area, from 0.06 m^2 to 1 m^2. The largest pilot trial (chapter 4) removed COD from a population equivalent of 6 people per day, or 1.04 kgCOD/m^3/d. In comparison, the previous trial (chapter 2) removed about 79% less, at 0.21 kgCOD/m^3/d.

The 1 m^2 electrodes would need to be 30 to 50 times bigger for full scale wastewater treatment. A scaled-up version of the existing configuration may bow or bend at the scale required for full scale treatment, but this problem should be alleviated with a spacer. If future research shows the configuration is not structurally viable when scaled-up further, there are two options to consider. The first, involves the use of the module in its current design as a package plant. This could be used to reduce the organic load on the system, decreasing the energy use of the STW. The second option would be to re-design.

Both trials produced a high hydrogen purity, with 98% ± 3 hydrogen in the first trial, and 93% ± 7 hydrogen in the second. The second trial showed continuous production of H$_2$ for more than 127 days, suggesting long term gas production is possible. The yield of hydrogen obtained in both trials was 2-3 times lower than achieved in studies of laboratory BES using real wastes. This may indicate that the system was under loaded, or it may reflect hydrogen loss in the MEC. Hydrogen yield decreased towards the end of the trial, and cathodic efficiency was consistently poor (below 10 %). Hydrogen loss by scavenging was the likely cause: acetogenic bacteria were present in the cathode samples, and cathodic VFA concentration increased during operation.

There are structural, hydraulic and analytical improvements that could be made to reduce hydrogen losses. There was a significant trade-off between the integrity of the modules' seal and the electrode spacing. The membrane separating the anode and cathode was sealed using a silicone-based adhesive, which is permeable to H$_2$. The design created hydraulic limitations: the strength of the seal, in comparison to a gasket, precluded the recirculation of catholyte, which may have enabled faster recovery of hydrogen and reduced activity by scavenging bacteria. Finding a solution which allows for the increased pressure created by recirculating the catholyte, without increasing electrode spacing (which would increase electrical

resistivity) will help to improve efficiencies in future reactors. Finally, to ensure reactor efficiencies are calculated accurately, the use of in line hydrogen gas analysis, as outlined in Jimenez *et al.,* 2015, would account for temperature and pressure differences affecting yield. Future design should also account for the gas production from the anode, which was not collected or measured in this study. Carbon dioxide and methane could be produced at the anode.

Perhaps the most important result was the ability to treat wastewater to an industrially viable level in an MEC: meeting the European standard for COD removal (<125 mg/L) without the need for a final clarification process. However, there were inconsistencies in COD removal throughout operation, which, on a day-to-day basis, may result in a failure to meet the industrial discharge limit. Increasing surface area or residence time may help to prevent these failures. Analysis of COD removal in the first pilot trial, led to a predicted requirement of 20 m^2 of anode surface area per m^3 of reactor. The second pilot exceeded this value at 34 m^2/m^3, although it was operated at a much shorter HRT. Failure to consistently meet effluent consent may have been due to limitations in the hydraulic design, rather than the electrode surface area. As reactor efficiencies were poor, examining COD removal in the absence of an applied voltage (by turning off the power supply for ~3 HRTs) should provide information on how much of the COD removal is due to bioelectrochemical processes.

The CFD and tracer study implied there was dead space and short-circuiting in the reactor. The measured hydraulic retention time from the tracer study was 31 minutes (10%) shorter than the expected HRT calculated from calibrated pumps. Better distribution of flow, through multiple inlets or a gravity feed, may have implications for the bacterial colonisation of electrode surface area, and therefore on the COD removed and the current generated.

An energy balance of the technology could not be carried out, because the values obtained for COD settlement and sludge production in the MEC were based on estimates. Future design of MECs should permit regular de-sludging of the base of the tank, instead of just the outlet. This would contribute to performance, prevent blockages from sludge build up, and allow for the quantification of settled solids and accurate COD removal. Composite sampling of COD should replace spot sampling, to provide accurate estimations of removal and reduce skew from influent variability.

Both trials showed poor nutrient removal, with limited nitrification and denitrification, as would be expected with an anaerobic technology. Nutrient removal remains a challenge for the uptake of MECs in domestic wastewater treatment, where regulations stipulate removal of total nitrogen to below 10-15 mg/L depending on the PE (UWWTD, 1991). As such, MECs are likely to require a chemical or biological downstream process to remove nitrogen and phosphorous. Martin *et al.,* (2009) demonstrated the use of a 4 % NaOH / 2 % NaCl solution with an ion exchange media to chemically remove phosphorous. The bioelectrochemical production of caustic, in a cathode chamber filled with NaCl, could provide a dual benefit: the sustainable production of the NaOH/NaCl solution, and the removal of phosphorous to meet the UWWTD discharge consent.

A greater understanding of external factors influencing the performance of MECs has been achieved through meta-analyses and experiments. Temperature, wastewater constituents and chemical dosing are likely to vary between sites: influencing MEC performance. Evaluation of specific constituents, such as sulphate, showed they may vary considerably between sites due to chemical dosing, or the surrounding catchment and the type of sewer feed to site. Sulphur-based compounds, such as gypsum and elemental sulphur, were found to be fouling the failed modules' membranes in the first pilot trial. Deposition of elemental sulphur on an electrode (or membrane) has been shown to increase ohmic resistance, and create a physical barrier which limits electrochemical performance (Dutta *et al*., 2008). This may have led to the deterioration to failure of some of the first pilot's modules.

Analysis of the anodic biofilm showed a significant difference between the communities in the two pilot trials: a finding in agreement with previous studies on anodic community variation (Jiang *et al.,* 2016; Zhou *et al.,* 2013). A comparison of the ten modules' communities within the first pilot trial showed they were not significantly different. These samples had been taken from the top corner of each module's anode. Molecular analysis following the second pilot trial supported this, but provided evidence to suggest spatial variation within each anodic community, based on the depth of submersion in the wastewater.

There was a strong alignment between the experimental data with a theoretical neutral community model (NCM). Pilot 1's community showed agreement with NCM, with 69 % of taxa located within the 95 % confidence limit of the model. *Geobacter* and SRB were found at greater frequencies than expected based on their relative abundance in the influent, suggesting these species are enriched in the MEC as proposed by Ishii *et al.,* (2014). The strong

correlation with the NCM, suggests the MEC community is very likely to be randomly assembled by stochastic processes. A greater understanding of community assembly and diversity could be achieved, if the number of individuals in the local community could be determined through quantitative PCR. Calculating the number of individuals would allow the colonisation of the local community, from the source community, to be determined.

Heterogeneity was observed in the gross colonisation of the biofilm. Fluorescent staining implied only 5% of the biofilm's surface area has sufficient coverage for the stain to be visualised under UV. Biofilm thickness correlates with current density (Ishii *et al.,* 2008, He *et al.,* 2011), but the influence of biofilm distribution on current production is not yet known. Analysing the distribution of biofilms in parallel reactors of high, medium and low current output could help to determine whether a correlation exists. If a correlation is observed, maximising colonisation of electrode surface area may provide a way to improve current density without the cost implications of using advanced materials.

In an anode transect from the second pilot trial, which represented 18% of the total surface area, *Geobacter* was found at <1% of the relative abundance. This is significantly lower than the proportion of *Geobacter* in the first pilot trial, where *Geobacter* was found to represent 7-10% of the relative abundance. However, these spot samples were taken from the same location each time, and only represent 2% of the total anode surface area. The proportion of *Geobacter* in the MEC could be enhanced by seeding from a population with a high relative abundance of *Geobacter.* The NCM model showed that *Geobacter* species were often found at a higher frequency than would be expected, based on their relative abundance in the source community. Increasing their abundance in the source community should further increase the frequency of detection in the target communities (i.e. MEC anodes), with positive implications for current generation (Ishii *et al.,* 2014).

Finally, a cost benefit analysis (CBA), based on a hypothetical scaled-up version of the pilot trial from this research, supported the production of caustic soda (sodium hydroxide) over hydrogen, methanol or hydrogen peroxide, in a wastewater application. Realistic scenarios implied the net present value (NPV) of MECs producing caustic exceeded the NPV of a conventional aerated process within 13-18 years, depending on the scenario. Therefore, the benefits of MEC-caustic production could in theory, outweigh the benefits of conventional wastewater treatment within three AMP cycles. This model did not account for several factors

including greenhouse gas emissions, increased operational complexity and economic and environmental factors outside the boundary of analysis.

Fault tree analysis (FTA) was used to understand why modules may have failed, and to identify areas to improve MEC robustness. Further development of the FTA could be beneficial to researchers and practitioners alike. Including probabilities in the FTA should help to determine the likelihood, as well as the mode, of failure. Probabilities could be assigned to one or both of; the likelihood of occurrence, and the likelihood of causing outright failure. The fault tree could also be used for gap analysis, to identify where to focus research effort to support the design of a more robust technology.

To conclude, MEC technology has advanced from the L to the m^3 scale, thanks to a 16-fold increase in electrode size and a reduction in HRT to 5 hours. The technology has moved on considerably from Heidrich's 'proof of concept' (Heidrich *et al.,* 2013, 2014), which equated to a technology readiness level (TRL) of 3 to 4. Significant technology development (TRL 5) and the beginnings of a pilot scale demonstration (TRL6) have been evidenced. The following improvements are deemed most important for the further development of the technology: (1) limiting scavenging by acetogenic bacteria, to increase yield of product; (2) improving the proportion and distribution of electrogenic bacteria, to improve the current density; and (3) decreasing the capital cost of the technology, to make it more competitive with existing assets. Achieving these improvements should take the technology to within reach of a commercial prospect.

References

Ahn, Y. and Logan, B.E. (2010) 'Effectiveness of domestic wastewater treatment using microbial fuel cells at ambient and mesophilic temperatures'. *Bioresource Technology*. **101(2):** 469-475.

Aiken, D. (personal communication) based on MSc study into rational design of MEC using current density.

Al-Amoudi, A and Lovitt, R.W. (2007) Fouling strategies and the cleaning system of NF membranes and factors affecting cleaning efficiency. *Journal of membrane science*. **303:** 4-28

Alibhai, K., Boon, A., Vincent, A. and Williams, J. (1995) Increasing sewer longevity by septicity control. 21st WEDC Conference on sustainability of water and sanitation systems. Kampala, Uganda, 1995.

Andersen, S.J., Hennebel, T., Gildemyn, S., Coma, M., Desloover, J., Berton, J., Tsukamoto, J., Stevens, C. and Rabaey, K. (2014) Electrolytic Membrane Extraction Enables Production of Fine Chemicals from Biorefinery Sidestreams. *Environmental Science & Technology*. **48**: 7135-7142

Anglian Water (2015) Greenhouse Gas Emissions Annual Report 2015 [online]. Available at http://www.anglianwater.co.uk/_assets/media/ghg_emissions_report_2015_H_res.pdf [accessed on 03/10/16]

Arrow, K.J. (1962) The economic implications of learning by doing. *The Review of Economic Studies*. **29** (3): 55-173

Baeza, A., Martínez-Miró, A., Guerrero, J., Ruiz, Y., and Guisasola, A. (2017) Bioelectrochemical hydrogen production at pilot scale from urban wastewater. *Journal of Power Sources*

Baudler, A., Schmidt, I., Langner, M., Greiner, A and Schröder, U. (2015) Does it have to be carbon? Metal anodes in microbial fuel cells and related bioelectrochemical systems. *Energy & Environmental Science.***8:** 2048-2055

Behera. M, Murthy, S.S.R., and Ghangrekar, M. M. (2011). Effect of operating temperature on performance of microbial fuel cell. *Water Science & Technology*. **64**(4): 917–926.

Bell, G. (2001) Neutral macroecology. *Science.* **293**: 2413–2418.

Birkhead, B.H. (2016) A CFD-based optimisation of a pilot-scale hydrogen producing MEC plant at Chester-Le-Street. MSc Dissertation in Environmental Engineering, Newcastle University.

Bloomberg (2016) Markets: Precious and Industrial Metals [online]. Available at http://www.bloomberg.com/markets/commodities/futures/metals [accessed on 03/10/16].

Boardman, A., Greenberg, D., Vining, A. and Weimer, D. (2014). Cost-benefit Analysis: concepts and practice 4th edition. Pearson Education Limited. ISBN 10: 1-292-02191-8

Brown, R.K., Harnisch, F., Wirth, S., Wahlandt, H., Dockhorn, T., Dichtl, N., and Schröder,

U. (2014) Evaluating the effects of scaling up on the performance of bioelectrochemical systems using a technical scale microbial electrolysis cell. *Bioresource Technology.* **163**: 206-213

Buffière, P., Fonade, C. and Moletta, R. (1998) Mixing and Phase Hold-Ups Variations Due to Gas Production in Anaerobic Fluidized-Bed Digesters: Influence on Reactor Performance. *Biotechnology and Bioengineering*. **60:** 36–43

Caccavo, F., Lonergan, D.J., Lovley, D.R., Davis, M., Stolz, J.F., and McInerney, M.J. (1994) Geobacter sulfurreducens sp. nov., a Hydrogen- and Acetate- Oxidizing Dissimilatory Metal-Reducing Microorganism. *Applied and Environmental Microbiology*. **60** (10): 3752-3759

Call, D.F., Wagner, R.C. and Logan, B.E. (2009) Hydrogen Production by Geobacter Species and a Mixed Consortium in a Microbial Electrolysis Cell. *Applied and Environemtnal Microbiology.* **75 (24):** 7579-7587

Call, D. and Logan, B.E. (2008) Hydrogen production in a single chamber microbial electrolysis cell lacking a membrane. *Environmental Science & Technology*. **42:** 3401-3406

Carepo, M., Baptista, J.F., Pamplona, A., Fauque, G., Moura, J.J.G. and Reis, M.A.M. (2002) Hydrogen metabolism in Desulfovibrio desulfuricans strain New Jersey (NCIMB 8313)—comparative study with D. vulgaris and D. gigas species. *Anaerobe.* **8:** 325–332

Chabert, N., Ali, O. A., and Achouak, W. (2015) All ecosystems potentially host electrogenic bacteria. *Bioelectrochemistry.* **106:** 88-96

Chae., K.Y., Choi, M.J., Lee, J.W., Kim, K.Y. and Kim, S. (2009) Effect of different substrates on the performance, bacterial diversity, and bacterial viability in microbial fuel cells. *Bioresource Technology*. **100** (14): 3518-3525

Chae., K.Y, Choi, M.J., Lee, J.W., Ajayi, F.F., and Kim., S. (2008) Biohydrogen production via biocatalyzed electrolysis in acetate-fed bioelectrochemical cells and microbial community analysis. *International Journal of Hydrogen Energy.* **33** (19): 5184-5192

Cheng, S., Xing, D., & Logan, B. E. (2011). Electricity generation of single-chamber microbial fuel cells at low temperatures. *Biosensors & Bioelectronics*. **26** (5). 1913–1917.

Cheng, S. and Logan, B.E. (2007) Sustainable and efficient biohydrogen production via electrohydrogenesis. *PNAS*. **104** (47): 18871-18873

Chernicharo, C.A.L (2007) Biological Wastewater Treatment. Vol 4: Anaerobic Reactors. IWA Publishing.

Clauwaert, P. and Verstraete, W. (2009) Methanogenesis in membraneless microbial electrolysis cells. *Biotechnological products and process engineering*. **82:**829-836

Comisari, P., Feng, L. and Freeman, B (2012) Valuation of water resources and water infrastructure assets. Australian Bureau of Statistics [online]. Available at: http://unstats.un.org/unsd/envaccounting/londongroup/meeting17/LG17_12.pdf [accessed on 15/11/2016].

Cordas, C.M., Tiago Guerra, L., Xavier, C. and Moura, J.J.G. (2008) Electroactive biofilms of sulphate reducing bacteria. *Electrochimica Acta*. **54:** 29-34

Cotterill, S., Heidrich, E. and Curtis T. (2016) Chapter 9: Microbial electrolysis cells for hydrogen production. In Scott, K., and Yu, E. ed. Microbial electrochemical and fuel cells: fundamentals and applications. Woodhead publishing. pp. 287-319

Croese, E., Keesman, K.J., Widjaja-Greefkes, A.H.C.A., Geelhoed, J.S., Plugge, C.M., Sleutels, T.H.J.A., Stams, A.J.M., and Euverink, G-J. W. (2013) Relating MEC population dynamics to anode performance from DGGE and electrical data. *Systematic and Applied Microbiology*. **36:** 408-416

Curtis, T.P. (2010) 13. Low-Energy Wastewater Treatment: Strategies and Technologies. In Mitchell, R. and Gu, J.D. (ed.) Environmental Microbiology. 2nd ed. New Jersey: Wiley-Blackwell

Curtis, T.P., Sloan, W.T., and Scannell, J.W. (2002) Estimating prokaryotic diversity and its limits. *PNAS*. **99 (16):** 10494 -10499

Cusick. R.D., Bryan. B., Parker. D.S., Merrill. M.D., Mehanna. M., Kiely. P.D., Liu. G., and Logan, B.E. (2011) Performance of a pilot-scale continuous flow microbial electrolysis cell fed winery wastewater. *Applied Microbiological Biotechnology.* **89:**2053–2063

Cusick, R.D., Kiely, P.D., and Logan, B.E (2010) A monetary comparison of energy recovered from microbial fuel cells and microbial electrolysis cells fed winery or domestic wastewaters. *International Journal of Hydrogen Energy.* **35:** 8855-8861

DECC (2016) Quarterly Energy Prices. Department of Energy & Climate Change. 30 June 2016 [online]. Available at: https://www.gov.uk/government/uploads/system/uploads/attachment_data/file/532712/QEP_June_2016_Final.pdf [accessed on 15/11/2016]

Deng, H. (1999) Multicriteria analysis with fuzzy pairwise comparison. *International Journal of Approximate Reasoning.* **21:** 215-231

Ditzig, J., Liu, H and Logan, B.E. (2007) Production of hydrogen from domestic wastewater using a bioelectrochemically assisted microbial reactor (BEAMR). *International Journal of Hydrogen Energy.* **32:** 2296-2304

Drainage Services Department (2013) Table 1 in Sewerage Manual Part 1. Third Edition, May 2013. Drainage Services Department, Government of Hong Kong Special Administrative Region. Accessed [online]. Available at: http://www.dsd.gov.hk/EN/Files/Technical_Manual/technical_manuals/Sewerage_Manual_1_Eurocodes.pdf on 27.10.2016 [accessed on 10/09/2016].

Department of Energy, DOE (2017) Hydrogen Fuel Cells [online]. Available at https://www.hydrogen.energy.gov/pdfs/doe_fuelcell_factsheet.pdf [accessed 09/03/2017].

Durham County Record Office (2016) Durham Collieries Search (for Fishburn Colliery and Pelton Fell) [online]. Available a: http://www.durhamrecordoffice.org.uk/Pages/AdvancedSearchDurhamCollieries.aspx [accessed on 17.10.2016]

Dutta, P.K., Rabaey, K., Yuan, Z. and Keller, J. (2008) Spontaneous electrochemical removal of aqueous sulfude. *Water Research*. **42:** 4965-4975

Edwards, K.J., Goebel, B.M., Rodgers, T.M., Schrenk, M.O., Gihring, T.M., Cardona, M.H., Hu, B., McGuire, M.M., Hamers, R.J. and Pace, N.R. (1999) Geomicrobiology of Pyrite (FeS$_2$) Dissolution: Case Study at Iron Mountain, California. *Geomicrobiology Journal*. **16**:155-179

Escapa, A., Mateos, R., Martinez, E.J., and Blanes, J. (2016) Microbial electrolysis cells: An emerging technology for wastewater treatment and energy recovery. From laboratory to pilot plant and beyond. *Renewable and Sustainable Energy Reviews*. **55**: 942-956

Escapa, A., San-Martin, M.I., Mateos, R. and Moran, A. (2015) Scaling-up of membraneless microbial electrolysis cells (MECs) for domestic wastewater treatment: Bottlenecks and limitations. *Bioresource Technology*. **180:** 72-78

Escapa, A., Lobato, A., Garcia, D.M. and Morán, A. (2013) Hydrogen production and COD elimination rate in a continuous microbial electrolysis cell: The influence of hydraulic retention time and applied voltage. *Environmental Progress and Sustainable Energy*. **32**(2): 263-268

Escapa, A., Gil-Carrera, L., Garcia, V., and Morán, A. (2012) Performance of a continuous flow microbial electrolysis cell (MEC) fed with domestic wastewater. *Bioresource Technology*. **117:** 55-62

European Commission (2013) Science for Environment Policy. Future Brief: Bioelectrochemical Systems. Wastewater treatment, bioenergy and valuable chemicals delivered by bacteria. February 2013. Issues 5.

Farhangi, S., Ebrahimi, S. and Niasar, M.S. (2014) Commercial materials as cathode for hydrogen production in microbial electrolysis cell. *Biotechnology Letters*. **36** (10): 1987-1992

Fauque G, Ollivier B. (2004) Chapter 17. Anaerobes: the sulfate-reducing bacteria asan example of metabolic diversity. In: Bull AT, editor. Microbial diversity and bioprospecting. New York: ASM Press. DOI. 10.1128/9781555817770

Foley, J.M., Rozendal, R.A., Hertle, C.K., Lant, P.A and Rabaey, K. (2010) Life Cycle Assessment of High-Rate Anaerobic Treatment, Microbial Fuel Cells, and Microbial Electrolysis Cells. *Environmental Science & Technology*. **44** (9). 3629-3637

Gil-Carrera, L., Escapa, A., Carracedo, B., Morán A, Gómez, X. (2013a) Performance of a semi-pilot tubular microbial electrolysis cell (MEC) under several hydraulic retention times and applied voltages. *Bioresouce Technology*. **146:** 63-69

Gil-Carrera, L., Escapa, A., Moreno, R. and Morán A (2013b) Reduced energy consumption during low strength domestic wastewater treatment in a semi-pilot tubular microbial electrolysis cell. *Journal of Environmental Management*. **122:** 1-7

Gil-Carrera, L., Escapa, A., Mehta, P., Santoya, G., Guiot, S.R., Moran, A., and Tartakovsky, B. (2013c) Microbial electrolysis cell scale-up for combined wastewater treatment and hydrogen production. *Bioresource Technology.* **130:** 584-59

Gildemyn, S., Verbeeck, K., Slabbinck, R., Andersen, S.J., Prévoteau, A. and Rabaey, K. (2015) Integrated production, extraction, and concentration of acetic acid from CO_2 through microbial electrosynthesis. *Environmental Science & Technology Letters*. **2:** 325-328

Giraldi, D., de'Machieli Vitturi, M., Zaramella, M., Marion, A. and Iannelli, R. (2009) Hydrodynamics of vertical subsurface flow constructed wetlands: tracer tests with rhodamine WT and numerical modelling. *Ecological Engineering*. **35:** 265-273

Gonzalez del Campo, A., Lobato, J., Cañizares, P., Rodrigo, M. A., & Fernandez Morales, F. J. (2013). Short-term effects of temperature and COD in a microbial fuel cell. *Applied Energy*. **101:** 213–217.

Hamelers, B., Sleutels, T.H.J.A., Jeremiasse, A.W., Post, J.W., Strik, D.P.B.T.B., and Rozendal, R.A. (2010) 10: Technological factors affecting BES performance and bottlenecks towards scale up. In Rabaey, K., Angenent, L., Schroeder, U. and Keller, J Edited: Bioelectrochemical systems: from extracellular electron transfer to biotechnological application. IWA Publishing, London. UK.

Hanley, N. and Spash, C.L. (1993) Cost-benefit analysis and the environment. Edward Elgar Publishing Limited. ISBN 978 1-85278-947-3

Hansen TA. (1994) Metabolism of sulfate-reducing prokaryotes. *Antonie van Leeuwenhoek.* **66**:165–85.

He, G. Gu, Y., He, S., Schröder, U., Chen, S., and Hou, H. (2011) Effect of fiber diameter on the behavior of biofilm and anodic performance of fiber electrodes in microbial fuel cells. *Bioresource Technology.* **102** (22): 10763-10766

Heidrich, E.S., Edwards, S.R., Dolfing, J., Cotterill, S.E., and Curtis, T.P. (2014) Performance of a pilot scale microbial electrolysis cell fed on domestic wastewater at ambient temperatures for a 12-month period. *Bioresource Technology.* **173:** 87-95

Heidrich, E.S., Dolfing, J., Scott, K., Edwards, S.R., Jones, C. and Curtis, T.P. (2013) Production of hydrogen from domestic wastewater in a pilot-scale microbial electrolysis cell. *Applied Microbiology and Biotechnology.* **97** (15): 6979-6989.

Heidrich, E.S, Curtis, T.P. and Dolfing, J. (2011) Determination of the internal chemical energy of wastewater. *Environmental Science & Technology.* **45** (2): 827–832

Heukelekian, A. H., Balmat, J. L., & Heukelekian, B. H. (2015). Chemical composition of the particulate fractions of domestic sewage. *Sewage and Industrial Wastes.* **31**(4): 413–423.

von Hippel, E. and Tyre, M.J. (1995) How learning by doing is done: problem identification in novel process equipment. *Research Policy.* **24**: 1-12.

Holmes, D.E., Bond, D.R., O'Neil, R.A., Reimers, C.E., Tender, L.R., and Lovley, D.R. (2004) Microbial Communities Associated with Electrodes Harvesting Electricity from a Variety of Aquatic Sediments. *Microbial Ecology.* **48** (2): 178-190

Houchins, C., Kleen, G.J., Spendelow, J.S., Kopasz, J. Peterson, D., Garland, N.L., Ho, D.L., Marcinkoski, J., Martin, K.E., Tyler, R. and Papageorgopoulos, D.C. (2012) U.S. DOE Progress Towards Developing Low-Cost, High Performance, Durable Polymer Electrolyte Membranes for Fuel Cell Applications. *Membranes.* **2:** 855-878

Hu, H., Fan, Y. and Liu, H. (2008) Hydrogen production using single-chamber membrane-free microbial electrolysis cells. *Water Research.* **42** (15): 4172-4178

Hubbell, S.P. (2001) The unified neutral theory of biodiversity and biogeography. Princeton University Press, Princeton, NJ.

Institution of Civil Engineers (2010) Asset Management. National Infrastructure Plan 2010. Accessed online at https://www.ice.org.uk/getattachment/disciplines-and-resources/best-practice/asset-management-policy/Asset-management-policy.pdf.aspx on 27.10.2016

Ishii, S., Watanabe, K., Yabuki, S., Logan, B.E. and Sekiguchi, Y. (2008) Comparison of electrode reduction activities of Geobacter sulfurreducens and an enriched consortium in an air cathode microbial fuel cell. *Applied and Environmental Microbiology*. **74** (23): 7348-7355

Ishii, S., Suzuki, S., Norden-Krichmar, T.M., Phan, T., Wanger, G., Nealson, K.H., Sekiguchi, Y., Gorby, Y.A. and Bretschger, O. (2014) Microbial population and functional dynamics associated with surface potential and carbon metabolism. *The ISME journal*. **8:** 963-978

Ivy, J. (2004) Summary of electrolytic hydrogen production: milestone completion report, NREL/MP-560-36734. National Renewable Energy Laboratory, USA, Tech. Rep. NREL/MP-560-36734; September 2004.

Jabari, L. Gannoun, H., Cayol, J-L., Hedi, A., Sakamoto, M., Falsen, E., Ohkuma, M., Hamdi, M., Fauque, g., Ollivier, B., and Fardeau, M.L. (2012) Macellibacteroides fermentans gen. nov., sp. nov., a member of the family Porphyromonadaceae isolated from an upflow anaerobic filter treating abattoir wastewaters. *International Journal of Systematic and Evolutionary Microbiology.* **62** (10): 2522- 2527

Jia, Y.H., Ryu, J.H., Kim, C.H., Lee, W.K., Thi, V.T.T., Lee, H.L., Zhang, R.H. and Ahn, D.H. (2012) Enhancing hydrogen production efficiency in microbial electrolysis cell with membrane electrode assembly cathode. *Journal of Industrial and Engineering Chemistry*. **18** (2): 715-719

Jia, Y.H., Choi., J.Y., Ryu, J.H., Kim, C.H., Lee, W.K., Tran, H.T., Zhang, R.H. and Ahn, D.H. (2010) Hydrogen production from wastewater using a microbial electrolysis cell. *Korean Journal of Chemical Engineering*. **27** (6): 1854-1859

Jiang, X., Shen, J., Lou, S., Mu, Y., Wang, N., Han, W., Sun, X., Li, J., and Wang, L. (2016) Comprehensive comparison of bacterial communities in a membrane-free bioelectrochemical system for removing different mononitrophenols from wastewater. *Bioresource Technology*. **216:** 645-652.

Jimenez, J., Latrille, E., Harmand, J., Robles, A., Ferrer, J., Gaida, D., Wolf, C., Mairet, F., Bernard, O., Alcarez-Gonzalez, V., Mendez-Acosta, H., Zitomer, D., Totzke, D., Spanjers, H., Jacobi, F., Guwy, A., Dinsdale, R., Premier, G., Mazhegrane, S., Ruiz-Filippi, G., Seco, A., Ribiero T., Pauss, A. and Steyer, J.P. (2015) Instrumentation and control of anaerobic digestion processes: a review and some research challenges. *Reviews in Environmental Science and Biotechnol*ogy. **14:** 615-648

Kennedy, A.C. (1999) Bacterial diversity in agroecosystems. *Agriculture, Ecosystems & Environment.* **74:** 65-76

Kiely, P.D., Regan, J.M. and Logan, B.E. (2011) The electric picnic: synergistic requirements for exoelectrogenic microbial communities. *Current Opinion in Biotechnology.* **22** (3): 378-385

Kim, M-S and Lee, Y-J (2010) Optimization of culture conditions and electricity generation using *Geobacter sulfurreducens* in a dual-chambered microbial fuel-cell. *International Journal of Hydrogen Energy*. **35** (23): 13028-13034

Klindworth, A., Prueese, E., Schweer, T., Peplies, J., Quast, C., Horn, M and Glöck, F.O. (2012) Evaluation of general 16S ribosomal RNA gene PCR primers for classical and next generation sequencing-based diversity studies. *Nucleic Acid Research*. **41** (1): e1

Kottek, M., Grieser, J., Beck, C., Rudolf, B., & Rubel, F. (2006). World map of the Köppen-Geiger climate classification updated. *Meteorologische Zeitschrift*. **15** (3): 259–263.

Kuntke, P., Sleutels, T.H.J.A., Saakes, M. and Buisman, C.J.N. (2014) Hydrogen production and ammonium recovery from urine by a Microbial Electrolysis Cell. *International Journal of Hydrogen Energy.* **39** (10): 4771-4778

Kyazze, G., Popov, A., Dinsdale, R., Esteves, S., Hawkes, F., Premier, G. and Guwy, A. (2010) Influence of catholyte pH and temperature on hydrogen production from acetate using a two chamber concentric tubular microbial electrolysis cell. *International Journal of Hydrogen Energy.* **35:** 7716-7722

Larrosa-Guerrero, A., Scott, K., Head, I. M., Mateo, F., Ginesta, A., & Godinez, C. (2010). Effect of temperature on the performance of microbial fuel cells. *Fuel.* **89** (12): 3985–3994.

Lee, H.S., Torres, C. I., Parameswaran, P., Rittmann, B. E. (2009) Fate of H_2 in an upflow single-chamber microbial electrolysis cell using a metal-catalyst-free cathode. *Environmental Science & Technology.* **43:**7971–7976.

Leitão, R.C., van Haandel, A.C., Zeeman, G. and Lettinga, G. (2006) The effects of operational and environmental variations on anaerobic wastewater treatment systems: a review. *Bioresource Technology.* **97:** 1105-1118

Lettinga, G., Hulshoff Pol, L.W., Koster, I.W., Wiegant, W.M., de Zeeuw, W.J., Rinzema, A., Grin, P.C., Roersma, R.E and Hobma, S.W. (1984) High rate anaerobic waste-water treatment using the UASB reactor under a wide range of temperature conditions. *Biotechnology and Genetic Engineering Reviews.* **2**(1): 253-284

Lettinga, G., van Velsen, A.F.M., Hobma, S.W., de Zeeuw, W.M. and Klapwijk, A. (1980) Use of the upflow sludge blanket (USB) reactor concept for biological wastewater treatment, especially for anaerobic treatment. *Biotechnology and Bioengineering.* **22** (4): 699-734

Lisdat, F and Schäfer, D. (2008) The use of electrical impedance spectroscopy for biosensing. *Analytical and Bioanalytical Chemistry.* **391:** 1555-1567

Li, L.H., Sun, Y.M., Yuan, Z.H., Kong, X.Y. and Li, Y. (2013) Effect of temperature change on power generation of microbial fuel cell. *Environmental Technology.* **34** (13-14): 1929-1934

Liu, H., Cheng, S., Huang, L and Logan, B.E (2008) Scale-up of membrane-free single-chamber microbial fuel cells. *Journal of Power Sources*. **179:** 274-279

Liu, H., Grot, S. and Logan. B.E (2005a) Electrochemically assisted microbial production of hydrogen from acetate. *Environmental Science & Technology*. **39:** 4317-4320

Liu, H., Cheng, S., & Logan, B. E. (2005b). Power generation in fed-batch microbial fuel cells as a function of ionic strength, temperature, and reactor configuration. *Environmental Science & Technology*. **39** (14): 5488–5493.

Liu, W., Wang, A., Ren, N., Zhao, X., Liu, L, Yu, Z. and Lee. D. (2008) Electrochemically Assisted Biohydrogen Production from Acetate. *Energy & Fuels*. **22:** 159-163

Logan, B.E., Wallack, M.J., Kim, K-Y., He, W., Feng, Y and Saikaly, P.E. (2015) Assessment of Microbial Fuel Cell Configurations and Power Densities. *Environmental Science & Technology Letters*. **2:** 206-214

Logan, B.E. and Rabaey, K. (2012) Conversion of Wastes into Bioelectricity and Chemicals by Using Microbial Electrochemical Technologies. *Science*. **337:** 686-690

Logan, B.E. (2010) 9: Materials for BES. In Rabaey, K., Angenent, L., Schroeder, U. and Keller, J Edited: Bioelectrochemical systems: from extracellular electron transfer to biotechnological application. IWA Publishing, London. UK.

Logan, B.E., Call, D., Cheng, S., Hamelers, H.V.M., Sleutals, T.H.J.A., Jeremiasse, A.W. and Rozendal, R.A. (2008) Microbial Electrolysis Cells for High Yield Gas Production from Organic Matter. *Environmental Science & Technology*. **42** (23): 8630- 8640

Logan, B.E and Regan, J.M. (2006) Microbial fuel cells: challenges and applications. *Environmental Science & Technology*. **40** (17): 5172- 5180

Logan, B.E., Murano, C., Scott, K., Gray, N.D., and Head, I.M. (2005) Electricity generation from cysteine in a microbial fuel cell. *Water Research*. **39 (5):** 942-952

Lu, L and Ren, Z.J. (2016) Microbial electrolysis cells for waste biorefinery: A state of the art review. *Bioresource Technology.* **215:** 254-264

Lu, L., Xing, D., Ren, N., & Logan, B. E. (2012). Syntrophic interactions drive the hydrogen production from glucose at low temperature in microbial electrolysis cells. *Bioresource Technology.* **124:** 68–76.

Madigan, M.T., Martinko, J.M., Stahl, D.A. and Clark, D.P. (2012) Brock Biology of Microorganisms. Global Edition. Thirteenth Edition. Pearson Education, Inc., ISBN 13: 978-0-321-73551-5

Manohar, A.K., He, Z. and Mansfeld, F. (2010). The use of electrochemical impedance spectroscopy (EIS) for the evaluation of the electrochemical properties of bioelectrochemical systems. In Rabaey, K., Angenent, L., Schroeder, U. and Keller, J Edited: Bioelectrochemical systems: from extracellular electron transfer to biotechnological application. IWA Publishing, London. UK.

Martin, B.D., Parsons, S.A. and Jefferson, B. (2009). Removal and recovery of phosphate from municipal wastewaters using a polymeric anion exchanger bound with hydrated ferric oxide nanoparticles. *Water Science & Technology*. **60** (10): 2637-2645

McCarty, P. L., Bae, J., & Kim, J. (2011). Domestic wastewater treatment as a net energy producer-can this be achieved? *Environmental Science & Technology.* **45**(17): 7100–7106.

Metal Miner (2016) Metal Miner Prices [online]. Available at: https://agmetalminer.com/metal-prices/ [accessed on 03/10/2016].

Michie I.S, Kim, J.R., Dinsdale, R.M., Guwy A.J., and Premier, G.C (2011) The influence of psychrophilic and mesophilic start-up temperature on microbial fuel cell system performance. *Energy & Environmental Science.* **4:** 1011-1019

Monpart, N., Rago, L., Baeza, J.A., and Guisasola, A (2015) Hydrogen production in single chamber microbial electrolysis cells with different complex substrates. *Water Research.* **68:** 601-615

Monpart, N., Ribot-Llobet, E., Garlapati, V.K., Rago, L., Baeza, J.A., and Guisasola, A. (2014) Methanol opportunities for electricity and hydrogen production in bioelectrochemical systems. *International Journal of Hydrogen Energy.* **39**(2): 770-777

Moon, H., Chang, I.S., Kim, B.H. (2006) Continuous electricity generation from artificial wastewater using a mediator-less microbial fuel cell. *Bioresource Technology.* **97:**621-627

Nam, J.Y., Tokash, J.C. and Logan, B.E (2011) Comparison of microbial electrolysis cells operated with added voltage or by setting the anode potential. *International Journal of Hydrogen Energy.* **36**(17): 10550-10556

Nam, J.Y. and Logan, B.E. (2010). Optimization of catholyte concentration and anolyte pHs in two chamber microbial electrolysis cells. *International Journal of Hydrogen Energy.* **37** (24): 18622- 18628

de Nardi, I.R., Zaiat, M. and Foresti, E. (1999) Influence of tracer characteristics on hydrodynamic models of packed-bed reactors. *Bioprocess Engineering*. **21:** 469-476

Nevin, K.P., Holmes, D.E., Woodard, T.L., Hinlein, E.S., Ostendorf, D.W and Lovley, D.R. (2005) Geobacter bemidjiensis sp. nov. and Geobacter psychrophilus sp. nov., two novel Fe(III)-reducing subsurface isolates. *International Journal of Systematic and Evolutionary Microbiology.* **55** (4): 1667-1674

Northumbrian Water Ltd (2009) Chapter 8: CBA and Carbon Accounting. Supplementary Information on Justification for Proposed Investment – including outcome of cost benefit analysis and carbon accounting. PR09 Final Business Plan [online]. Available at: https://www.nwl.co.uk/_assets/documents/C8__CBA_and_Carbon_Accounting.pdf [accessed on 10/08/2016]

Ofiteru, I.D., Lunn, M., Curtis, T.P., Wells, G.F., Criddle, C.S., Francis, C.A., and Sloan, W.T. (2010). Combined niche and neutral effects in a microbial wastewater treatment community. *PNAS.* **107** (35): 15345-15350

Olsson, G. (2012) Chapter 15. Energy and carbon footprint of water operations. Water and Energy: Threats and Opportunities. IWA Publishing, London

Orhon, D., Okutman, D. and Insel, G (2002) Characterisation and biodegradation of settleable organic matter for domestic wastewater. *Water SA*. **28** (3): 299-306

Parker, C.D. (1945) The corrosion of concrete. *Australian Journal of Experimental Biology and Medical Science.* **23**: 81-90

Parameswaran, P., Torres, C.I., Lee, H.S., Krajmalnik-Brown, R., Rittmann, B.E. (2009) Syntrophic interactions among anode respiring bacteria (ARB) and Non-ARB in a biofilm anode: electron balances. *Biotechnology Bioengineering*. **103:**513–523.

Patil, S. A., Harnisch, F., Kapadnis, B., & Schröder, U. (2010). Electroactive mixed culture biofilms in microbial bioelectrochemical systems: the role of temperature for biofilm formation and performance. *Biosensors & Bioelectronics*. **26** (2): 803–808.

Pikaar, I., Sharma, K.R., Hu, S., Gernjak, W., Keller, J. and Yuan, Z. (2014) Reducing sewer corrosion through integrated urban water management. *Science*. **345** (6198): 812-814

Pisano, G.P. (1996) Learning-before-doing in the development of new process technology. *Research Policy*. **25**: 1097-1119

Popescu, D.M. (2016) Doctoral thesis submitted to Newcastle University.

Prosser, J.I., Bohannan, B.J.M., Curtis, T.P., Ellis, R. J., Firestone, M.K., Freckleton, R.P., Green, J.L., Green, L.E., Killham, K., Lennon, J.J., Osborn, A.M., Solan, M., van der Gast, C.J. and Young, J.P.W (2007). The role of ecological theory in microbial ecology. *Nature Reviews*. **5:** 384-392

Protopopoff, E. and Marcus, P. (1988) Poisoning of the cathodic hydrogen evolution reaction by sulphur chemisorbed on platinum (110). *Journal of the Electrochemical Society.* **135** (12): 3073-3075

Qu, Y., Feng, Y., Wang, X., Liu, J., Lv, J., He, W. and Logan, B.E. (2012) Simultaneous water desalination and electricity generation in a microbial desalination cell with electrolyte recirculation for pH control. *Bioresource technology.* **106:** 89-94

Rabaey, K., Bützer, S., Brown, S., Keller, J. & Rozendal, R.A. (2010) High current generation coupled to caustic production using a lamellar bioelectrochemical system. *Environmental Science & Technology.* **44:** 4315-4321.

Rabaey, K., van de Sompel, K., Maigien, L., Boon, N., Aelterman, P., Clauwert, P., de Schamphelaire, L., Pham, H.T. Vermeulen, J., Verhaege, M., Lens, P. and Verstraete, W. (2006) Microbial Fuel Cells for Sulfide Removal. *Environmental Science & Technology.* **40:** 5218-5224

Rago. L., Ruiz, Y., Baeza, J.A., Guisasola, A., Cortés, P. (2015) Microbial community analysis in a long-term membrane-less microbial electrolysis cell with hydrogen and methane production. *Bioelectrochemistry.* **106:** 359-368

Rajput, R.K. (2004) A textbook of electrical engineering materials. U.P. Technical University, Lucknow. Firewall Media. ISBN: 8170084016, 9788170084013.

Rauch, W. and Kleidorfer, M. (2014) Replace contamination, not the pipes. *Science.* **345** (6198): 734-735

Raunkjær, K., Hvitved-Jacobsen, T., & Nielsen, P. H. (1994). Measurement of pools of protein, carbohydrate and lipid in domestic wastewater. *Water Research.* **28** (2): 251–262.

Ravot, G., Magot, M., Fardeau, M-L., Patel, B.K.C., Thomas, P., Garcia, J-L., and Ollivier, B. (1999) Fusibacter paucivorans gen. nov., sp. nov., an anaerobic, thiosulfate-reducing bacterium from an oil-producing well. *International Journal of Systematic and Evolutionary Microbiology.* **49** (3): 1141-1147

Reysenbach, A.L., Giver, L.J., Wickham, G.S. and Pace, N.R. (1992) Differential amplification of rRNA genes by polymerase chain reaction. *Applied and Environmental Microbiology.* **58** (10): 3417-3418

Ringelberg, D.B., Foley, K.L., and Reynolds, C.M. (2011) Electrogenic capacity and community composition of anodic biofilms in soil-based bioelectrochemical systems. *Applied Microbiology Technology*. **90:** 1805 - 1815

Rodriguez-Añòn, J. A., Proupin, J., González- Añòn, M., and Núñez-Regueira, L. (1998) Energy recovery from municipal solid waste in small communities. *Journal of Thermal Analysis and Calorimetry*. **52** (3): 1005–1012

Rozendal, R.A., Hamelers, H.V.M., Rabaey, K., Keller, J. and Buisman, C.J.N. (2008a) Towards practical implementation of bioelectrochemical wastewater treatment. *Trends in Biotechnology*. **26**(8): 450-459.

Rozendal, R.A., Jeremiasse, A.W., Hamelers, H.V.M., and Buisman, C.J.N. (2008b) Hydrogen production with a microbial biocathode. *Environmental Science & Technology* **42**: 629-634.

Rozendal, R.A., Hamelers, H.V.M., Molenkamp, R.J., and Buisman, C.J.N. (2007) Performance of single chamber biocatalyzed electrolysis with different types of ion exchange membranes. *Water Research*. **41** (9): 1984-1994

Rozendal, R.A., Hamelers, H.V.M., Euverink, G.J.W., Metz., S.J. and Buisman, C.J.N. (2006) Principle and perspectives of hydrogen production through biocatalyzed electrolysis. *International Journal of Hydrogen Energy*. **31** (12): 1632-1640

Ruiz, Y., Baeza, J.A., Guisasola A. (2013) Revealing the proliferation of hydrogen scavengers in a single-chamber microbial electrolysis cell using electron balances. *International Journal of Hydrogen Energy*. **38:**15917-15927.

Ruiz, V., Ilhan, Z.E., Kang, D.W., Krajmalnik-Brown, R., Buitrón, G. (2014) The source of inoculum plays a defining role in the development of MEC microbial consortia fed with acetic and propionic mixtures. *Journal of Biotechnology*. **182-183**: 11-18

Schiel-Bengelsdorf, B. and Dürre, P (2012). Pathway engineering and synthetic biology using acetogens. *FEBS letters*. **586** (15): 2191-2198

Schloss, P.D., and Handelsman, J. (2004) Status of the microbial census. *Microbiol. Mol. Biol.Rev.* **68** (4): 686-691

Scott, K. (2016) Chapter 2: Electrochemical principles and characterization of bioelectrochemical systems. In Scott, K., and Yu, E. ed. Microbial electrochemical and fuel cells: fundamentals and applications. Woodhead publishing. 29-66

Sedlak, R. (1991) Phosphorus and Nitrogen Removal from Municipal Wastewater. Principles and Practice. 2nd Edition.

Seghezzo, L., Zeeman, G., van Lier, J.B., Hamelers, H.V.M. and Lettinga, G. (1994) A review: the anaerobic treatment of sewage in UASB and EGSB reactors. *Bioresource Technology.* **65:** 175-190

Sigma Aldrich (2017) Hydrogen Peroxide [online]. Available at http://www.sigmaaldrich.com/catalog/substance/hydrogenperoxidesolution3401772284111?lang=en&region=GB [Accessed 09/03/2017].

SGL (2016) SIGRACELL Battery Felt Material Data [online] Available at: http://www.sglgroup.com/cms/international/products/product-groups/cfrc_felt/specialty-graphites-for-energy-storage/material.html?__locale=en [accessed on 03/10/2016]

Sharma, M., Bajracharya, S., Gildemyn, S., Patil, S.A., Alvarez-Gallego, Y., Pant, D., Rabaey, K., and Dominguez-Benetton, X. (2014) A critical revisit of the key parameters used to describe microbial electrochemical systems. *Electrochimica Acta.* **140:**191-208

Shih, W-Y., Rahardianto, A., Lee, R-W., and Cohen Y. (2005) Morphometric characterization of calcium sulfate dihydrate (gypsum) scale on reverse osmosis membranes. *Journal of Membrane Science.* **252:** 253–263

Shizas, I., & Bagley, D. M. (2004). Experimental Determination of Energy Content of Unknown Organics in Municipal Wastewater Streams. *Journal of Energy Engineering.* **130** (2): 45–53.

Shröder, U and Harnisch, F. (2010) 7: Electrochemical Losses. In Rabaey, K., Angenent, L., Schroeder, U. and Keller, J. ed., Bioelectrochemical systems: from extracellular electron transfer to biotechnological application. IWA Publishing, London. UK

von Sperling, M., and Gonçalves, R.F. (2007) Chapter 2: Sludge Characteristics and Production. In: Andreoli, C.V., von Sperling, M. and Fernandes, F., ed. Sludge Treatment and Disposal Volume Six. IWA Publishing.London. 4-28

Spirito, C.M., Richter, H., Rabaey, K., Stams, A.J.M. and Angenent, L.T. (2014) Chain elongation in anaerobic reactor microbiomes to recover resources from waste. *Current Opinion in Biotechnology*. **27**: 115-122

Stairs, D.B. (1993) Flow characteristics of constructed wetlands: tracer studies of the hydraulic regime. MSc thesis for Bioresource Engineering, Oregon State University.

Stolten, D. (2010) Hydrogen and Fuel Cells: Fundamentals, technologies and applications. Wiley-VCH.

Sun, D., Wang, A., Cheng, S., Yates, M., and Logan, B.E (2014) Geobacter anodireducens sp. nov., an exoelectrogenic microbe in bioelectrochemical systems. *International Journal of Systematic and Evolutionary Microbiology.* **64:** 3485-3491

Tchobanoglous, G., Burton, F.L., and Stensel, H.D (2004) Wastewater Engineering Treatment and Reuse. Fourth Edition. McGraw Hill.

Teefy, S.M., and Singer, P.C. (1990) Performance and analysis of tracer tests to determine compliance of a disinfection scheme with SWTR. *American Water Works Association (AWWA).* 88-98.

Tenca, A., Cusick, R.D., Schievano, A., Oberti, R., and Logan, B.E. (2013) Evaluation of low cost cathode materials for treatment of industrial and food processing wastewater using microbial electrolysis cells. *International Journal of Hydrogen Energy.* **38** (4): 1859-1865

Thomke, S. and Reinertsen, D. (2012) Six myths of product development. *Harvard Business Review*. May 2012. 85-94

Torres, C.I., Krajmalnik-Brown, R., Parameswaran, P., Marcus, A.K., Wanger, G., Gorby, Y.A. and Rittmann, B.E. (2009) Selecting Anode-Respiring Bacteria Based on Anode Potential: Phylogenetic, Electrochemical, and Microscopic Characterization. *Environmental Science & Technology*. **43**(24): 9519-9524

Turner, J.A. (2004) Sustainable Hydrogen Production. *Science*. **305** (5686): 972-974

Ullery, M.L. and Logan, B.E (2014) Comparison of complex effluent treatability in different bench scale microbial electrolysis cells. *Bioresource Technology*. **170:** 530-537

UniQuest (2012) Bilexys wins international water prize [online]. Available at https://www.uniquest.com.au/news/bilexys-wins-international-water-prize [accessed on 09/03/2017].

Venkataraman, A., Bassis, C.M., Beck, J.M., Young, V.B., Curtis, J.L., Huffnagle, G.B. and Schmidt, T.M. (2015) Application of a Neutral Community Model to Assess Structuring of the Human Lung Microbiome. *mBio.* **6** (1): e02284-14

Verea, L. Savadogo, O., Verde, A., Campos, J., Ginez, F. and Sebastian, P.J. (2014) Performance of a microbial electrolysis cell (MEC) for hydrogen production with a new process for the biofilm formation. *International Journal of Hydrogen Energy*. **39** *(17):* 8938-8946

Vesilind, P. A., and Ramsey, T. B. (1996) Effect of drying temperature on the fuel value of wastewater sludge. *Waste Management and Research*. **14** (2): 189–196

Water UK (2012) Sustainability Indicators 2010/11 [online]. Available at: http://www.water.org.uk/news-water-uk/latest-news/water-industry-sustainability-latest-indicators. Updated on 5 Jan 2012. [accessed on 03/10/2016]

Wagner, R.C., Regan, J.M., Oh, S., Zuo, Y. and Logan, B.E. (2009) Hydrogen and methane production from swine wastewater using microbial electrolysis cells. *Water Research.* **43** (5): 1480-1488

Wang, A., Liu, W., Ren, N., Zhou, J and Cheng, S. (2010) Key factors affecting microbial anode potential in a microbial electrolysis cell for H_2 production. *International Journal of Hydrogen Energy.* **35:** 13481-13487

Wang, J.J., Jing, Y.Y., Zhang, C.F. and Zhao, J.H. (2009) Review on multi-criteria decision analysis aid in sustainable energy decision-making. *Renewable and Sustainable Energy Reviews.* **13:** 2263-2278

Wang, Y., Guo, W., Xing, D., Chang, J. and Ren, J. (2014) Hydrogen production using biocathode single-chamber microbial electrolysis cells fed by molasses wastewater at low temperature. *International Journal of Hydrogen Energy.* **39**(33): 19369-19375

Weber, K.A., Achenbach, L.A., and Coates, J.D (2006a) Microorganisms pumping iron: anaerobic microbial oxidation and reduction. *Nature Reviews*. **4:** 752-764

Weber, K.A., Urrutia, M.M., Churchill, P.F., Kukkadapu, R.K., and Roden, E.E. (2006b) Anaerobic redox cycling of iron by freshwater sediment microorganisms. *Environmental Microbiology*. **8** (1):100-113

Wei, L., Han, H., & Shen, J. (2013). Effects of temperature and ferrous sulfate concentrations on the performance of microbial fuel cell. *International Journal of Hydrogen Energy*. **38** (25): 11110–11116.

Wu, T., Zhu, G., Jha, A.K., Zou, R., Liu, L., Huang, X., and Liu, C. (2013) Hydrogen production with effluent from an anaerobic baffled reactor (ABR) using a single-chamber microbial electrolysis cell (MEC). *International Journal of Hydrogen Energy.* **38** (25): 11117-11123

Xu, Y. Jiang, Y., Chen, Y., Zhu, S., and Shen, S. (2014) Hydrogen Production and Wastewater Treatment in a Microbial Electrolysis Cell with a Biocathode. *Water Environment Research*. **86** (7): 649-653

Yang, Q., Feng, Y., and Logan, B.E. (2012) Using cathode spaces to minimise reactor size in air cathode microbial fuel cells. *Bioresource Technology*. **110:** 273-277

Yossan, S. Xiao, L., Prasertsan, P. and He, Z. (2013) Hydrogen production in microbial electrolysis cells: Choice of catholyte. *International Journal of Hydrogen Energy*. **38** (23): 9619-9624

Zanoni, A. E., and Mueller, D. L. (1982) Calorific value of wastewater plant sludges. *Journal of Environmental Engineering Division.* **108** (1): 187–195

Zeng, W., Bai, X., Zhang, L., Wang, A. and Peng, Y. (2014) Population dynamics of nitrifying bacteria for nitritation achieved in Johannesburg (JHB) process treating municipal wastewater. *Bioresource Technology.* **162:** 30-37

Zhang, F., Zheng G., Grimaud, J., Hurst, J. and He, Z. (2013) Long-Term Performance of Liter-Scale Microbial Fuel Cells Treating Primary Effluent Installed in a Municipal Wastewater Treatment Facility. *Environmental Science & Technology*. **47**: 4941-4948

Zhang, F., Pant, D., Logan, B.E. (2011) Long-term performance of activated carbon air cathodes with different diffusion layer porosities in microbial fuel cells. *Biosensors and Bioelectronics*. **30** (1): 49-55

Zhang, G., Wang, K., Zhao, Q., Jiao, Y., Lee, D.J. (2012a) Effect of cathode types on long-term performance and anode bacterial communities in microbial fuel cells. *Bioresource Technol*ogy. **118:** 249-256

Zhang, T., Shao, M.F. and Ye, L. (2012b) 454 Pyrosequencing reveals bacterial diversity of activated sludge from 14 sewage treatment plants. *ISME Journal*. **6:**1137–1147

Zhang, X., He, W., Ren, L., Stager, J., Evans, P. J., & Logan, B. E. (2015). COD removal characteristics in air-cathode microbial fuel cells. *Bioresource Technology*. **176:** 23–31.

Zhang, Y., Sun, J., Hu, Y., Wang, Z., & Li, S. (2014). Effects of periodically alternating temperatures on performance of single-chamber microbial fuel cells. *International Journal of Hydrogen Energy*. **39** (15): 8048–8054.

Zhang, Y. and Angelidaki, I. (2014) Microbial electrolysis cells turning to be a versatile technology: Recent advances and future challenges. *Water Research*. **56:** 11-25

Zheng, M.X., Wanh, K.J., Zuo, J.E., Yan, Z., Fang, H. and Wu, J.W. (2012) Flow pattern analysis of a full-scale expanded granular sludge bed-type reactor under different organic loading rates. *Bioresource Technology*. **107:** 33-40

Zhou, J., Liu, W., Deng, Y., Jiang, Y-H., Xue, K., He, Z., Van Nostrand, J.D., Wu, L., Yang, Y., and Wang, A. (2013) Stochastic assembly leads to alternative communities with distinct function in a bioreactor microbial community. *mBio*. **4** (2): e00584-12

Zhuang, L., Zhou, S., Li., Y. and Yuan, Y. (2010) Enhance performance of air-cathodetwo-chamber microbial fuel cells with high-pH and low-pH cathode. *Bioresource Technology*. **101:** 3514-3519

Züttel. A (2003) Materials for hydrogen storage. *Materials Today.* **6** (9): 24-33

Zuur, A., Ieno, E. and Smith, G.M (2007) Chapter 15. Principal coordinate analysis and non-metric multidimensional scaling. In: Analyzing Ecological Data. Springer, New York pp 259-264 ISBN: 978-0-387-45967-7

Appendices

Appendix A Tables from review of 33 MEC papers (2005-2015)

A1. Synthetic Wastes.

The key operational variables from 15 MEC papers published from 2005-2015 using synthetic wastes such as sodium acetate. A dash indicates the value was missing from the publication (either not collected, recorded or directly reported).

Study	Duration (days)	Scale (L)	CE (%)	Electrical Efficiency (%)	Total Energy Efficiency (%)	COD removal (%)	Temp (°C)	Volumetric H$_2$ production (m^{3}H$_2$/m^3/d)
Farhangi *et al.*, 2014	-	0.385	73-79	-	44-54	-	-	0.22-0.3
Xu *et al.*, 2014	-	0.08	63	67	-	90	33	0.39
Brown *et al.*, 2014	30	16-30	11	-	-	67	25-36	-
Verea *et al.*, 2014	-	0.1	5-21	-	-	-	37	0.82
Yossan *et al.*, 2013	10	0.24	8-43	-	-	86-98	20	0.034-0.237
Nam *et al.*, 2011	103	0.028	79-87	71-187	26-58	93-95	30	3.6-7.9
Hu *et al.*, 2008	-	0.5	24-75	204-267	27-60	-	30	0.2-0.69
Chae *et al.*, 2008	150	0.36	48-68	-	-	-	26-28	0.052
Liu *et al.*, 2008	66	0.9	-	-	-	-	28-30	-
Call & Logan 2008	-	0.028	92	194-406	72-78	-	30	1.99- 3.12
Rozendal *et al.*, 2008b	-	0.028	-	-	-	-	30	0.63
Rozendal 2007	-	6.6	23	-	-	-	30	0.33
Cheng & Logan 2007	-	0.042	-	288	62–86	-	30	0.11-1.23
Rozendal *et al.*, 2006	8	6.6	92	-	-	-	30	0.02
Liu, Grot & Logan 2005	120	0.31	60-78	-	-	-	-	-

A2. Real Wastewaters.

The key operational variables from 18 MEC papers published from 2005-2015 using real wastes such as domestic and industrial wastewaters. A dash indicates the value was missing from the publication (either not collected, recorded or directly reported).

Study	Duration (days)	Scale (L)	CE (%)	Electrical Efficiency (%)	Total Energy Efficiency (%)	COD removal (%)	Temp (°C)	Volumetric H_2 production ($m^3H_2/m^3/d$)
Monpart et al., 2015	100	0.028	15-52	-	-	73.5-100	23	0-0.94
Heidrich et al., 2014	>365	100	41.2	48.7	-	33	1-22	0.007
Wang et al., 2014	25	0.025	83.6-95	110-244	-	-	9	0.72-1.69
Ullery and Logan, 2014	40	0.005-0.032	18-169	-	-	66-92	30	-
Monpart et al., 2014	28	0.028	60-90	60	20	-	~25	0.1
Kuntke et al., 2014	12	0.9	84-97	-	-	29-46	30	49
Gil-Carrera et al., 2013a	>730	2	9-30	-	-	80	20	0.006- 0.045
Wu et al., 2013	-	0.085	-	138	-	99	35	1.31
Heidrich et al., 2013	149	120	55	70	30	34	16.6	0.015
Escapa et al., 2013	-	0.5	7-25	97	-	46-90	25	1.42
Gil-Carrera et al., 2013b	>730	2	10-94	-	-	85	20	0.045
Tenca et al., 2013	-	0.028	7–12	-	-	85-89	30	0.8-1.8
Gil-Carrera et al., 2013c	45	10	23-129	-	-	66-76	24	0.04
Escapa et al., 2012	35	0.2	38-65	-	-	76	30	0.3
Cusick et al., 2011	100	1000	-	-	-	62	31	Trace
Jia et al., 2010	-	0.72	9-30	124	4-14	48	-	0.061
Wagner et al., 2009	15	0.028	29-70	91-190	-	19-72	30	0.8-1
Ditzig, Lui Logan 2007	-	0.6	10-26	-	-	95	30	-

Appendix B. Efficiency Calculations

There are four efficiency calculations which can be made to evaluate how well the system is performing.

a) **Electrical Energy Efficiency (η_E) - this is the amount of electrical energy put into the reactor that is recovered as hydrogen.**

$$Electrical\ Energy\ Efficiency = \frac{Energy\ recovered\ in\ H_2}{Electrical\ energy\ input}$$

The electrical energy input $W_{E\,is}$ calculated as:

$$W_E = \sum_1^n (I\ E_{ps}\Delta t - I^2 R_{ex}\Delta t) \tag{1}$$

The electrical energy input (W_E) given in kWh is determined by integrating the product of the voltage added at each measured current over the experiments duration. Where I is the current calculated for the circuit based on the measured voltage E and external resistor R_{ex} ($I=E/R_{ex}$). An external resistor is required to calculate the current that the cell produces from the voltage that the data logger records. As the external resistor increases resistance in the system, the smallest value resistor suitable for the system should be used in order to minimise electrical losses. E_{ps} is the applied voltage of the power supply, this value is adjusted for the losses caused by the external resistor ($I^2 R_{ex}$), with integration over n data points measured over time intervals Δt.

The energy recovered in H_2 (W_{out}) is calculated from the measured moles of hydrogen produced $N_{H2,}$ and the standard higher heating value of hydrogen of 285.83 kJ/mol, i.e. ΔH_{H2}. The higher heating value of hydrogen is chosen over the lower heating value which takes into account the heat lost through the production of water vapour during burning. It is expected that this H_2 product would be used either as a commercial product for industry, or in a clean H_2 consuming fuel cell to create electricity, not for combustion. The kJ are then converted to kWh using the unit of conversion of 3600 kJ/kWh.

$$W_{out} = [\Delta H_{H2}\ N_{H2}]/\ 3600 \tag{2}$$

Electrical energy efficiency (η_E) (excluding pump requirements) can then be calculated as follows:

$$\eta_E = \frac{W_{out}}{W_E} \tag{3}$$

Energy efficiency is expressed as a percentage, and is over 100% when the MEC is energy producing- when additional energy is being gained from the substrate.

Example

The following MEC conditions will be assumed throughout the four calculations:

A cell operates with an input voltage of 0.5V, producing an average voltage of 6 mV over a 1 Ω resistor for 20 hours. During this time, it produces 20 mL of gas, which is 94% pure H_2, measured at standard atmospheric pressure and at 20°C. 150 mg/L of COD are removed during this operation.

Calculation a

The current $I = (6/1000)/1 = 0.006$ Amps

The current is supplied at 0.5 V, meaning the watts supplied $= 0.006 * 0.5 = 0.003$ W

The adjustment for the external resistor $I^2R_{ex} = 0.006^2 * 1 = 0.000036$

The total energy supplied is $= ((0.003 - 0.000036) *20)/1000 = 5.9*10^{-5}$ kWh

The volume of hydrogen gas $= 20 * 0.94 = 18.8$ mL

This is converted to moles using the ideal gas equation $PV = nRT$, where P = pressure (1 atmosphere), V = volume (L), n = number of moles, R = the gas constant (0.08206 L/atm/mol), and T = temperature (294.15 K).

Moles $H_2 = (1*(18.8/1000))/ (0.08206*294.15) = 0.00078$ moles

Energy in H_2 produced $= 0.00078*285.83 / 3600 = 6.2*10^{-5}$ kWh

Electrical Energy Efficiency $= (6.2*10^{-5} / 5.9*10^{-5}) *100 = 105\%$

b) Maximum energy efficiency (η_E max)

The equation in a (1) can be re-written as:

$$W_E = F \eta_E E_{ps} \tag{4}$$

as 1 J= 1 W x t (s), and 1 Watt = 1 Amp x 1 Volt. The product of I (1 A= 1 c/s) and Δt (s) is the number of Coulombs transferred. For each mole of hydrogen produced, we require 2 mol of e⁻ so the energy required is:

$$F \eta_E E_{ps} = (96,500 \text{ C/mol e}^-) (2 \text{ [mol e}^- / \text{ mol } H_2]) E_{ps}$$

$$W_E \text{ (J/ mol } H_2) = 1.93 \times 10^5 E_{ps} \text{ (V)} \tag{5}$$

The energy yield relative to electrical energy input is defined as: $\eta_{E} = W_{H2} / W_{E}$ (6)

where W_{H2} is the energy in the hydrogen gas produced, based either on combustion energy ($\Delta H_{H2} = -285.8$ kJ) or the Gibbs Free energy ($\Delta G_{H2} = -237.1$ kJ). Entropic energy cannot be recovered, therefore, Gibbs Free energy is used:

$\eta_{E} = W_{H2} / W_{E} = (-237,100 \text{ J/mol}) / - (1.93 \times 10^{5}) \text{ E}_{ps} \text{ (V) (mol}^{-1})$ (7)

$\eta_{E} = W_{H2} / W_{E} = 1.23 \text{ E}_{ps}^{-1} \text{ (V)}$ (8)

Therefore, the maximum energy recovery at 0.9 V is 137% and at 1.2 V is 103%.
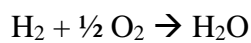
c) **Substrate efficiency** (η_{S}) **- the amount of hydrogen produced compared to the amount theoretically possible based on substrate removed in the reactor.**

$$Substrate\ efficiency\ = \frac{Moles\ of\ H_2\ recovered}{Theoretical\ moles\ of\ H_2\ in\ the\ substrate\ removed}$$ (9)

The number of moles of hydrogen produced (N_{H2}) is compared to the amount theoretically possible based on the amount of substrate removed (N_S) this is calculated as:

$$N_S = 0.0625\ \Delta COD \Delta t$$ (10)

Chemical oxygen demand (COD) is the amount of oxygen required for full oxidation of an organic compound. To oxidise 1 mole of H_2, 0.5 moles of O_2 are required - equating to 16g COD.

$H_2 + \frac{1}{2} O_2 \rightarrow H_2O$

1 mole of hydrogen = 2g   0.5 moles of oxygen = 16g

If 16 g COD are converted in to 1 mole of H_2, each g COD is equivalent to 0.0625 moles of H_2. The COD removal is measured to give ΔCOD over the time interval of the experiment.

Substrate efficiency (S_E) is then calculated as:

$$S_E = \frac{N_S}{N_{H2}}$$ (11)

Again this is expressed as a percentage, and it gives an indication of how well the reactor is converting the substrate energy into hydrogen.

Calculation b

Moles H_2 recovered = 0.00078 moles

If 150 mg/L COD is removed,

Moles H_2 in substrate removed = 0.065 * (150/1000) = 0.0096 moles

Substrate Efficiency = 0.00078 / 0.0096 *100 = 8%

d) **Cathodic coulombic efficiency (CCE) - the amount of hydrogen produced compared to the amount theoretically possible based on the current or total charge passing through the cell.**

$$Cathodic\ coulombic\ efficiency\ = \frac{Moles\ of\ H_2 recovered}{Theoretical\ moles\ of\ H_2\ in\ the\ current\ produced} \qquad (12)$$

The theoretical moles of hydrogen based on current (N_{CE}) is calculated as:

$$N_{CE} = \frac{\sum_1^n I\Delta t}{2F} \qquad (13)$$

Where I am the current calculated from the measure voltage, Δt is the time interval and F is Faradays constant (96485 coulombs/mol e⁻), 2 is the number of electrons in the hydrogen evolution reaction to give moles of H_2.

Cathodic coulombic efficiency CCE [eq. 4.8] is then calculated as:

$$CE = \frac{N_{CE}}{N_{H2}} \qquad (14)$$

This is again expressed as a percentage; it should not exceed 100%.

Calculation c

Moles H_2 recovered = 0.00078 moles

Moles H_2 in the current = (0.006*30*60*20)/ (2*96485) = 0.00111 moles

CCE = 0.00078/0.00111*100 = 70%

This correlates directly to the electrical energy efficiency (η_E) by re-arrangement of their respective equations. It is assumed that the effect of the external resistor over time, denoted by the term $I^2 R_{ex}\Delta t$ in calculating W_E , is negligible in comparison to the first term:

166

$$\eta_E = \frac{\Delta H_{H2} \times 1000}{2F \times E_{ps}} CCE \tag{15}$$

This means that halving the E_{ps} doubles the η_E, if the CCE can be maintained. An increase in CCE at the same E_{ps} causes a linear increase in η_E.

e) Total energy efficiency (η_{E+S})- the amount of input energy both electrical and substrate that is recovered as hydrogen.

$$Energy\ recovery = \frac{Energy\ recovered\ in\ H_2}{Electrical\ and\ substrate\ energy\ input} \tag{16}$$

The substrate energy (W_s) is calculated as:

$$W_s = \Delta COD\ \Delta H_{ww/COD} \tag{17}$$

Where ΔCOD is the change in COD in grams, usually estimated as the difference in COD of the influent and effluent at the end of each batch. The energy content per gCOD $\Delta H_{ww/COD}$ is the internal energy of the substrate (given as kJ/mol in thermodynamic tables) converted to an equivelent gram of COD, i.e. for acetate this would be 13.6 kJ/gCOD. Thermodynamic values are not known for wastewater as it contains a mix of compounds, therefore an estimate of 17.8 kJ/gCOD is used here, based on the measurement of a domestic wastewater sample used in a previous study (Heidrich *et al.,* 2011).

Total energy efficiency is then calculated as:

$$\eta_{E+S} = \frac{W_{out}}{W_E + W_S} \tag{18}$$

This quantity is again measured as a percentage and can be low especially with real wastewaters, where the substrate energy is estimated based on the internal chemical energy which is higher than the free energy actually available.

Calculation d

Energy out = 6.2×10^{-5} kWh

Electrical energy input = 5.9×10^{-5} kWh

Energy in wastewater substrate = 0.15 $\times 17.8$ /3600 = 7.4×10^{-4} kWh

Total energy efficiency = $6.2*10^{-5}$ / $(5.9*10^{-5} + 7.4*10^{-4})$ *100 = 7.7%

These four calculations form the basis on which to evaluate MECs system and can give an indication as to where the greatest losses lie.

Power densities and current densities can also be used to provide information about the level of electrical performance within the system; these are measured the same way as with MFCs. A further measurement that is useful for comparison between systems is the volumetric hydrogen production rate, expressed as the volume of hydrogen produced per reactor volume per unit time i.e. m^3-H_2/m^3/day as used in Table 5.2 and 5.3. To compare MECs to other wastewater treatment systems, it may also be necessary to calculate the organic loading rate, expressed as the amount of COD removed per reactor volume per unit time i.e. gCOD/m^3/hr.

Appendix C. Description of rocket and bomb calorimetry method

C1. Collection of sample

Three spot samples (influent, effluent and sludge; each using a two litre Duran bottle) were taken from the MEC reactor on site at Chester le Street STW, on three separate visits. The sample was transported back to the university in a cool box, stored in a refrigerator at 4°C before subsequent drying in the evaporator within the same day.

C2. Drying method and control

Each sample was dried (for 18 hours and 40 minutes; until all visible liquid had disappeared) using low pressure steam under vacuum in a Rocket Synergy centrifugal evaporator (Genevac, UK). For the first three runs, two vials containing 400 mL of liquid were put in to the evaporator for each distinct sample, totalling 800 mL of liquid per sample. After the Rocket Synergy run was complete the vials were left to air dry in a box containing desiccating crystals for 3 days before the vials were re-weighed to calculate the amount of dry solid yielded by the drying process. Following this, the sample was scraped out of the vial and stored in a sterile container prior to further analysis.

Unfortunately, due to the low strength of the wastewater (100-250 mg/L-COD) 800ml of liquid only produced 0.35-0.4 g of dry solid. When analysed on the bomb calorimeter, this heat of combustion from this amount of solid did not mask the spike from the standard and therefore the calorific value recorded was negligible or negative. It was decided that the sampling and drying process would be repeated with 3 flasks per sample, totalling 1200 mL of liquid to be dried. This volume yielded 0.55-0.6 g of dry solid, a value comparable with Heidrich *et al.,* 2011, and sufficient to give accurate measurements in the bomb calorimeter.

A control (of 40 mL per sample) was run via the same procedure to determine how effective the drying process was at retaining the COD fractions in the dry solid, and to compare this with oven and freeze drying. The dry solid (from 40 mL of evaporated sample) was rehydrated with 40 mL of deionised water and sonicated for 10 minutes to encourage disintegration of the solid and thorough mixing of the solution. After sonication, the solution was transferred to a 50 mL centrifuge tube and mixed thoroughly by pipetting the solution up and down. Samples were then taken from this rehydrated solution for COD analysis. The triplicate rehydrated COD measurements were divided by the triplicate COD measurements taken from the original sample to calculate the recovery of COD by the drying process. This value is expressed as a percentage.

C3. Wastewater analysis

Total solids (TS), total chemical oxygen demand (tCOD) and soluble chemical oxygen demand (sCOD) were carried out immediately after placing the samples in the evaporator, on the same day as sampling. Both tCOD and sCOD were measured in triplicate using Hach LCK314 (range 40-150 mg/L) and LCK514 (range 100-2000 mg/L) COD cuvette test kits with a LT200 laboratory analysis dry thermostat and a DR3900 spectrophotometer (Hach Lange, UK). To calculate TS three crucibles for each samples were weighed; filled with wastewater and reweighed; and then dried in a 104°C oven for 24 hours before weighing for a third and final time. This enabled the following calculation: weight of dry solids divided by liquid weight.

C4. Bomb calorimetry method

The calorific value of the dry solids was determined using an adiabatic bomb calorimeter, as described by Heidrich *et al.,* 2011. The heat capacity of the system had been determined using triplicate samples of benzoic acid. This was used to calibrate the system: prior to every set of experimental samples (which were run in standardisation mode), the instrument was run in determination mode with 1g of benzoic acid until a satisfactory reading was given (±0.5% of the theoretical calorific value of the standard) to ensure it was operating within its calibrated points. As shown previously, the dried wastewater sample struggles to combust alone (Heidrich *et al.,* 2011; Shizas and Bagley, 2004) and therefore the 0.6g dry sample was supplemented with 0.4g of paraffin wax, which was used as a combustion aid. The exact weight (in grams; to four decimal places) and the temperature rise of the surrounding water jacket of the bomb calorimeter were recorded along with the calorific value (in kJ/g). Given the exact volume of liquid and the exact weight of dry sample were known – it was possible to calculate the calorific value of the wastewater (kJ/L) by dividing the kJ/g of sample by the amount of sample obtained from the known volume of liquid (g/L). Then, using the COD measurements (mg-COD/L) it was possible to calculate kJ/g-COD.

Appendix D. Molecular and microbial methods

D1. Location of samples for 16S DNA sequencing

Samples were taken evenly across the top, middle and bottom of the front and rear anodes of one of the high performing modules from pilot 1 (chapter 2). These samples functioned as transects of the biofilm, so the heterogeneity of the community could be determined. This was carried out through16S DNA Illumina sequencing (red squares) and SEM imaging (yellow squares). Samples were numbered sequentially left to right and top to bottom.
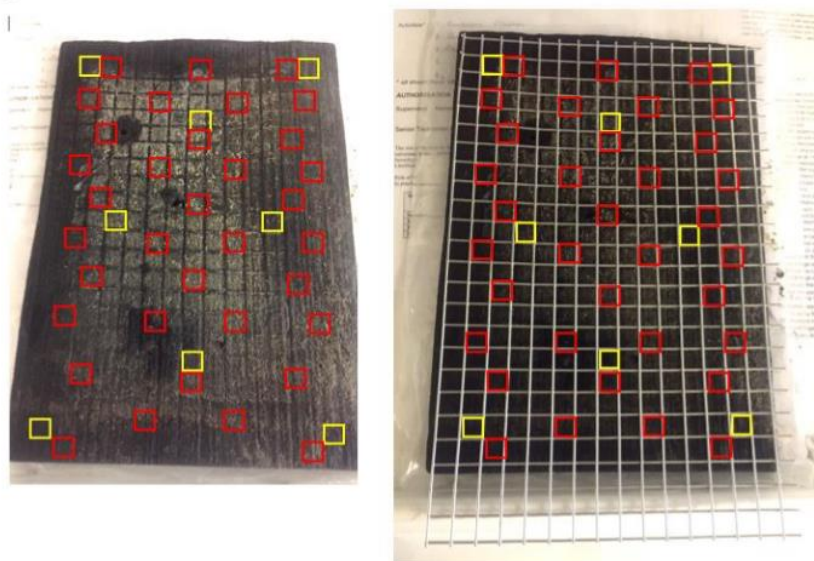

D2. All 16 SEM images

The distribution of the anodic biofilm was visualised after six-months' inoculation in domestic sewage, at a variety of magnifications, using scanning electron microscopy (SEM). The distribution is heterogeneous at an overview level of magnification (100x), but when each fibre is visualised individually (2000x magnification) it is clear to see a biofilm surrounding each fibre. Each of the images from the 16 samples are paired and positioned relative to their positioning on the original anode.
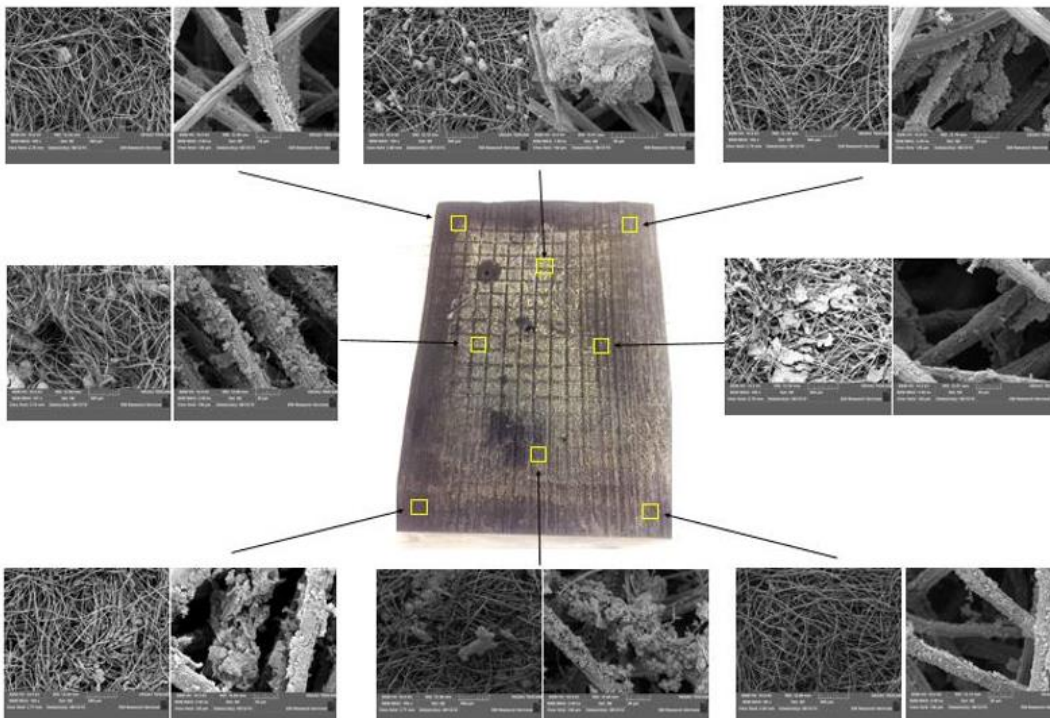
Scanning electron microscopy images at 100x (left of each pair) and 2000x (right of each pair) magnification for eight samples taken from the front of one of the high performing modules from pilot 1 (chapter 2). The anode is shown with magnification centrally, to highlight the location of each of the respective samples.
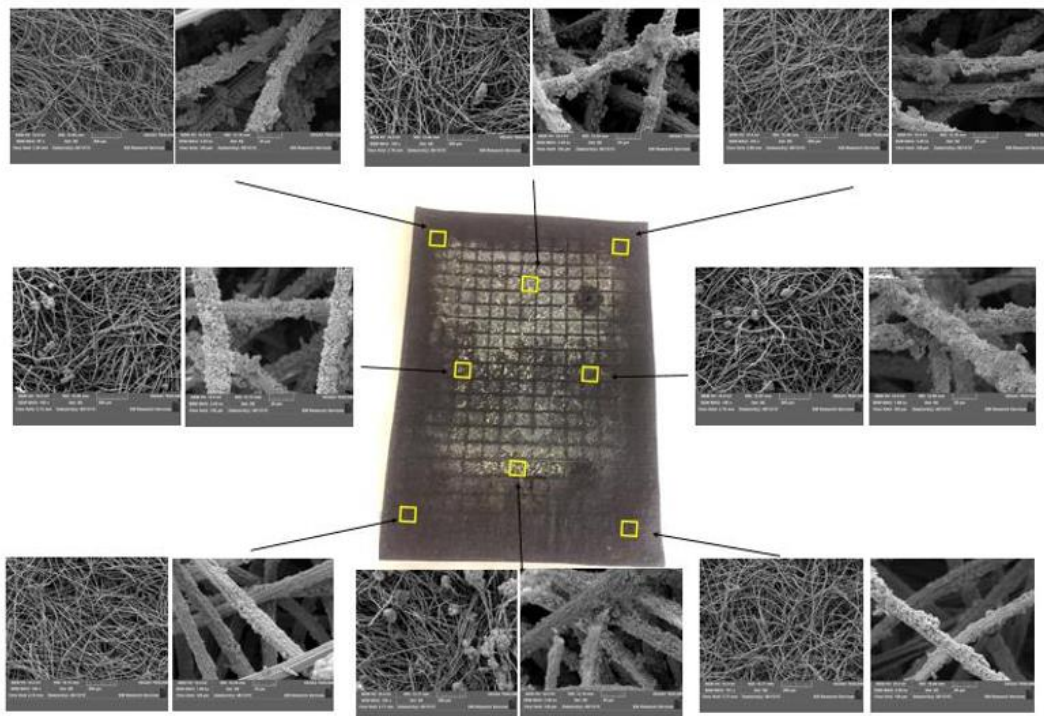
Scanning electron microscopy images at 100x (left of each pair) and 2000x (right of each pair) magnification for eight samples taken from the back of one of the high performing modules from pilot 1 (chapter 2). The anode is shown with magnification centrally, to highlight the location of each of the respective samples.

Appendix E. Quantification of Fe(II) and Fe(tot) via the 1,10-phenanthroline method

Quantification of reduced iron (Fe^{2+}) and total iron was performed using the 1,10-phenanthroline method.

The following reagents were prepared (as described below) in advance to running the method:

- **HCl:** 5 M Hydrochloric acid

- **1,10-phenanthroline**: 0.15 g of 1,10-phenanthroline was dissolved in 150 mL of de-ionised (DI) water which had been acidified with 3 drops of concentrated HCl

- **Reductant**: 15 g of hydroxylamine hydrochloride was dissolved in 150 mL DI water

- **Ammonium Acetate Buffer**: 14.3 g of ammonium acetate was dissolved in 8.57 mL DI water, before adding 40 mL of glacial acetic acid

- **Ammonium Fluoride:** 450 mM ammonium fluoride

Fe (II) standards were prepared by diluting ferrous ammonium sulfate in 0.1 N H_2SO_4 in the range of 1-100 µM. Standards were stored in a refrigerator until time of use.

For analysis of Fe (II) alone:
- Add 1000 µL to the micro centrifuge tube before acidifying with 40 µL HCl
- Add 200 µL 1,10-phenanthroline
- Add 200 µL acetate buffer

For analysis of Fe(II) in the presence of Fe(III)
- Add 1000 µL to the sample tube before acidifying with 40 µL HCl
- **Add 50 µL ammonium fluoride**
- Add 200 µL 1,10-phenanthroline
- Add 200 µL acetate buffer

For analysis of Fe(tot)
- Add 1000 µL to the sample tube before acidifying with 40 µL HCl
- **Add 30 µL of reductant (hydroxylamine)**
- **Leave to react for >5 minutes**
- Add 200 µL 1,10-phenanthroline
- Add 200 µL acetate buffer

Incubate in the dark for >30 minutes for maximum colour development.
Transfer each sample from the micro-centrifuge tube into a photometer cuvette.
Measure the absorbance at 510 nm with a UV-vis photometer**.**